Vjeran Hukic, BSc.

2D and 3D FE analyses to investigate the behaviour of reinforced slopes

Master Thesis

To achieve the university degree of

Diplom-Ingenieur

submitted to

Graz University of Technology

Supervisor

Ass. Prof. Dipl.-Ing. Dr. techn.
Franz Tschuchnigg

Institute of Soil mechanics and Foundation Engineering

Second supervisor

Dipl.-Ing. Simon Oberhollenzer BSc.

Graz, November 2018.

Eidesstattliche Erklärung

Ich erkläre an Eides statt, dass ich die vorliegende Arbeit selbstständig verfasst, andere als die angegebenen Quellen/Hilfsmittel nicht benutzt, und die den benutzten Quellen wörtlich und inhaltlich entnommenen Stellen als solche kenntlich gemacht habe. Das in TUGRAZonline hochgeladene Textdokument ist mit der vorliegenden Arbeit identisch.

....

Datum Unterschrift

Acknowledgement

First of all, I would like to thank Ass.Prof. Dipl.-Ing. Dr.techn. Franz Tschuchnigg for assigning me an interesting thesis topic, the outstanding guidance through the whole procedure, the helpful tips and mostly for his patience.

A great thanks goes to Simon, who always took time for me in this process, no matter where he or I were and no matter how busy he was.

I would also like to thank Prof. Schubert who taught me that there are simple solutions for the most complicated problems and Prof. Marte for teaching me to think a little outside the box.

A special thanks is reserved for my friends from home and the ones that I learned to know here in Graz, inside and outside the University. Here, I would also like to address my thanks to my “Kammerl-roommate” with who I spent a few long nights working on the thesis. Without all of them the past six years would have been much harder and monotone.

But my biggest thanks gets my family. My four younger brothers Egi, Dadni, Loki and Dudi, my little sister Nika and of course my parents, Danijel and Ivanka, who always believed in me, no matter how bad it seemed. They showed me what life really is about.

Kurzfassung

In der Geotechnik werden Bodennägeln üblicherweise verwendet um Geländesprünge und alle Arten von Baugruben zu stabilisieren. Mit dem Sicherheitsfaktor wird die Stabilität von Geländesprüngen bewertet. Eine numerische Studie mit dem Finite Elemente Programm PLAXIS 2D würde durchgeführt, um den Einfluss der Bodennägel auf die Sicherheitsfaktorberechnung zu bestimmen. Die Bodennägel würden als Geogrid, modelliert.

In PLAXIS 2D ist es möglich mit zwei verschiedenen Fließregeln, mit der assoziierten und der nicht-assoziierten Fließregel den Sicherheitsfaktor zu bestimmen. Die zwei Fließregel unterscheiden sich bei der Annahme des Dilatanzwinkels. In dieser Diplomarbeit werden die zwei Fließregeln, bezüglich den generierten Bruchflächen, den berechneten Sicherheitsfaktor und den Spannungen entlang der Bruchfläche mit einander verglichen. Die Berechnungen mit der assoziierten Fließregel ergaben größere Sicherheitsfaktoren mit längeren Bruchflächen. Außerdem war auch die Einwirkung der Bodennagel auf die effektiven Spannungen entlang der Bruchfläche untersucht und zeigte einen wesentlichen Einfluss auf die untersuchten Spannungen. Die Resultate werden auch mit den Resultaten des Grenz-Gleichgewichtverfahren Programms *Slide* verglichen.

Schließlich wird eine Fallstudie von einer Bodennagelwand, in PLAXIS 3D durchgeführt. Bodennägel mit unterschiedlichen Steifigkeiten würden untersucht. In der 3D Studie liegt der Fokus, neben der Sicherheitsfaktorberechnung, in dem Deformationsverhalten und den Kräften in den Bodennägeln. Die Berechnungen mit den steiferen Bodennägeln ergaben kleinere Verformungen und größeren Sicherheitsfaktor.

Abstract

In geotechnical engineering, soil nails are commonly used to stabilize slopes and different kinds of excavations. The slope stability is assessed by means of a factor of safety (FoS) calculation. To determine the influence of the soil nails on the slope stability, stability analyses were carried out using the displacement finite element software PLAXIS 2D. Thereby, the soil nails were modelled using the Geogrids structural type.

The factor of safety of reinforced slopes is strongly influenced by the flow rule (the associated $\psi'=\varphi'$ and the non-associated flow rule $\psi'<\varphi'$). In this thesis, numerical analyses based on the associated and the non-associated flow rule are compared, by means of the constituted slip surface of the slope, the calculated factor of safety and the generated stresses along the slip surface. Whereas the associated plasticity generates a longer slip surface with a higher FoS. Furthermore, the soil nail influence on the effective stresses along the slip surface was investigated and revealed to be significant. Additionally, a comparison with the Limit Eqilibrium Analysis (LEA) using the software *Slide* was performed.

Finally, a case study of a soil nail wall was conducted by varying the soil nail stiffness in PLAXIS 3D. Besides the FoS calculation, the main focus of the 3D research was the soil nail deformation and the internal forces of the soil nails. The stiffer soil nails results displayed higher FoS and lower deformations.

Inhalt

List of figures

List of tables

List of symbols and abbreviations

Small letters

c'	[kN/m²]	Effective cohesion
d	[m]	Diameter
f	[-]	Plastic yield
l	[m]	Slice base length
p'	[kN/m²]	Effective hydrostatic stress
q	[kN/m²]	Deviatoric stress
c_u	[kN/m²]	Undrained shear strength
u	[m]	Displacement
x, y, z	[m]	Cartesian coordinates

Capital letters

A	[m²]	Area
E	[kN/m²]	Elasticity Modulus
E_{50}	[kN/m²]	Secant Stiffness Modulus
E_{oed}	[kN/m²]	Tangent Stiffness Modulus
E_{ur}	[kN/m²]	Unloading Reloading Modulus
G	[kN/m³]	Soil self-weight
I	[m^4]	Moment of Inertia
K_0	[-]	Earth pressure coefficient “at rest”
M_{sf}	[-]	Factor of safety (in PLAXIS 2D and PLAXIS 3D)
N'	[kN/m²]	Effective base normal force acting along the failure mechanism (LEA)
N_p	[kN/m]	Maximum axial tension force (in-plane)
R	[m]	Radius of circular failure sip surface about origin 0
R_{inter}	[-]	Interface strength
S	[kN/m²]	Shear force acting along the failure mechanism
Y_0	[kN/m²]	Stress at yield
$L_{spacing}$	[m]	Out-of-plane spacing of the soil nails

Small Greek letters

α	[°]	Slip surface inclination (LEA)
β	[°]	Inclination of the slip surface
γ	[kN/m³]	Soil weight
σ_1'	[kN/m²]	Major effective principal stress
σ_3'	[kN/m²]	Minor effective principal stress
σ_{xx}'	[kN/m²]	Cartesian effective stress in x-direction
σ_{yy}'	[kN/m²]	Cartesian effective stress in y-direction
σ_{zz}'	[kN/m²]	Cartesian effective stress in z-direction
σ_n'	[kN/m²]	Effective normal stresses
ν	[-]	Poisson´s ratio
ε	[m]	Strains
ε_e	[m]	Elastic strains
ε_p	[m]	Plastic strains
φ'	[°]	Effective friction angle
ψ'	[°]	Effective dilatancy angle
τ_{rel}	[-]	Relative shear stress
τ_{mob}	[kN/m²]	Mobilized shear stress
τ_{max}	[kN/m²]	Shear stress at failure
$\Delta\gamma_s$	[m]	Deviatoric incremental strain

Capital Greek letters

K	[1/m]	Bending

Abbreviations

EB	Embedded beam
EBR	Embedded beam row
FoS	Factor of Safety
FEM	Finite Element method
HS	Hardening Soil model
LE	Linear-Elastic model
MC	Mohr-Coulomb model
LEA	Limit Equilibrium Analysis
SRFEA	Strength Reduction Finite Element Analysis

1 Introduction

1.1 Slope stability

In practical engineering, factors of safety for slope stability analyses are still mostly determined employing the limit equilibrium approach. However, the limit equilibrium method involves several assumptions regarding the equilibrium of moments and forces, as well as the failure surface. Furthermore, all the programs used for limit equilibrium analyses need to perform a global search in order to identify the failure mechanism with the lowest factor of safety (Schweiger, 2014). Recently, displacement finite element method is increasingly being used for determination of slope stability. Other than the limit equilibrium approach, there is no need to define the failure mechanism in advance, since it is automatically determined in the zones where the shear stress exceeds the failure criterion (strength reduction method). Nevertheless, concerns exist about this method when dealing with non-associated plasticity. The main objective of this thesis is the evaluation of the influence of the flow rule on the failure mechanism of the slope.

A slope model is implemented in PLAXIS 2D considering both associated and non-associated plasticity. Slope stability in PLAXIS is calculated by means of φ'/c' reduction. In order to simulate the same failure mechanisms for associated (ψ'=φ') and non-associated (ψ'<φ') plasticity, a thin layer modelled with MC is defined on the failure line obtained from the calculation of a homogeneous slope modelled with MC and associated flow rule. The other part of the slope is modelled as linear elastic material. Consequently, the failure mechanism is forced to go through the layer modelled with MC. The results for associated and non-associated plasticity are evaluated in terms of factors of safety, normal forces, principal stress directions and relative shear stresses along the slip surface. PLAXIS results regarding the factors of safety are subsequently compared with results obtained from software *Slide*, which is based on the limit equilibrium method.

Additionally, slopes supported by a soil nail horizon as well as three soil nail horizons are modelled using the same procedure as for the unsupported slope, to get the same failure mechanism for associated and non-associated plasticity. The soil nails are modelled by means of geogrid. The factors of safety, normal forces along the slip surface, relative shear stresses and axial forces in the nails are investigated for both associated and non-associated flow rule. A comparison with *Slide* related to the factors of safety is also performed.

Finally, a case study of an excavation pit is presented and discussed. The calculation is performed using PLAXIS 3D software. The main focus is on the deformation behaviour of soil nails. Therefore, the Hardening Soil model was selected to describe the soil behaviour, since it considers a stress dependent

stiffness. The results for the factor of safety, soil nail deformation and axial forces in soil nails are evaluated for non-associated plasticity.

2 Theoretical background

2.1 Limit equilibrium analysis

2.1.1 Methods of slices

A limit equilibrium of a soil body is reached when the mobilised shear stresses τ_{mob} reach the shear strength of the soil. The shear strength of the soil is defined according to Eq. (1) based on the Mohr-Coulomb failure criterion.

$$\tau_f = c' + tan(\varphi') \tag{1}$$

τ_f Shear strength at failure (maximal shear strength)

(Oberhollenzer, 2017) shows three approaches to determine the factor of safety. The first option (Eq.(2)), defines the FoS as the relation between the shear stress at failure τ_f and the mobilized shear stress τ_{mob}. The FoS can also be defined as the ratio between the resisting forces to driving forces (Eq. (3)). Finally, the third definition (Eq. (4)) calculates the FoS as the ratio of resisting moments to driving moments.

$$FoS = \frac{\tau_f}{\tau_{mob}} \tag{2}$$

$$FoS = \frac{Sum\ of\ resisting\ forces}{Sum\ of\ driving\ forces} = \frac{S}{G \times sin(\alpha_{Slice})} \tag{3}$$

$$FoS = \frac{Sum\ of\ resisting\ moments}{Sum\ of\ driving\ moments} = \frac{R \times \int_0^L Sdl}{G \times x} \tag{4}$$

The calculation of the FoS based on LEA has a number of disadvantages. A circular or a polygonal failure slip surface has to be determined in advance. Additionally, kinematic admissibility of the failure mechanism is not ensured. Furthermore, the distribution of interslice forces is assumed differently in various methods. Finally, a global search is needed to identify the failure mechanism with the lowest FoS (Schweiger, 2014).

As stated, the FoS can be determined based on several approaches. All LEA methods got developed based on the Ordinary Method of Slices by Fellenius (1936). They assume a circular failure mechanism (Figure 1). The forces acting on each slice are predetermined. Afterwards, the FoS is calculated through the equilibrium of moments.

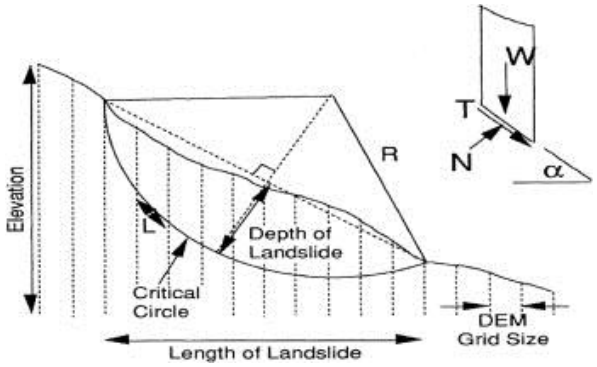

Figure 1 Illustration of the Fellenious method of slices (ResearchGate, 2014)

$$FoS = \frac{\sum\left(c' \times l + N' \times tan(\varphi')\right)}{\sum G \times sin(\alpha_{Slice})} \tag{5}$$

N' effective base normal force acting on shear force

G self-weight of the slice

u pore water pressure

l slice base length

α_{Slice} inclination in the middle of the slice

The other more advanced LEA methods (based on the one by Fellenius) were thoroughly described by Oberhollenzer (2017) and will therefore not be further discussed in this sections.

2.2 Soil nail

Soil nails are steel bars that are installed into the ground with a machine called Soil nail launcher, to stabilize slopes, landslides, construction pit walls and different kinds of excavations.

In practice, soil nails are inserted into the ground in a raster, and act as a group that forms sort of monolithic supporting body. As a result of arching, of the soil between the soil nail raster, the soil volume shores up on the sufficiently tight soil nail raster (Figure 2). Soil nails are a passive support system. This means that a small deformation of the soil body is needed to mobilize the reinforcement forces of the soil nails. Furthermore, a shotcrete support is needed. The soil nails need to be long enough to transfer the forces behind the slip surface. Usually, soil nails have a length of 50% to 70% of the slope height (Lehner, 2016).

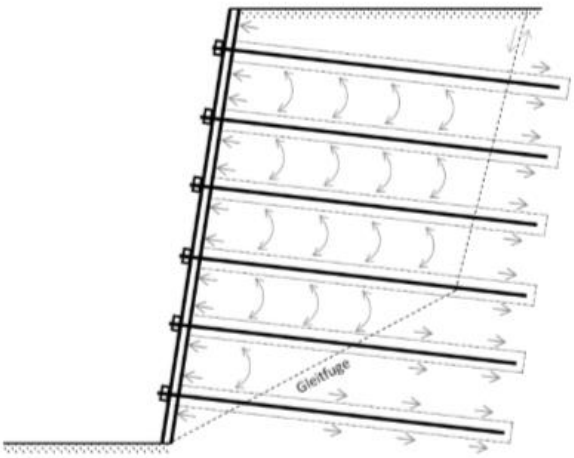

Figure 2 Soil arching between the soil nails (Lehner, 2016)

The combination of soil nails with shotcrete (or also reinforced shotcrete) is called a soil nail wall, which is constructed using the so-called top down technique. Firstly, the ground has to be excavated. The excavation depth depends on the soil properties. Secondly, shotcrete has to be installed (with or without reinforcement). The necessary thickness of the shotcrete wall depends not only on to the soil properties, but also on the planned duration of the wall. Temporary soil nail wall has a thickness of about 8 to 15 cm. For permanent soil nail walls a thickness up to 25 cm is constructed (Lehner, 2016). The next step is to install the soil nails into the ground, by ramming or drilling. The difference between various soil nail installation concepts is well explained in the Master thesis of Lehner (2016).

According to Byrne et al. (1998), three types of soil nail failure exist. The first is an internal failure, if the failure slip surface is cutting through the soil nails.

Secondly, an external failure, if the failure slip surface is formed behind the soil nails, and thirdly, a mixed failure, when the failure slip surface cuts some of the nails. These three failure modes are shown in the pictures below (Figure 3).

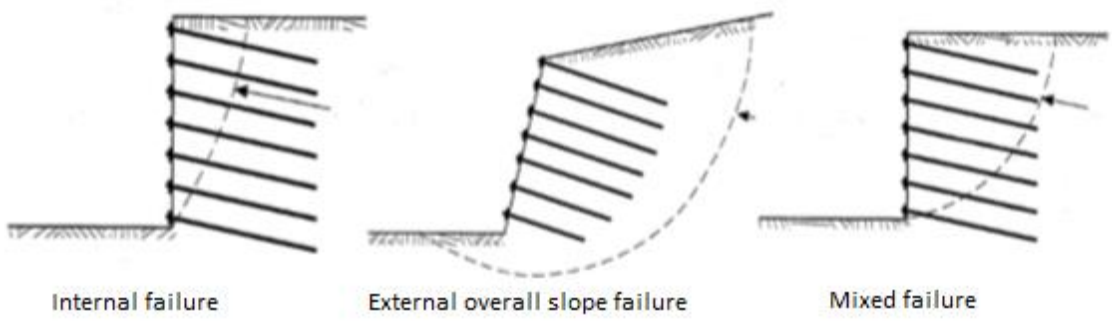

Figure 3 Three types of soil nail failure (Mosser, 2016)

2.2.1 Flow rule

When the failure stress state of a material is reached, the material cannot take any more stress increments, subsequently, plastic strains occur. In principle, the flow rule dictates how plastic strain evolves after failure (Oberhollenzer, 2017).

Two flow rules are distinguished: the associated and the non-associated flow rule. The associated flow rule assumes a dilatancy angle equal to the friction angle ($\psi'=\varphi'$), due to the fact that the plastic strains (ε_p) are oriented perpendicular to the yield function (Figure 4). On the other hand, the plastic strains of the non-associated flow rule act perpendicularly to the plastic potential Q and not to the yield friction (F in Figure 4). Consequently, a dilatancy angle smaller than the friction angle ($\psi'<\varphi'$) is assumed for the non-associated plasticity. Thereby the plastic volumetric strains are reduced, which is a more realistic representation of the soil behaviour (Oberhollenzer, 2017).

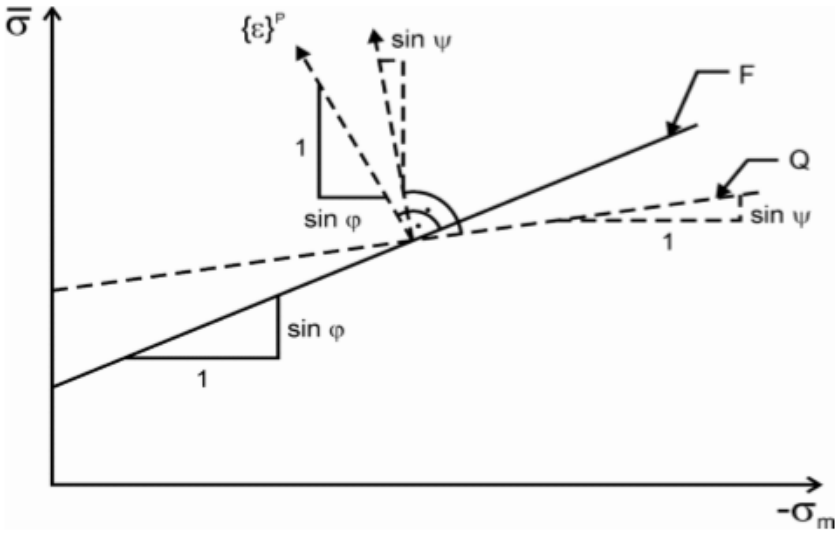

Figure 4 Illustration of the associated and non-associated flow rule (Schweiger, 2014)

2.2.2 Strength reduction finite element analysis

The soil shear strength is given by the friction angle φ' and the effective cohesion c'. With the φ'/c' reduction (Figure 5), both soil parameters are simultaneously decreased until no equilibrium is present. The friction angle φ' is successively reduced by means of tan(φ'). If the soil body submitted to the φ'/c' reduction also has a dilatancy, its dilatancy angle ψ' can be affected by the safety calculation. The friction angle is always higher than the dilatancy angle. With the stepwise reduction of the friction angle, the friction angle can at some point reach the same value as the dilatancy angle. Whereby, with further decrement of the friction angle the dilatancy is subsequently subjected to the same reduction as the friction angle (Brinkgreve, 2018).

The FoS in PLAXIS 2D is given as M_{sf}, whose formulation is described with the Eq. 7, from the PLAXIS 2D manual.

$$\sum M_{sf} = \frac{tan(\varphi \quad)}{tan(\varphi_{mobilized})} = \frac{c}{c_{mobilized}} = \frac{c_u}{c_{u,mobilized}} \tag{7}$$

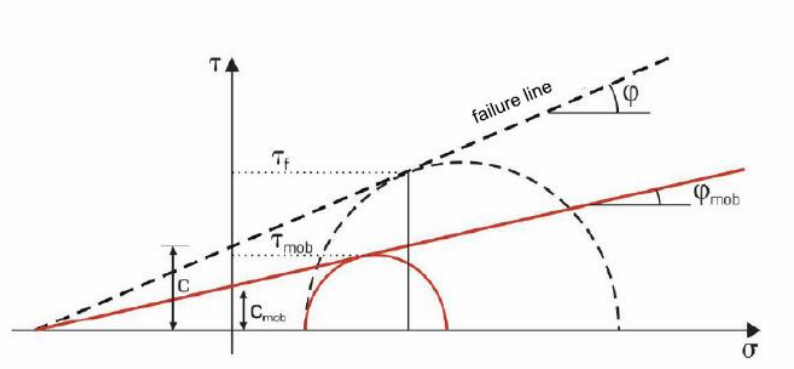

Figure 5 Illustration oft he φ/c reduction method (Havinga, 2016)

2.2.3 Soil nail simulation

The soil nails in this thesis were modelled using embedded beam rows and geogrids in the 2D simulations and with embedded beams in the 3D simulations. In the limit equilibrium analysis softwere *Slide*, the soil nails were simulated with the "Soil nail" support type.

2.2.3.1 Geogrid (PLAXIS 2D)

Geogrids in PLAXIS 2D are continuous elements with an axial stiffness (EA), but no bending stiffness (EI). Therefore, their input parameters are the axial stiffness EA and the limited tension force $N_{p,1}$. With the input of $N_{p,1}$, the failure by tension of the geogrid structure can be simulated. For a more detailed description of the geogrid behaviour, it is advised to consult the PLAXIS 2D manual (Brinkgreve, 2018).

To simulate the soil-structure interaction, so called interfaces must be added to geogrids. The interfaces have also to be added on plate elements.

2.2.3.2 Embedded beams (PLAXIS 3D)

In PLAXIS 3D the embedded beam (EB) consists of beam elements with implemented interface elements for the soil-structure interaction. The EB does not have a volume, however, by using EB, the reinforcement modelled by the EB is simulated so that plasticity of the soil around the EB is not possible. This elastic soil region around the EB is dependent on the chosen pile diameter. Embedded beams are described more in detail in the PLAXIS 3D manual (Brinkgreve, 2018).

3 Introduction to numerical studies

The undertaken slope stability studies of this thesis can be separated into the 2D analysis and the 3D with different soil and soil nail material sets.

The first 2D studies were conducted on an unsupported slope model with the software PLAXIS 2D. The soil was modelled according to a Mohr-Coulomb material. The main focus of the analyses was to determine the difference between the factor of safety, the slip surface and the stresses acting for the associated ($\psi'=\varphi'$) and the non-associated ($\psi'<\varphi'$) plasticity. The stresses along that slip surface were evaluated (the methodology behind that evaluation is described in the Methodology (4.1) chapter of this thesis). The results of the two flow rules were compared.

Afterwards, the same research and procedure was carried out for a homogeneous slope with a reinforced soil nail. The reinforcement was composed of a single soil nail and a shotcrete wall. The soil nail was modelled with geogrid. Therefore, the geogrid-reinforced slopes of the two flow rules were evaluated and compared. The shotcrete wall was modelled with a plate element. Same analysis was conducted with three soil nail horizons.

The FoS and the slip surface location were compared. The stresses along the two slip surfaces of the two identical models with different flow rules could not be compared, since the generated slip surfaces were not the same. In order to compare the two flow rules by means of the computed stresses along the failure mechanism, they have to be situated on the same (or almost the same) slip surface. To achieve this, firstly, the safety calculation (φ'/c' reduction) of the unsupported slope model with the associated flow rule ($\psi'=\varphi'$) was conducted. Afterwards, the generated failure mechanism (depicted with the deviatoric incremental strains) of the associated calculation was implemented into a new model with the same geometry, as an individual soil layer. The individual soil layer was modelled as a very thin (<20 cm) Mohr-Coulomb material. The surrounding soil of the model with the implemented associated failure mechanism was modelled as linear-elastic. This model (which will be referred to as MC-LE model) is used for the flow rule comparison. The safety calculation with the MC-LE model was performed for both flow rules and the resulting stresses along the two identical failure slip surfaces were compared. The same procedure follows for the same model with one soil nail and with a three soil nail reinforcement. The safety factors of all numerical analyses were compared to the results of the analytical limit equilibrium analysis (LEA) using *Slide*.

At the end, 3D analyses of the soil nails were conducted on a practical example of a soil nail wall. The focus of this investigation were the soil nail deformation, the forces acting in the soil nails and the factor of safety. The displacements and

internal forces of the soil nail were evaluated for a chosen soil nail column with a given cross section.

4 Numerical studies on a homogeneous slope

4.1 Methodology

A homogenous slope model without reinforcement and with reinforcements (soil nail and a shotcrete wall) was analysed for both flow rules. The soil nails were modelled using geogrid with interfaces. The shotcrete wall was created as a plate element with interface.

Since the goal of this thesis is to compare the two flow rules, this investigation was conducted with both, the associated ($\psi'=\varphi'$) and the non-associated flow rule ($\psi'=0$).

A Mohr-Coulomb material model was used to model the homogeneous soil body. Later on, in this thesis, the homogeneous slope will be compared to the Linear-elastic – Mohr-Coulomb model (LE-MC model) with the implemented associated slip surface (description follows).

The failure slip surface of a slope model in PLAXIS 2D can be received with the so-called "Safety calculation". After the completed safety calculation (φ/c reduction), the slip surface can be presented by displaying the incremental deviatoric strains. An example of this slip surface illustration can be seen in the Figure 6.

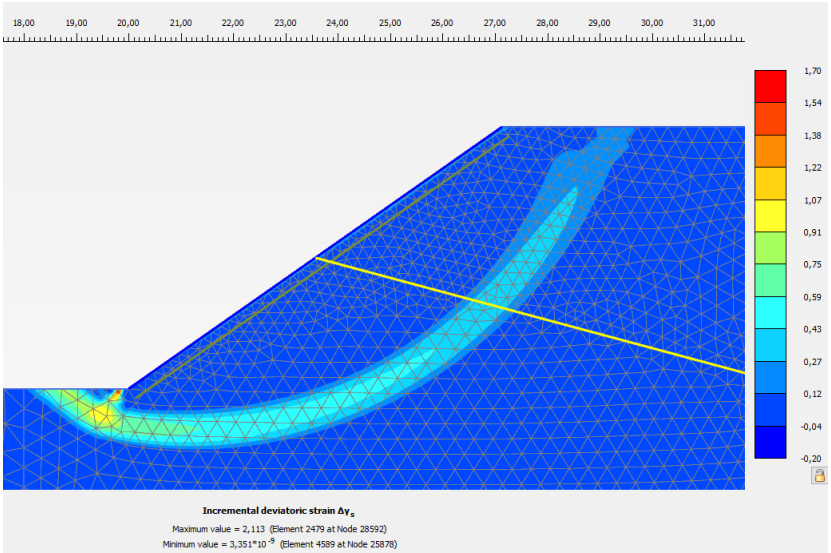

Figure 6 Illustration of the incremental deviatoric strains after the safety calculation

The slip surface location (coordinates) and the stresses along the slip surface can be displayed over the stress points situated on the incremental deviatoric strain surface.

For every chosen stress point along the slip surface, the following stress indicators are discussed, for both flow rules:

- Principal effective stresses (σ_1', σ_2', σ_3')
- Effective Cartesian stresses (σ_{xx}', σ_{yy}', σ_{zz}')
- Effective hydrostatic (p') and deviatoric (q) stresses
- Principal stress directions
- Relative shear stress (τ_{rel}) in combination with the corresponding axial soil nail force

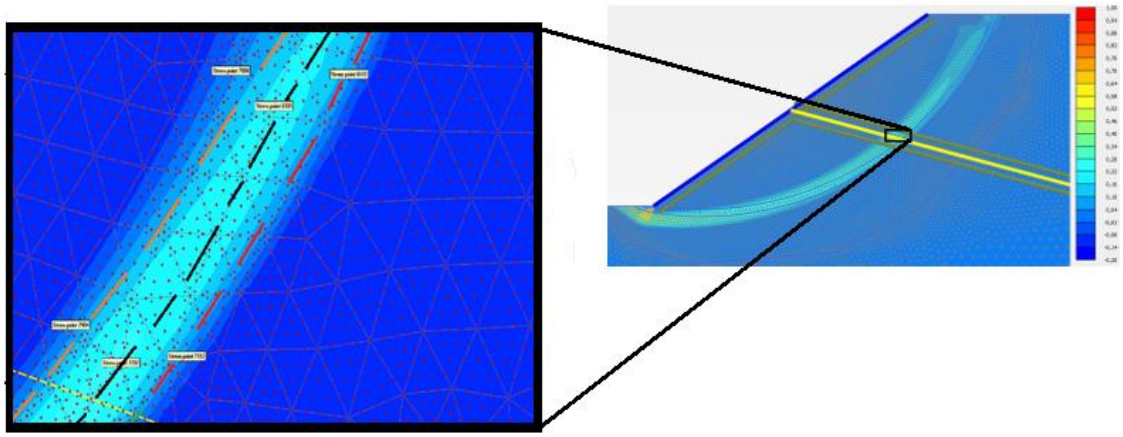

Figure 7 Handpicking of stress points along the three parallel stress point polygons (zoomed in)

To get the desired stress indicators along the slip surface (through the middle of the "light blue" incremental strain surface (black dashed line in Figure 7)), the individual stress points along the slip surface were selected. Afterwards, the computed stresses of the selected stress points were evaluated. This procedure was also performed for two parallel stress point polygonals on the upper and lower border of the slip surface (orange and red dashed lines in Figure 7). As a result, the influence of the stress point handpicking can be assessed. It should be noted that the picked stress points are very close to the actual slip surface, but not on the slip surface.

The stress development along the slip surface with the safety calculation progression was analysed. To analyse the stress-trend the different stress indicators

were evaluated for different safety calculation steps. By plotting the Msf over the total displacements |u| a similar curvature to Figure 8 was obtained. The trend relevant stresses are the stresses generated in the calculation step before the φ'/c' reduction calculation (Nil step or Support installation) and the last step of the safety calculation. Furthermore, in order to display a stress trend more safety calculation steps, between the initial step and the final step were necessary. Therefore, the steps shown in the Figure 8 were chosen for the stress trend evaluation.

The trend-relative calculation steps were selected depending on the height between the initial step (0%-step) and the first step on the $M_{sf}/|u|$ plateau line (100%*-step). The calculation steps at the 33% of the height, as well as the 50%, 67%, 100%* were utilized for the stress trend evaluation. Furthermore, the stresses from the last calculation step (100%final-step) and the 100% were evaluated for the stress trend study. With 100% always being the point at which the end-FoS (FoS at the last,100%final point) first appeared before the curvature jump. Due to the fact that the soil experiences large deformations at the end step of the φ'/c' reduction, the 100% and 100%* were also evaluated. However, if there is no jump in the $M_{sf}/|u|$ curvature, then the 100% point and the 100%* are the same point which will be referred to as 100% stress point. An additional M_{sf} %-step was used, only for the investigation of the relative shear stress τ_{rel}, which is the 20%-step (at the 20% of the 0%-100%* height).

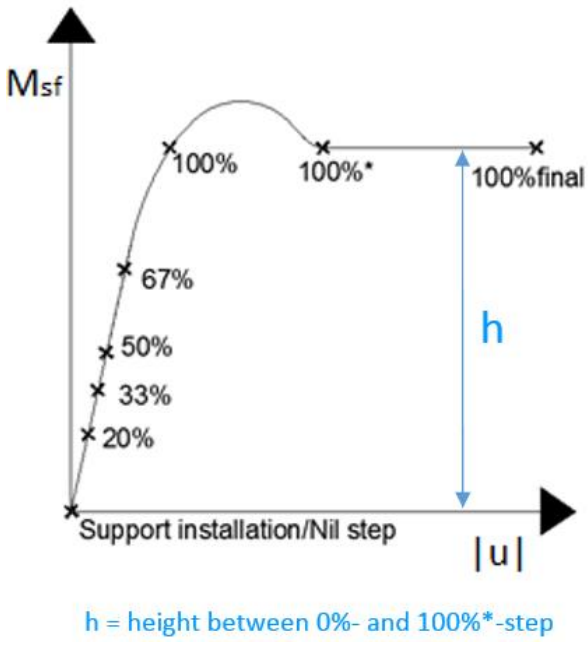

Figure 8 Illustration of the FoS over the total displacement diagram

Only the effective normal stresses will be discussed in this thesis, the other evaluated stress indicators are depicted in the Appendix C, D, E, F, G and H. The effective normal stresses σ_n' of the stress points were calculated over the σ_{xx}', σ_{yy}' and the inclination of the slip surface (α) at the corresponding stress point of the slip surface.

Afterwards the same procedure and assessment were performed for a Linear-elastic - Mohr-Coulomb model.

As it was described in the chapter 3., a MC-LE model was created to allow the comparison of the two distinct flow rules. The MC-LE model was modelled in a way that the failure slip surface of the MC model (Figure 9) calculated with the associated flow rule ($\psi'=\varphi'$) was "traced" in the MC-LE model as a second soil layer (brown soil layer in Figure 9 (right)), with the same MC properties. The remaining soil body was modelled with the same properties, but as a LE soil body (blue soil layer in Figure 9 (right)). The MC soil layer was modelled as thin as possible (<20 cm). Subsequently the MC-LE model was computed with the associated ($\psi'=\varphi'$) and the non-associated flow rule($\psi'<\varphi'$). The aim was to compare associated and non-associated analyses with the same failure mechanism. Both slip surfaces went through the traced MC soil layer of the MC-LE model, which is evident in Figure 23, Figure 36 and Figure 46 (Results chapter).

Furthermore, the FoS of the MC-LE model with the associated flow rule had to be equal or almost equal to the FoS of the MC model calculated with the associated flow rule.

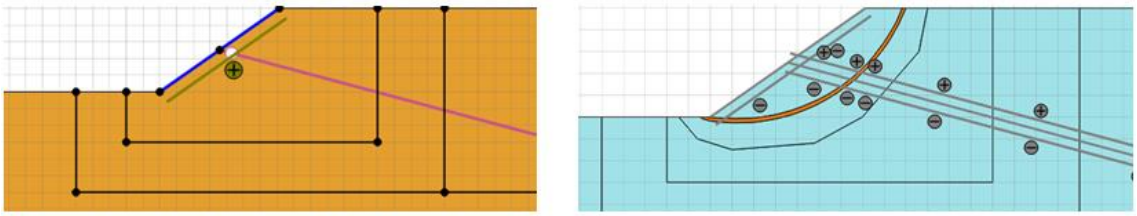

Figure 9 MC model (left) and the MC-LE model (right)

4.2 Model

4.2.1 Model dimensions and parameters

The chosen dimensions of the model can be observed in Figure 10. The homogeneous slope is disposed 35° to the horizontal and shows a height equal to five meters. In order for the boundaries of the model not to influence the result, the

depth of the soil body is chosen to be 15 m (starting from the slope toe) and the model width is 20 m to the left and 25 m to the right of the slope. All model dimensions are shown in Figure 10.

The soil body was modelled as a Mohr-Coulomb material. The chosen parameters for the soil body are presented in the **Fehler! Verweisquelle konnte nicht gefunden werden.**. The difference between both parameter sets is the dilatancy angle (non-associated $\psi'=0$; associated $\psi'=\varphi'$).

The soil nail has a length of 20 m with an inclination of 20° to the horizontal. It is placed in the middle point of the shotcrete wall (for the one soil nail reinforced model). For the 3 soil nail reinforced slope, the soil nails have the same length and inclination as the soil nail used in the one soil nail reinforced slope study. However, the axial tension force is reduced (Table 4) to get an internal failure slip surface for the case with three soil nails.

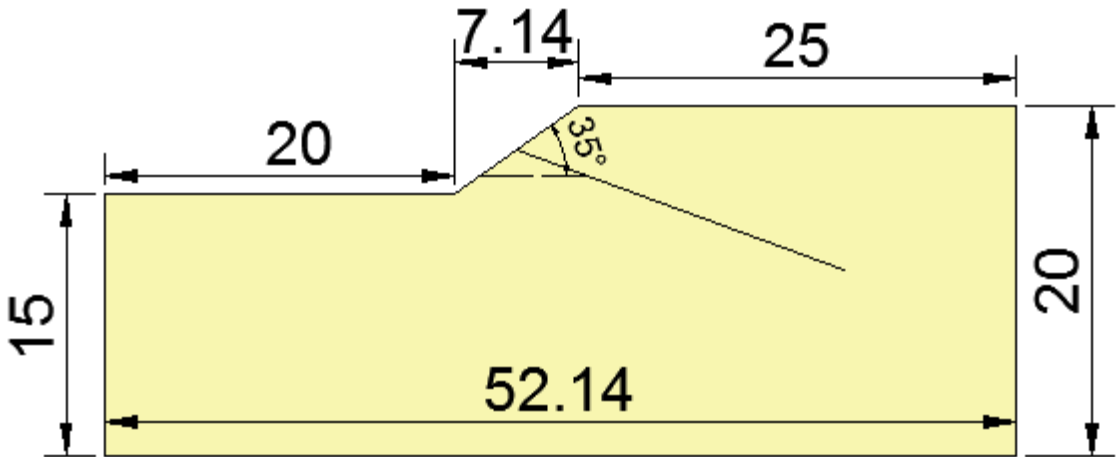

Figure 10 Homogeneous slope model dimensions

Since geogrid is a continuous “plate”, the EA and the N_{p1} are divided by a spacing of 1.5 m between the soil nails, which has to be taken into account (Table 2 and Table 4).

Table 1 Geogrid parameters for the one soil nail reinforced slop models

Soil parameters		
Material model:	Mohr-Coulomb	
Drainage type:	Drained	
	CASE 1	CASE 2

	Non-associated	Associated
E [kN/m²]	30.000	30.000
ν [-]	0.3	0.3
γ [kN/m³]	20	20
c' [kN/m²]	5	5
φ' [°]	30	30
ψ' [°]	0	30

Table 2 Geogrid parameters for the three soil nail reinforced slop models

Soil nail parameters (1-soil nail models)	
Soil nail:	Geogrid
Material type:	Elastoplastic
EA_1 [kN/m]:	5716.0
N_{p1} [kN/m]:	66.67

Table 3 Shotcrete parameters

Shotcrete parameters	
Shotcrete:	Plate
Isotropic:	Yes
End bearing:	Yes
Material type:	Elastic
EA_1 [kN/m]	$4*10^6$
EI [kNm²/m]	$13.33*10^3$

ν [-]	0.25

Table 4 Geogrid parameters for the three soil nail reinforced slop models

Soil nail parameters (3-soil nail-models)	
Soil nail:	Geogrid
Material type:	Elastoplastic
EA_1 [kN/m]:	5716.0
N_{p1} [kN/m]:	10.00

The shotcrete has a thickness of 0.2 m and it is modelled as a plate element with an interface on the soil side of the slope that simulates the soil-shotcrete connection (Table 3).

4.2.2 Discretisation

The model is separated into 4 parts with different mesh coarseness factor. Depending on the distance to the slope of the different "mesh areas", the coarseness changes. The closer the area is to the slope, the finer it is discretised. The 4 different "mesh areas" are shown in Figure 11. The coarseness factor gets higher with the increasing distance from the slope. The 15 nodded elements were used for the 2D calculations. The total number of the computed finite elements for the MC model is 5,065 (Figure 12).

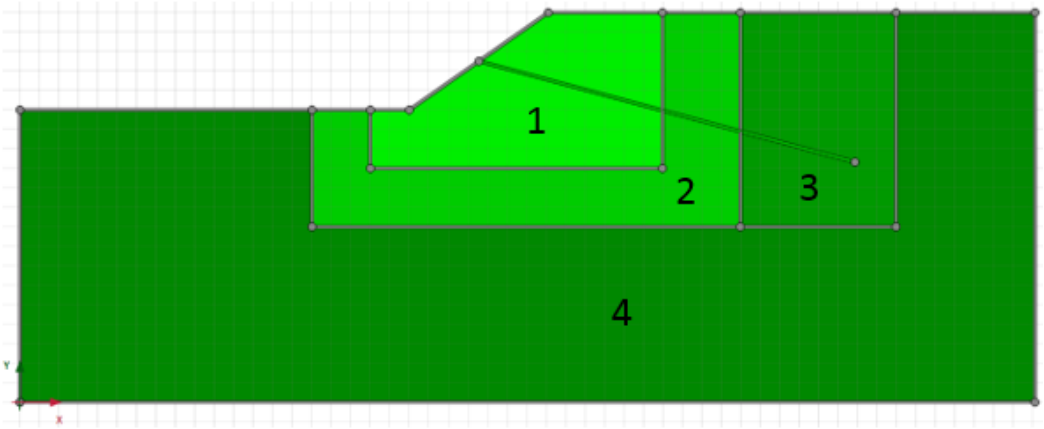

Figure 11 Four mesh areas of the MC model with one soil nail horizon

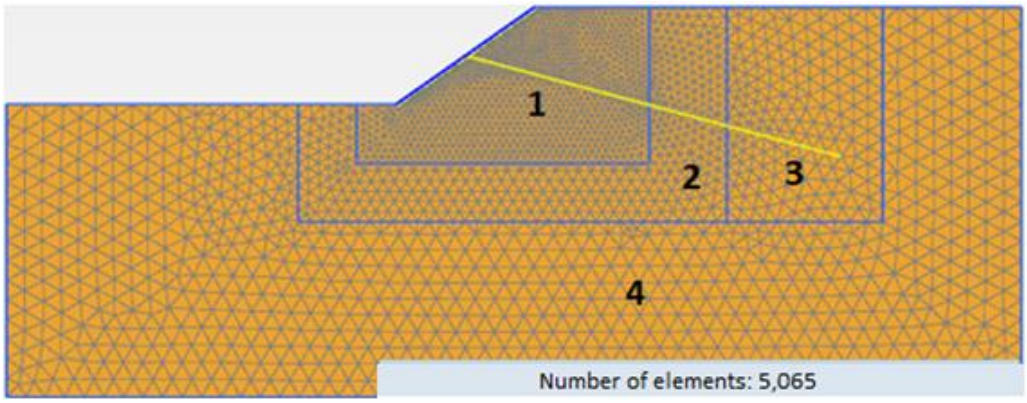

Figure 12 Four mesh areas of the MC model with one soil nail horizon

For the three-soil nail model, the discretization was done as for the one soil nail slope model.

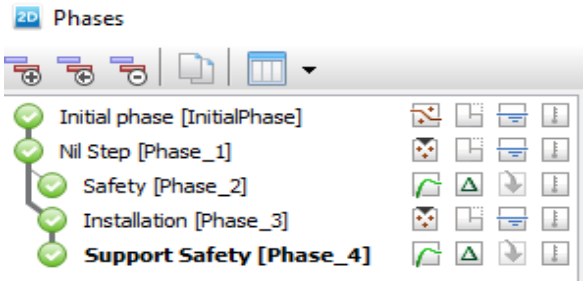

4.2.3 Calculation phases

Figure 13 Calculation phases for the MC and MC-LE model

The five calculation phases according to Figure 13 are used to determine the stability of the slope.

These phases were used for all calculated slope models (1 soil nail models and 3 soil nail models), for both flow rules.

The initial stresses were calculated by means of “Gravity loading”. Thereby the initial stresses are calculated from the volumetric weight of the soil. By using the gravity loading, the K_0 value firmly depends on the Poisson's ratio (Eq. 8). For this phase, the tolerated error margin is reduced from the standard value to 0.5% in order to get a higher calculation accuracy.

$$K_0 = \frac{\nu}{1-\nu} \tag{8}$$

The second phase is the so called plastic Nil step. This step is widely used to restore equilibrium in the model, so that the failure condition is kept. The option “Reset displacements to zero” is used in this step, so that the additional displacements, computed in the previous step are ignored.

Table 5 Used steps and chosen step features for the FoS calculation of the supported and unsupported slope, for both, the MC an the MC-LE model

PLAXIS 2D stages – Homogeneous Mohr-Coulomb slope					
Stages:	Initial phase	Nil step	Safety	Support installation	Support safety
Start from phase:	-	Initial phase	Nil step	Nil step	Support installation
Calculation type:	Gravity loading	Plastic	Safety	Plastic	Safety
Loading type:	Staged constructi-on	Staged constructi-on	Incremental multiplier	Staged constructi-on	Incremental multiplier
Max steps	50	1000	100	1000	Varies
Tolerated error:	0.005	0.01	0.01	0.01	0.01
Arc-length control type	On	On	On	On	On
Support:	Off	Off	Off	On	On

The third phase is the safety calculation (φ/c reduction) for the non-reinforced slope. In that step the factor of safety of the unsupported slope is calculated. For the case with reinforcement, however, there is a step before the safety calculation, the installation of the reinforcement, where the shotcrete-plate and the soil nail (geogrid) are activated. Afterwards, the safety calculation is conducted, where the factor of safety for the reinforced slope is calculated.

4.3 Results

4.3.1 Comparison of FoS and the failure mechanism

4.3.1.1 2D studies - unsupported slope model

- **Mohr-Coulomb model**

As mentioned before, the failure mechanisms with corresponding FoS were evaluated for the two flow rules, for the MC model.

The results presented in this section focus on the numerical analyses using geogrids.

A study of the EBR-d/$L_{spacing}$ dependency was also conducted. Different $L_{spacing}$ were examined for the chosen diameter of 32 mm in the FoS calculation. This study is available in the Appendix A.

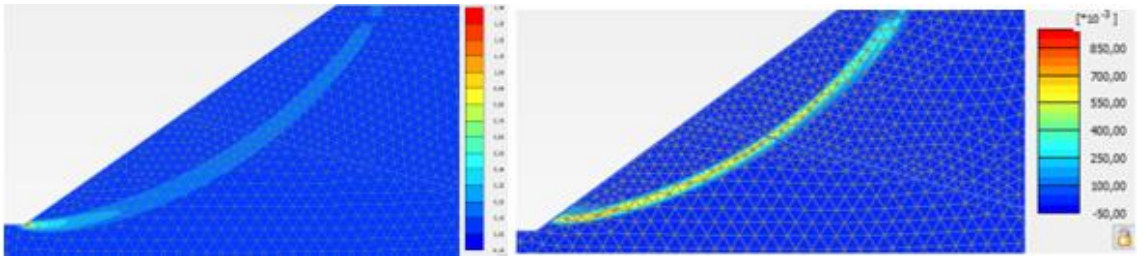

Figure 14 Incremental deviatoric strains with the associated (left) and the non-associated flow rule (right) for the unsupported MC slope model

The two slip surfaces computed with PLAXIS 2D for the unsupported MC model are shown in the Figure 13. The associated case (ψ'=φ') is on the left hand side and the non-associated (ψ'=0) is displayed on the right hand side. It can be seen that both failure mechanisms differ slightly.

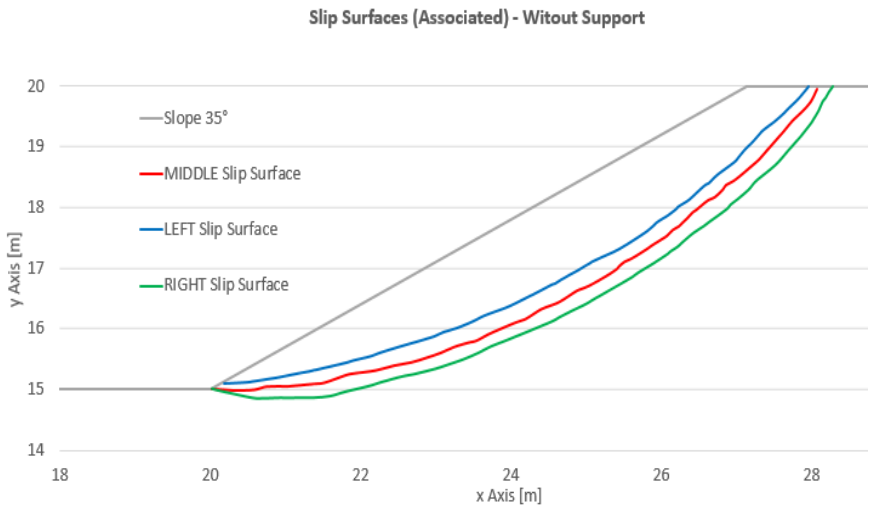

Figure 15 Illustration of the three "slip surfaces" of the unsupported associated MC model

In Figure 15 and Figure 16 the three parallel slip surfaces are presented. The red line is the assumed failure mechanism that goes through the middle of the deviatric strain surface. The blue line shows the upper border of the incremental deviatoric strain. The green polygon represents the lower border of the deviatoric strain area.

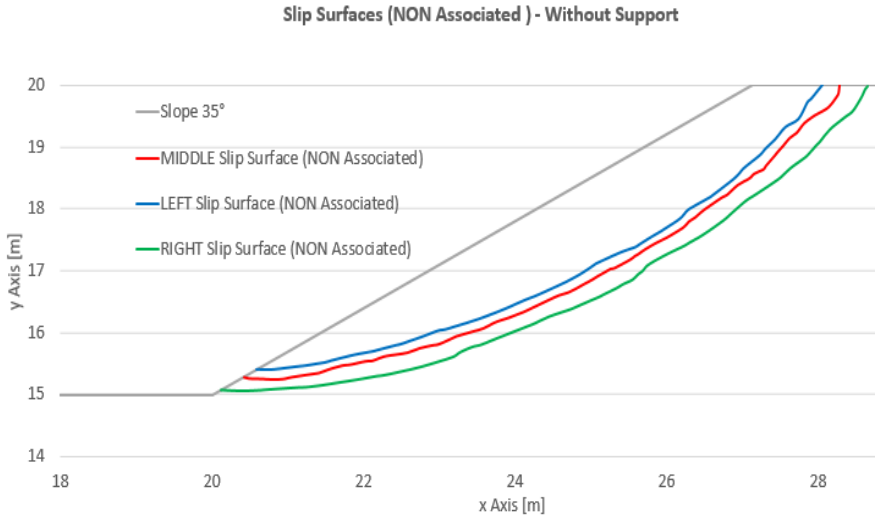

Figure 16 Illustration of the three "slip surfaces" of the unsupported non-associated MC model

Figure 18 shows that the failure mechanism for the non-associated flow rule (visualised with the solid lines; Figure 17) leads to a smaller sliding mass, in other words, a shorter slip surface, than the one with associated flow rule (visualised with the dotted lines). This behaviour is based on the different dilatancy angles. The slip surface for $\psi'=\varphi'$ is longer and the sliding mass bigger compared to $\psi'=0$.

Furthermore, the failure mechanisms discussed in this section are slightly influenced by the chosen stress points.

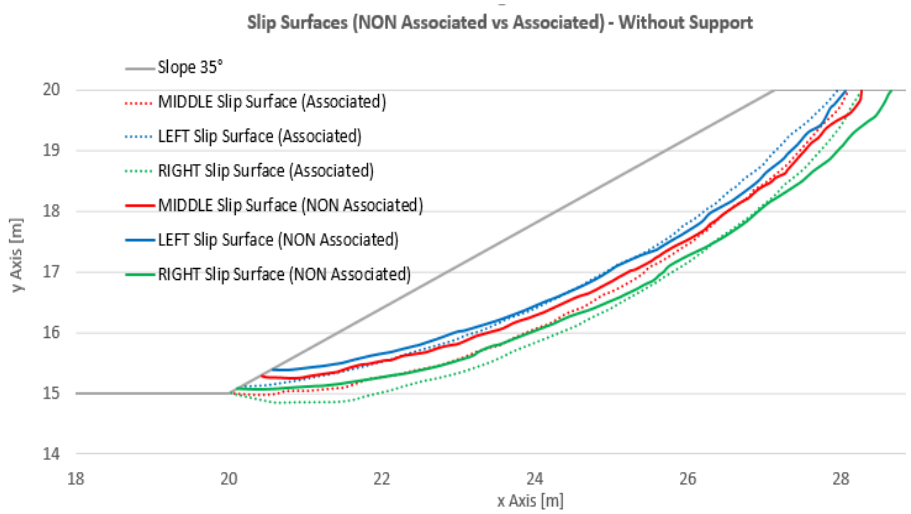

Figure 17 Comparison of the associated (full lines) and non-associated (dotted lines) flow rules by means of slip surfaces of the unsupported MC model

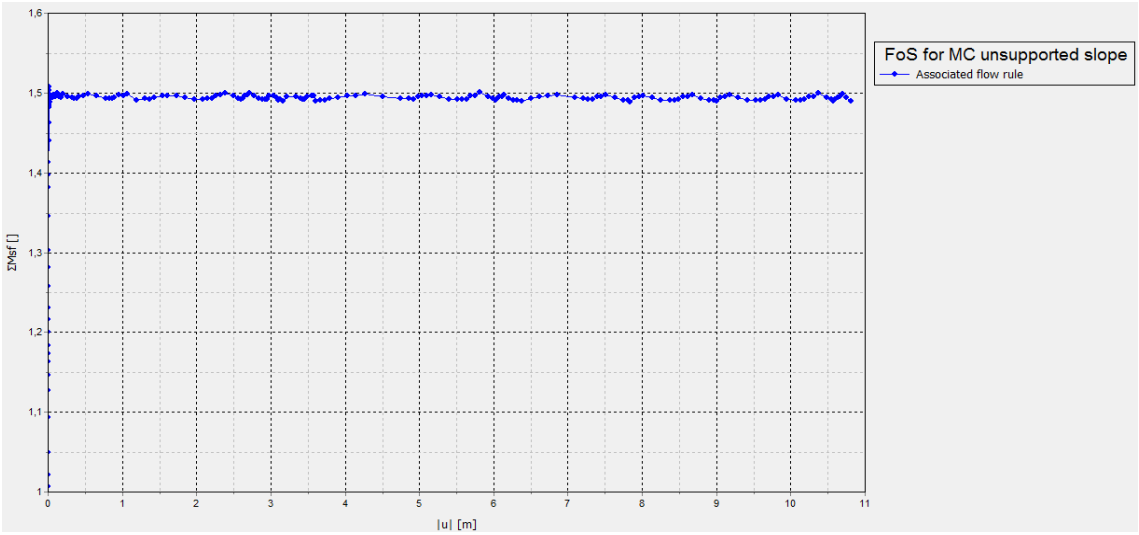

Figure 18 $M_{sf}/|u|$ diagram for the unsupported case calculated with the associated flow rule (MC model) – FoS=1.50

The factor of safety for the MC model with no support (associated flow rule) is 1.50 (Figure 18). The FoS of the non-associated calculation is 1.40 (Figure 20). The slip surfaces of the two distinct flow rules are depicted in Figure 19.

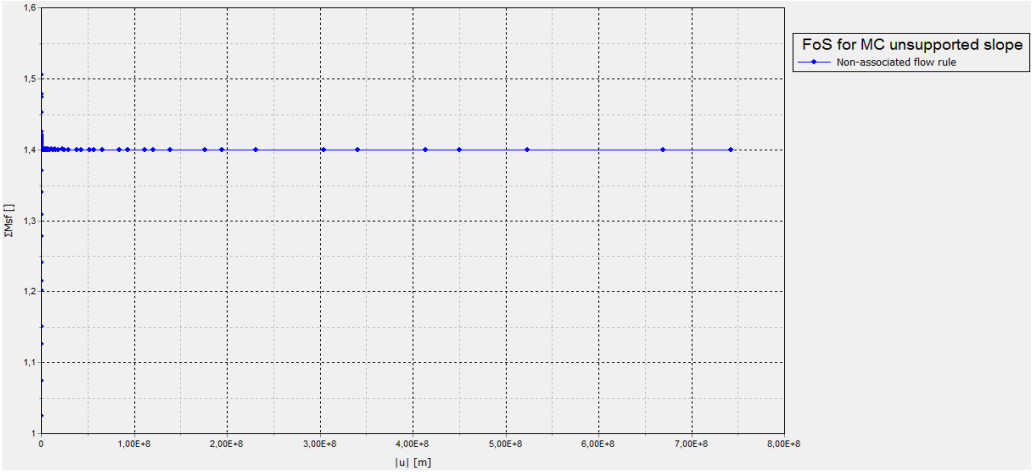

Figure 19 Msf/|u| diagram for the unsupported case calculated with the non-associated flow rule (MC model) – FoS=1.40

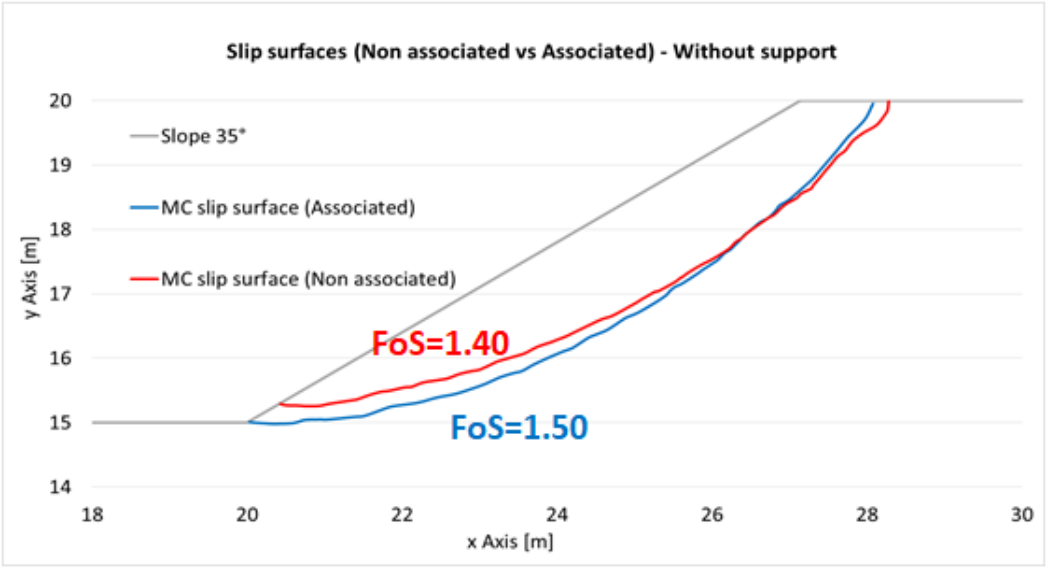

Figure 20 Slip surfaces generated for the unsupported slope with the associated and non-associated flow rule, with PLAXIS 2D (MC model)

- **Mohr-Coulomb – Linear-elastic model**

As stated before, the next step was to take the MC model discussed above and to change the soil material of the model to linear-elastic (LE) outside the failure mechanism (Figure 9). Afterwards, a MC soil layer with the maximal thickness of 20 cm was created along the area where the slip surface of the MC model was situated. In the following pages of this thesis, the models that were created in that manner will be referred to as MC-LE model.

An important point that had to be taken into account in the creation of the MC-LE model was that the FoS of the MC-LE model should be the same or almost the same as the one in the MC model. Due to the fact that the two different slope models have the same failure mechanism. The Msf/|u| diagram in Figure 22 shows

that the FoS for the MC-LE model calculated with the associated flow rule is the same as the one calculated with the associated MC model.

The middle slip surface was implemented into the MC-LE PLAXIS 2D model as a 20 cm thick MC layer in the LE soil model. The resulting slip surfaces of the unsupported MC-LE model, calculated with the two flow rules and their corresponding FoS are depicted in the Figure 23.

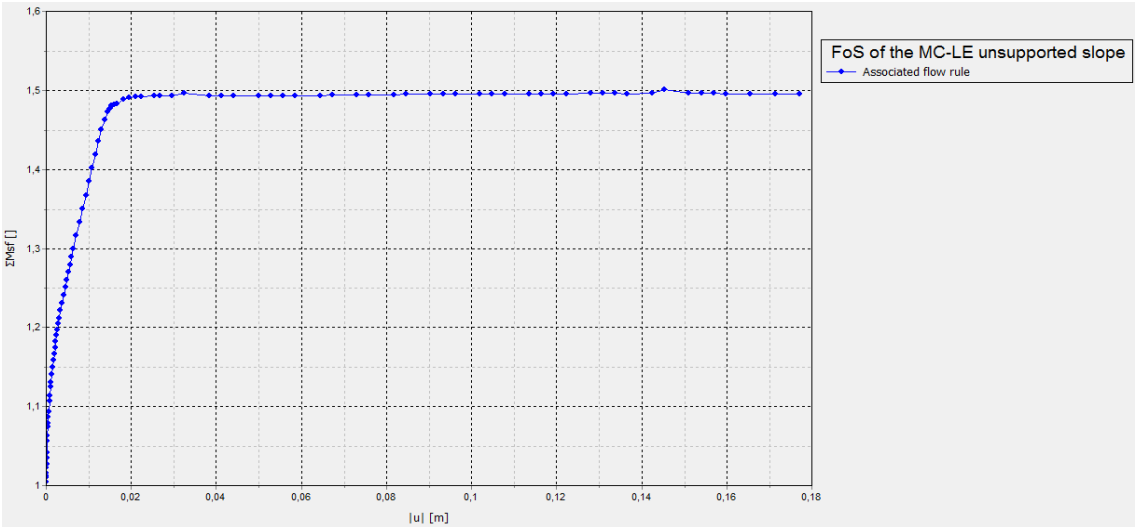

Figure 21 M_{sf}/|u| diagram for the unsupported case calculated with the associated flow rule (MC-LE model) – FoS=1.50

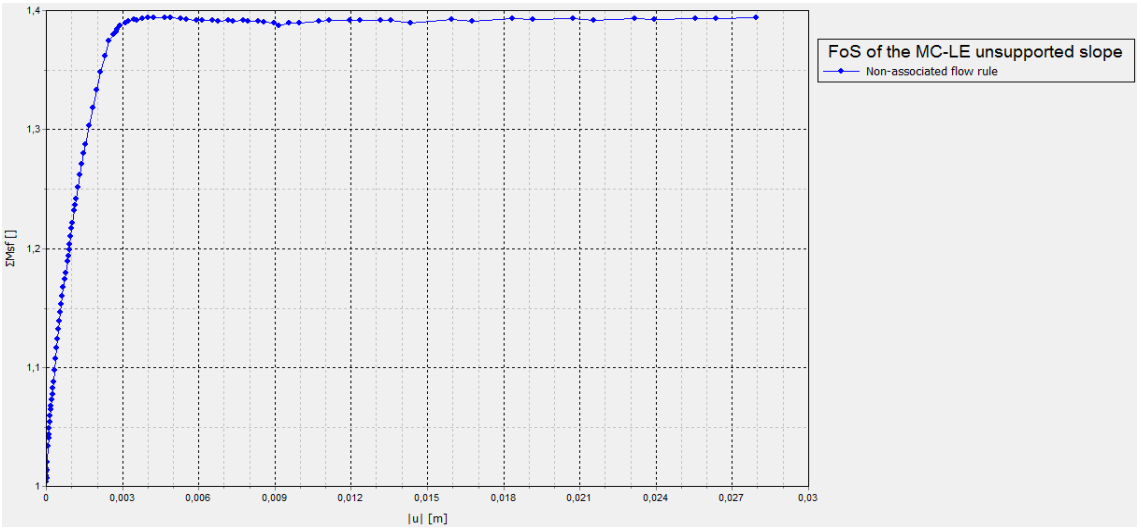

Figure 22 M_{sf}/|u| diagram for the unsupported case calculated with the non-associated flow rule (MC-LE model) – FoS=1.39

The non-associated calculation of the MC-LE model gives a FoS of about 1.39 (Figure 21), which is almost the same as in the non-associated FoS calculation of the MC model.

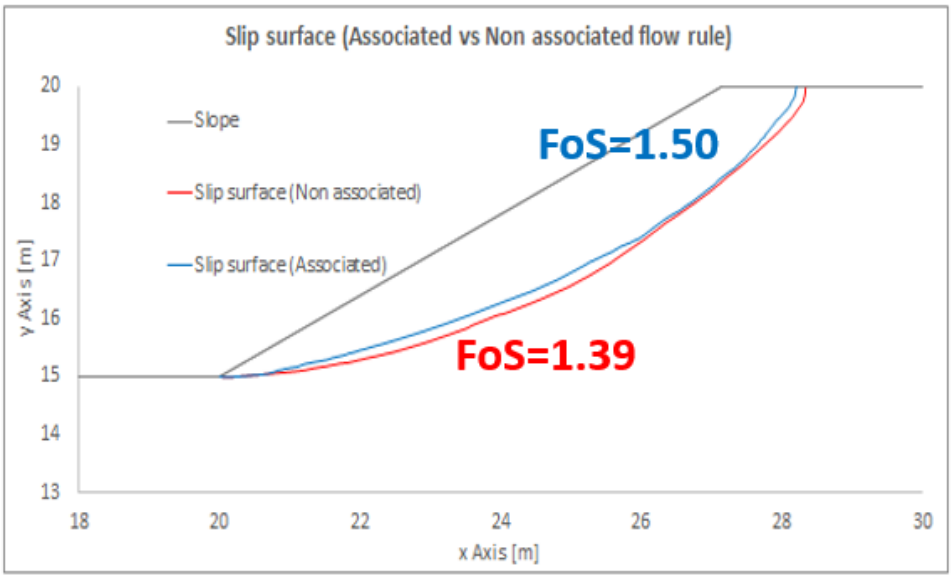

Figure 23 Slip surfaces generated for the unsupported slope with the associated and non-associated flow rule, with PLAXIS 2D (MC-LE model)

Figure 23 shows the evaluated stress points over the slip surface of the MC-LE models calculated with the two flow rules (blue and red lines). Figure 23 and Figure 24 show that the associated flow rule generates a slip surface that is moving along the upper border of the drawn MC soil layer (traced slip surface of the corresponding MC model), whereas, the non-associated flow rule generates a slip surface along the lower MC soil layer border.

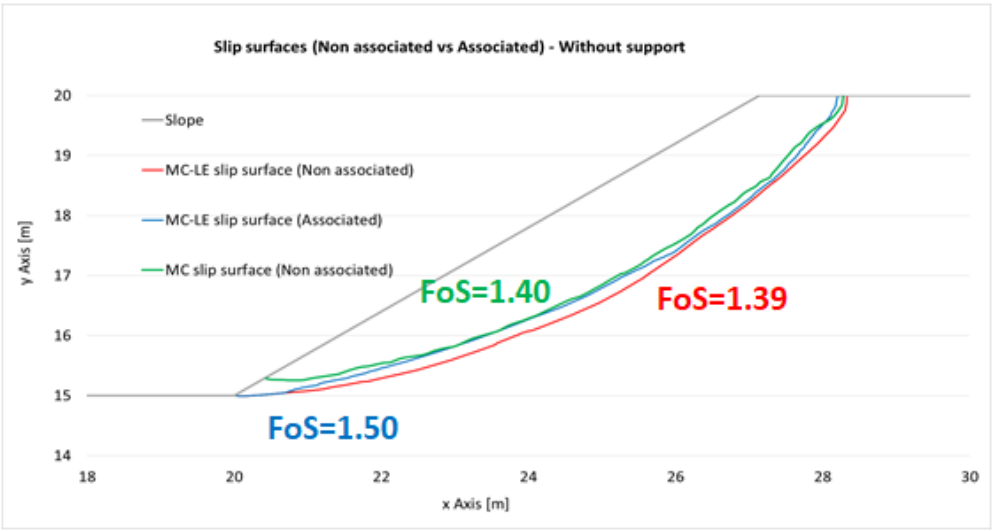

Figure 24 Slip surfaces generated for the unsupported slope with the two flow rules, in PLAXIS 2D (MC-LE model + non-associated MC model)

- **Comparison with limit equilibrium analysis**

Morgenstern-Price was used to determine the factor of safety via *Slide*.

The reason for the different FoS between the slope model calculated with the limit equilibrium analysis and the same model calculated with the finite element analysis is that the two computed slip surfaces are not the same. This statement is backed up by Figure 25.

The details regarding parameters and the modelling of the slope in the LEA programme *Slide* can be found in Appendix B.

Figure 25 shows that *Slide* calculates a slip surface that is situated deeper in the ground than the two slip surfaces calculated with PLAXIS 2D (with the associated and non-associated flow rule).

For that reason, one more *Slide* vs. PLAXIS 2D study has been undertaken. The slip surface generated by *Slide* was implemented in PLAXIS 2D as Mohr-Coulomb soil layer (same procedure as for the MC-LE model) and the surrounding soil was modelled as linear-elastic material. This implemented "*Slide*- PLAXIS 2D" model will be referred to as *Slide*-MC-LE PLAXIS 2D model.

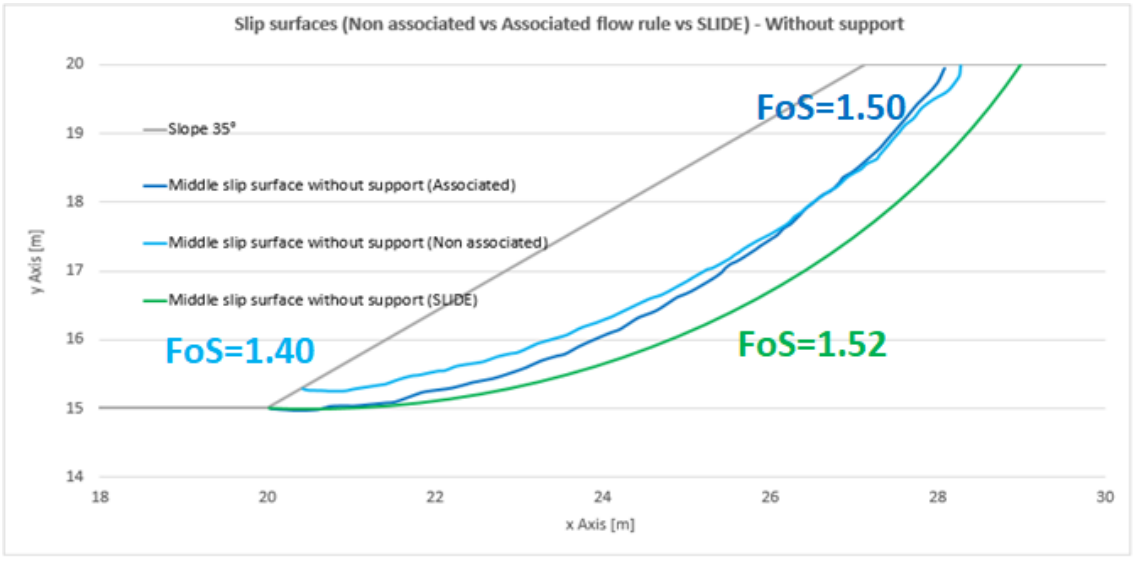

Figure 25 Slip surfaces generated with PLAXIS 2D (associated + non-associated) and *Slide* for the same unsupported slope model (geometry and parameters)

- **Comparison of the *Slide* model with *Slide*-MC-LE PLAXIS 2D model**

Figure 27 shows the slip surface generated in *Slide*, and the slip surface (stress points) which was evaluated from the *Slide*-MC-LE PLAXIS 2D model. It can be observed that these slip surfaces are almost identical.

Now the FoS of the two failure slip surfaces of the *Slide* model and *Slide*-MC-LE PLAXIS 2D model are equal (Figure 26).

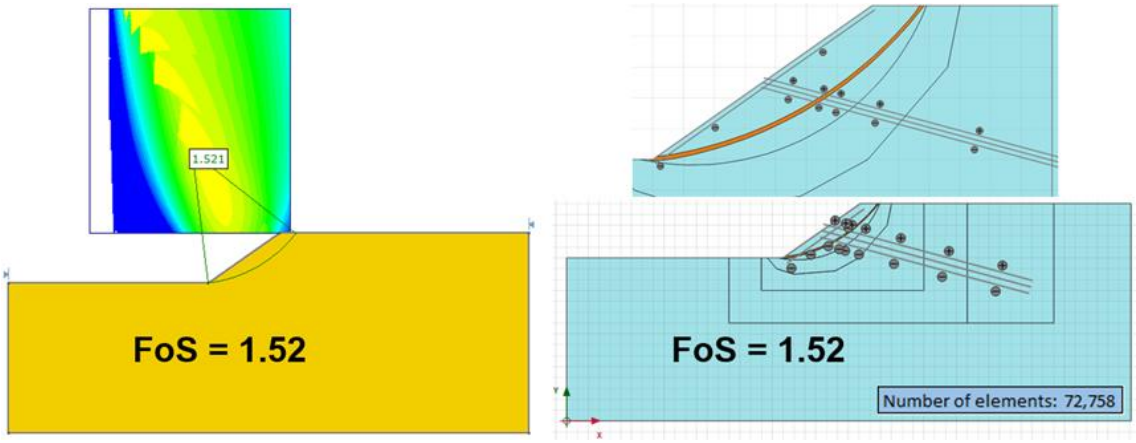

Figure 26 *Slide*-slip surface of the unsupported slope and the *Slide*-MC-LE PLAXIS 2D-slip surface with their FoS

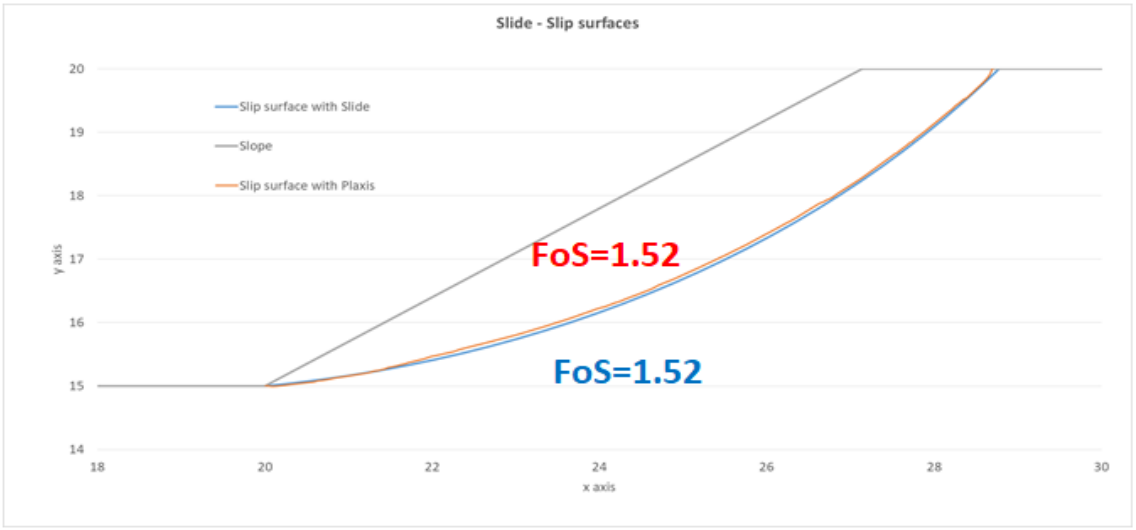

Figure 27 Illustration of the *Slide*-slip surface and the *Slide*-MC-LE PLAXIS 2D-slip surface

4.3.1.2 2D studies – one soil nail horizon

- **Mohr-Coulomb model**

The same study was conducted for the equal homogeneous slope supported by a 20 m long soil nail. The inclination of the soil nail is 20° to the horizontal.

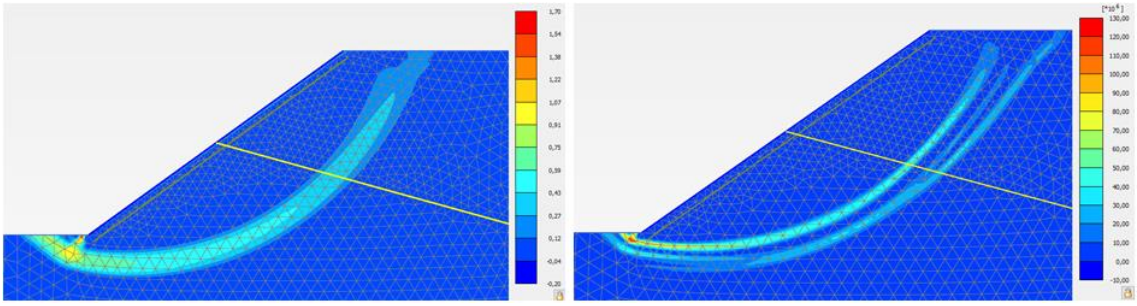

Figure 28 Slip surfaces of the reinforced slope; non-associated (left) and associated flow rule (right) for the MC model

The two slip surfaces of the reinforced MC model computed with PLAXIS 2D are shown in Figure 28. The associated ($\psi'=\varphi'$) case can be seen on the left hand side and the non-associated ($\psi'=0$) is displayed on the right. The images show how the slip surface moves further into the soil body compared with the unsupported cases (Figure 14).

The same colouring as before for the unsupported slope (Figure 15, Figure 16 and Figure 17) applies to the supported slip surface visualization of the case with associated (Figure 30) and non-associated flow rule (Figure 29) for the middle, upper-bound and lower-bound lines.

For the supported MC cases, the difference between the slip surfaces of the two flow rules is evident. The dashed associated case shows a longer slip surface (Figure 29). Hence, the failure mechanism depends strongly on the flow rule.

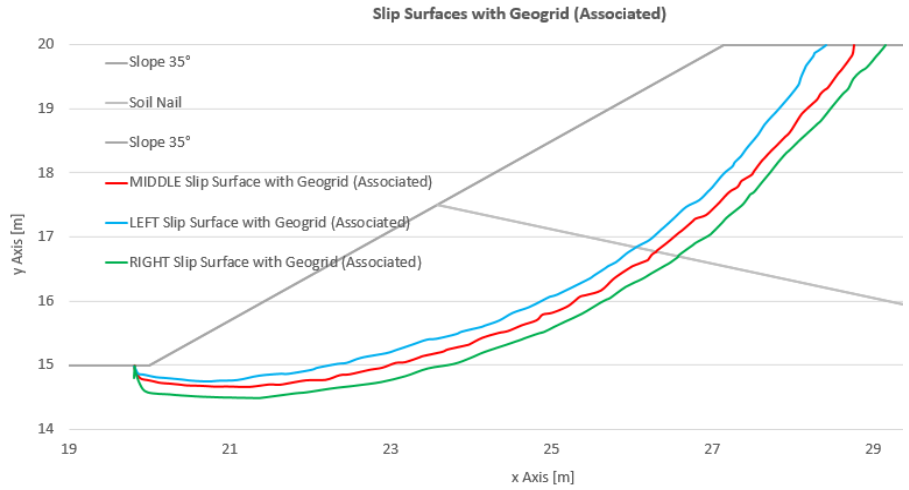

Figure 30 Visualization of the "slip surfaces" generated with the associated flow rule

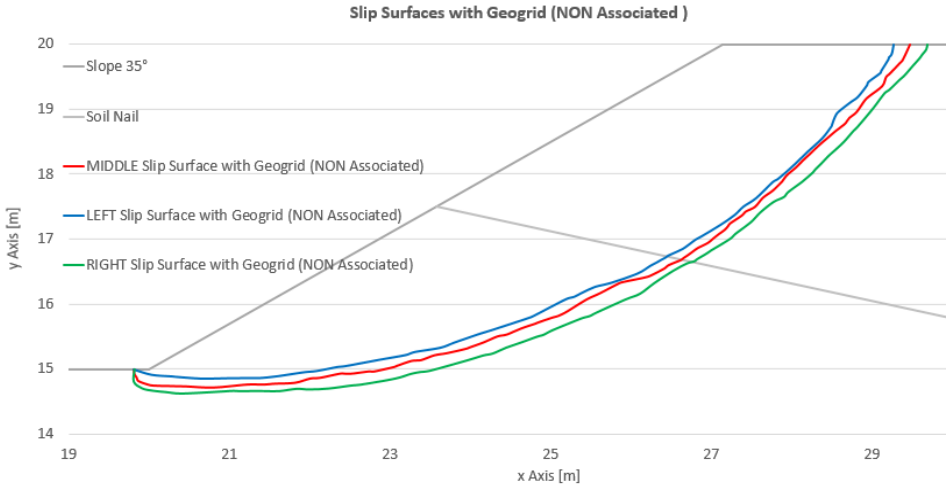

Figure 29 Visualization of the "slip surfaces" generated with the associated flow rule

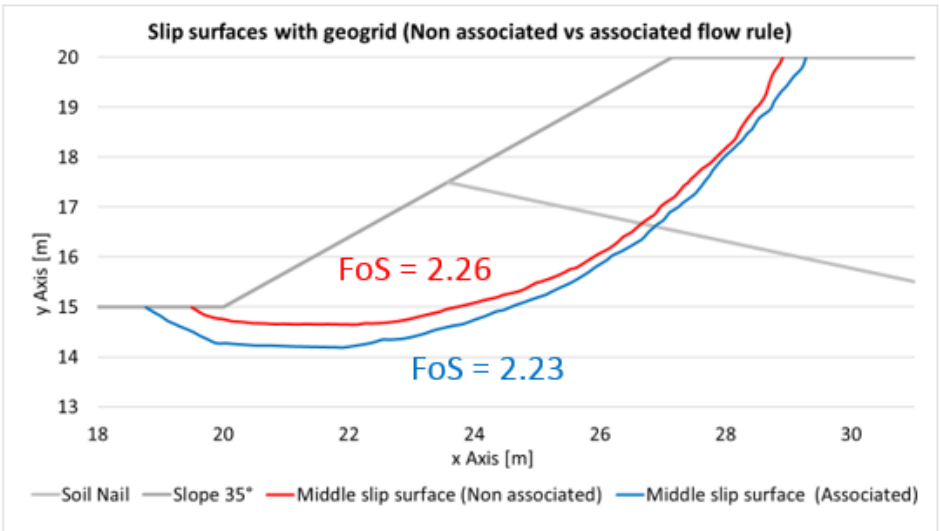

Figure 31 Comparison of the slip surfaces generated with the associated (red line) and non-associated flow rule (blue line) for the reinforced (1 soil nail horizon) case

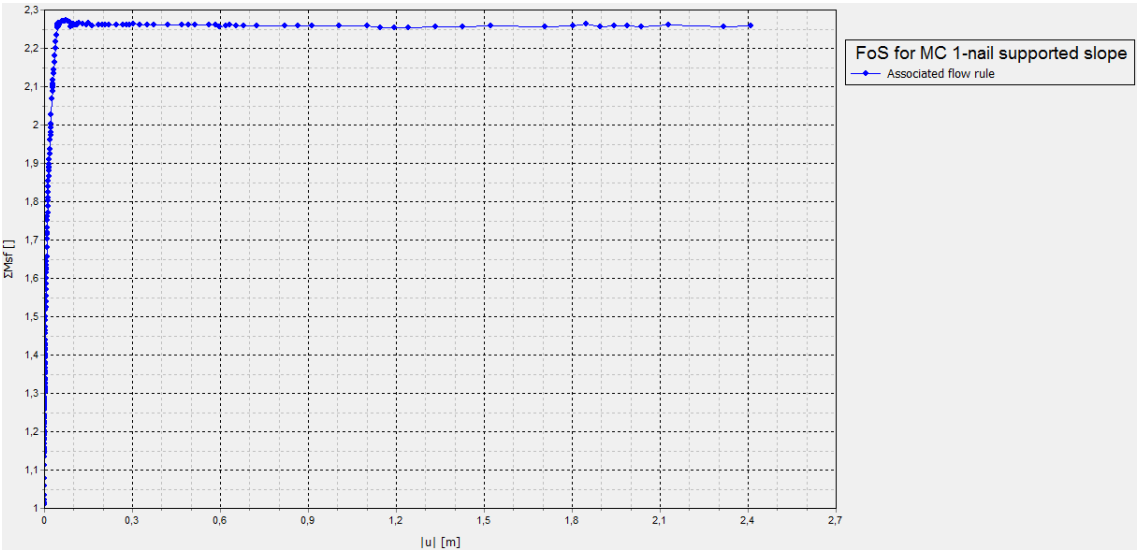

Figure 32 $M_{sf}/|u|$ diagram for the reinforced (1 soil nail) case calculated with the associated flow rule (MC model) – FoS=2.26

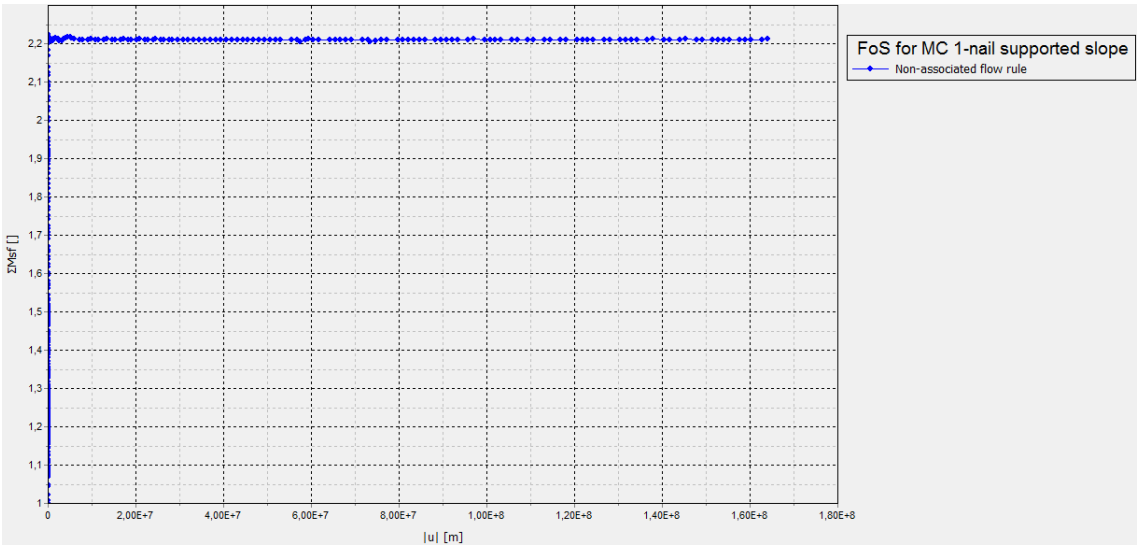

Figure 33 $M_{sf}/|u|$ diagram for the reinforced (1 soil nail) case calculated with the non-associated flow rule (MC model) – FoS=2.23

The FoS of the 1 soil nail reinforced slope MC model, calculated with the associated flow rule, is equal to 2.26 (Figure 32). On the other hand, the FoS for non-associated plasticity is slightly lower (FoS=2.23; Figure 33). As expected the FoS based on the non-associated plasticity leads to a smaller safety level.

- **Mohr-Coulomb – Linear-elastic model**

The FoS of the MC-LE model (FoS=2.26, Figure 34), with a soil nail is almost the same as for the MC model (FoS=2.29). The same MC-LE model calculated with

the non-associated flow rule has a safety value of 2.25 (Figure 35) – a slightly higher as the FoS of the non-associated –MC model.

The following MC-LE reinforced slopes are evaluated only over the one "real-middle" slip surface.

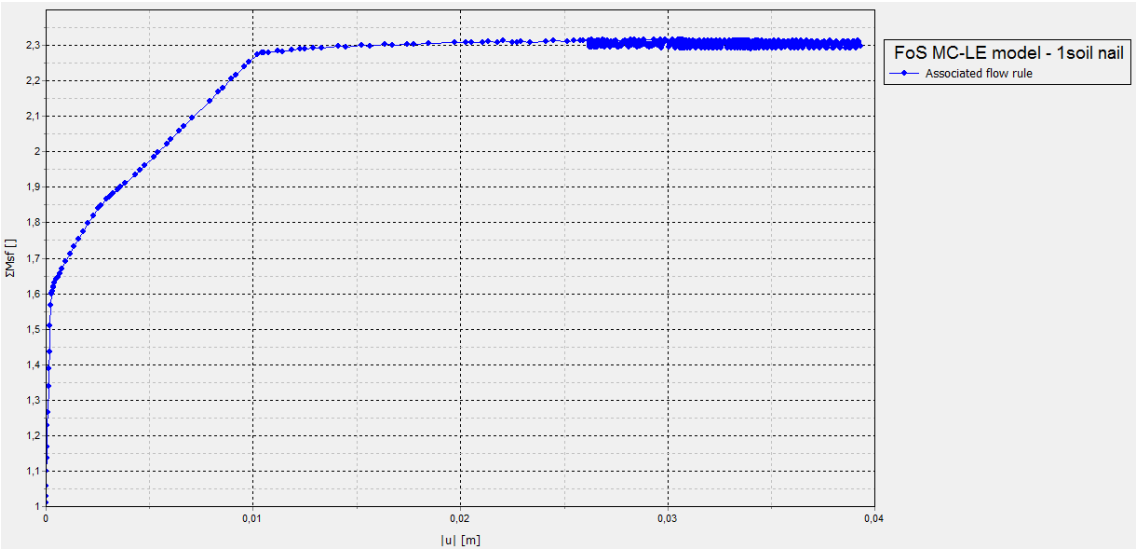

Figure 34 M_{sf}/|u| diagram for the reinforced (1 soil nail) case calculated with the associated flow rule (MC-LE model) – FoS = 2.29

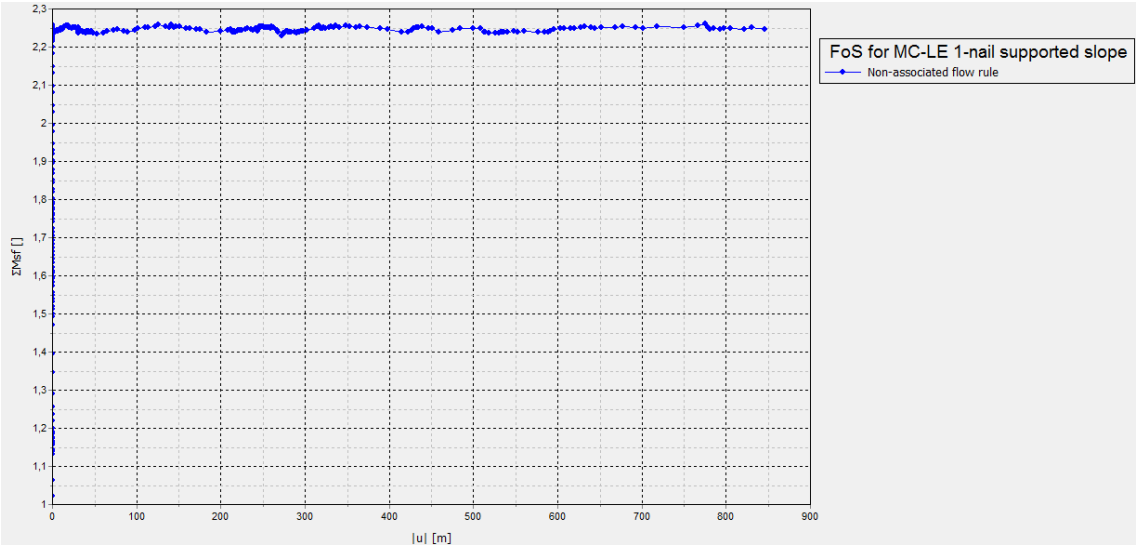

Figure 35 M_{sf}/|u| diagram for the reinforced (1 soil nail) case calculated with the non-associated flow rule (MC model) – FoS = 2.23

In Figure 36 the slip surfaces generated with the 1-nail-supported MC-LE models, calculated with the two flow rules are shown. They are moving over the same failure line. The FoS of the associated calculation is slightly higher than the FoS calculated with the non-associated plasticity.

Figure 37 presents the evaluated stress points over the slip surface of the 1-nail-reinforced MC-LE models calculated with the two flow rules (blue and red lines) Furthermore, the slip surface of the MC model calculated with the non-associated flow rule is also depicted (green line).

The slip surface calculated with the associated flow rule for the MC model is not illustrated in Figure 37, because it was traced by the blue line in the mentioned figure (and also has the same FoS).

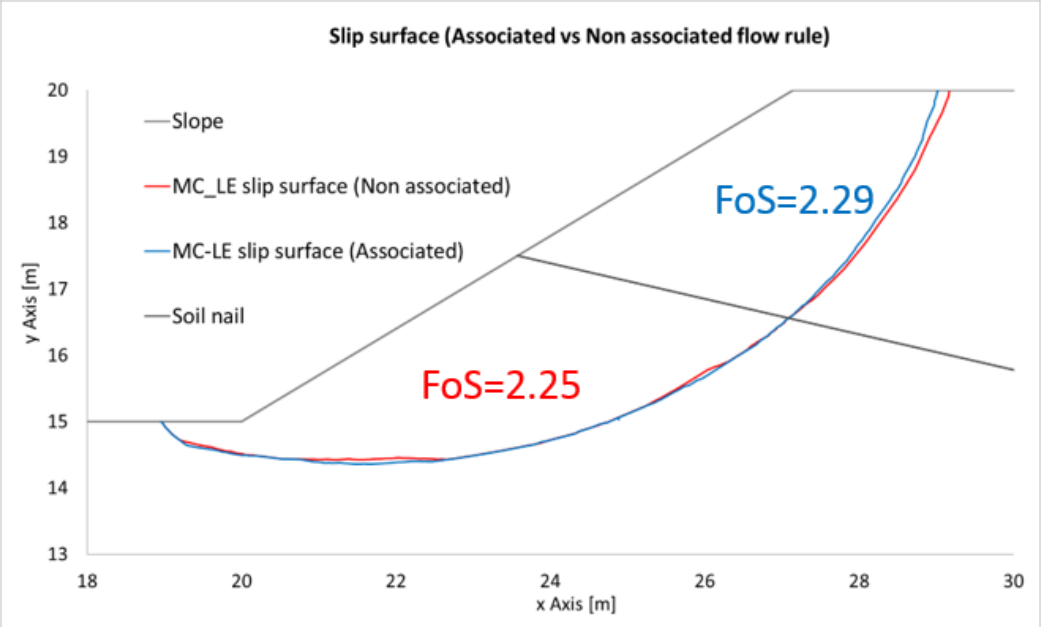

Figure 36 Slip surfaces generated with the associated and non-associated flow rule with corresponding factor of safety (MC-LE model of the 1-nail supported slope)

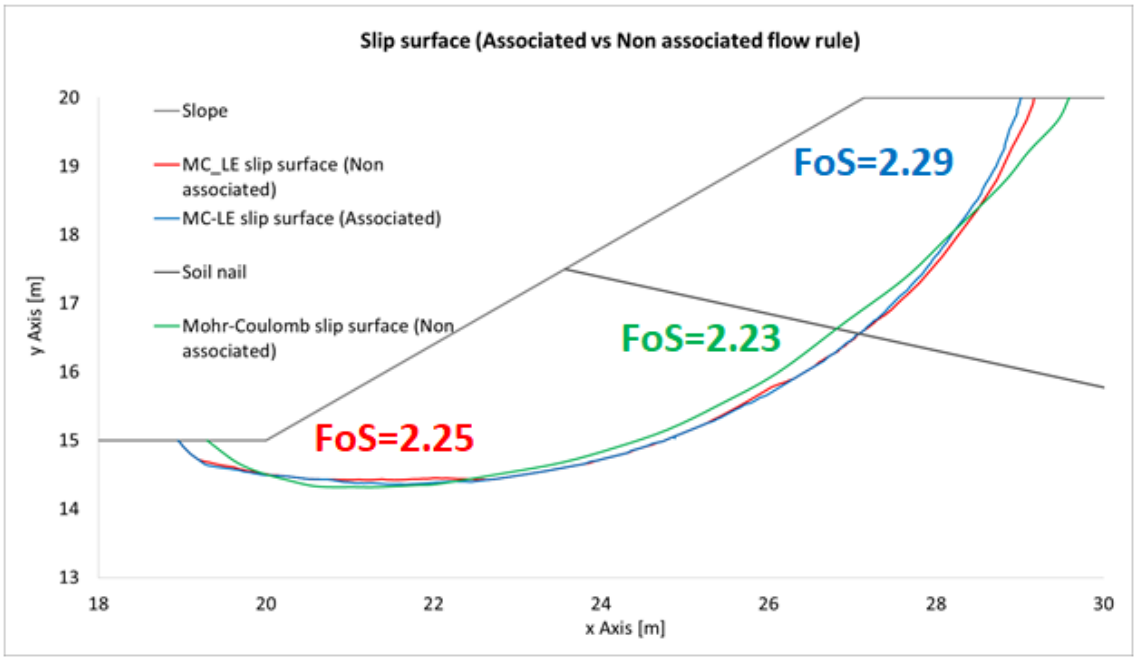

Figure 37 Slip surfaces generated for the 1-nail-reinforced slope with the two flow rules, with PLAXIS 2D (MC-LE model + non-associated MC model)

- **Comparison with Limit equilibrium analysis**

For the limit equilibrium analysis, the same soil model was examined as in PLAXIS 2D. The soil nail parameters had to be changed to take the 1.5 m spacing into account. In *Slide*, the spacing between the soil nail rows can be defined, but for geogrids in PLAXIS 2D this is not possible. Therefore, the tensile strength in *Slide* is 100 [kN] (the axial strength of the geogrids multiplied by 1.5).

The slip surfaces calculated in *Slide* and PLAXIS 2D are not the same. Consequently, the FoS cannot be equal for analytical and numerical analyses.

The details behind parameters and the modelling of the slope in the LEA program *Slide* can be found in Appendix B.

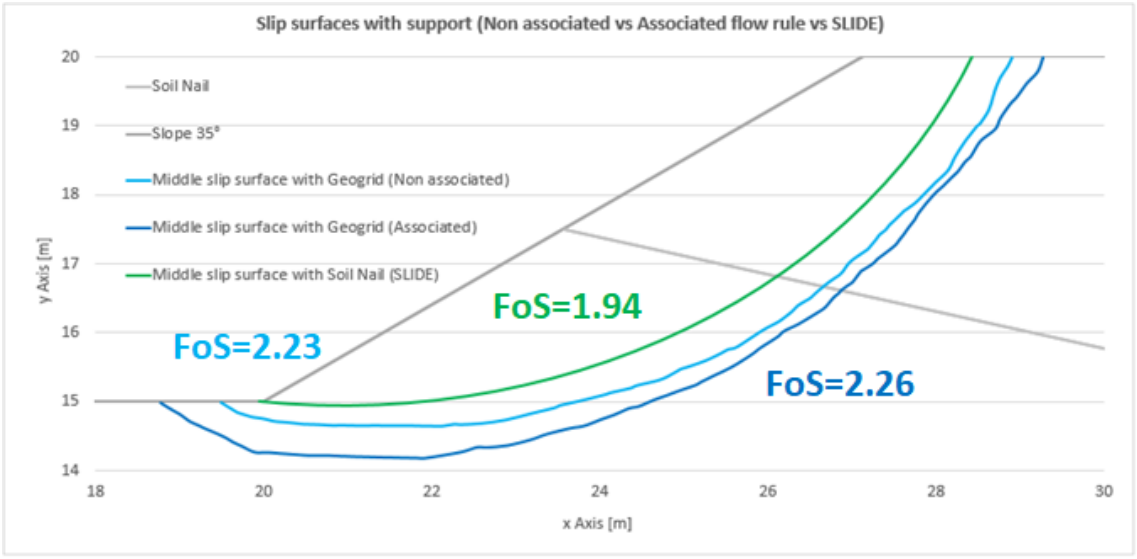

Figure 38 Slip surfaces generated with PLAXIS 2D (associated + non-associated) and *Slide* for the same reinforced slope model (geometry, parameters and reinforcement)

Again, the slip surface generated by *Slide* was implemented in PLAXIS 2D as a Mohr-Coulomb soil layer and the surrounding soil was modelled as linear-elastic. This was done to see whether the two programs show the same FoS for the same reinforced slope if they consider the same slip surface. Figure 38 shows the difference between the slip surface generated by *Slide* and the two surfaces generated by PLAXIS 2D.

- **Comparison of the *Slide* model with the *Slide*-MC-LE PLAXIS 2D model**

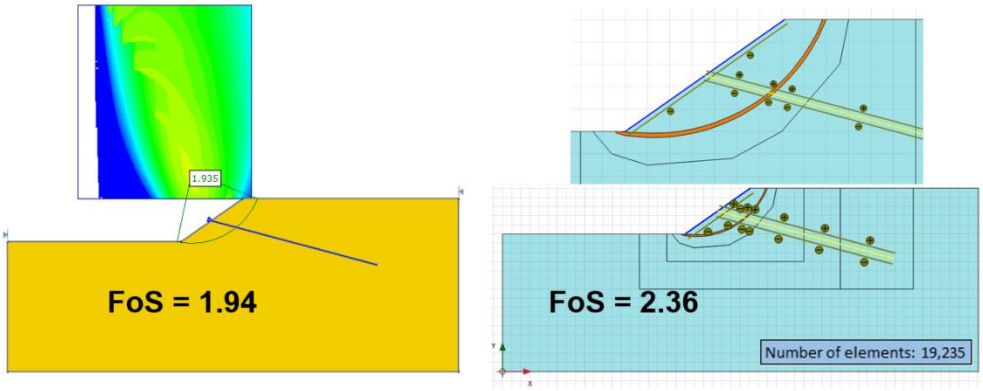

Figure 39 *Slide* model of the reinforced slope (left) with the calculated FoS and *Slide*-MC-LE PLAXIS 2D model calculated with the associated flow rule (right), with the corresponding FoS

After the implementation of the *Slide* failure slip surface in the PLAXIS 2D as a MC soil layer, the FoS of the *Slide*-MC-LE PLAXIS 2D model (Figure 39) is still not equal as the FoS calculated with *Slide*. Further analyses lead to the revelation of the origin for the distinct FoS to be the different generation of the soil nail forces (Figure 40).

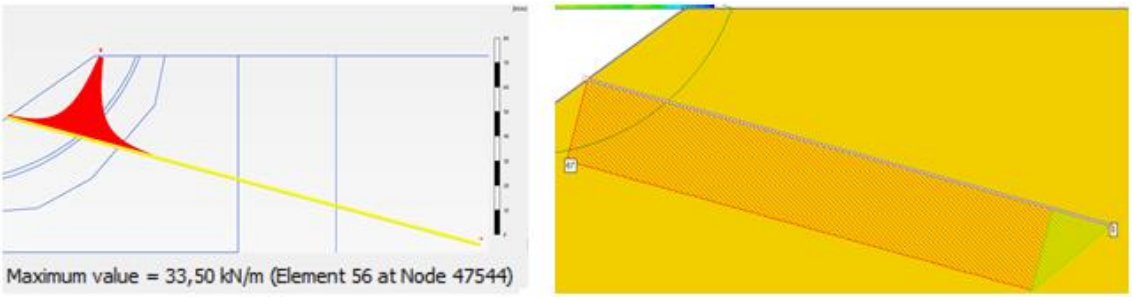

Figure 40 The qualitative trend of the normal forces in the soil nail in PLAXIS 2D (right) and *Slide* (right)

The internal normal forces in the *Slide*-soil nail are activated over the whole length of the soil nail, whereas the normal forces of the PLAXIS 2D soil nail (modelled with geogrid) are activated depending on the deformation. In PLAXIS 2D, the axial forces are successively decreasing with increasing distance from the shotcrete wall.

Table 6 The FoS of the *Slide*-MC-LE PLAXIS 2D model calculated with PLAXIS 2D with the corresponding maximal soil nail internal tension force N

"*Slide*" model in PLAXIS 2D mit geogrid	
Tension force N [kN/m]	**Factor of safety**
66.67	2.36
50.00	2.13
40.00	2.01
35.00	1.95
34.00	1.95
33.50	**1.93**
33.00	1.93

33.00	1.93
30.00	1.89

To determine the influence of the different normal force activation mechanisms in *Slide* and PLAXIS 2D, the axial force of the geogrid (N_p) in the *Slide*-MC-LE PLAXIS 2D model (calculated with the associated flow rule) was varied until the same FoS as in *Slide* (**Fehler! Verweisquelle konnte nicht gefunden werden.**) is reached. The FoS of 1.93 (which is close to the FoS_{SLIDE}=1.94) is reached after the geogrid axial force was decreased to about 50% (from 66.67 to 33.5 [kN/m]).

4.3.1.3 2D studies –three soil nail horizons

- **Mohr-Coulomb model**

The next analysis was conducted for the same MC slope model used in previous two points in research plain laid out above. This time three soil nails were used. All three soil nails have the same length (20 m) and inclination (20° to the horizontal).

Figure 43 shows the slip surfaces generated for the MC model (both flow rules), where the non-associated case calculates a bigger sliding mass, hence a longer and deeper located slip surface. Furthermore, the corresponding FoS of the slip surfaces calculated with the two distinct flow rules are displayed.

The safety calculation for the associated MC model delivered a FoS of 1.86 (Figure 41). The FoS for the non-associated MC model is equal to 1.80 (Figure 42).

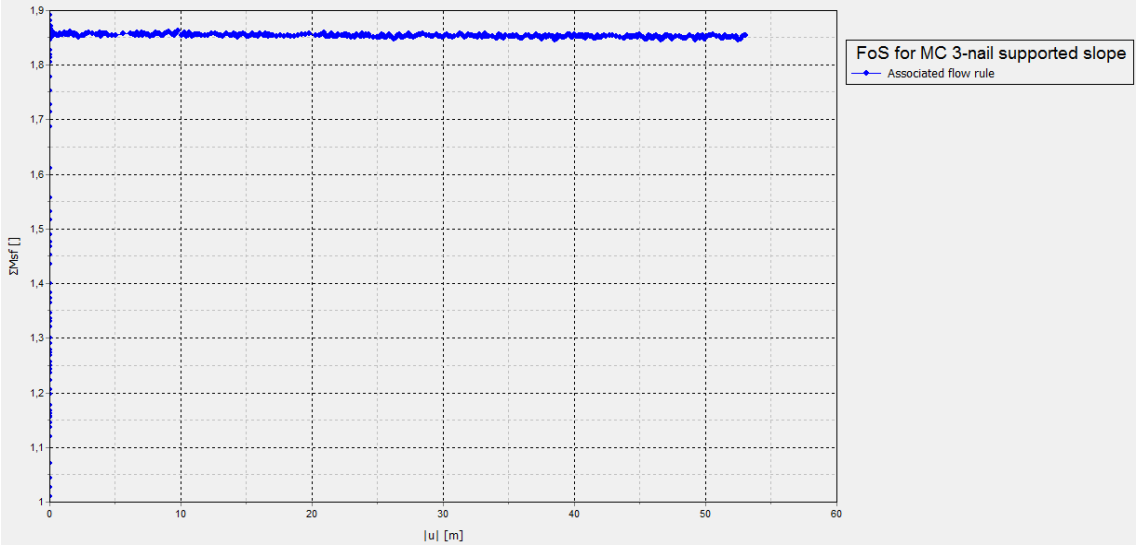

Figure 41 M_{sf}/|u| diagram for the reinforced (3 soil nail) case calculated with the associated flow rule (MC model) – FoS = 1.86

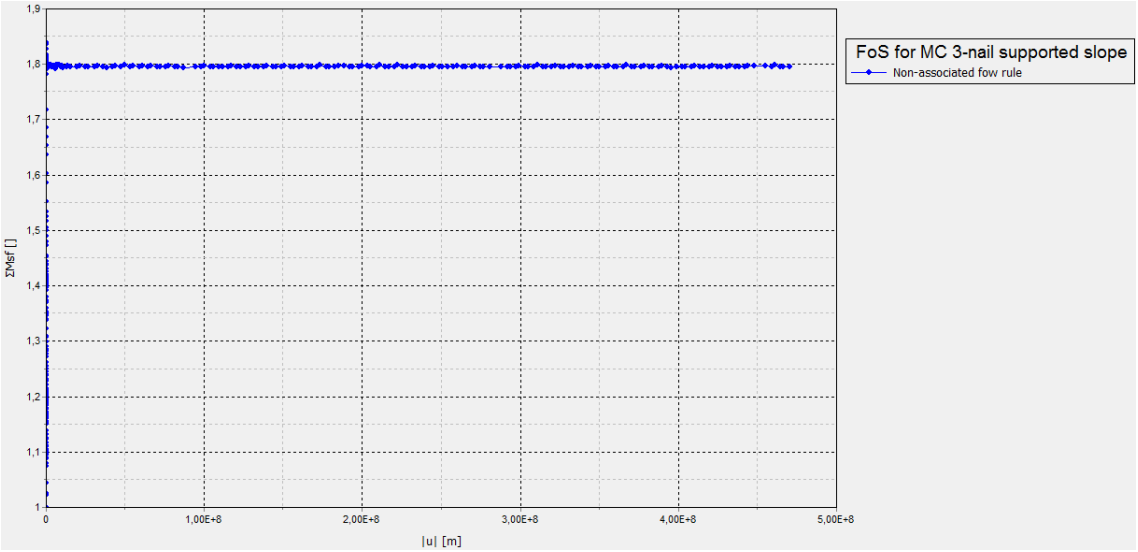

Figure 42 M_{sf}/|u| diagram for the reinforced (3 soil nail) case calculated with the non-associated flow rule (MC model) – FoS = 1.86

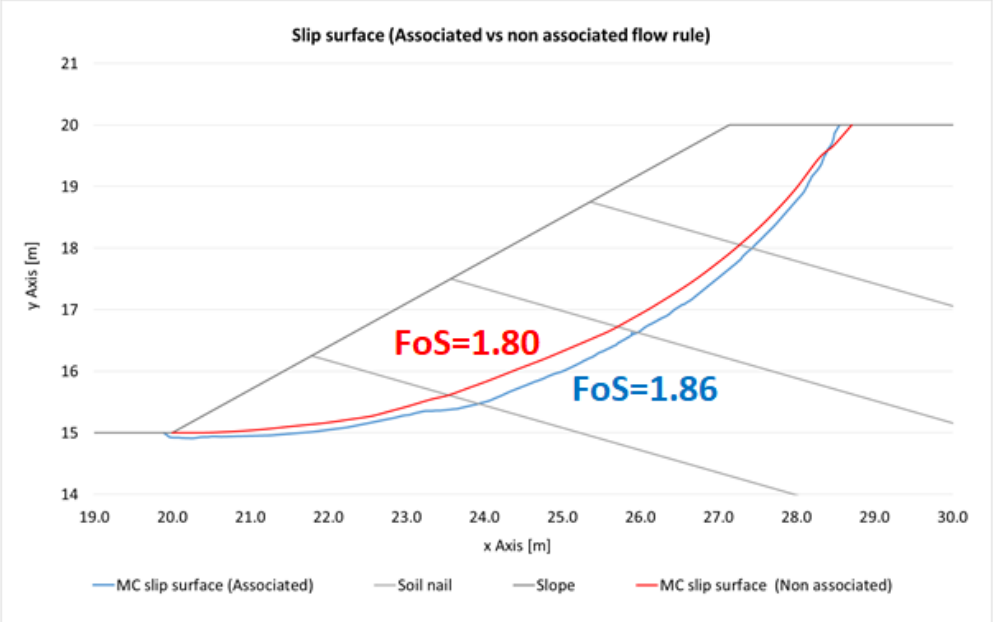

Figure 43 Generated slip surfaces of the 3-nail-reinforced MC model (both flow rules)

- **Mohr-Coulomb – Linear-elastic model**

By implementing the associated ($\psi'=\varphi'$) failure slip surface of the MC model into the MC-LE model, the two resulting slip surfaces of the two flow rules are identical (Figure 46). Here it is also evident how the associated incremental strains $\Delta\gamma_s$ (blue line) are moving along the upper border of the MC soil layer (blue line) and the non-associated $\Delta\gamma_s$ along the lower border (red line).

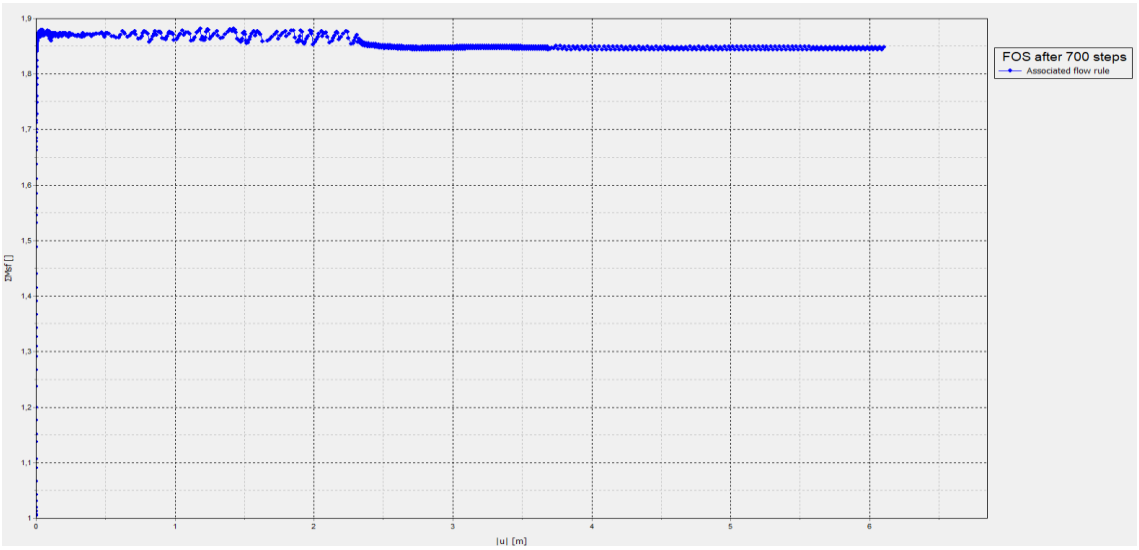

Figure 44 $M_{sf}/|u|$ diagram for the reinforced (3 soil nail) case calculated with the associated flow rule (MC-LE model) – FoS = 1.85

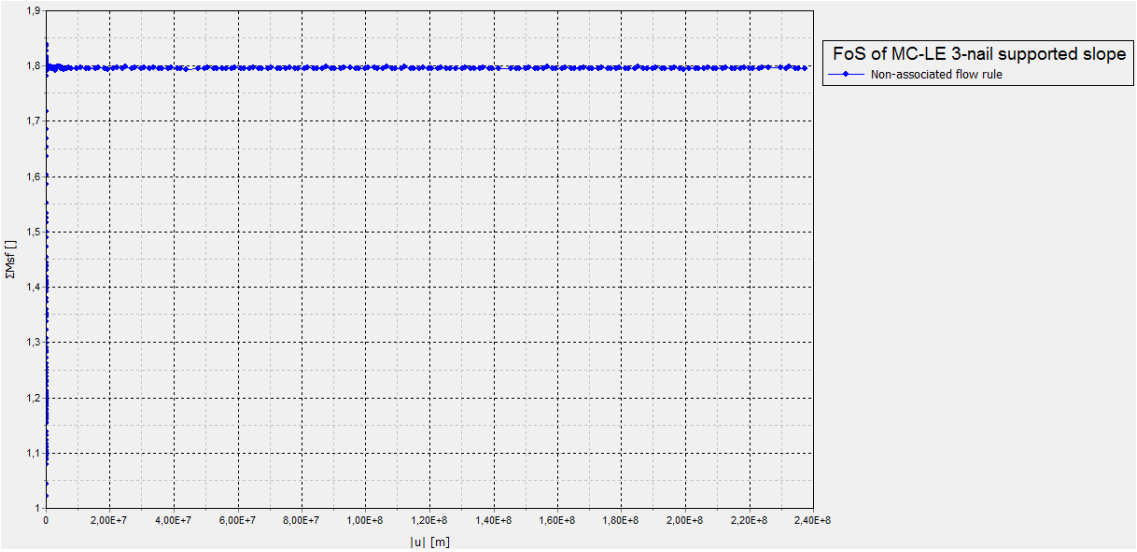

Figure 45 M_{sf}/|u| diagram for the reinforced (3 soil nail) case calculated with the non-associated flow rule (MC-LE model) – FoS = 1.80

The FoS of the associated MC-LE model is almost the same as the FoS of the associated three soil nail MC model, which is shown in Figure 44 of the Msf/|u| diagram, leading to a difference of about 1%. The non-associated flow rule calculates a lower FoS for the MC-LE model with a three soil nail reinforcement, as the associated plasticity.

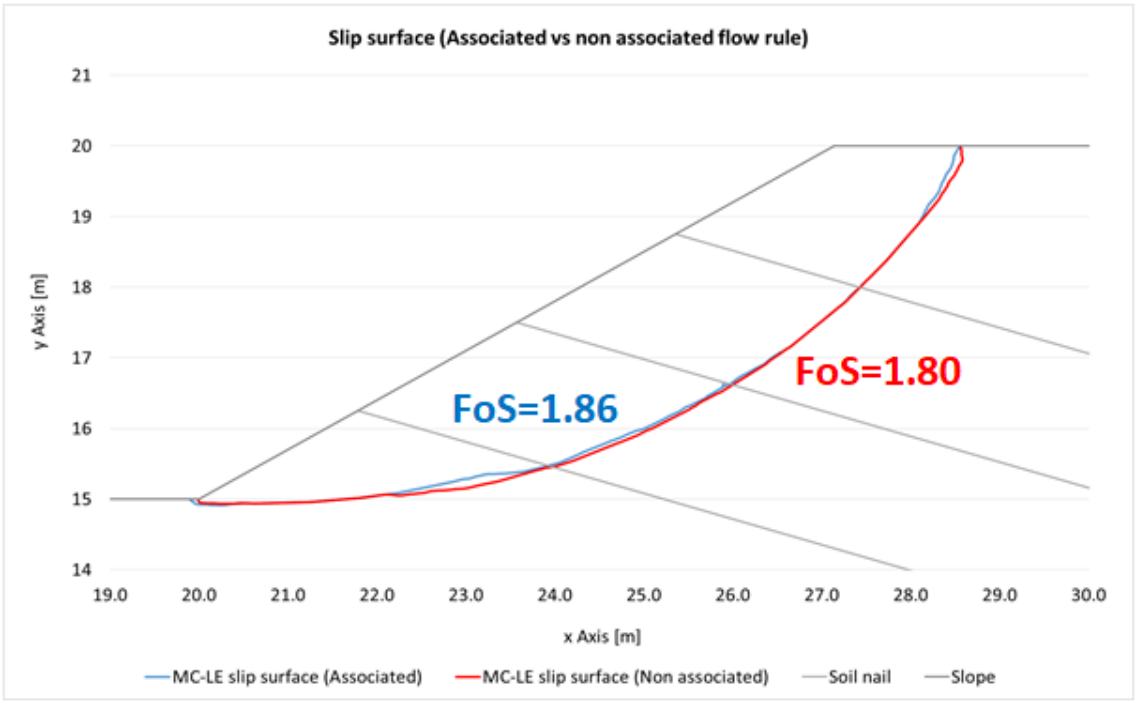

Figure 46 Generated slip surfaces of the 3-nail-reinforced MC-LE model (both flow rules)

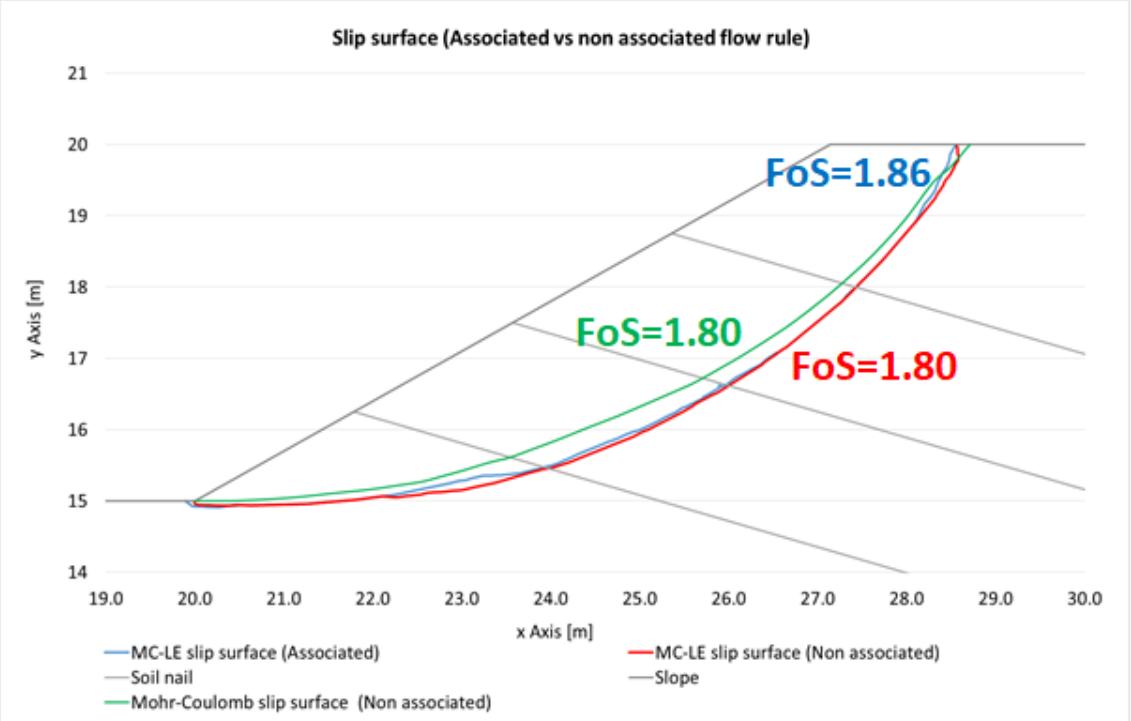

Figure 47 Slip surfaces generated for the 3-nail-reinforced slope with the two flow rules, with Plaxis 2D (MC-LE model + non-associated MC model)

Figure 47 depicts the two slip surfaces shown in Figure 46 plus the slip surface generated via the non-associated calculation of the MC model (green line).

- **Comparison with Limit equilibrium analysis**

The LEA programme *Slide* was used only for the FoS comparison with PLAXIS 2D, for three soil nail model. Morgenstern-Price method was used for the FoS calculation. The soil parameters are the same as in the PLAXIS 2D calculation. The soil nail and plate tensile capacity are chosen to be 15 [kN] with a spacing of 1.5 m. The axial force of the three geogrids in PLAXIS 2D is 10 [kN/m], a 33% lower axial force as in *Slide*, in order to take the spacing of 1.5 m into account.

The limit equilibrium analysis provides a lower FoS value, than the FoS calculated with the non-associated and the associated flow rule in PLAXIS 2D (about 8% lower than the associated, and 5% lower than the non-associated). The difference in the FoS is existing due to the different failure slip surfaces and the difference in the activation of the soil nail normal forces.

- **Trend summary**

The following tables show the FoS calculated with the associated and non-associated flow rule of the discussed MC and MC-LE models for the unsupported, one soil nail supported and three soil nail supported slope model.

The comparison between the FoS calculated with the LEA programme *Slide* and the PLAXIS 2D software is also given in the following tables.

Table 7 Comparison of FoS for the unsupported model calculated in *Slide* and PLAXIS 2D (MC and MC-LE model)

Factor of safety – without reinforcement				
Limit equilibrium analysis-*Slide*	**Finite element analysis – PLAXIS 2D-*Slide*-MC-LE model**			
	MC without support		MC-LE without support	
Without support	Associated	Non-associated	Associated	Non-associated
1.52	1.50	1.40	1.50	1.39

Table 8 Comparison of the FoS for the MC and MC-LE model, for the 1-soil nail supported slope

Factor of safety – 1 soil nail				
LEA - *Slide*	**FEA – PLAXIS 2D**			
With support	MC model with geogrid		MC-LE model with geogrid	
	Associated	Non-associated	Associated	Non-associated
1.94	2.26	2.23	2.29	2.25

Table 9 Comparison of the FoS calculated with *Slide* and with the PLAXIS 2D model with the implemented *Slide* failure slip surface (for the 1-soil nail supported slope)

Factor of safety – 1 soil nail					
LEA - *Slide*		**FEA – PLAXIS 2D – *Slide*-MC-LE model**			
With support	Without support	Without support		Geogrid as support	
		Associated	Non-associated	Associated	Non-associated
1.52	1.94	1.52	1.42	2.36	2.27

Table 10 Comparison of the FoS for the MC and MC-LE model, for the 1-soil nail supported slope

Factor of safety – 3 soil nails				
LEA- *Slide*	**FEA – PLAXIS 2D**			
With support	MC model with geogrid		MC-LE model with geogrid	
	Associated	Non-associated	Associated	Non-associated
1.73	1.86	1.80	1.85	1.80

4.3.2 Comparison of the normal effective stresses σ_n' along the slip surface

In this section of the thesis, the stresses generated with the two flow rules along the failure slip surface are compared. The stresses along the slip surface of the MC-LE models are compared and discussed, due to the fact that the slip surfaces generated with the two distinct rules are identical. Different stress indicators were compared over the slip surface of all the investigated models, for the two flow rules. Here, only the effective normal stresses σ_n' are discussed and compared. The remaining stresses (σ_1', σ_3', σ_{xx}', σ_{yy}' and the principal stress directions) are displayed in Appendix C, D, E, F, G and H.

The stresses of the same safety calculation step, have the same colour, they are depicted on the same coloured line. Every calculation step has its own colour scheme. The stresses of the Nil step (for the unsupported cases) or the Support installation-step (for the supported cases) are represented by a red line, 33%-step stresses by a blue line, 67%-step stresses by a violet line, 90%-step stresses by an orange line, 100%-step stresses by a green line and the 100%final-step stresses by a black line (for example see Figure 48).

The software PLAXIS 2D does not calculate the effective normal stresses. However, the Cartesian effective stresses (σ_{xx}', σ_{yy}' and σ_{zz}') can be calculated and displayed for all the stress points, including the ones in the slip surface. By knowing the Cartesian effective stresses in the slip surface and the slip surface inclination at every stress point, the normal effective stresses can be calculated using Eq. (9).

$$\sigma_n' = \sigma_{xx}' \times \cos(\alpha) + \sigma_{yy}' \times cos(90° - \alpha) \quad (9)$$

α Slip surfaces inclination on a certain stress point

In this chapter, first the effective normal stresses and afterwards all stress indicators will be displayed in a diagram and discussed for both the associated flow rule and the non-associated flow rule. These results will be presented for the MC-LE model with no reinforcement, followed by the results of the one soil nail reinforced slope and at the end, the results of the slope model with three soil nail horizons will be presented. Finally, a summary of the results is included. The section 4.4 was done with the same description structure.

4.3.2.1 2D studies – unsupported slope model

For the case without reinforcement, the results of the normal effective stress over the slip surface (of the associated flow rule) are shown (Figure 48 and Figure 49). Figure 49 shows the evolution of the effective normal stresses over the slip surface length (from left to right) with the increase of steps in the safety calculation. The effective normal stresses σ_n' are shown for the following steps: Nil step, 33%-, 67%-, 90%-, 100%*- and 100%final-step, which are explained in section 4.1.

In Figure 48 it can be seen that σ_n' (calculated with the associated flow rule) does not change significantly between the steps. Since the 100%final and the 100%* step do not divulge much more than the previous steps, these steps were excluded from further investigation of the stress behaviour for the associated flow rule.

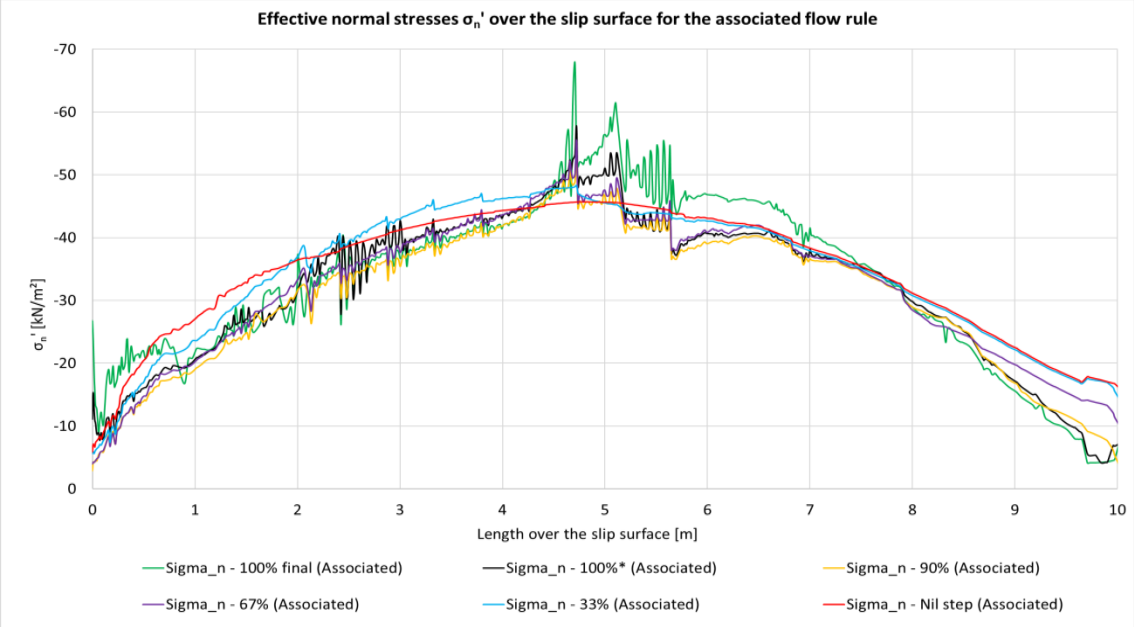

Figure 48 σ_n'/Slip surface length for the associated flow rule without reinforcement

By removing the 100%- and 100%final-step lines the diagram looks as follows in Figure 49. This diagram shows that σ_n' remains almost the same with the increase of steps. The stresses slightly decrease with the step increase of the safety calculation, but this might be a result of the stress point handpicking.

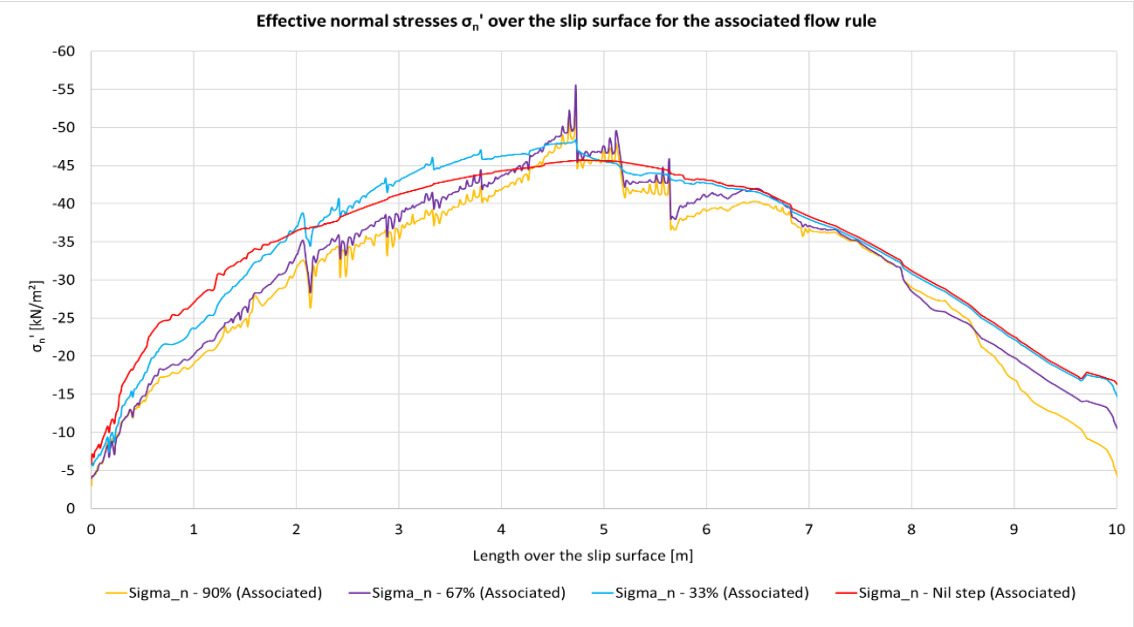

Figure 49 σ_n'/Slip surface length for the associated flow rule without reinforcement

In the unsupported slope calculated with the associated flow rule, the σ_n' result does not alter much between the calculation steps of the safety calculation.

The following four diagrams (Figure 51, Figure 50, Figure 53, Figure 52) show all the stress indicators σ_i' (σ_1', σ_3', σ_{yy}', σ_{xx}', σ_n') evaluated for the selected safety calculation steps (Nil-, 33%-, 67%-, and 90%-step) over the slip surface length (from the slope toe to the top of the slope).

The different coloured lines show the different stress indicators at the corresponding slip surface stress points. The following coloured lines correspond to the related stress indicators:

- σ_1' – red line
- σ_3' – green line
- σ_{yy}' – violet line
- σ_{xx}' – orange line
- σ_n' – blue line

This colour scheme is used for all the σ_i'/Slip surface length diagrams in this thesis (unsupported and supported MC-LE models).

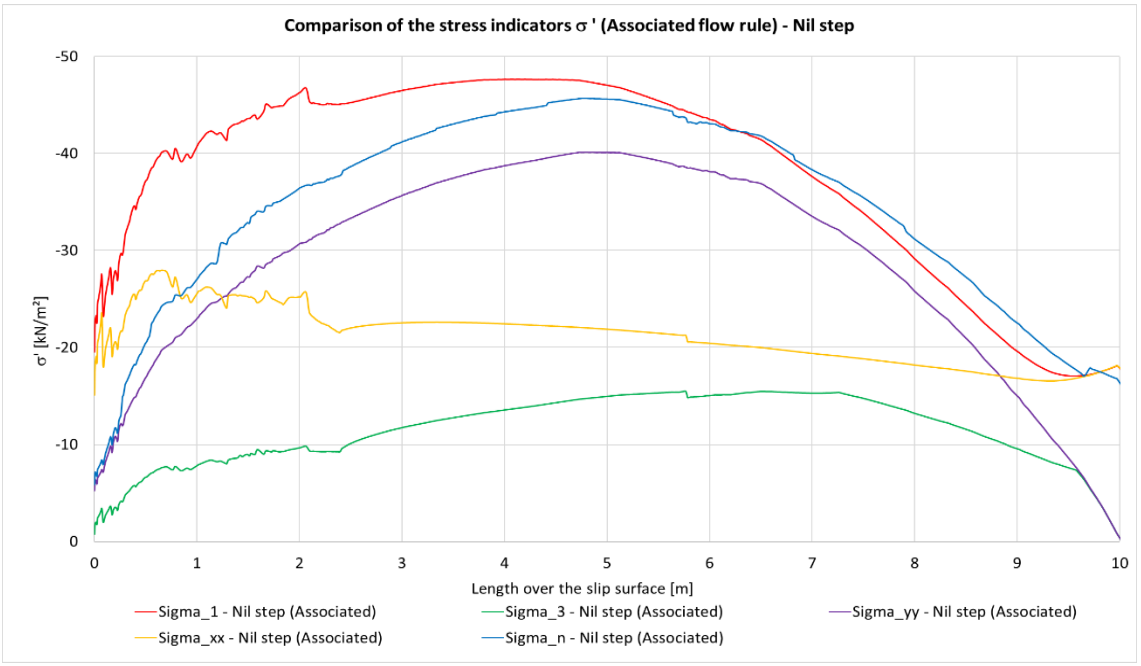

Figure 51 σ_i'/Slip surface length for the associated flow rule of the MC-LE model without reinforcement (Nil-step stress indicators)

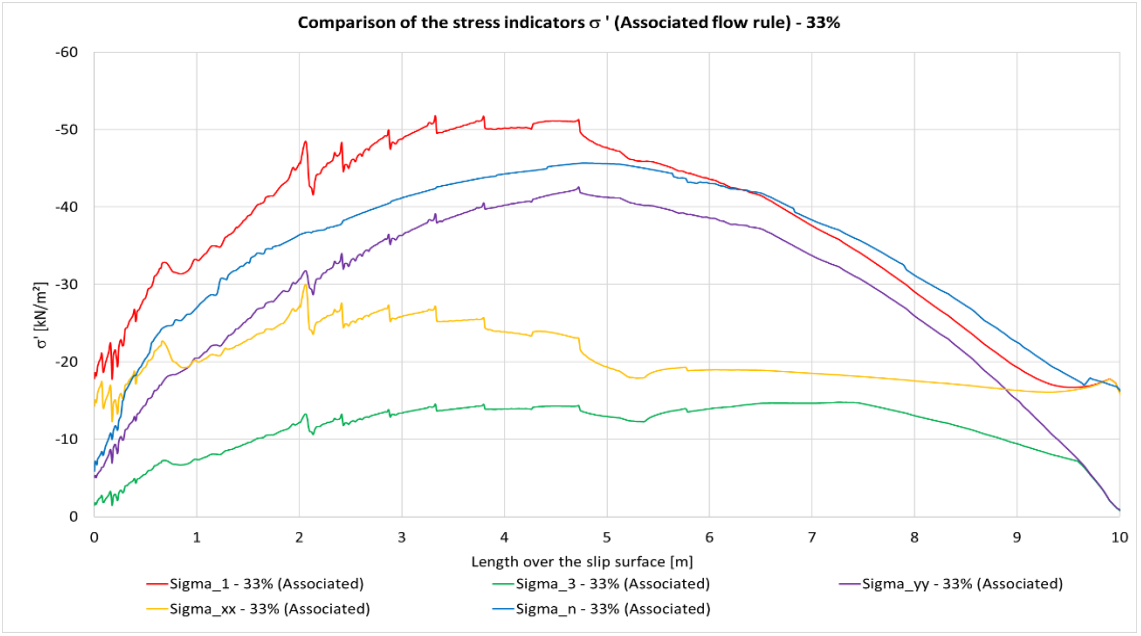

Figure 50 σ_i'/Slip surface length for the associated flow rule of the MC-LE model without reinforcement (33%-step stress indicators)

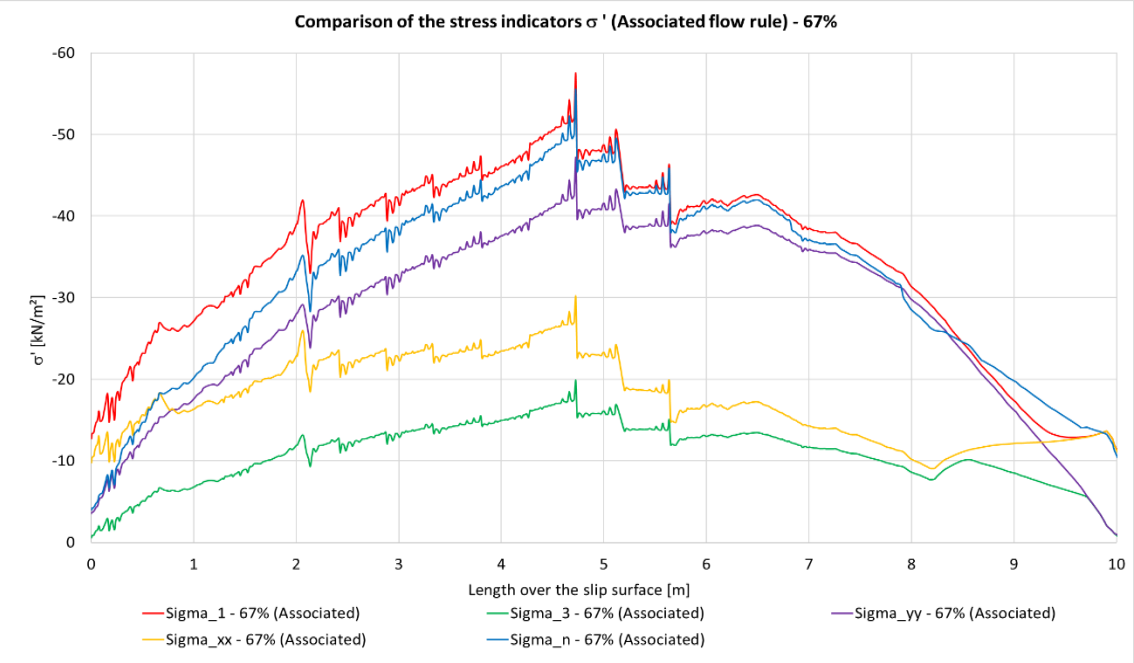

Figure 53 σ_i'/Slip surface length for the associated flow rule of the MC-LE model without reinforcement (67%-step stress indicators)

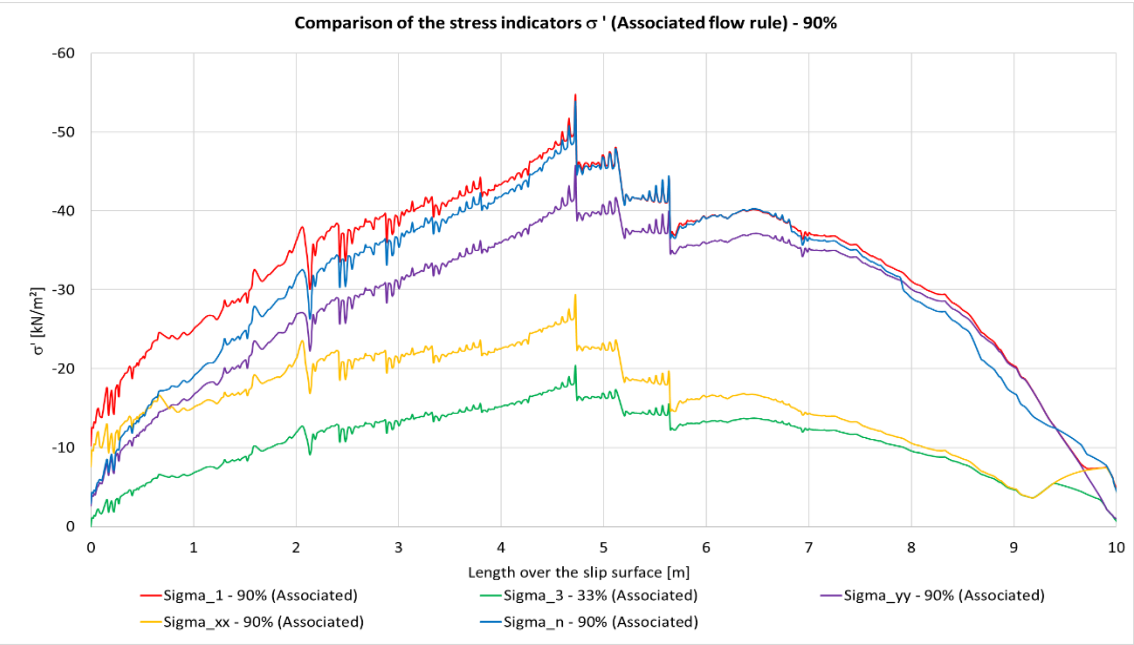

Figure 52 σ_i'/Slip surface length for the associated flow rule of the MC-LE model without reinforcement (90%-step stress indicators)

This evaluation shows that all the stress indicators have the same trend for the same steps. The lower the step number, the less the lines are scattered. The order from the highest stress indicator to the lowest is: $\sigma_1' > \sigma_n' > \sigma_{yy}' > \sigma_{xx}' > \sigma_3'$.

These different stress indicators are showed in detail and compared (considering the different safety calculation steps) in Appendix F. Furthermore, the principal stress directions of the evaluated stress points are also shown in Appendix F.

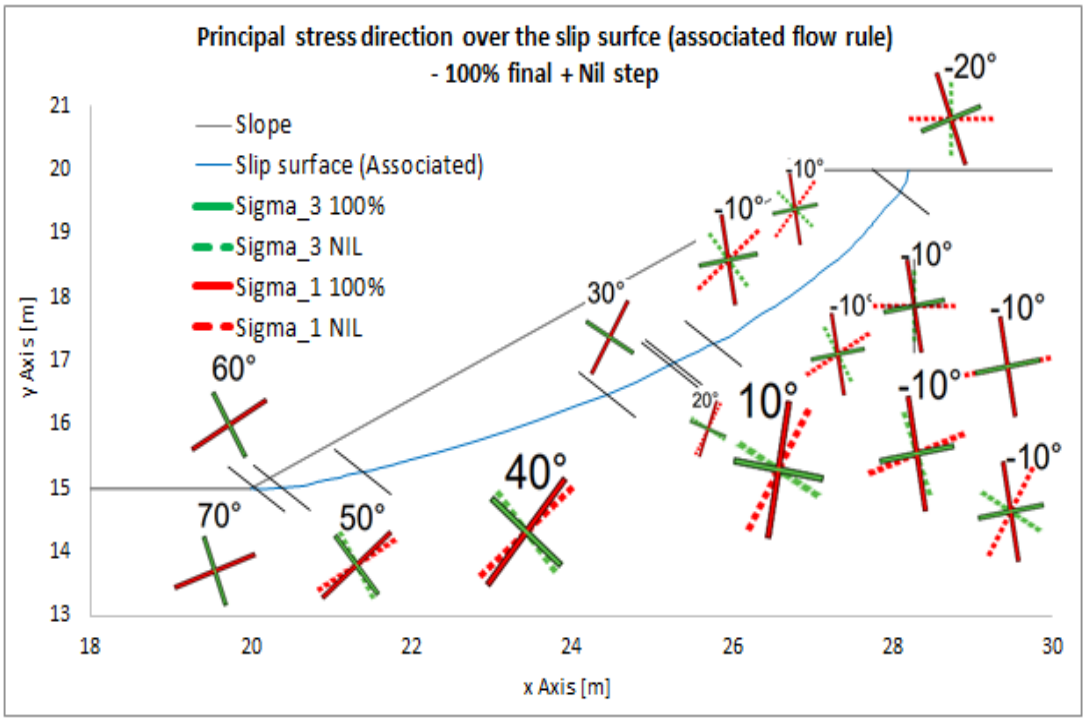

Figure 54 Principal stress directions for the associated flow rule (MC-LE model)

Figure 54 illustrates the principal stress orientation evolution with the safety calculation progress. The dashed principal stress crosses represent the principal stress orientation at Nil step. The soilid principal stress crosses represent the principal stress orientation at the final safety calculation step (100%final-step).

The slip surface in Figure 54 is separated into parts with the same principal stress orientation. The degree-value above the stress crosses shows the maximal principal stress orientation at the final step of the safety calculation for the corresponding slip surface section (and the minimal inclination of that section is then 10° lower compared to the maximal). Therefore, the slip surface is divided in 10°-principal stress orientation (direction) groups.

The conclusion behind the Figure 54 is that the slip surface stress orientation depends on the slip surface formation. The principal stress directions cross is approximately parallel to the generated slip surface

The same study was conducted for the non-associated case. In Figure 55, σ_n' over the non-associated slip surface length is shown for the steps: Nil-, 33%-, 67%- and the 90%, 100%*-, 100%** and 100%final-step. The high scattering of the σ_n'-lines can be related to the non-associated. Therefore, for the non-associated investigation the 100%*-, 100%**- and 100%final-step results will not be shown and discussed further in this thesis. The 100%**-line was inserted somewhere (in between 100%* and 100%final) at the plateau-line-part of the $M_{sf}/|u|$ line in order to investigate the scattering.

The σ_n' results without the 100%*-, 100%**- and 100%final-line are depicted in the Figure 56.

Figure 56 shows that for the non-associated flow rule, σ_n' does not change much between the safety calculation steps. It is also visible that the non-associated analysis result in a stress field around the slip surface with a scattering principal stress direction (Figure 57). The scattering principal stresses directions explain the high fluctuation of the stresses along the slip surface.

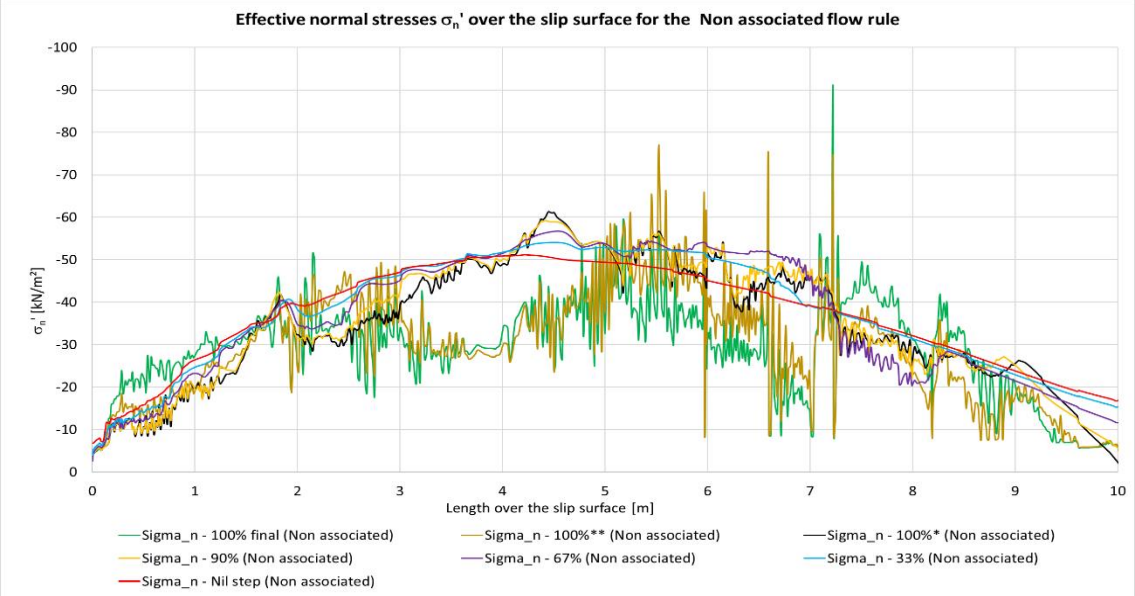

Figure 55 σ_n'/Slip surface length for the non-associated flow rule of the MC-LE slope model without reinforcement

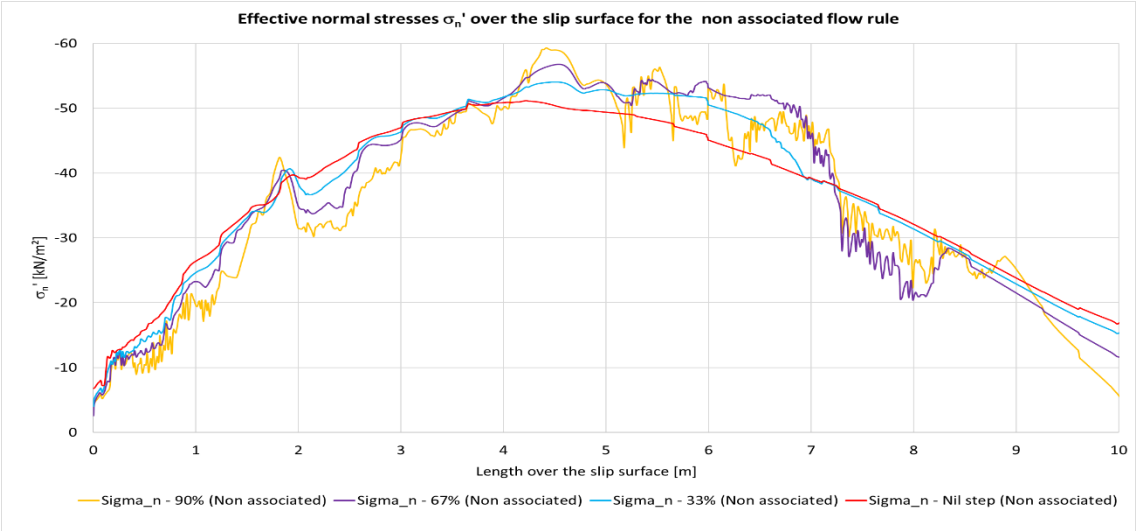

Figure 56 σ_n'/Slip surface length for the non-associated flow rule of the MC-LE slope model without reinforcement

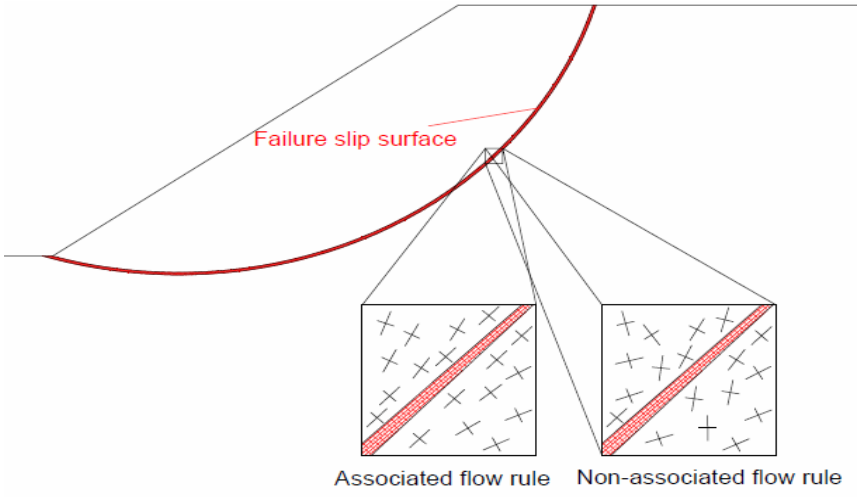

Figure 57 Illustration of the different principal stress directions calculated with the associated and non-associated flow rule

The following four diagrams show all the stress indicators over the slip surface length for the non-associated calculation of the unsupported MC-LE model. These stresses were evaluated (in order) from the Nil-, 33%-, 67%- and 90%-step.

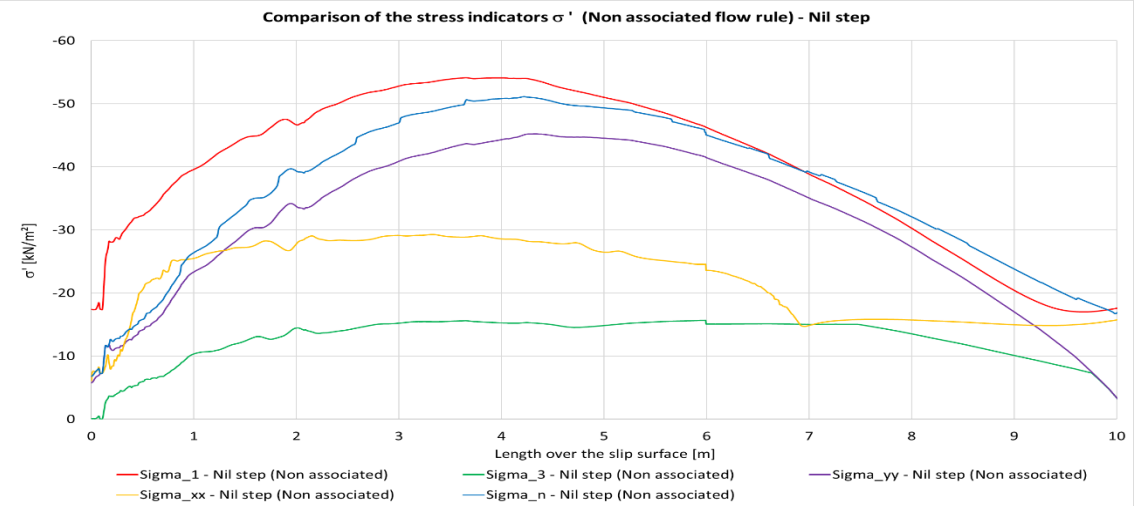

Figure 59 σ_i'/Slip surface length for the non-associated flow rule of the MC-LE slope model without reinforcement (Nil step)

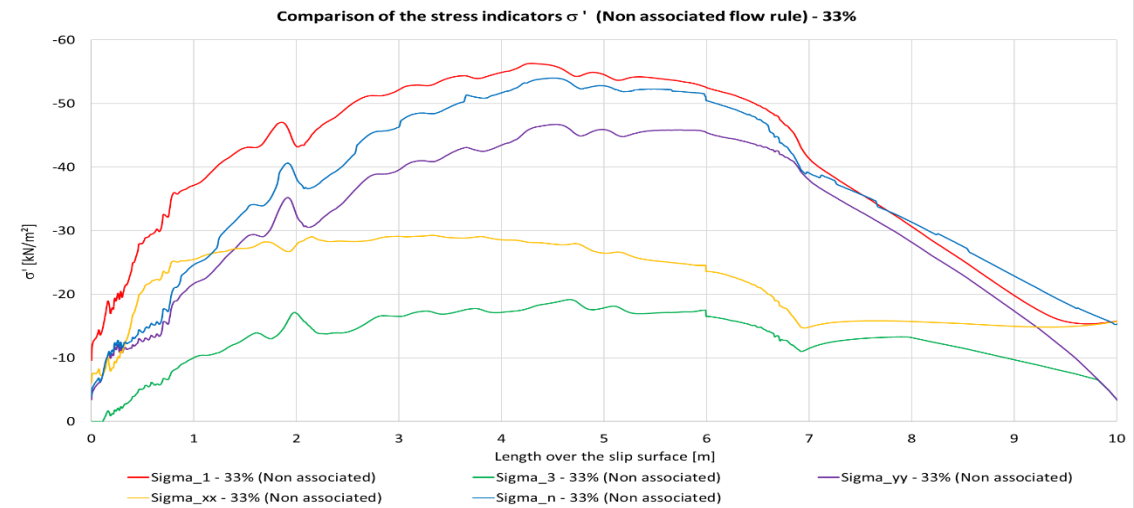

Figure 58 σ_i'/Slip surface length for the non-associated flow rule of the MC-LE slope model without reinforcement (33%-step)

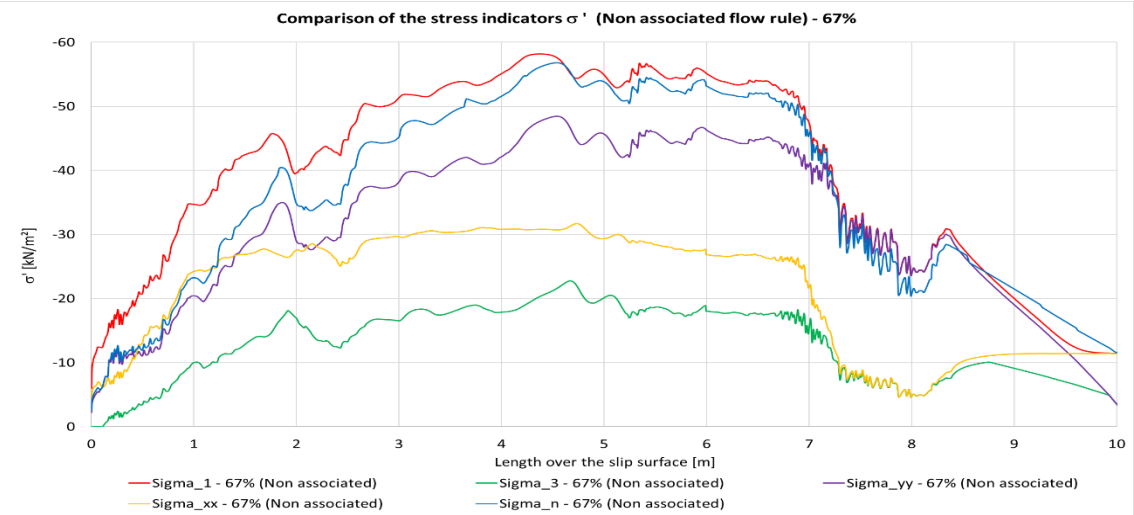

Figure 60 σ_i'/Slip surface length for the non-associated flow rule of the MC-LE slope model without reinforcement (67%-step)

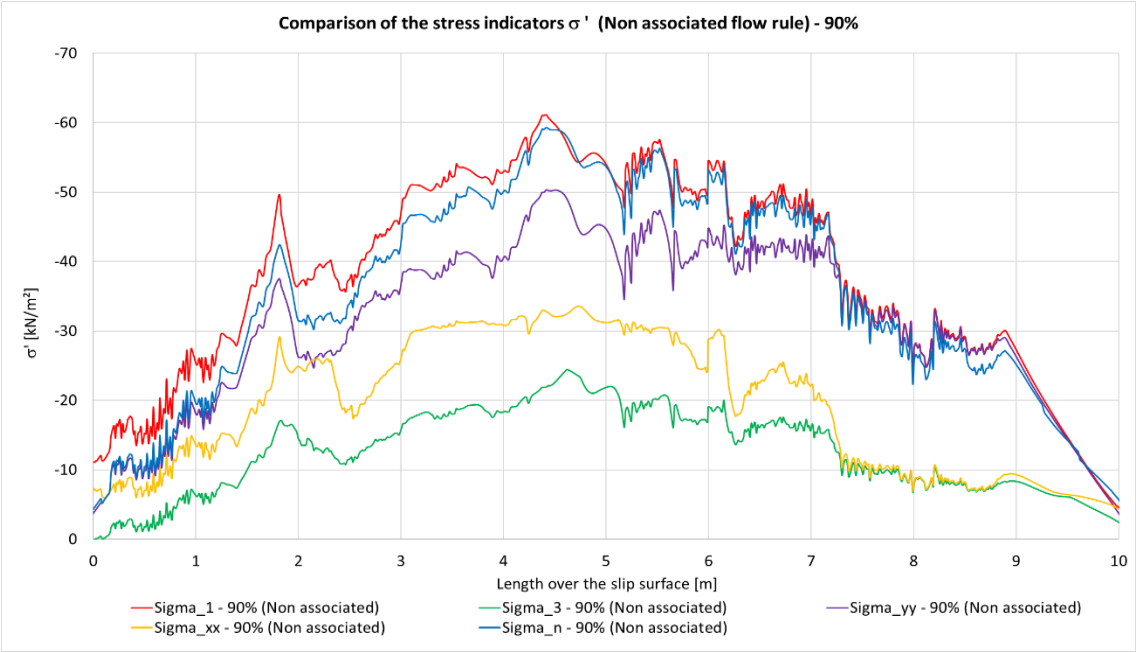

Figure 61 σ_i'/Slip surface length for the non-associated flow rule of the MC-LE slope model without reinforcement (90%-step)

The σ_i'/Slip surface length diagrams (Figure 60, Figure 59, Figure 58 and Figure 61) show that the different stress indicators have the same trend over the slip surface length through the examined safety calculation steps. With the increase of steps, the scatter increases in height and frequency. A more detailed description and comparison of these stress indicators can be found in Appendix F.

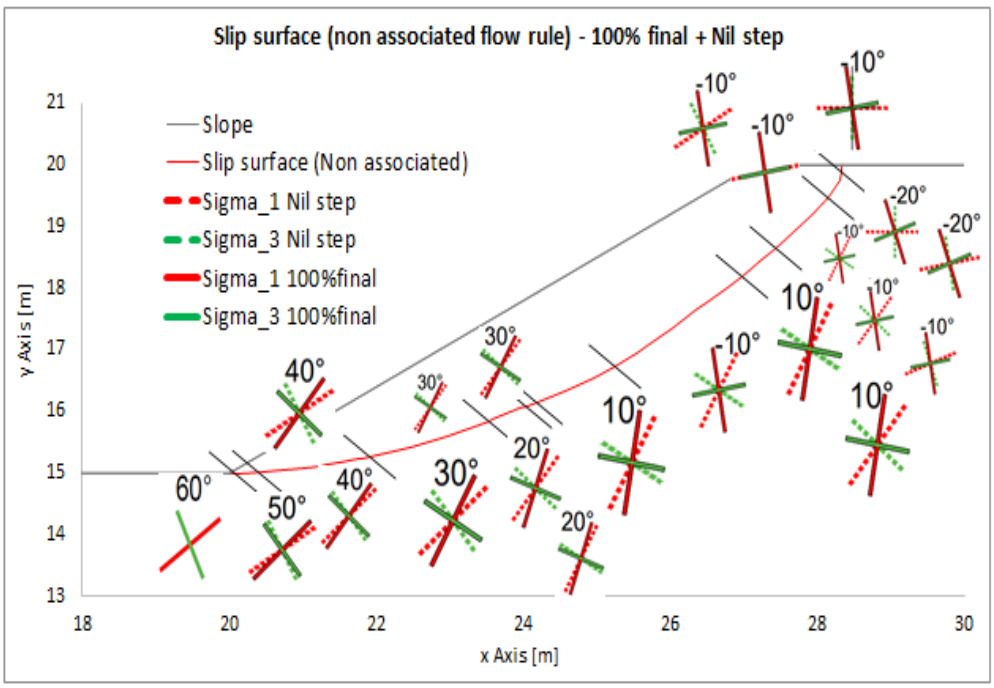

Figure 62 Principal stress directions for the non-associated flow rule (MC-LE model)

Figure 62 presents the principal stress orientation evolution. The slip surface of the non-associated plasticity is divided into more principal stress direction parts then the associated case, which is a result of the high scattering of the stresses. For the non-associated case, the principal stress direction crosses are also roughly parallel to the slip surface generated with the non-associated flow rule.

4.3.2.2 2D studies – one soil nail horizon

The following diagrams show the influence of one soil nail (indicated by the black vertical line) on the stresses in the slip surface. Figure 63 shows the distribution of σ_n' over the slip surface of the reinforced MC-LE model ($\psi'=\varphi'$).

It can be seen that the normal stresses σ_n' are increase during the φ'/c' reduction. The stresses have a higher increase in the area of the soil nail, which is depicted by the stress peak, near the black vertical line (the soil nail).

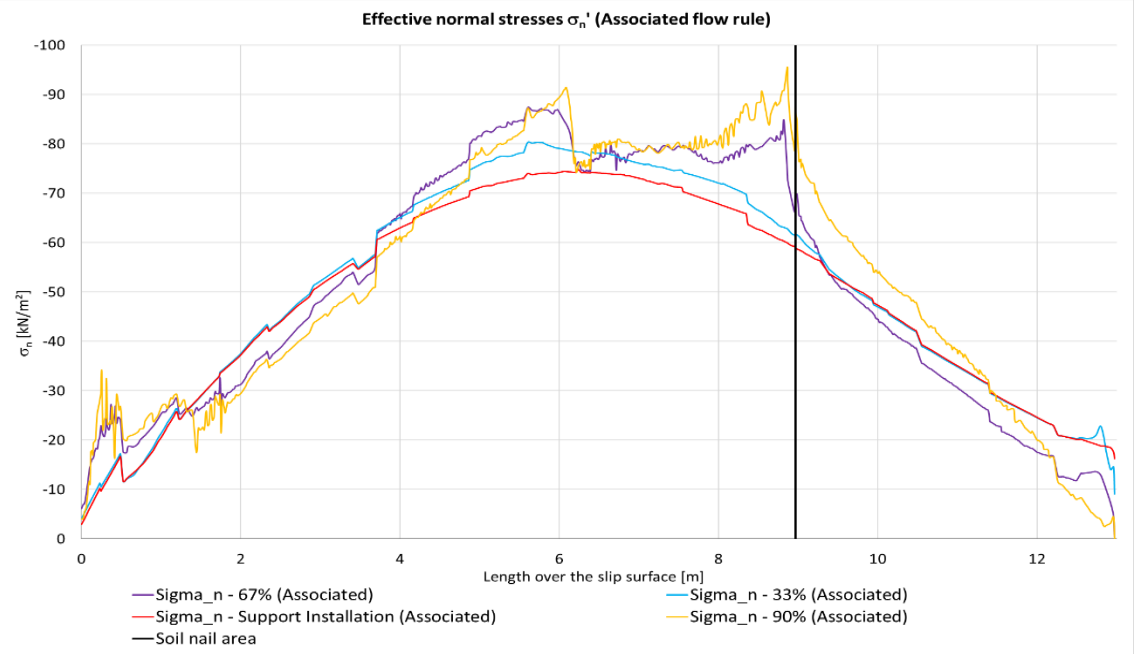

Figure 63 σ_n'/Slip surface length for the associated flow rule with one nail reinforcement of the MC-LE slope model

The following four diagrams (Figure 64, Figure 65, Figure 66 and Figure 67) show the development of all the stress indicators in the slip surface of the MC-LE model (for the associated flow rule).

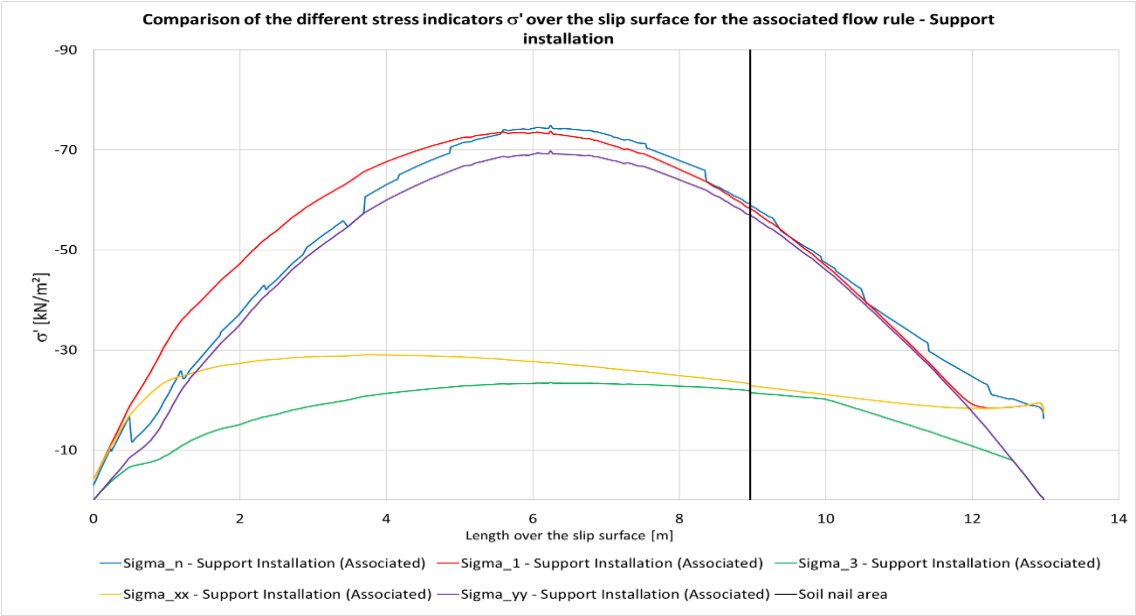

Figure 64 σ_i'/Slip surface length for the associated flow rule with one nail reinforcement of the MC-LE slope model (Support installation step)

The development of the stresses in the slip surface of a reinforced slope model (for the associated case) shows that the evolution of all the differently orientated stresses shows the same trend. In the first two evaluated steps (Support installation- and 33% step), the soil nail does not have a significant effect on the stresses along the slip surface. The soil nail effect cannot be observed until the 67%-step, where the stresses increase around the soil nail area and can be proven by the stress peaks near the soil nail (vertical black line) line in the Figure 66 and Figure 67. The σ_1', σ_3', σ_{yy}', σ_{xx}' results for the reinforced associated case are depicted and compared in detail in Appendix G.

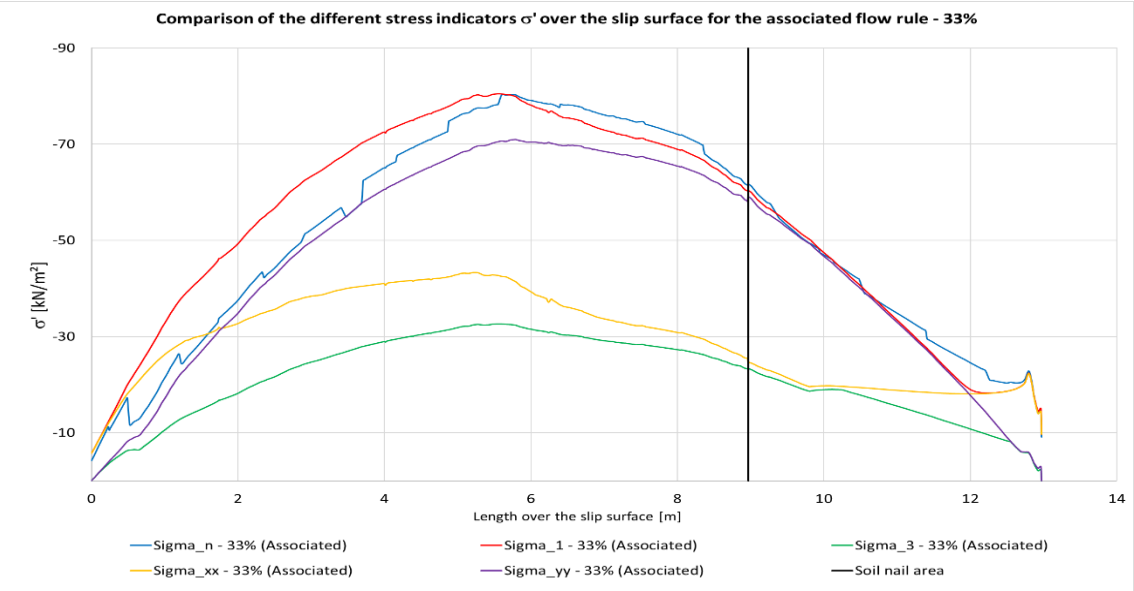

Figure 65 σ_i'/Slip surface length for the associated flow rule with one nail reinforcement of the MC-LE slope model (33%-step)

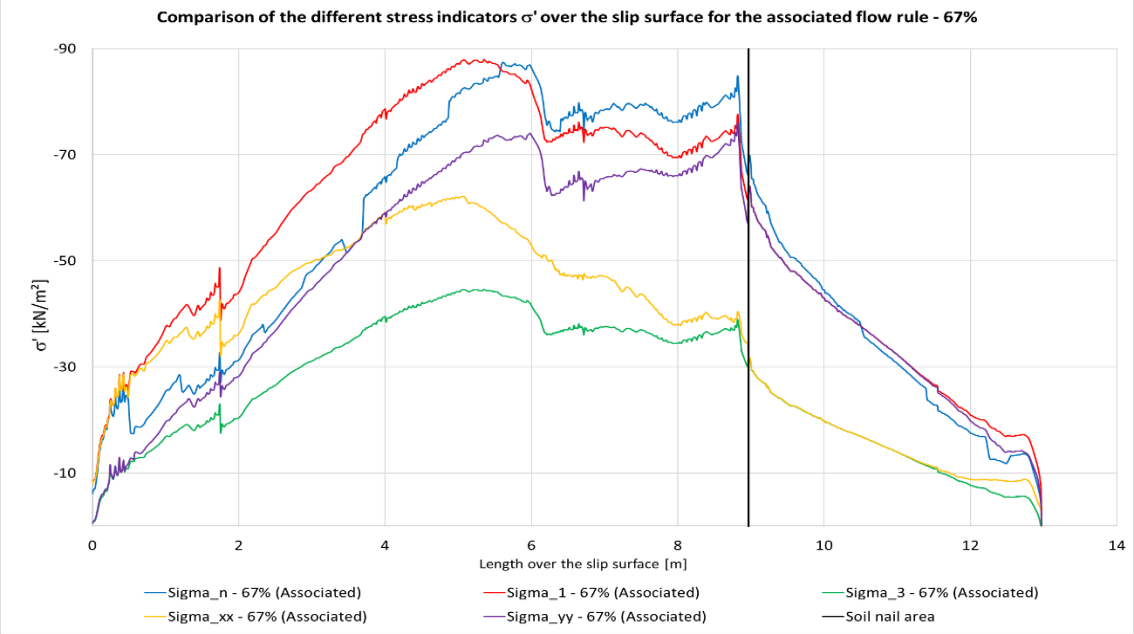

Figure 66 σ_i'/Slip surface length for the associated flow rule with one nail reinforcement of the MC-LE slope model (67%-step)

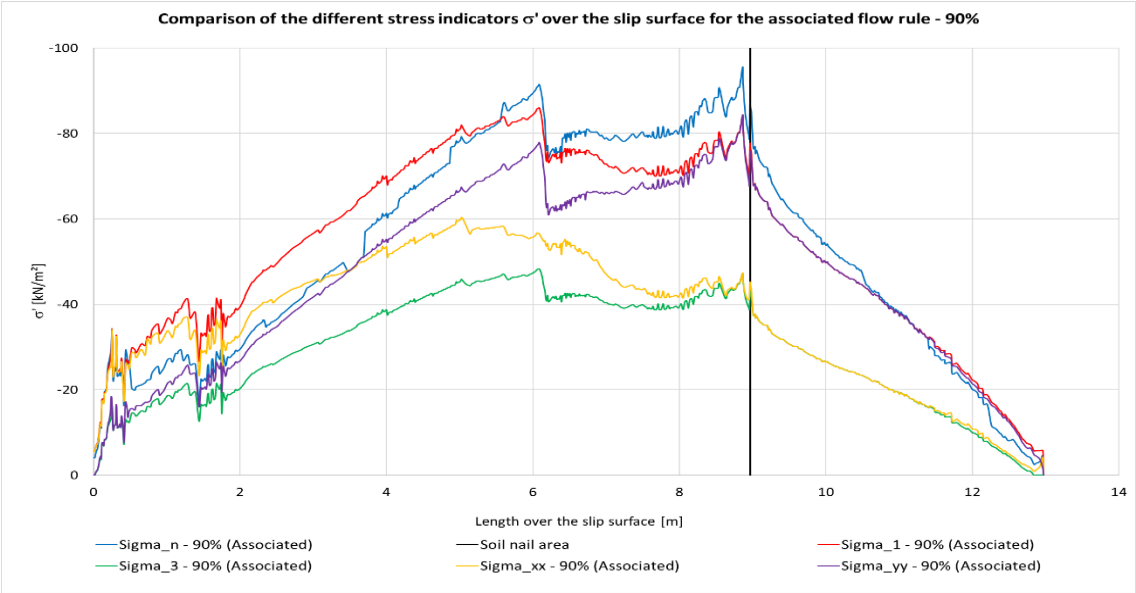

Figure 67 σ_i'/Slip surface length for the associated flow rule with one nail reinforcement of the MC-LE slope model (90%-step)

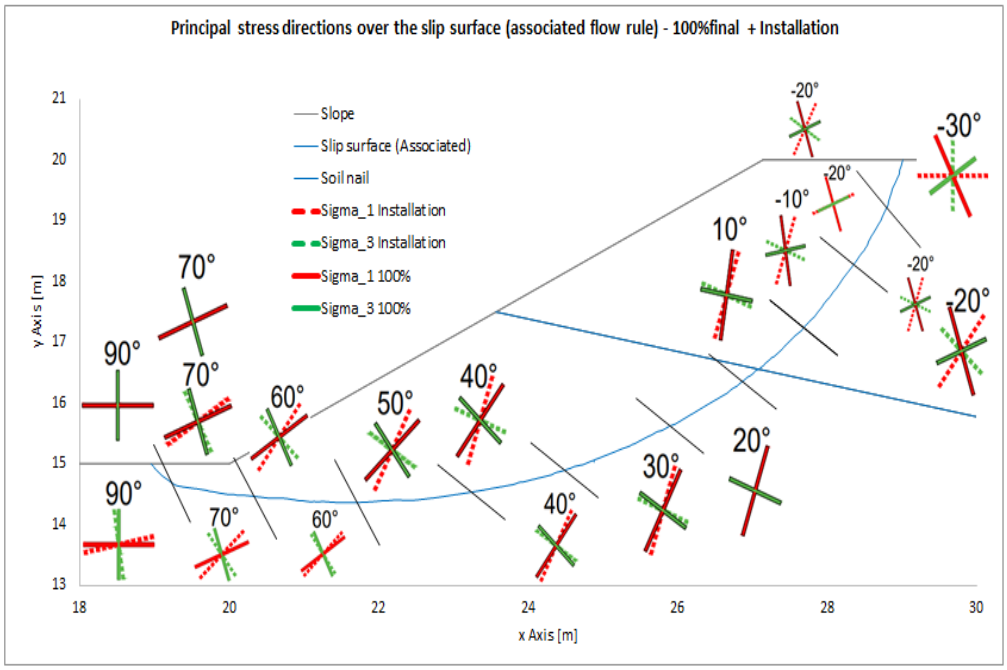

Figure 68 Principal stress directions for the non-associated flow rule with one nail reinforcement of the MC-LE slope model

The principal stress orientation depends on the slip surface formation.

Figure 69 shows σ_n' over the slip surface for the non-associated case of the 1-soil nail reinforced MC-LE model. The non-associated flow rule once again shows much more scattering in the final steps than the associated flow rule.

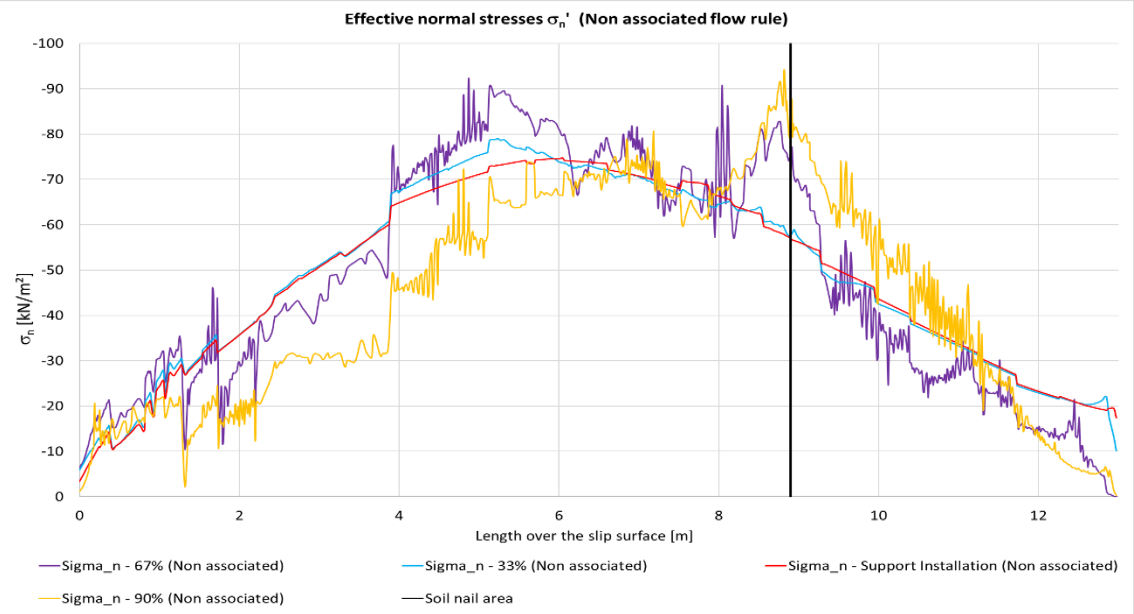

Figure 69 σ_n'/Slip surface length for the non-associated flow rule with one nail reinforcement of the MC-LE slope mode

The normal effective stresses fluctuate between the steps, but are increasing near the soil nail area. It can be seen that the soil nail effects on the distribution of effective normal stresses along the failure mechanism.

The next diagrams (Figure 70, Figure 71, Figure 72 and Figure 73) show all the stress indicators over the slip surface for the non-associated flow rule of the MC-LE model. Again, the stress distributions show much more scattering for non-associated plasticity compared to associated plasticity.

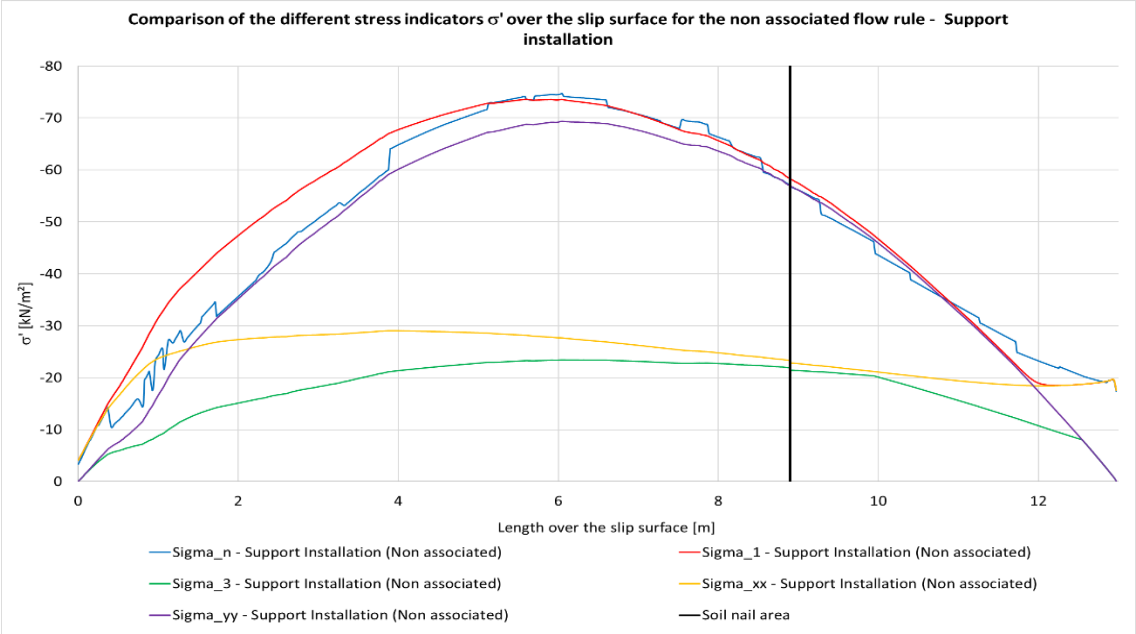

Figure 70 σ_i'/Slip surface length for the non-associated flow rule with one nail reinforcement of the MC-LE slope model (90%-step)

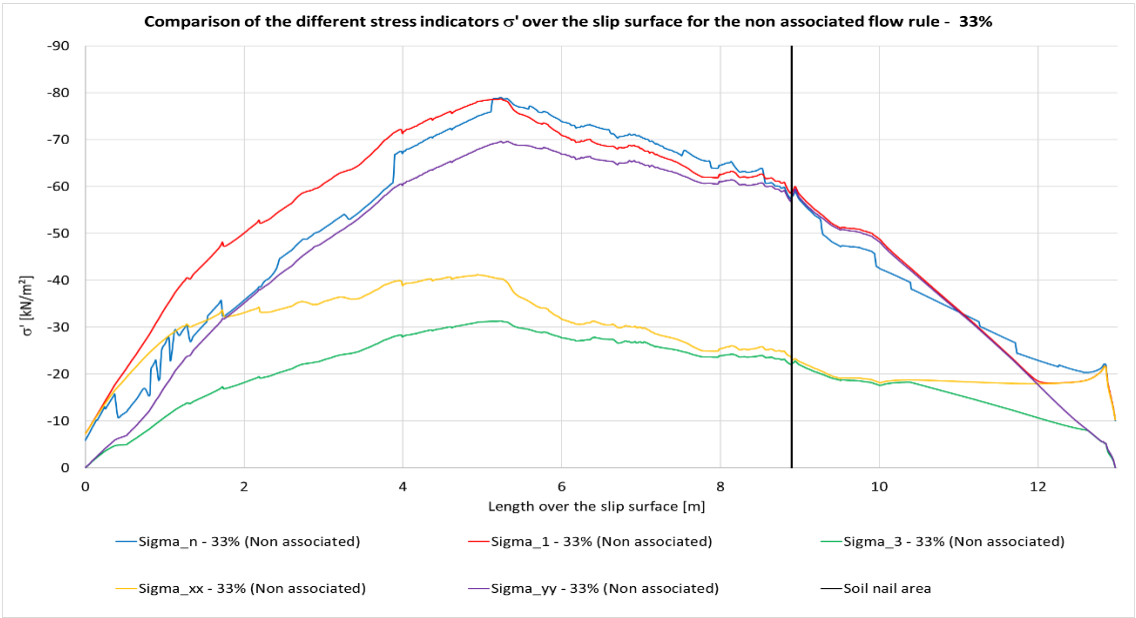

Figure 71 σ_i'/Slip surface length for the non-associated flow rule with one nail reinforcement of the MC-LE slope model (33%-step)

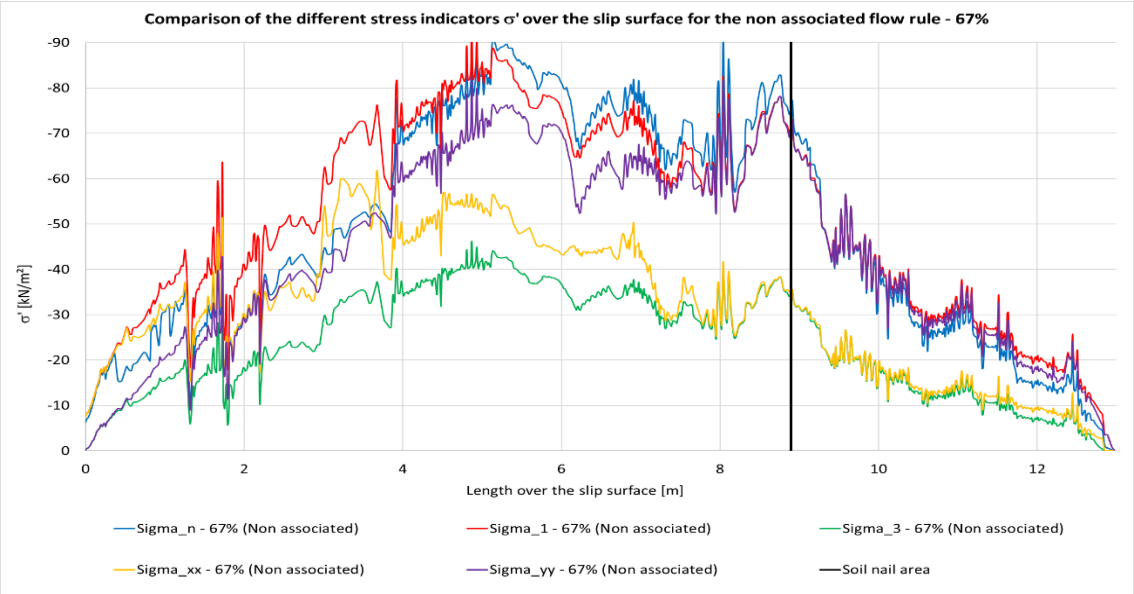

Figure 72 σ_i'/Slip surface length for the non-associated flow rule with one nail reinforcement of the MC-LE slope model (67%-step)

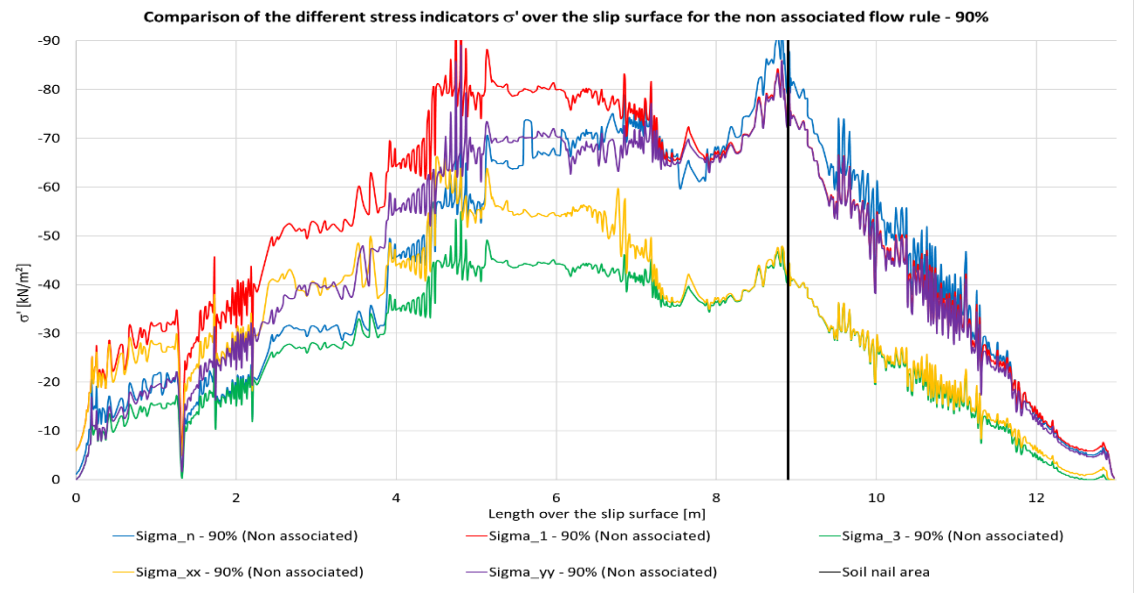

Figure 73 σ_i'/Slip surface length for the non-associated flow rule with one nail reinforcement of the MC-LE slope model (90%-step)

The soil nail of the non-associated case of the reinforced model is acting earlier (at 33%-step) on the stresses in the slip surface, then for the associated flow rule (an effect cannot be seen until at 67%).

The σ_1', σ_3', σ_{yy}', σ_{xx}' results for the reinforced non-associated case are discussed in detail in Appendix G.

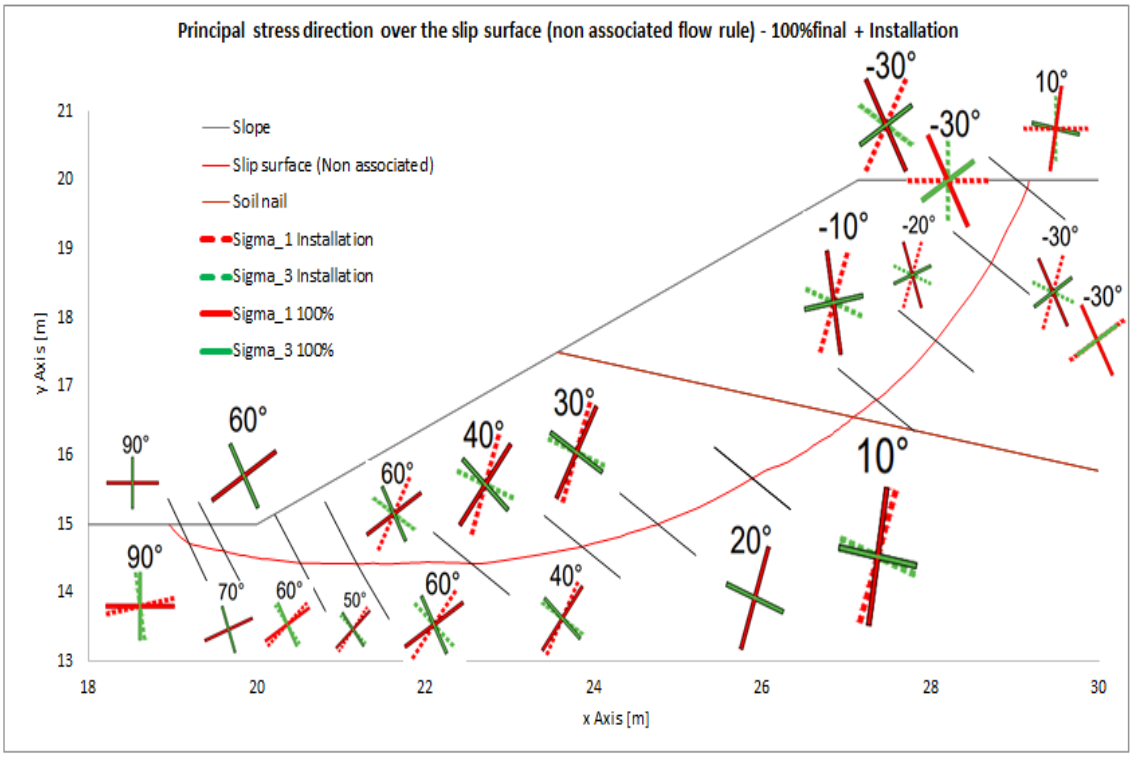

Figure 74 Principal stress direction evolution for the non-associated case of the one nail supported slope (MC-LE model)

Again, the (non-associated) principal stresses (Figure 74) show high scattering over the slip surface and their orientation depends on the slip surface course.

The direct comparison of the principal stress direction calculated with the associated and non-associated plasticity are shown in Appendix G

4.3.2.3 2D studies – three soil nail horizons

After the evaluation of the slope supported with one soil nail, the same analysis and evaluation were performed for the same slope, but reinforced by three soil nails (and a shotcrete wall). These three soil nails were modelled with a lower N_p (maximum axial tension soil nail force) in order, to obtain a slip surface through the three soil nails. The vertical black lines (in Figures: 75-84) indicate the three points of the slip surface where the three soil nails cut the slip surface.

The first results (Figure 75) show the effective normal stresses over the slip surface of the three soil nail supported slope (associated flow rule).

The stress line peaks near the soil nail lines indicate an influence of the soil nails on the effective normal stresses. The effective normal stresses increase with the safety calculation progression. For the three soil nail supported slope model, the stress increase stretches out over a longer section of the slip surface.

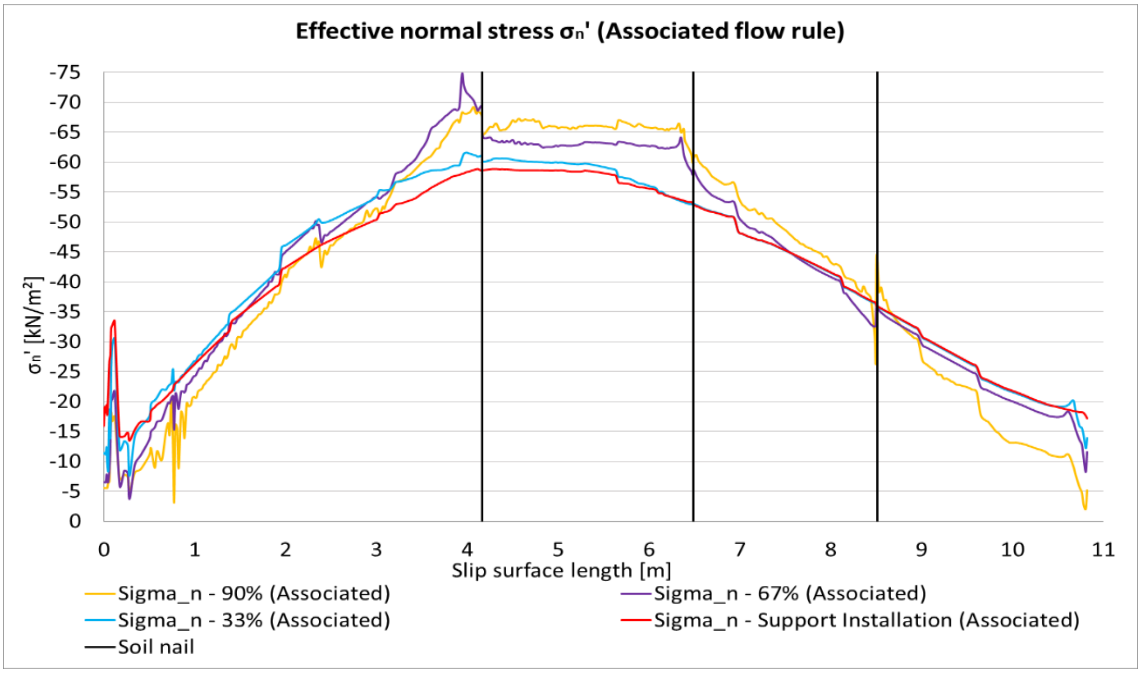

Figure 75 σ_n'/Slip surface length for the associated flow rule with 3 soil nails

The effect of the three soil nails on the effective normal stresses for the associated case cannot be observed until 67%-step (Figure 78). The peaks in Figure 78 and Figure 79 indicate the soil nail effect on the stresses along the slip surface. The lowest soil nail (left vertical black line) has an influence on the effective stresses in an earlier safety calculation step (at the 33%-step; Figure 77) in comparison to the other two soil nails.

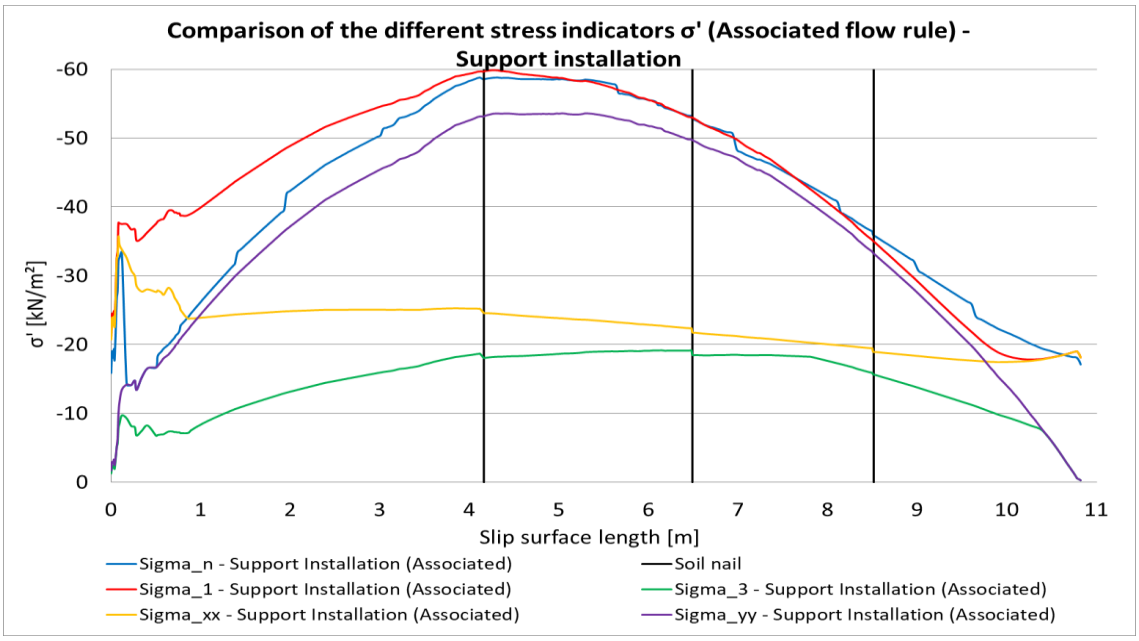

Figure 76 σ_i'/Slip surface length for the associated flow rule with 3 soil nails

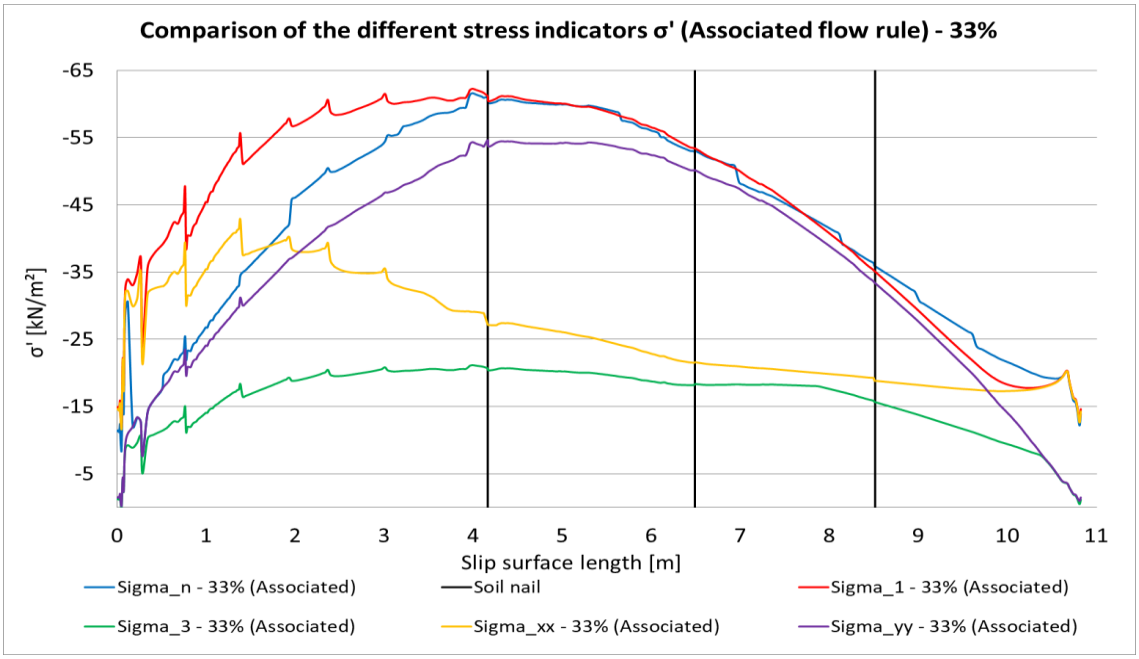

Figure 77 σ_i'/Slip surface length for the associated flow rule with 3 soil nails

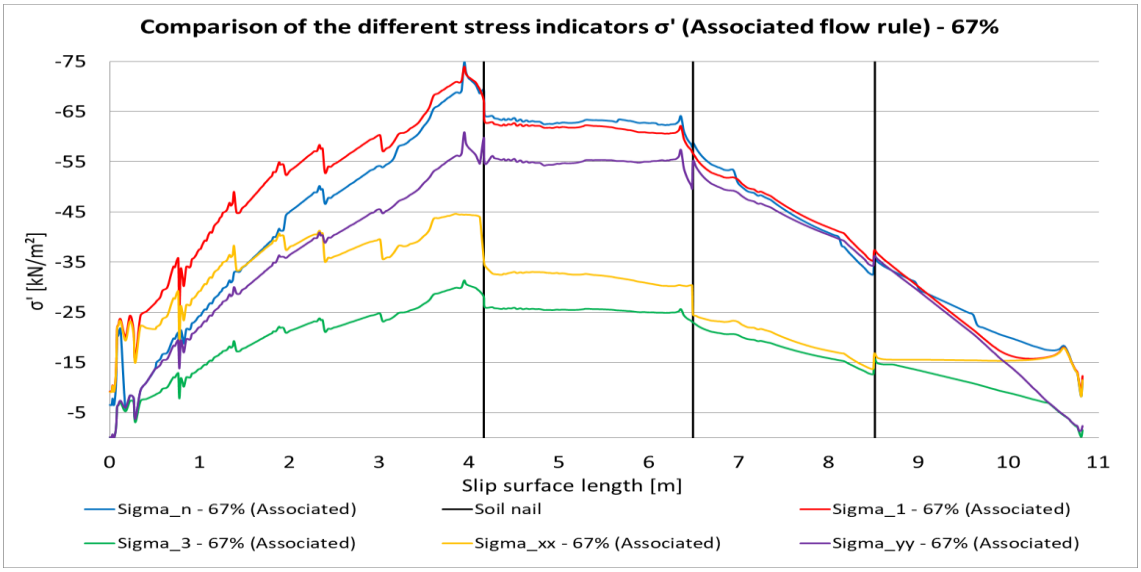

Figure 78 σ_i'/Slip surface length for the associated flow rule with 3 soil nails

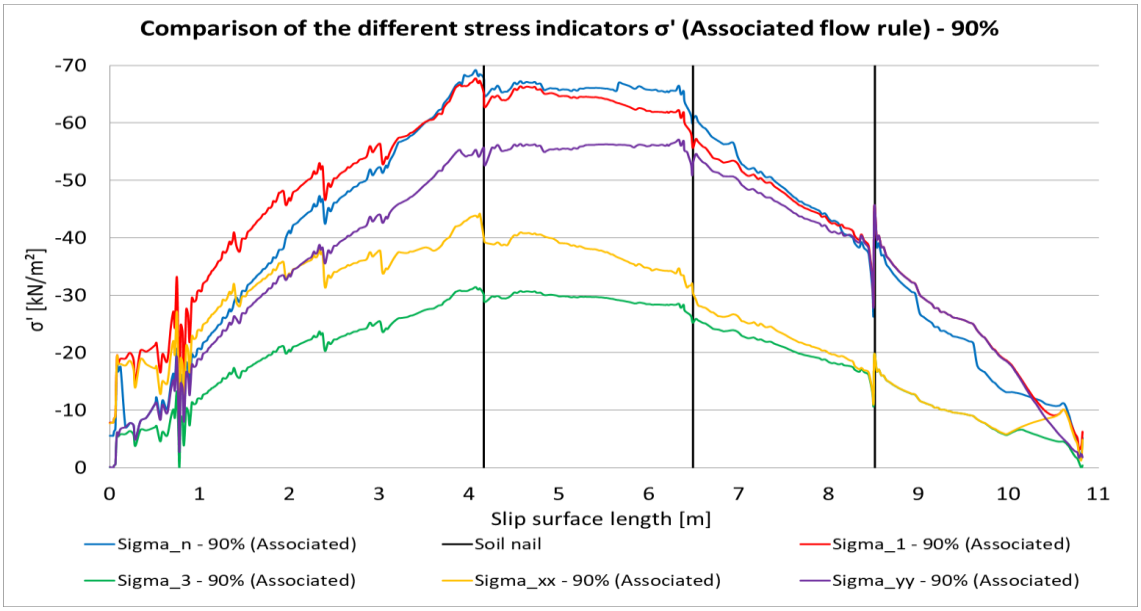

Figure 79 σ_i'/Slip surface length for the associated flow rule with 3 soil nails

The distribution of the normal effective stresses over the slip surface of the MC-LE model calculated with the non-associated flow rule are depicted in Figure 80. The stress scattering is strongly affected by the non-associated flow rule, so that the influence of the soil nail on the normal effective stresses is barely visible. A stronger increase of the 67%- (violet) and 90%- (orange) lines in the soil nail area indicate the soil nail influence.

There is no significant progression of the normal stresses between the steps of the non-associated calculation. Because of the scattering of the stress-lines, it is hard to detect the development of the normal effective stresses.

The σ_1', σ_3', σ_{yy}', σ_{xx}' results for the reinforced associated case of the three soil nail reinforced slope are shown in Appendix H.

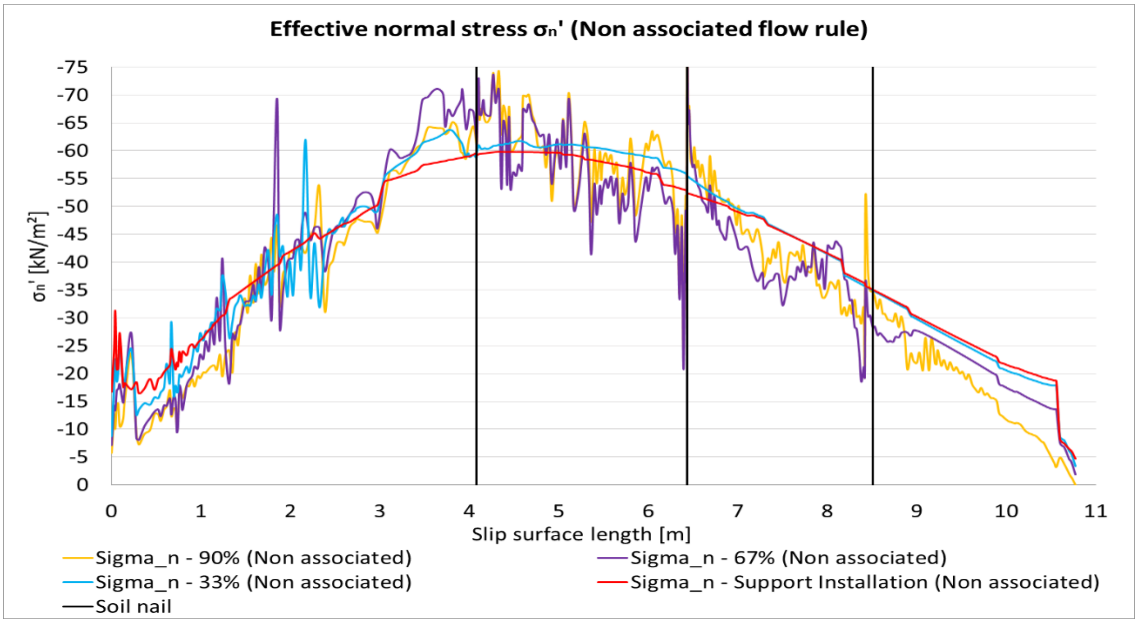

Figure 80 σ_n'/Slip surface length for the non-associated flow rule with 3 soil nails (MC-LE model)

The following σ'/|u| diagrams show all the stress indicators over the slip surface of the non-associated MC-LE model with a three soil nail horizon.

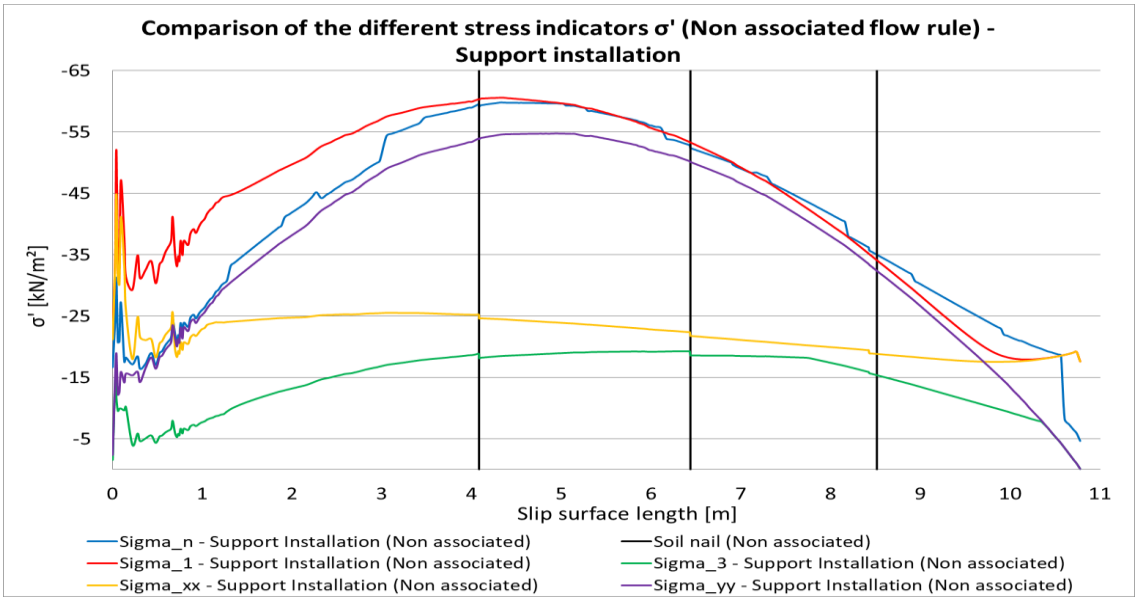

Figure 81 σ_i'/Slip surface length for the non-associated flow rule with 3 soil nails (MC-LE model) – Support installation-step

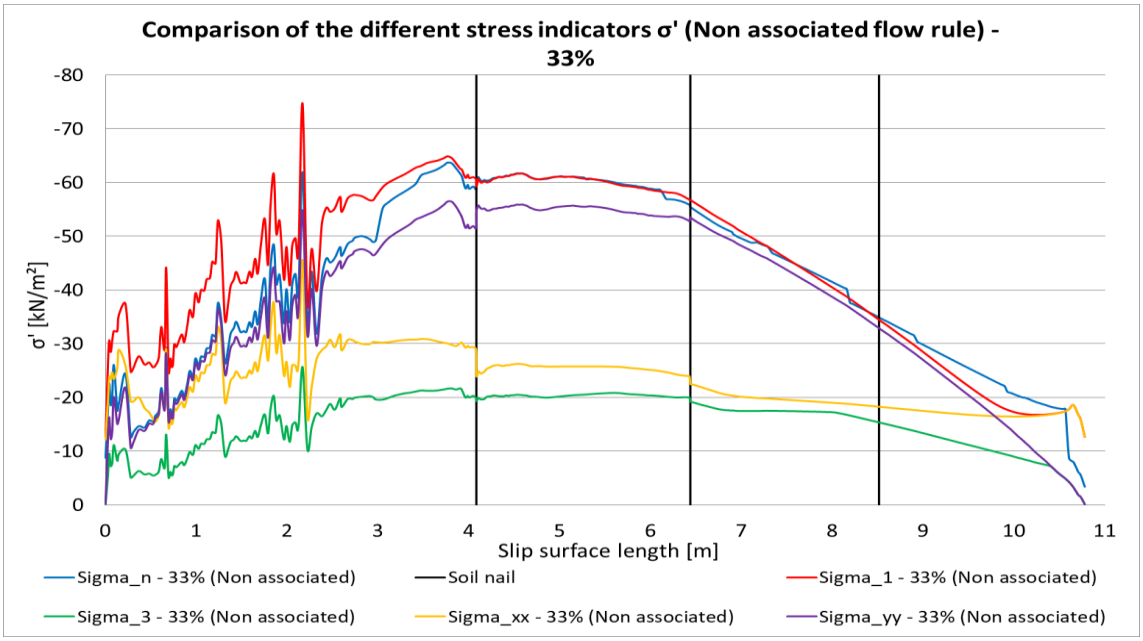

Figure 82 σ_i'/Slip surface length for the non-associated flow rule with 3 soil nails (MC-LE model) – 33%-step

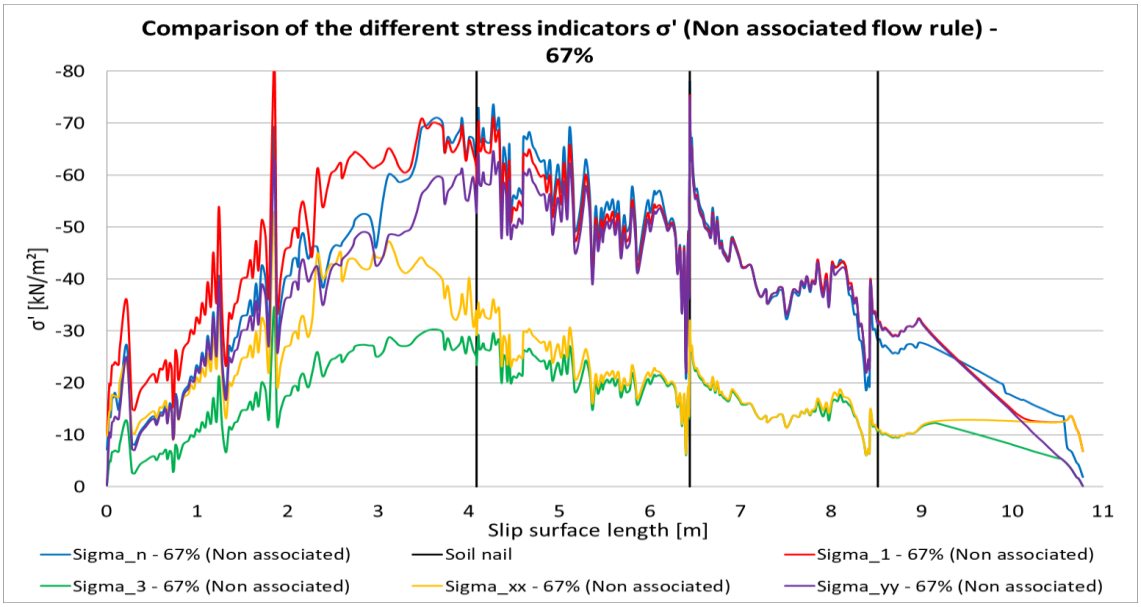

Figure 83 σ_i'/Slip surface length for the non-associated flow rule with 3 soil nails (MC-LE model) – 67%-step

The influence of the lowest soil nail (far left vertical black line) is visible in the 33%-step of the safety calculation (Figure 83).

The influence of the three soil nails is evident in Figure 82 and Figure 84. Higher stress line jumps occur in the soil nail areas.

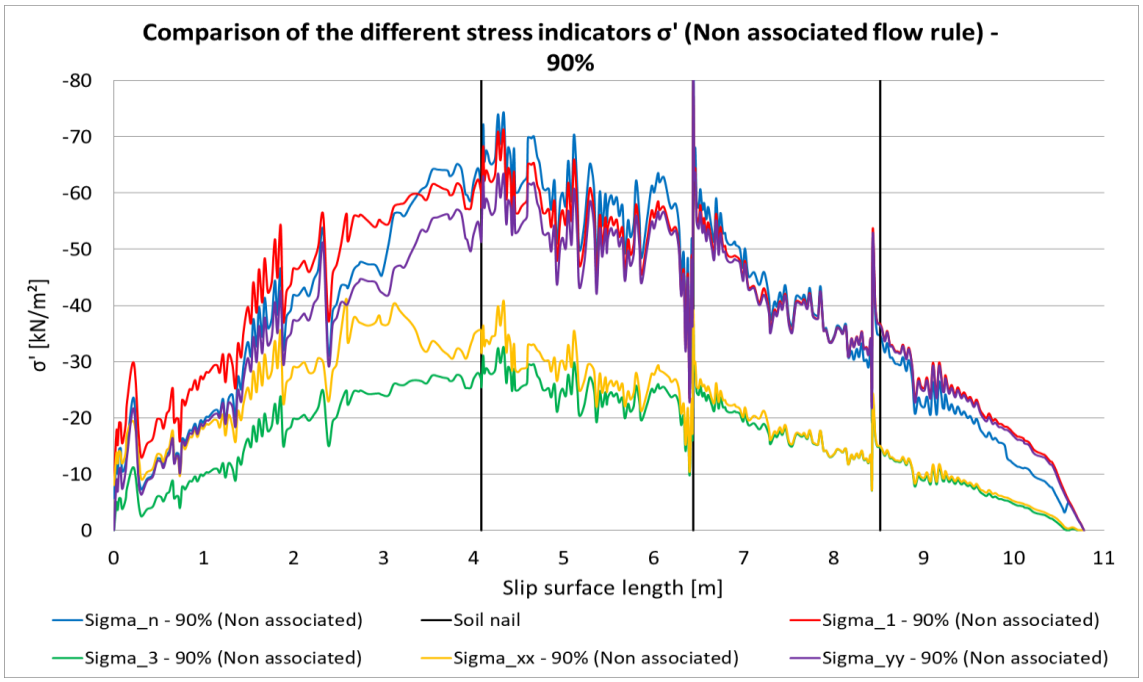

Figure 84 σ_i'/Slip surface length for the non-associated flow rule with 3 soil nails (MC-LE model) – 90%-step

The σ_1', σ_3', σ_{yy}', σ_{xx}' results for the reinforced non-associated case of the 3-soil nail-reinforced slope are discussed and compared to the stresses calculated with the associated plasticity in Appendix H.

- **Trend summary**

The effective stresses calculated with the associated flow rule show well shaped stress lines over the slip surface length. The effective stresses of the unsupported slope do not show a significant change between the calculation steps, but with the installation of the soil nails, the effective stresses in the slip surface are increasing with the increasing steps. For both supported cases (with 1 and with 3 soil nail horizons) the stress trend is an increasing one. Hence, the soil nails have an influence on the effective stresses. With one soil nail (N_p=66.67 [kN/m]) σ_n' shows an increase of about 80%. With three soil nails (N_p=10 [kN/m] for each one) the increase of σ_n' is about 45% compared to the stresses of the unsupported model. The 90%-stress lines were considered for this estimation.

The soil nail influence on the effective stresses begins at 67% for the one-soil nail-support. The influence of one of the three soil nails in the three-soil nail support starts at 33%-step, all three are having an effect at the effective stresses at 67%-step stress line.

The main problem in the stress results is the high fluctuation of the stresses calculated with the non-associated flow rule, which complicates the result interpretation.

The effective stresses calculated with the non-associated flow rule scatter immensely, as described previously. Because of this, no exact trend for the unsupported slope can be stated. However, an increase of the effective stresses with support compared to the unsupported case is evident. The increase of σ_n' of the one soil nail supported slope is about 60% and for the three-soil nail-supported slope it is about 30%.

The effective stresses calculated at different calculation steps of the non-associated flow rule do not show a tendency for the single soil nail supported slope, due to the high scattering of the stress lines. However, a tendency of the effective stresses of the three soil nail supported slope is at hand. The effective stresses increase with the step increase in the slip surface of the three-soil nail- supported slope

The effective stress influence of the soil nails for both reinforced cases (with one and with three soil nails) starts at the 33%-step stress line, which is evident earlier for the non-associated flow rule as it is for the associated flow rule.

4.4 Comparison of τ_{rel} + axial normal forces

In this chapter the relative shear stress, which is the ratio between the mobilised and the maximal shear stress, over the slip surface of the different MC/LE models calculated for both plasticity rules will be discussed. First, the unsupported case, the reinforced case with one and subsequently the case with three soil nail horizons is shown in this chapter.

For all cases, the relative shear stresses are approximating the maximal value of 1 with the increase of steps of the φ'/c' reduction.

For the unsupported cases and the 1-nail-supported cases, the 67%-step and the 90%-step relative shear line are not shown for the reason that they are almost equal to the 100%-step line. In addition, the 20%-step relative shear stress line was added to get a better understanding of the shear stress propagation. For the 3-nail-supported soil nail wall, the 67%- τ_{rel} line is shown, because of its dissimilarity to the other τ_{rel} lines.

The different coloured lines illustrate the calculated τ_{rel} for the corresponding step. The following coloured lines correspond to the related calculation steps:

- Nil step (for unsupported slope)/Support installation (for supported slope)– red line
- 20%-step of FoS – light green line
- 33%-step of FoS – light blue line
- 67%-step of FoS – violet line
- 100%-step of FoS – green line

The results calculated with the non-associated flow rule scatter slightly.

4.4.1 2D studies – unsupported slope

The relative shear stresses based on the non-associated plasticity reach the value of 1 faster (at an earlier calculation step), than during a φ'/c' reduction using an associated flow rule.

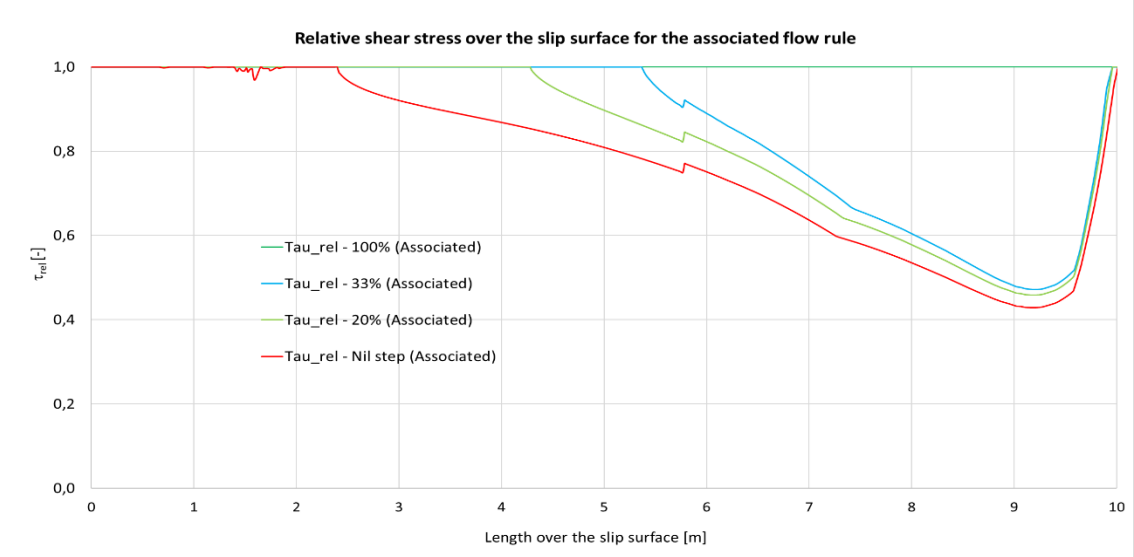

Figure 85 Relative shear stress over the slip surface for the unsupported MC-LE model (associated flow rule)

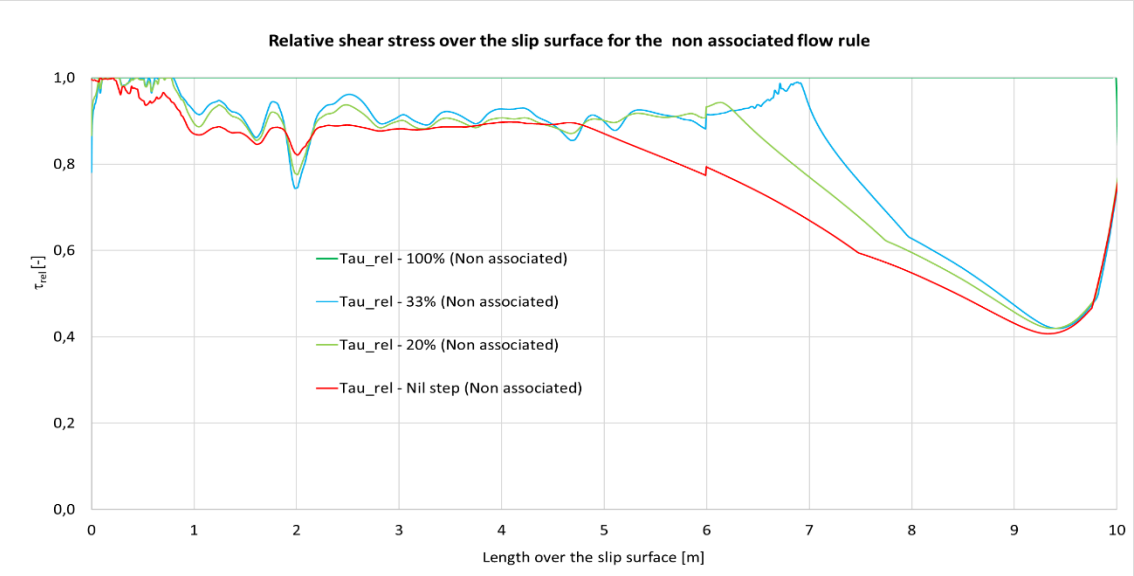

Figure 86 Relative shear stress over the slip surface for the unsupported MC-LE model (non-associated flow rule)

4.4.2 2D studies – one soil nail horizon

The diagrams of the relative shear stress of the one soil nail supported slope (Figure 87 for the associated and Figure 88 for the non-associated case) also show the maximum mobilised normal force in the nail for the corresponding safety calculation step. The colour of the soil nail force value corresponds to the same coloured step line.

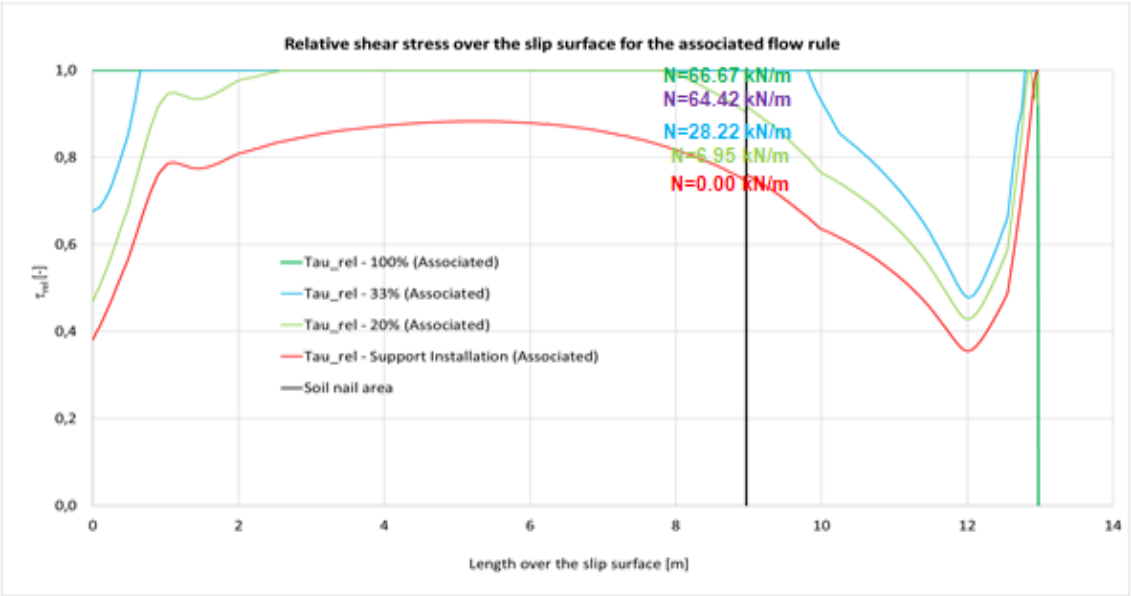

Figure 87 Relative shear stress over the slip surface for the supported MC-LE model (1 soil nail) calculated with the associated flow rule

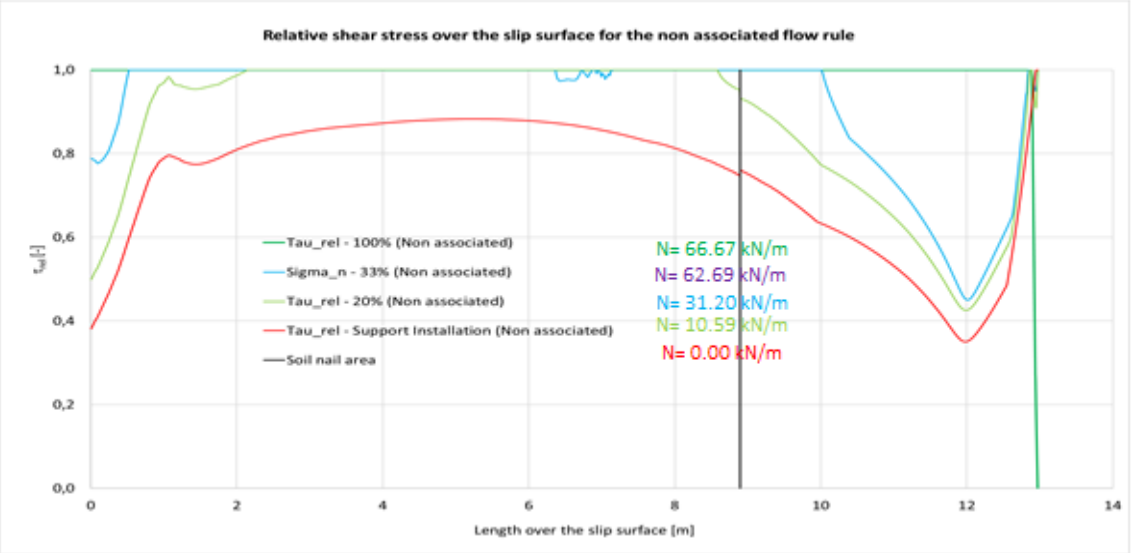

Figure 88 Relative shear stress over the slip surface for the supported MC-LE model (1 soil nail) calculated with the non-associated flow rule

The soil nail normal fore is increasing with the increase of the relative shear stress. It is evident that the internal normal forces of the soil nail do not increase linearly during the φ'/c' reduction. The internal soil nail normal force increases slightly faster for the non-associated calculation in comparison to the associated calculation.

4.4.3 2D studies – three soil nail horizons

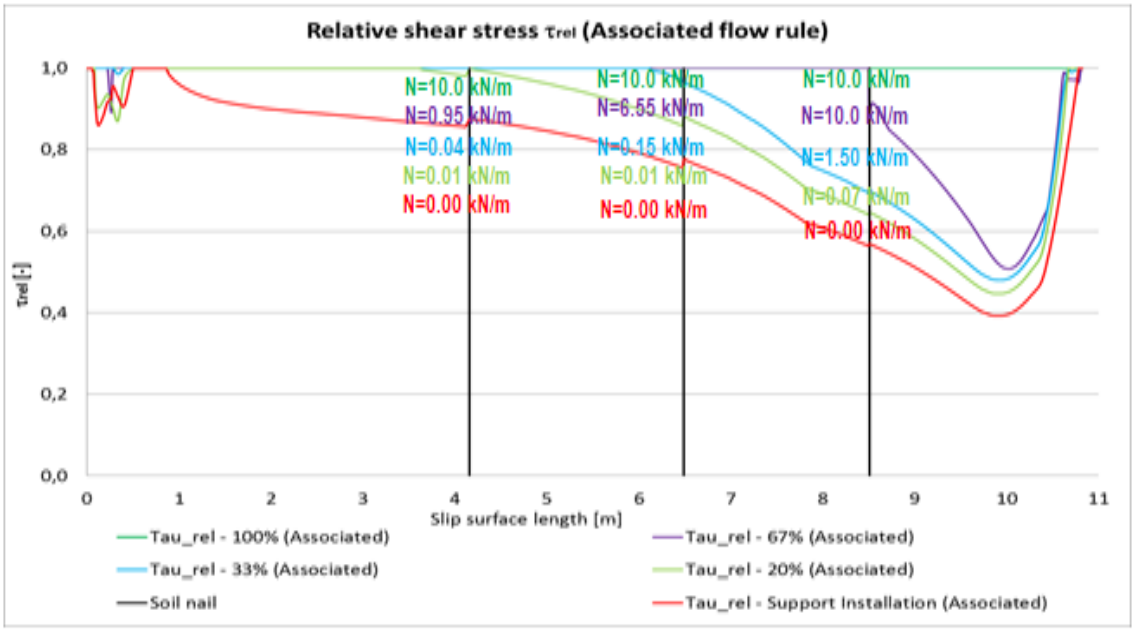

Figure 89 Relative shear stress over the slip surface for the supported MC-LE model (3 soil nails) calculated with the associated flow rule

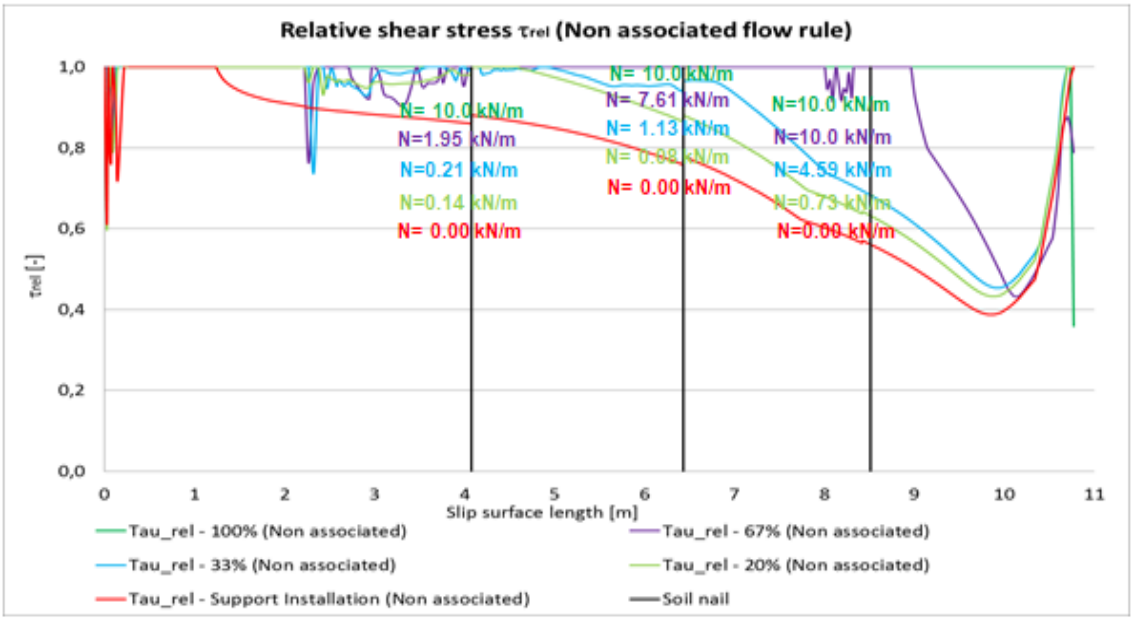

Figure 90 Relative shear stress over the slip surface for the supported MC-LE model (3 soil nails) calculated with the non-associated flow rule

For the cases with three soil nails (Figure 89 and Figure 90), it is also evident that the increase of the shear stress is proceeding faster for the non-associated flow rule than for the associated flow rule.

The third soil nail (the soil nail at the highest point of the slope) reaches its maximum tensile capacity ($N_{p,\,max}$) first (in the 67%-step).

5 Case study

5.1 Introduction

An existing excavation pit is investigated in a three dimensional analysis using PLAXIS 3D. The construction pit is supported by soil nail walls. Three types of soil nails are considered for the calculation: IBO, CLHS (t = 0) and CLHS (t = ∞), which are characterized by different stiffness's. The key point of interest of the analysis is the deformation behaviour of soil nails. Therefore, the HS model is used to describe the soil behaviour, since the HS model, in contrast to the standard MC model, takes the stress dependency of the stiffness into account. The results are evaluated in terms of factors of safety, soil nail deformations, axial forces in soil nails and bending of soil nails.

5.2 Model geometry and parameters

The excavation has a length of nearly 20 m and a width of almost 40 m. The ground surface inclination is assumed 4°. The shotcrete wall is disposed about 11° to the vertical. A total of 102 nails with an inclination of 11.3° are modelled on 4 horizons. The soil nails installed after the first excavation have a length of 4.5m and the other soil nails have a length of 7.5m. Figure 91 illustrates the finite element model as implemented in PLAXIS 3D.

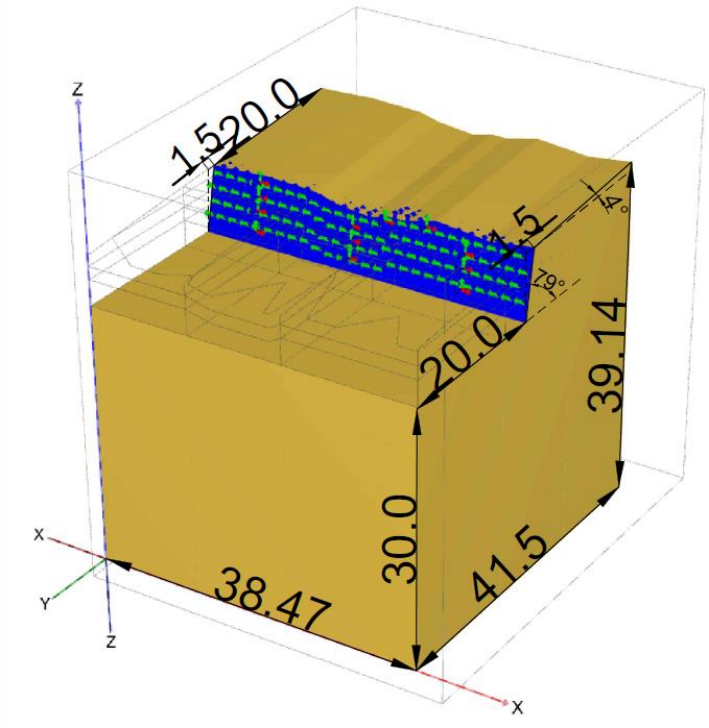

Figure 91 Geometry of the 3D PLAXIS model

The soil behaviour is modelled using the HS model and employing non-associated plasticity. Because of the uncertainties regarding the real behaviour of soil, two cases are considered for the non-associated plasticity. In the first case, the dilatancy angle is assumed 0° and in the latter 7°. The necessary input parameters for the soil are listed in Table 11.

The soil nails are modelled by means of Embedded Piles. Further information about the embedded pile approach is given in Chapter 2.2.3.2. For the IBO, a circular tube was selected, whereas the CLHS are modelled as „user defined“ EP, since only the cross sectional area was available to describe the geometry of these soil nails. The skin friction and yield stress are the same for all the soil nail types. The soil nails parameters are summarized in Table 12 and Table 13.

The shotcrete wall is modelled as an elastic plate element with a thickness of 20cm. The input parameters can be found in Appendix 1.

Table 11 Input parameters for HS soil

Soil parameters		
Material mode:	Hardening soil	
Drainage type:	Drained	
	CASE 1	CASE 2
γ_{unsat} [kN/m³]	20	20
γ_{sat} [kN/m³]	20	20
E_{50} [kN/m²]	40,000	40,000
E_{oed} [kN/m²]	40,000	40,000
E_{ur} [kN/m²]	120,000	120,000
m [-]	0.7	0.7
ν_{ur} ' [-]	0.2	0.2
c' [kN/m²]	0	0
φ' [°]	32.5	32.5
ψ' [°]	0	7

R_{inter}	0.8	0.8

Table 12 CLHS soil nail parameters

CLHS soil nail parameter sets		
	CLHS (t=0)	**CLHS (t=∞)**
Set type:	Embedded beams	Embedded beams
Material type:	Elastoplastic	Elastoplastic
E [kN/m²]	$4.728*10^{6}$	$7.626*10^{6}$
γ [kN/m³]	79	79
Pile type:	User defined	User defined
A [m²]:	$5.212*10^{-3}$	$5.212*10^{-3}$
I_2 [m⁴]	$4.353*10^{-6}$	$4.353*10^{-6}$
I_3 [m⁴]	$4.353*10^{-6}$	$4.353*10^{-6}$
Yield stress σ_y [kN/m²]	$470*10^{3}$	$470*10^{3}$
W_2 [m³]	$0.05027*10^{-3}$	$0.05027*10^{-3}$
$T_{skin,start,max}$ [kN/m]	30	30
$T_{skin,end,max}$ [kN/m]	30	30
F_{max} [kN]	210	210

Table 13 IBO soil nail parameters

IBO soil nail parameters	
Set type:	Embedded beams
Material type:	Elastoplastic
E [kN/m²]	$210*10^{6}$
γ [kN/m³]	79

Pile type:	Predefined
Predefined pile type:	Circular tube
d [m]:	0.032
t [m]:	0.0101
Yield stress σ_y [kN/m²]	$470*10^3$
$T_{skin,start,max}$ [kN/m]	30
$T_{skin,end,max}$ [kN/m]	30
F_{max} [kN]	210

For the discretization of the model 10-noded elements are used. A finer mesh is generated in the soil region near the shotcrete wall, where the soil nails are situated. The model consists of nearly 236,000 elements (Figure 92)

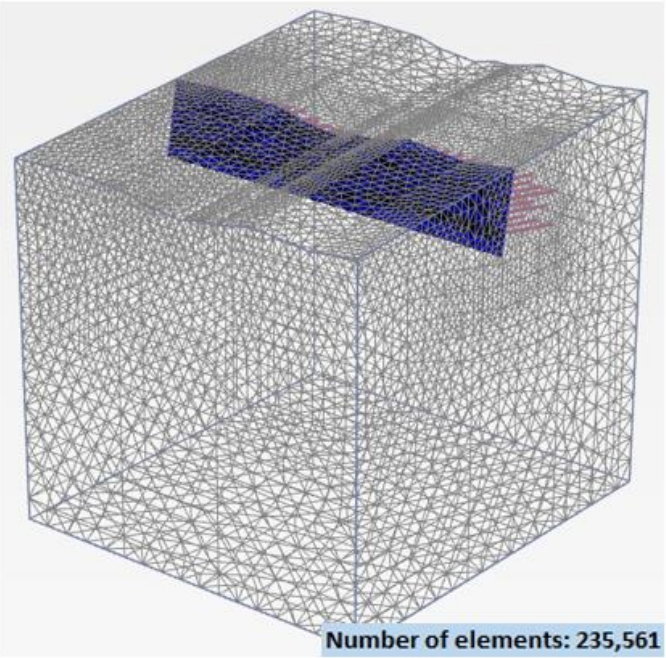

Figure 92 Model mesh in Plaxis 3D

5.3 Calculation phases

To obtain realistic representation of the deformation behaviour and stress distribution after the excavation, it is necessary to simulate the real construction process. The excavation is carried out in four excavation steps. The soil nails are installed 0.5 m above the bottom level of each excavation step. The following phases are preformed in the calculation:

- Generation of initial stresses by gravity loading
- Plastic nil step
- First excavation step to -1.3m (soil body deactivated, activation of shotcrete wall and soil nails)
- Second excavation step to -2.8m (soil body deactivated, activation of shotcrete wall and soil nails)
- Third excavation step to -4.3m (soil body deactivated, activation of shotcrete wall and soil nails)
- Fourth excavation step to -5.6m (soil body deactivated, activation of shotcrete wall and soil nails)
- Safety Calculation

An overview of the excavation steps performed in PLAXIS 3D is given in the following figure (Figure 93).

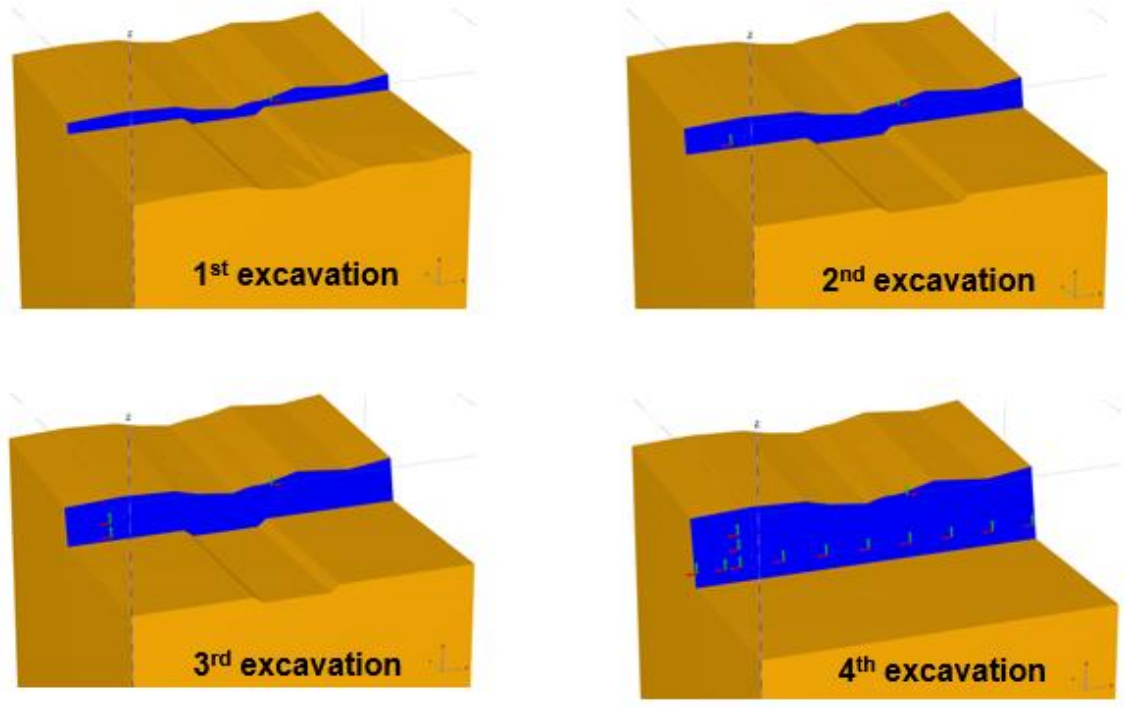

Figure 93 Excavation steps in PLAXIS 3D

5.4 Results

For the investigation of the soil nails behaviour a cross section is selected. A schematization of the selected cross section is illustrated in Figure 94.

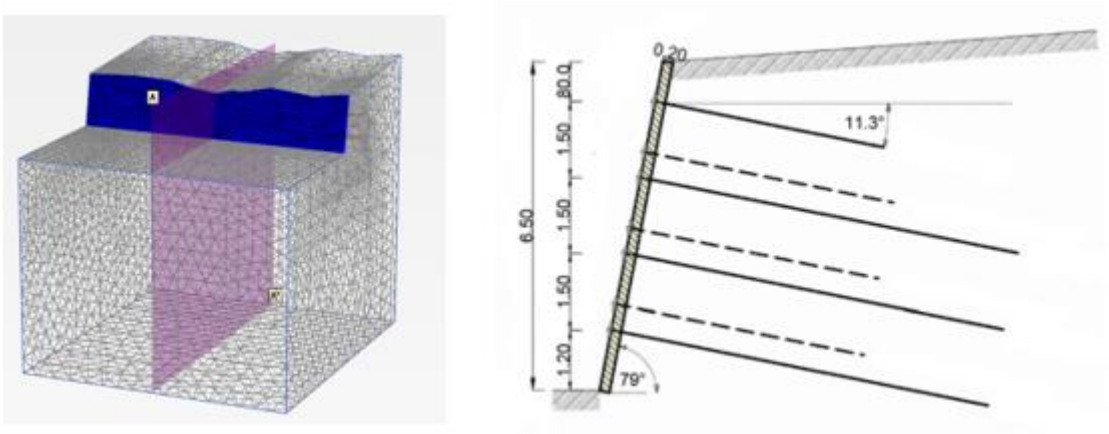

Figure 94 Selected cross section (left) and the cross section geometry (right)

The factors of safety for the different soil nails are calculated in PLAXIS 3D. Furthermore, the results for the „2nd soil nail“ and the „4th soil nail“ are evaluated in terms of deformations, axial forces and bending. The results for the other soil nails are provided in Appendix K. The evaluation of bending of soil nails can be found in Appendix K.

5.4.1 Factor of safety

As previously mentioned, the soil model employs non-associated plasticity with two different dilatancy angles, namely 0° and 7°. Factors of safety are calculated for the different soil nails and both soil parameter sets. The results of the computation are summarized in Table 14 The plots for „Msf/|u|“ for all investigated cases can be found in Appendix J.

Table 14 FoS for all the three analysed soil nails for the two different soil parameters

Soil nail type	Factor of safety	
	φ'=32.5° and ψ'=0°	φ'=32.5° and ψ'=7°
IBO	1.47	1.49
CLHS (t=0)	1.50	1.52

CLHS (t=∞)	1.50	1.52

The results show that the safety factor is affected by the dilatancy angle. For all types of soil nails, the FoS increases with increasing dilatancy angle.

Furthermore, it can be seen that the FoS for the stiffer IBO is slightly higher than for CLHS soil nails.

Figure 95 shows the failure mechanisms for the case with a dilatancy angle of 0°. As it can be seen, the failure mechanisms are similar for all soil nail types.

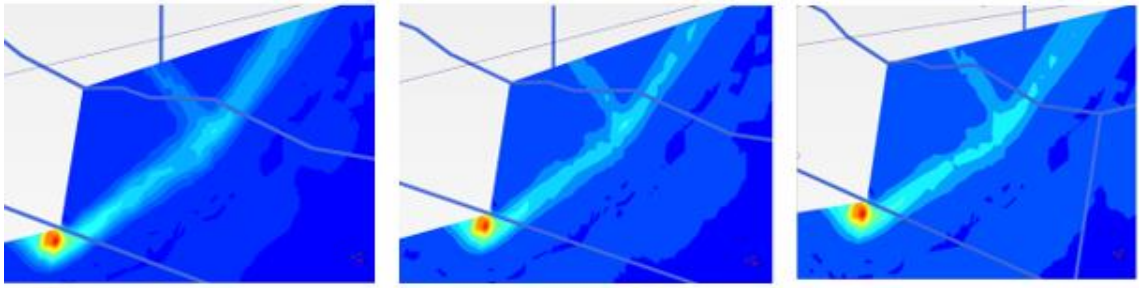

Figure 95 Failure mechanisms for IBO (left), CLHS (t=0)(middle) and CLHS (t=∞) (right) ($\psi = 0°$)

5.4.2 Soil nail deformation

To analyse the deformation behaviour of soil nails, only the case with dilatancy angle equal to 0° is considered. The displacements in the vertical direction along the soil nail for the 2nd and 4th soil nails are illustrated in Figure 96 and Figure 97, respectively. The different colours indicate the different soil nail types (red – IBO, green - CLHS (t=∞), blue - CLHS (t=0)). To distinguish between the excavation stages, different line styles are used (dotted – 2nd excavation stage, dashed – 3rd excavation stage, solid – 4th excavation stage).

The maximum displacements occur at the connection point to the shotcrete wall and decrease along the length of the soil nails. A minimal displacement is still present at the end of the nails.

Obviously, the stiffer soil nails (IBO) show less displacements compared to CLHS (t=0) and CLHS (t=∞), which has the lowest Young´s modulus and as a result shows the highest deformations.

The discrepancies between the displacements of the different soil nails become more evident when progressing the excavation process. After the last excavation

step, the displacements of the flexible CLHS (t=∞) are significantly higher than the displacements shown by IBO.

The same behaviour is observed for the 4th soil nail, as shown in Figure 97.

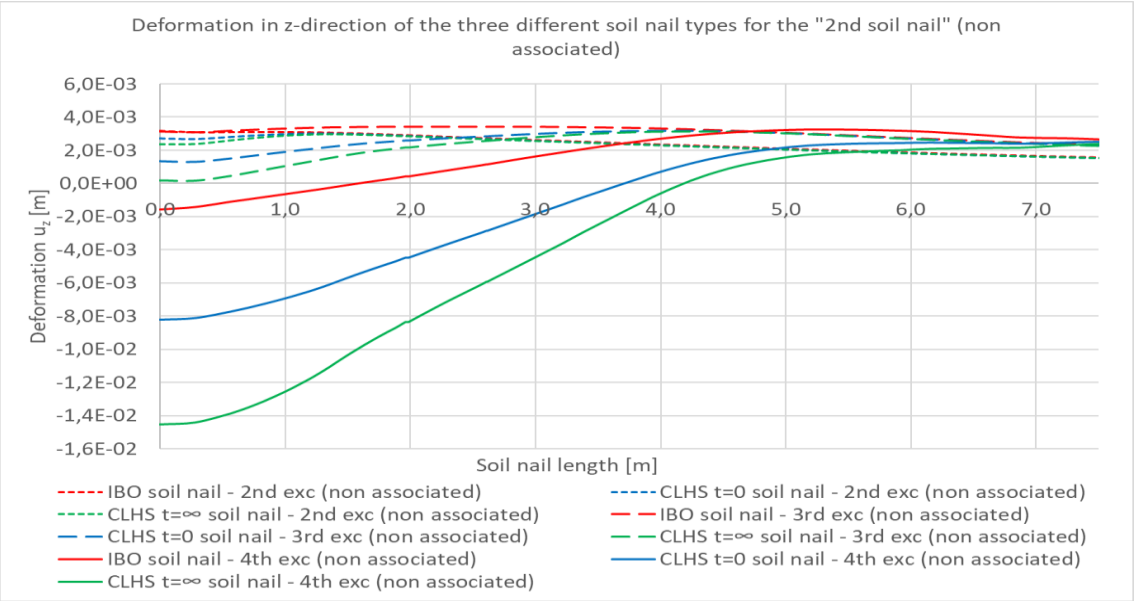

Figure 96 Displacements of the 2nd soil nail in the z-direction, from the 2nd to the 4th excavation

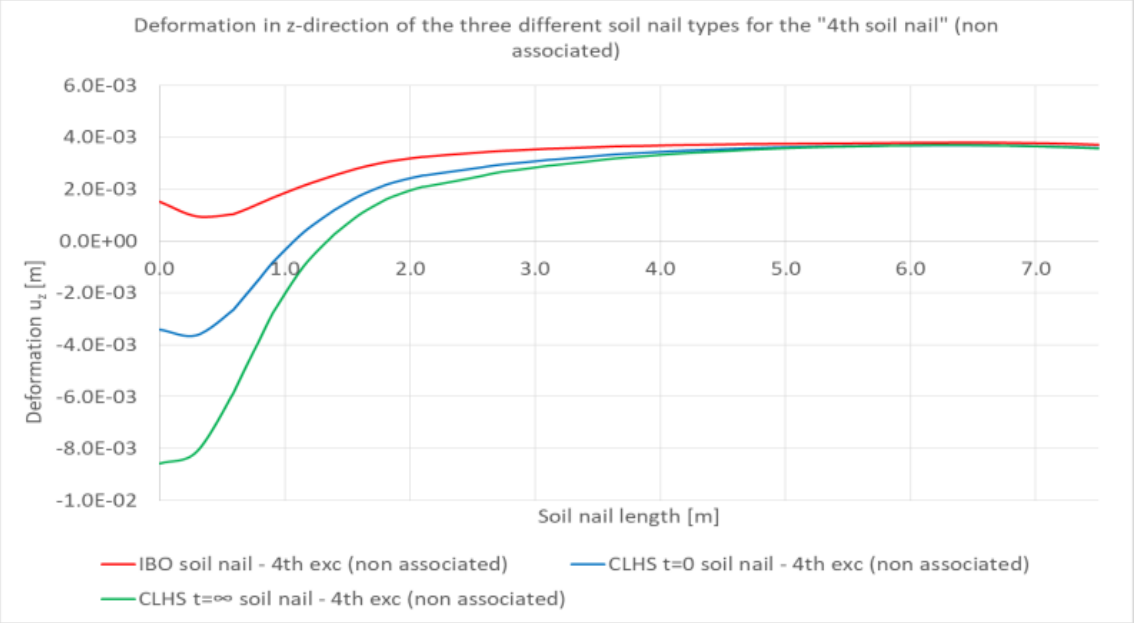

Figure 97 Displacements in z-direction of the 4th soil nail after the 4th excavation

5.4.3 Axial forces of soil nails

The normal force distribution is evaluated for non-associated plasticity, assuming a dilatancy angle of 0°. The axial forces for the 2nd and 4th soil nail are presented in Figure 98 and Figure 99 respectively. It can be seen that the axial forces in the soil nails increase during the excavation process.

The axial forces in the soil nails after the second and third excavation step reveal a different behaviour compared to the end stage. While in the former case (2nd and 3rd excavation stage), the maximum force is reached in about 0.5m distance from the shotcrete wall and then decreases almost linearly towards the soil nail end, in the latter a significantly higher mobilisation of the axial forces along the entire soil nail length is observed.

Furthermore, it can be observed that the stiffness of the soil nails affects the axial force generated in the nails. Stiffer soil nails (IBO) transfer a higher load along their length. The difference in the axial force distribution for CLHS (t = ∞) and CLHS (t = 0) is minimal.

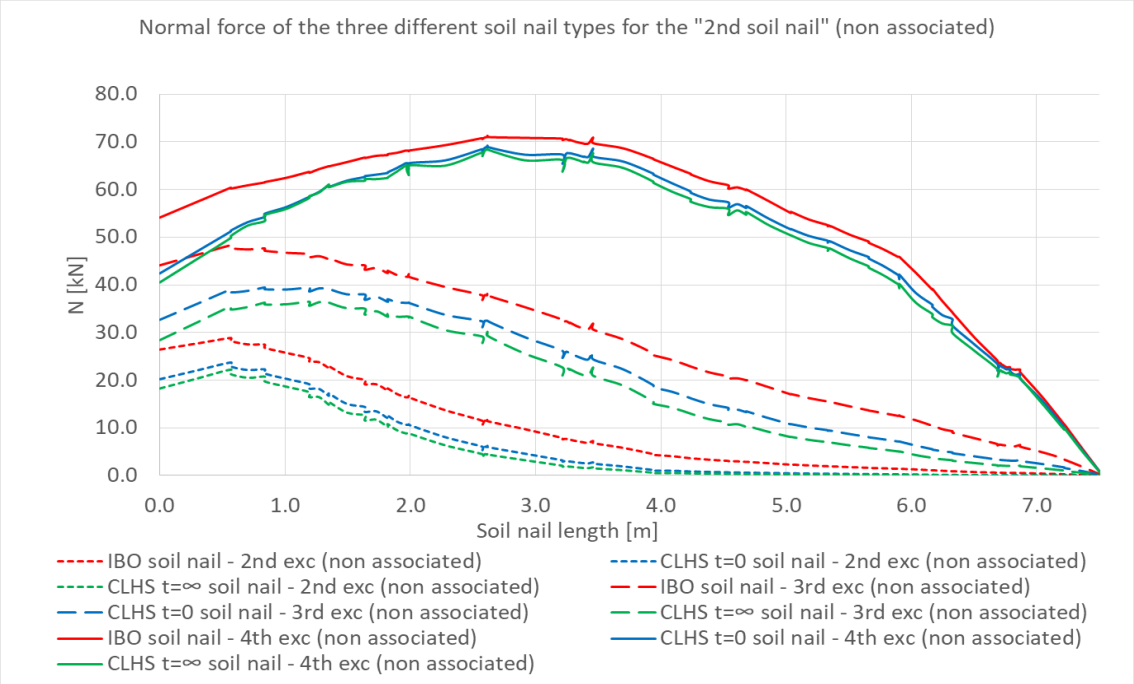

Figure 98 Axial forces in the 2nd soil nail for various excavation steps (ψ = 0°)

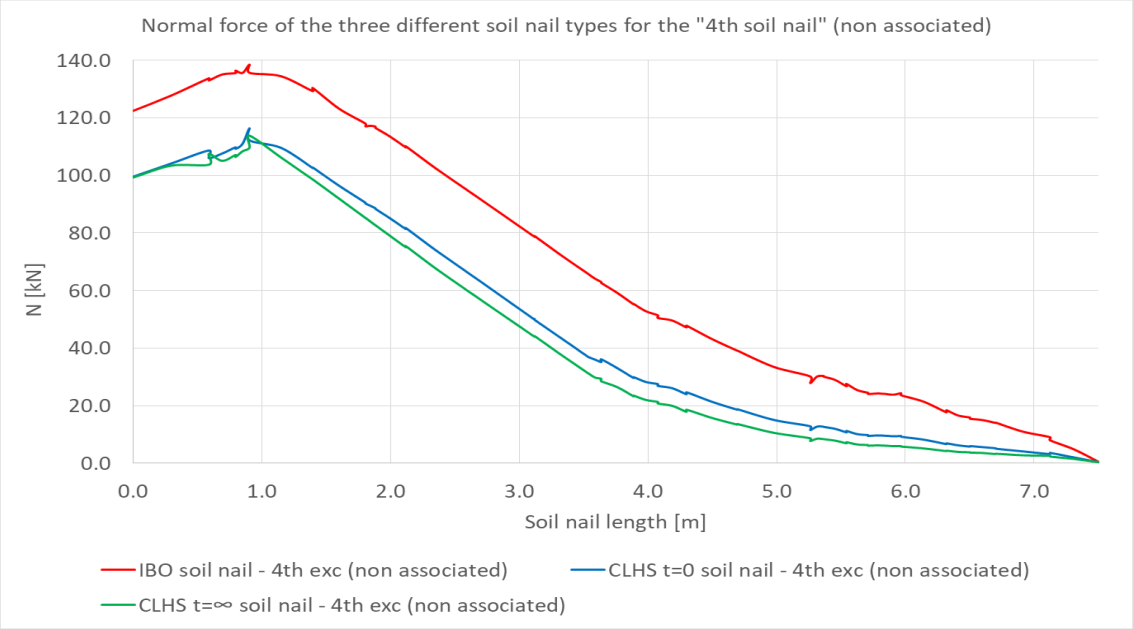

Figure 99 Axial forces in the 4th soil nail for various excavation steps ($\psi = 0°$)

6 Conclusion

The flow rule generally affects the safety analyis. The influence of the flow rule on the failure mechanism of unsupported and supported slopes was investigated in this study. Following conclusions can be drawn regarding homogeneous slopes modelled with MC:

- The safety factor for homogeneous slopes modelled with MC and associated flow rule is slightly higher compared to the case with non-associated plasticity.

- When assuming non-associated plasticity, the stresses on the slip surface of the unsupported slope decrease during the Phi/c reduction. For associated plasticity, no clear statement can be given.

- The soil nails affect the stress distribution along the failure surface. For both associated and non-associated flow rule, the stresses increase during the safety calculation.

- The failure mechanisms obtained from limit analyses and Phi/c reduction agree well for unsupported slopes. In case of supported slopes, different safety factors are calculated, due to the different forces generated in the geogrid (PLAXIS 2D) and soil nail (SLIDE).

A special model was implemented in PLAXIS 2D in order to get the same failure mechanism for associated and non-associated plasticity. The numerical study lead to the following conclusions:

- When employing associated flow rule, the stresses along the slip surface of the unsupported slope decrease during the phi/c reduction. The non-associated case gives erratic stress results, which are not easily interpretable.

- In the case of supported slope by one soil nail horizon, the results obtained with associated plasticity do not reveal a clear stress tendency, while assuming non-associated plasticity leads to higher normal effective stresses during the strength reduction procedure.

- The results of the calculation for the slope supported by three soil nail horizons and in which associated flow rule is applied, show an increasing tendency of the stresses. On the other hand, the stresses computed assuming non-associated plasticity remain constant during the safety calculation.

- The deviatoric stresses show a decreasing trend for all the investigated cases.

- The shear stresses, together with the normal forces in soil nails increase with the proceeding of the safety calculation.

- The direction of principle stresses depends on the slip surface orientation. The principal stresses rotate towards the slip surface during the Phi/c reduction.

7 Literature

Brinkgreve, R. &. e. a., 2018. *PLAXIS 2D 2018 - Material Models Manual.* Delft, The Netherlands: Plaxis bv..

Brinkgreve, R. &. e. a., 2018. *PLAXIS 2D 2018 - Reference Manual.* Delft, The Netherlands: Plaxis bv..

Brinkgreve, R. &. e. a., 2018. *PLAXIS 3D - Reference Manual.* Delft, The Netherlands: Plaxis bv..

Havinga, M., 2016. *Advanced Soil Mechanics: Lecture notes.* Graz University of Technology: Institute of Soil Mechanics and Foundation Engineering.

Lehner, P., 2016. *Untersuchungen zum Tragverhalten von Bodennägel,* Graz: Graz University of Technology.

Marte, R., 2016. *Advanced Soil Mechanics: Lecture notes.* Graz University of Technology: Institute of Soil Mechanics and Foundation Engineering.

Mosser, C., 2016. *Numerical Study on the Behaviour of Soil Nails. Master´s Thesis,* Graz: Graz University of Technology.

NPTEL, 2009. *NPTEL.* [Online]
Available at: https://nptel.ac.in/
[Accessed 29 October 2018].

Oberhollenzer, S., 2017. *Numerical studies on slope stability analysis. Master thesis,* Graz, Austria: Technical University of Graz.

ResearchGate, 2014. *researchgate.* [Online]
Available at: https://www.researchgate.net/figure/Illustration-of-Fellenius-method_fig3_260296356
[Accessed 28 10 2018].

Rocscience Inc., 2016. *Slide User´s Guide.* Canada: s.n.

Sallinger, M., 2017. *Slope stability analysis by means of strength reduction technique,* Graz: Graz University of Technology.

Schweiger, H., 2014. *Computational Geotechnics: Lecture notes.* Graz University of Technology: Institute of Soil Mechanics and Foundation Engineering.

Torggler, N., 2016. *Numerical Studies of Embedded Beam Row in Safety Analysis in PLAXIS 2D. Master´s Thesis,* Graz: University of Technology Graz.

Tschuchnigg, F., Schweiger, H. & Sloan, S., 2015. *Slope stability analysis by means of finite element limit analysisand finite element strengthreduction techniques. Part II: Back analysis of a case history* , s.l.: Computers and Geotechnics 70, 178-189.

Appendix A

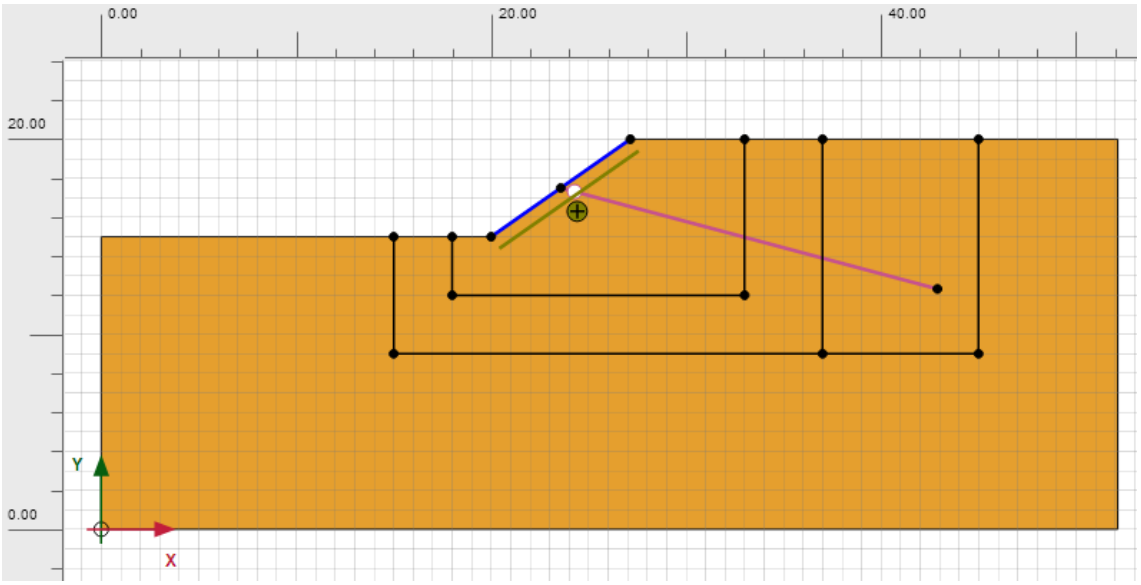

Figure A 1 Mohr-Coulomb model with embedded beam row (hinged connection to shotcrete-plate)

Plaxis 2D model with EBR	
Soil nail:	
	Embedded beam row
Material type:	Elastoplastic
E [kN/m²]:	$21*10^6$
γ [kN/m³]:	77
Diameter [m]:	0.0228
Spacing length [m]:	1.5
N_p [kN]:	100
Skin resistance:	Linear
Tskin,start,max [kN]:	30
Tskin,end,max [kN]:	30
Base resistance force [kN]:	0

Figure A 2 EBR parameters

The following Figures display the varied $L_{spacing}$/d with corresponding factor of safety ($L_{spacing}$ = 1.5 m, 3.0 m, 5.0 m, 7.5 m for the calculations with the associated flow rule and $L_{spacing}$ = 1.5 m, 3.0 m, 5.0 m, 7.5 m, 8.0 m, 8.5 m for the non-associated calculations). The plateau of the M_{sf}/|u| diagram occurs at a $L_{spacing}$ of 7.5 m (Figure A 3; lower right diagram) for the associated flow rule. With a FoS of 2.25.

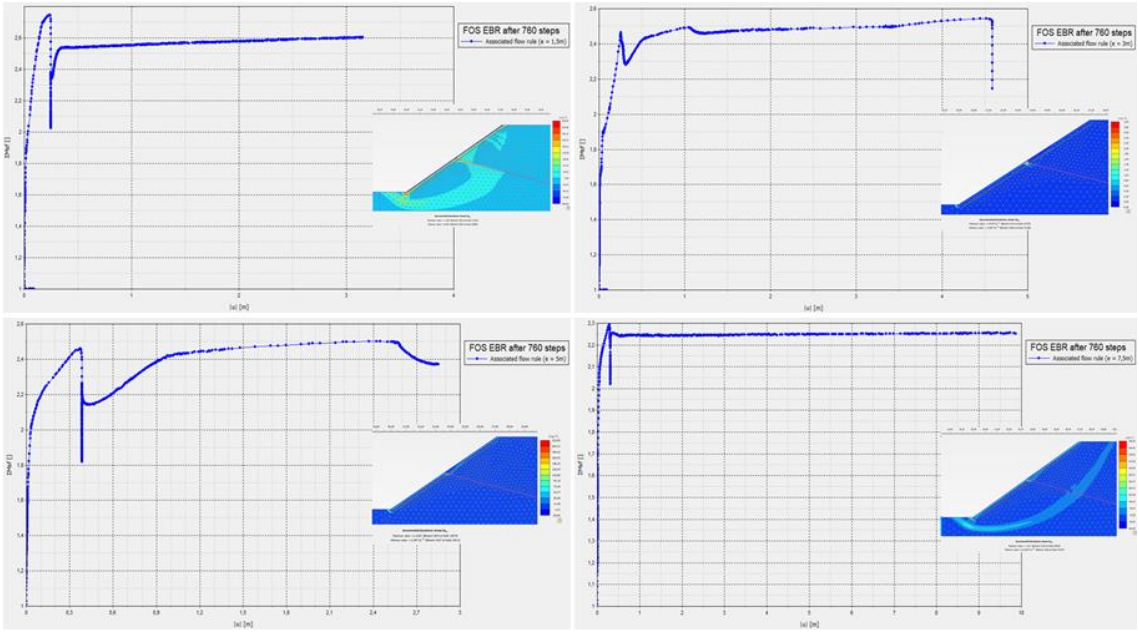

Figure A 3 M_{sf}/|u| diagram with corresponding incremental strain illustration after the safety calculation (upper left: $L_{spacing}$ = 1.5 m, upper right: $L_{spacing}$ = 3.0 m, lower left: $L_{spacing}$ = 5.0 m, lower right: $L_{spacing}$ = 7.5 m)

For the variation of $L_{spacing}$ for the non-associated flow rule the plateau of the M_{sf}/|u| diagram is reached at a $L_{spacing}$ = 8.5 m (Figure A 4; lower left diagram). With a FoS of 2.15.

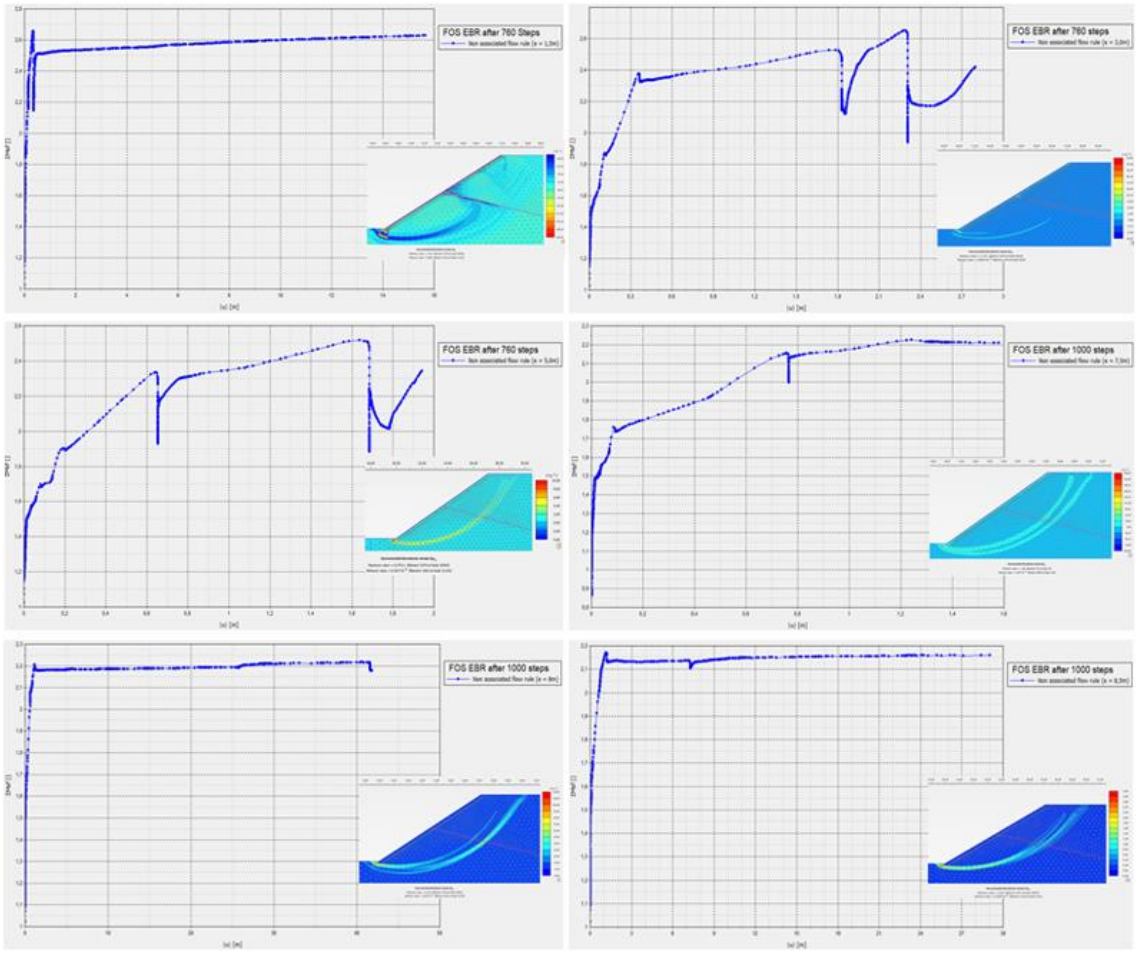

Figure A 4 $M_{sf}/|u|$ diagram with corresponding incremental strain illustration after the safety calculation (upper left: $L_{spacing}$ = 1.5 m, upper right: $L_{spacing}$ = 3.0 m, middle left: $L_{spacing}$ = 5.0 m, middle right: $L_{spacing}$ = 7.5 m, lower left: $L_{spacing}$ = 8.0 m, lower right: $L_{spacing}$ = 8.5 m)

Appendix B

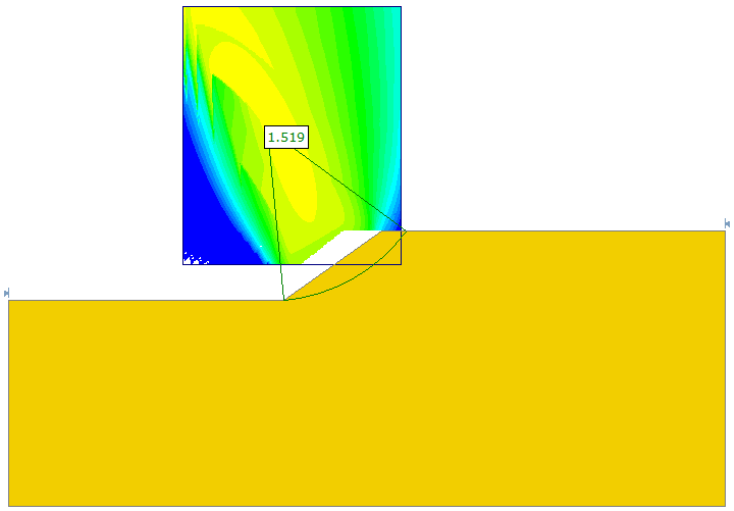

Figure B 1 Unsupported slope model in *Slide* with a calculated $FoS^{LEA} = 1.519$

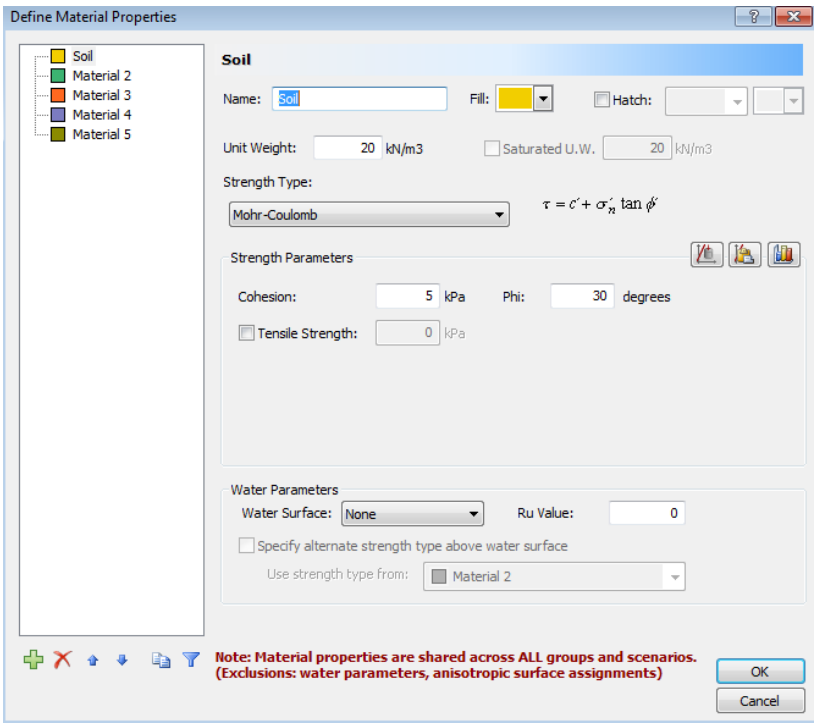

Figure B 2 Soil parameters for all the *Slide* models

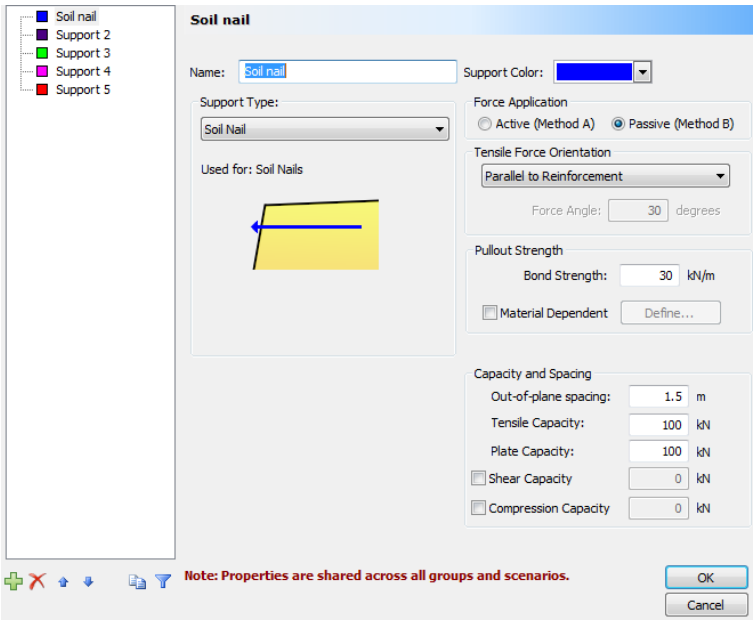

Figure B 3 Soil nail properties for the One-soil nail *Slide* model

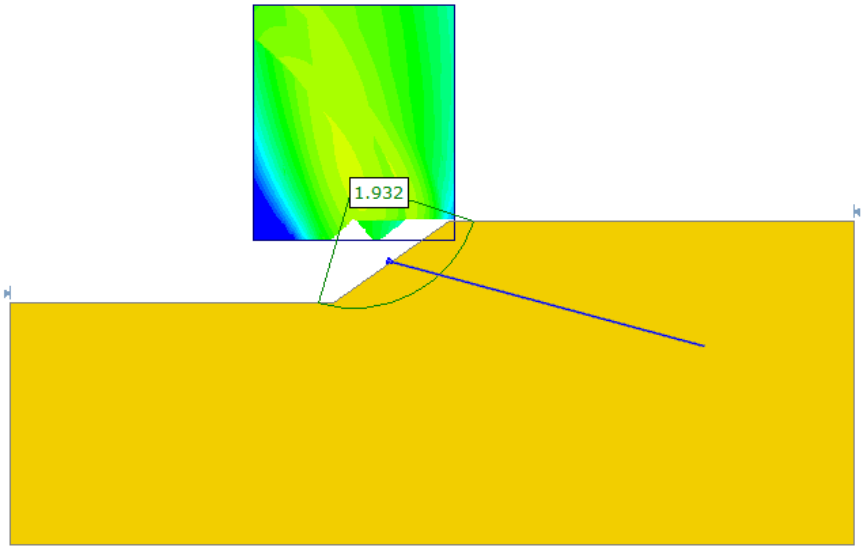

Figure B 4 One-soil nail *Slide* model with a calculated FoS^{LEA} = 1.932 (N=66.67 kN)

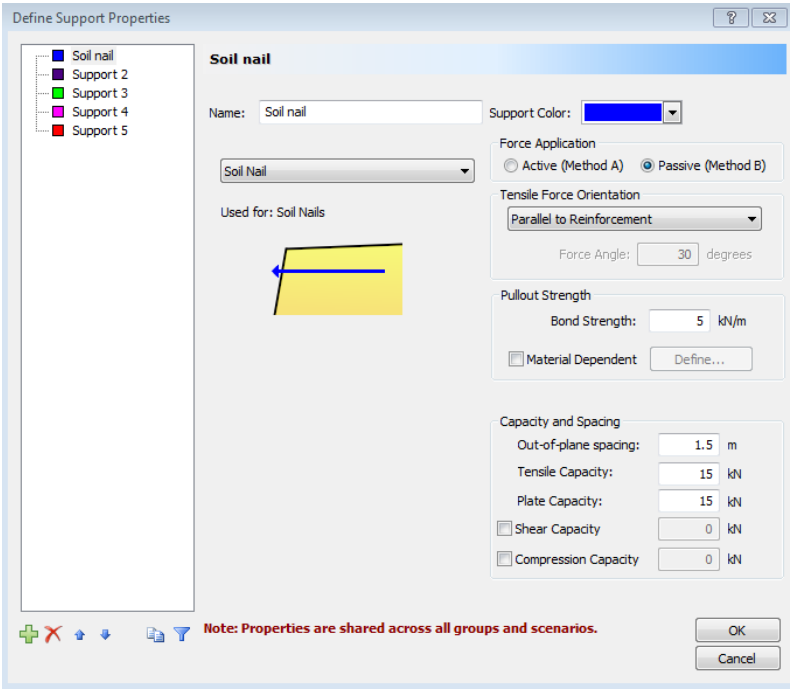

Figure B 6 Soil nail properties for the three-soil nail *Slide* model

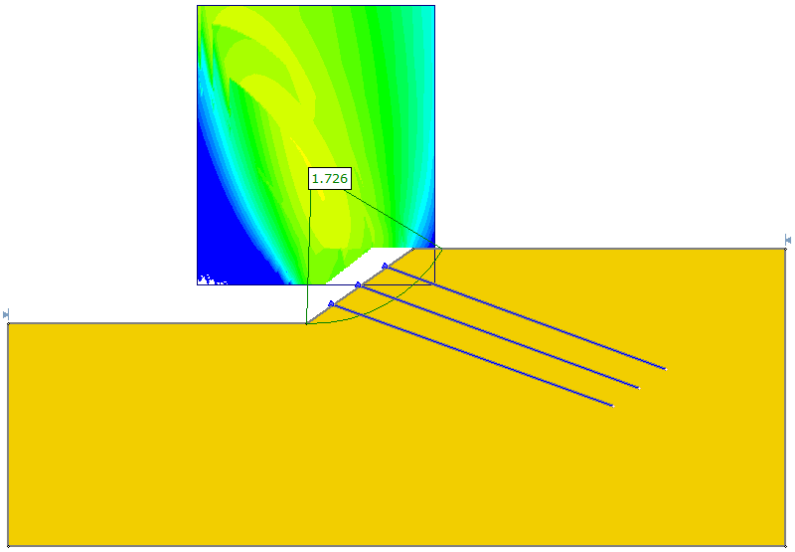

Figure B 5 Three-soil nail *Slide* model with a calculated FoS^{LEA} = 1.726 (N=15 kN)

Appendix C

The results displayed in this appendix show the stress indicators over the slip surface for the associated and non-associated flow rule of the MC model of the unsupported slope.

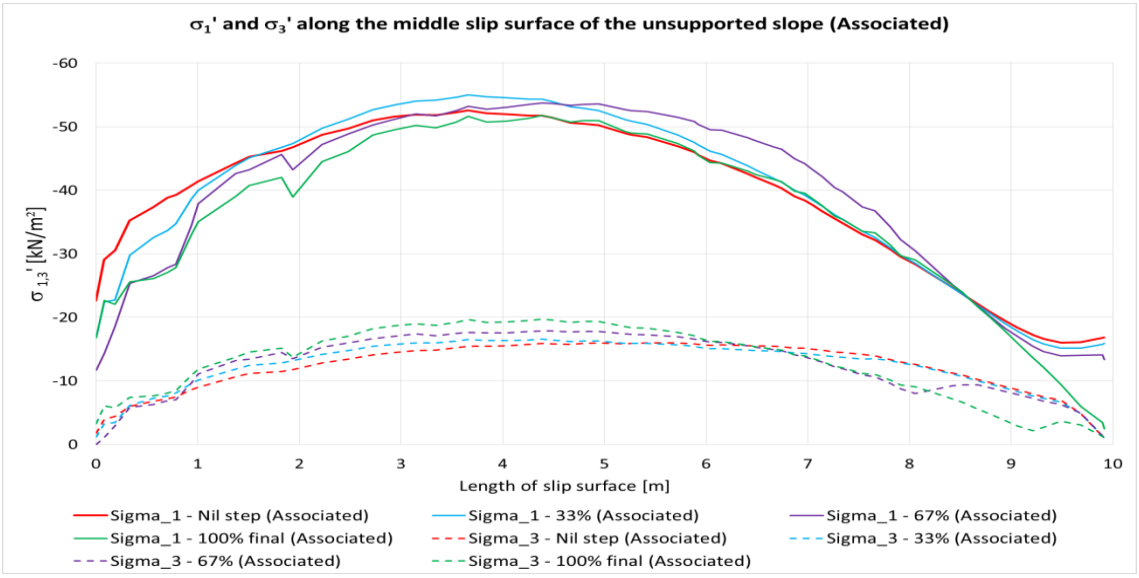

Figure C 1 Principal effective stresses $\sigma_{1,3}'$ over the slip surface length for the associated calculation of the unsupported MC model

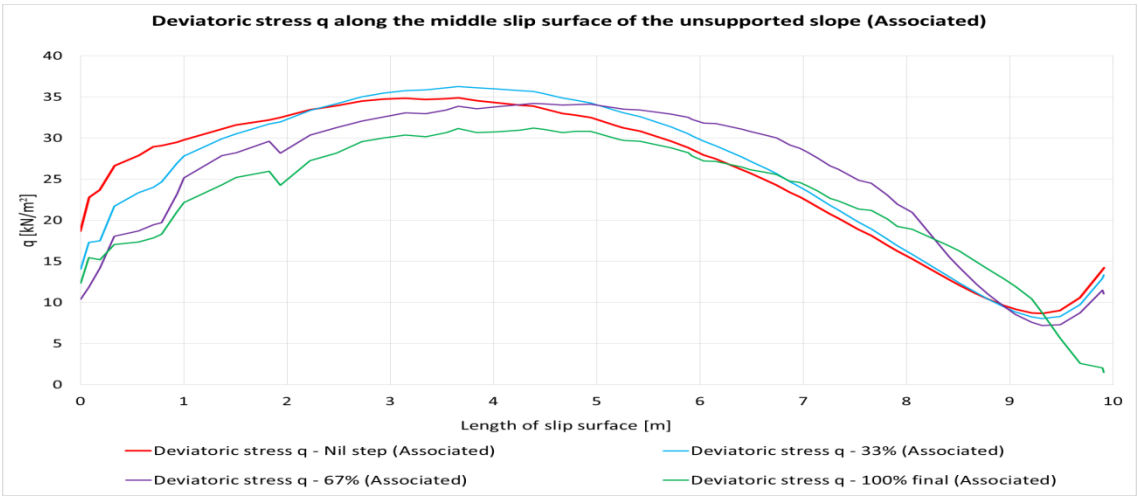

Figure C 2 Deviatoric stress q over the slip surface of the unsupported MC model (associated flow rule)

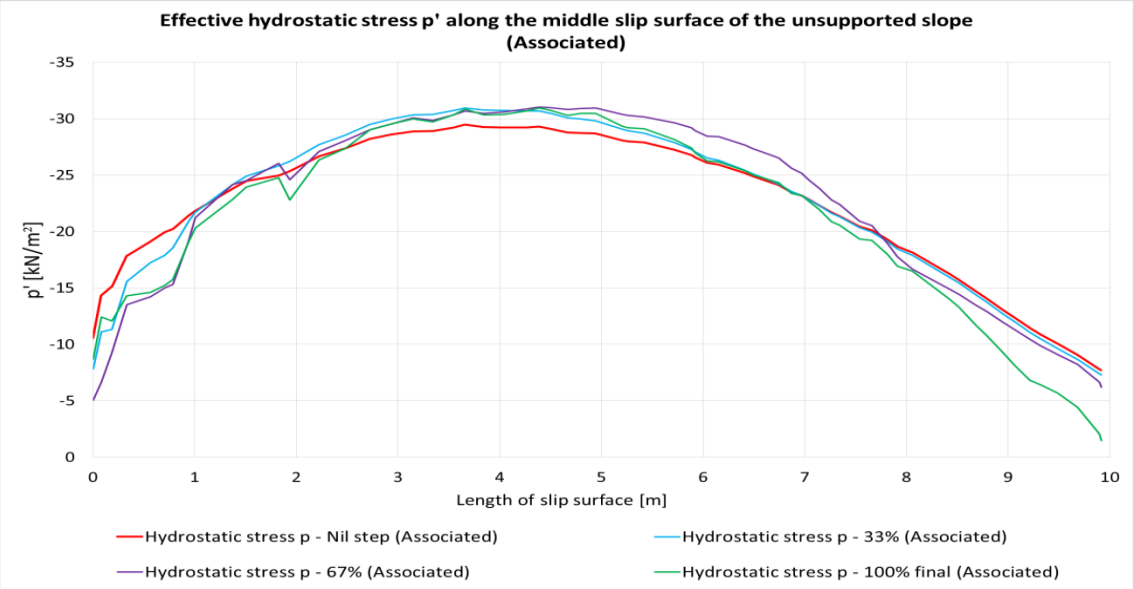

Figure C 3 Hydrostatic effective stress p' over the slip surface of the unsupported MC model (associated flow rule)

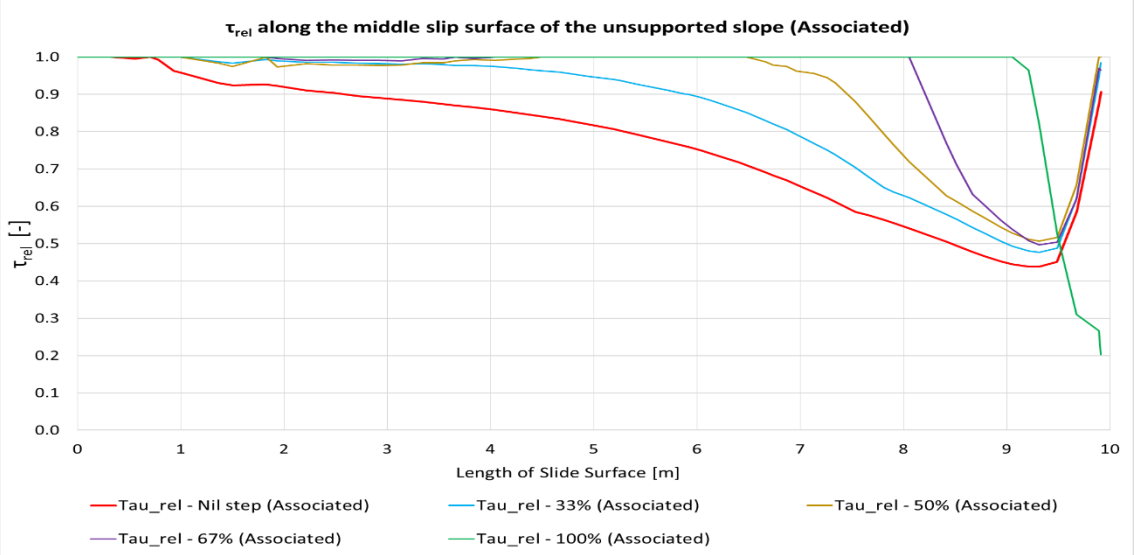

Figure C 4 Relative shear stresses over the unsupported MC slip surface length (associated)

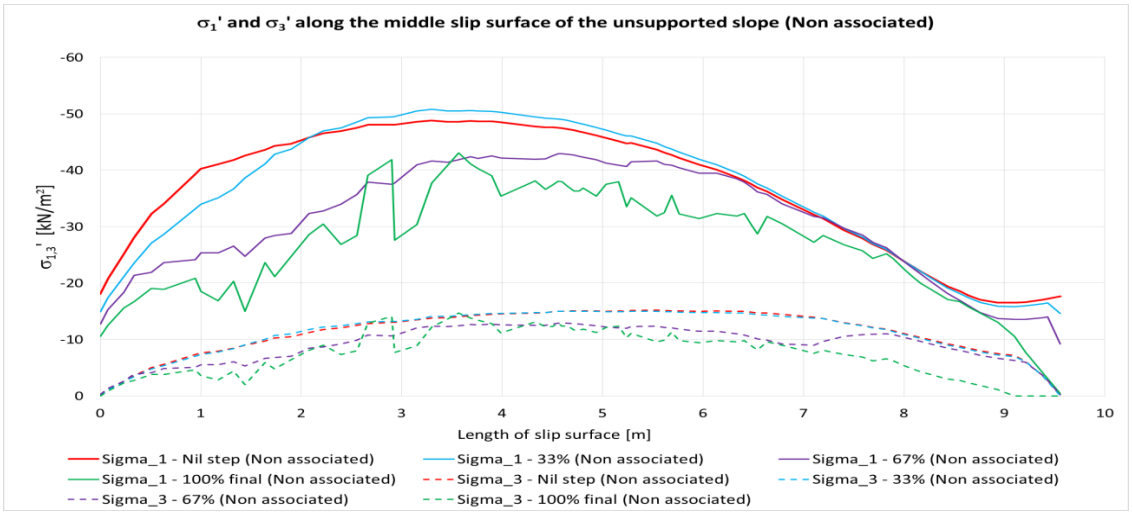

Figure C 5 Principal effective stresses $\sigma_{1,3}'$ over the slip surface length for the non-associated calculation of the unsupported MC model

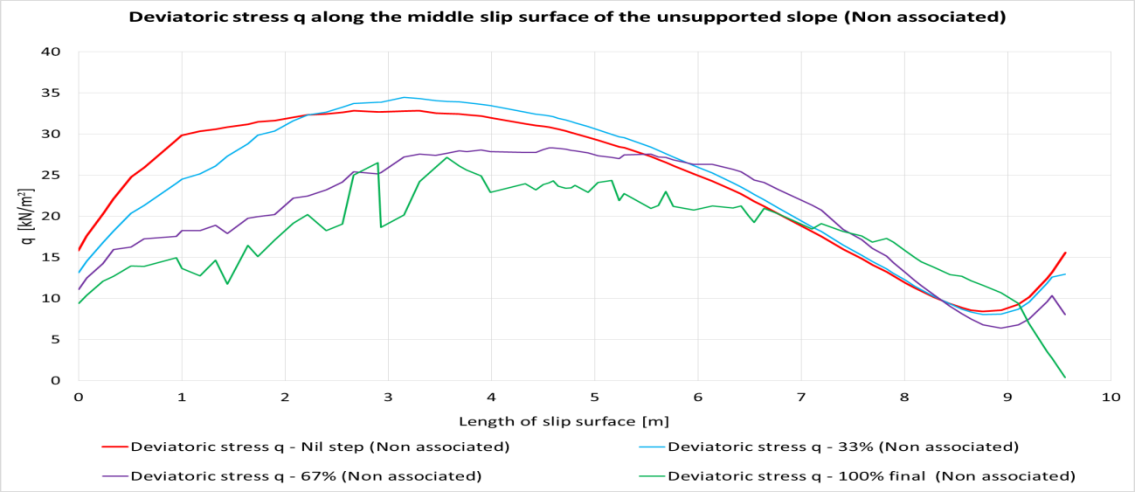

Figure C 6 Deviatoric stress q over the slip surface of the unsupported MC model (non-associated flow rule)

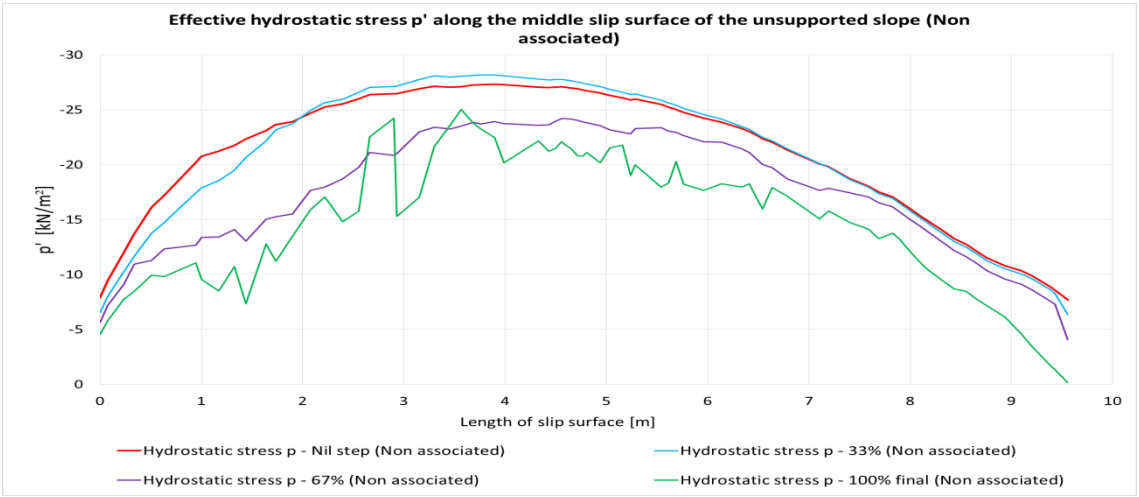

Figure C 7 Effective hydrostatic stress p' over the slip surface length for the non-associated calculation of the unsupported MC model

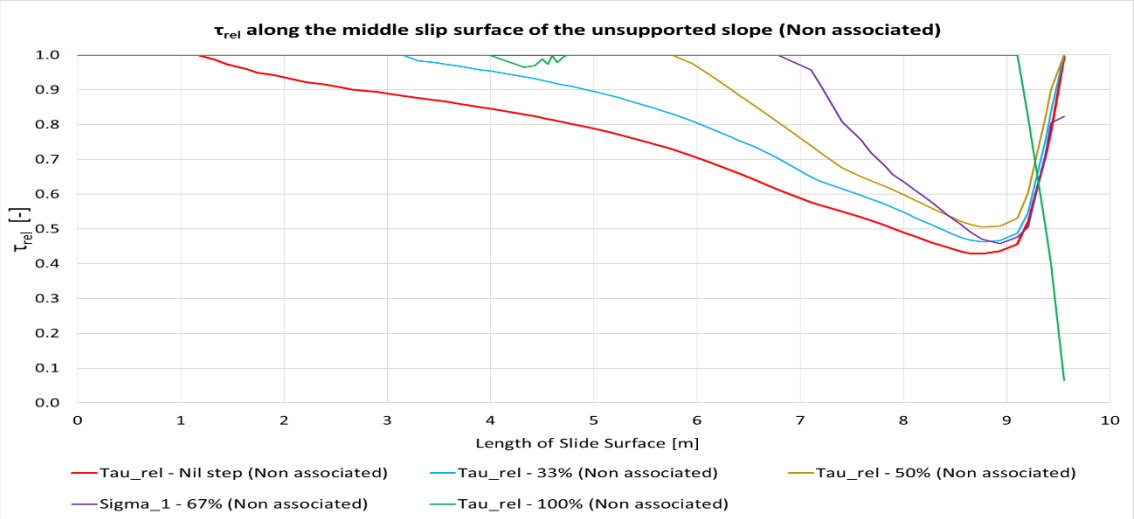

Figure C 8 Relative shear stresses over the unsupported MC slip surface length (non-associated)

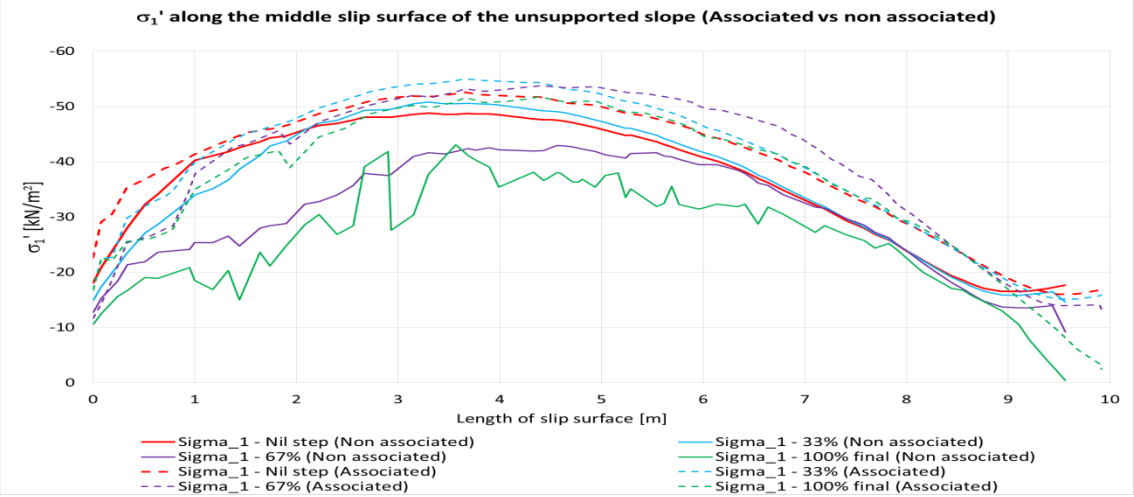

Figure C 9 σ_1' over the slip surface length for the unsupported MC model (associated vs. non-associated flow rule)

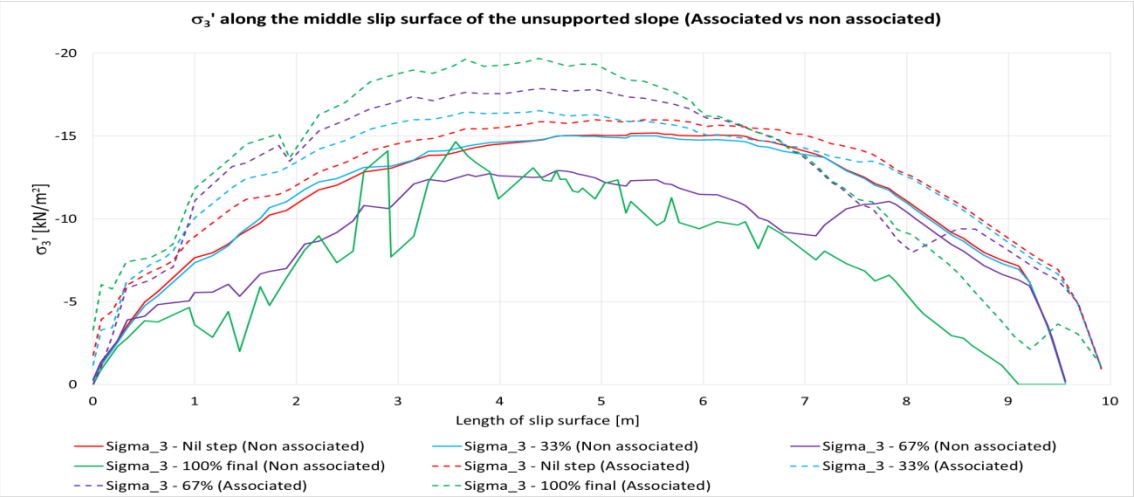

Figure C 5 σ_3' over the slip surface length for the unsupported MC model (associated vs. non-associated flow rule)

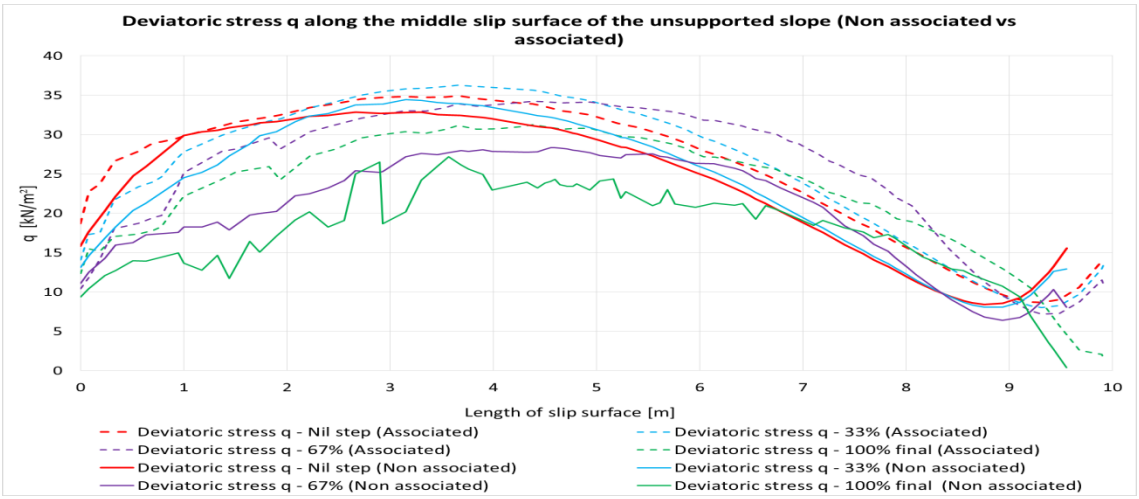

Figure C 11 Deviatoric stress q over the slip surface length for the unsupported MC model (associated vs. non-associated flow rule)

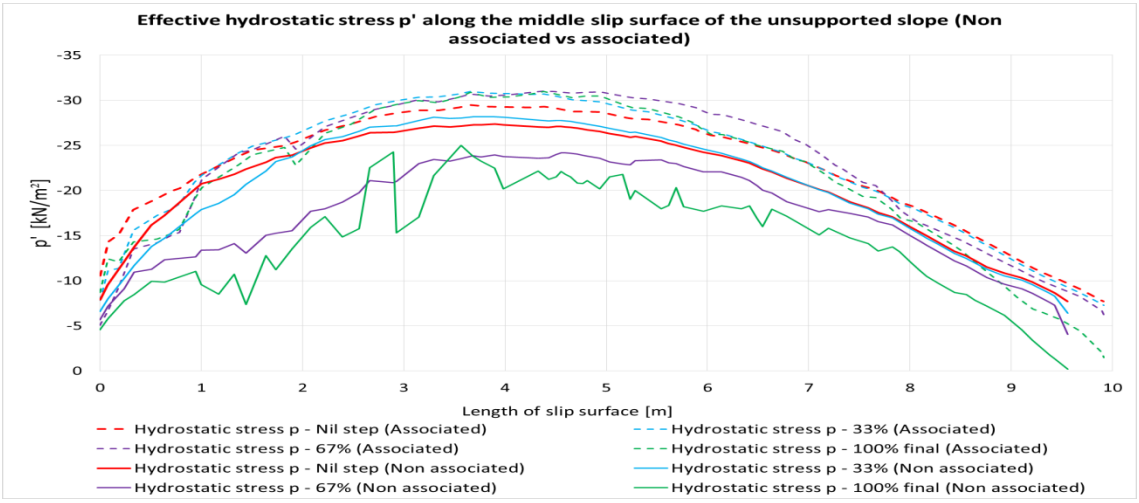

Figure C 6 Effective hydrostatic stress p' over the slip surface length for the unsupported MC model (associated vs. non-associated flow rule)

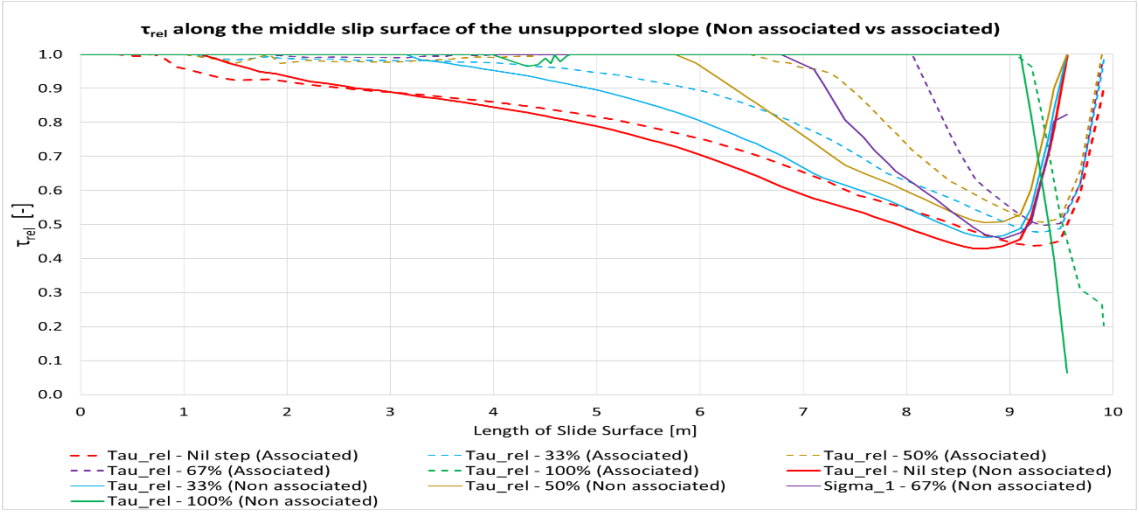

Figure C 13 Relative shear stresses over the unsupported MC slip surface length (associated vs non-associated)

MC unsupported slope			
Stress	Associated		Non-associated
σ_n'	↗	/	↗
σ_1'	↕	>	↓
σ_3'/σ_2'	↑	>	↓
σ_{yy}'	↗	/	↗
σ_{xx}'	↗	/	↗
p'	-	>	↓
q	↓	>	↓
τ_{rel}	↑	>	↑

Trend between steps over the slip surface:
↑ increasing trend
↓ decreasing trend
- no bigger change between steps
↕ scattering/no evident trend

> associated shows higher stresses
< non-associated shows higher stresses
= almost equal

Figure C 7 Trend of the stress indicators for the unsupported MC model

Appendix D

The results displayed in this appendix are the stress indicators over the slip surface for the associated and non-associated flow rule of the MC model with a 1-nail reinforced slope.

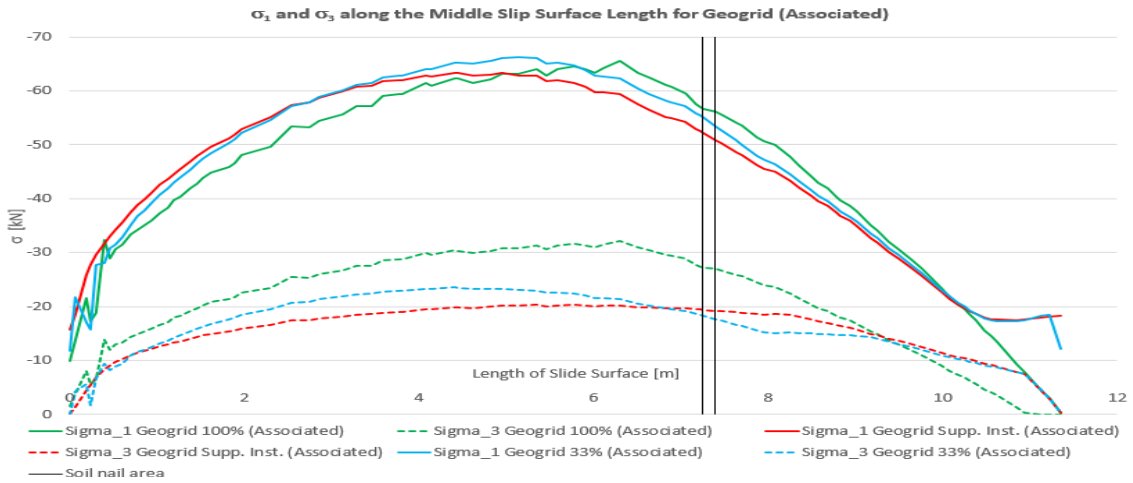

Figure D 1 $\sigma_{1,3}$' over the slip surface length for the associated calculation of the 1-nail supported MC model

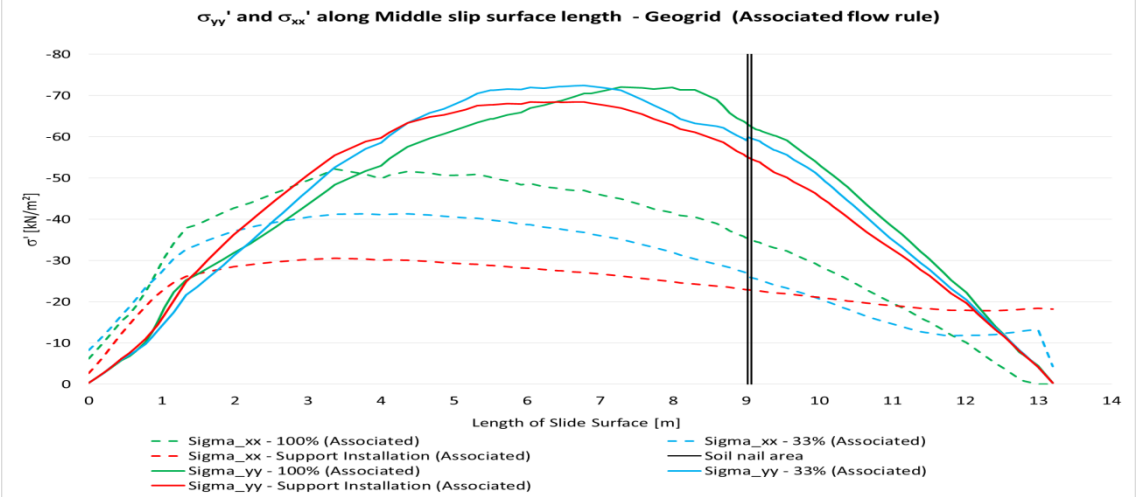

Figure D 2 $\sigma_{xx,yy}$' over the slip surface length for the associated calculation of the 1-nail supported MC model

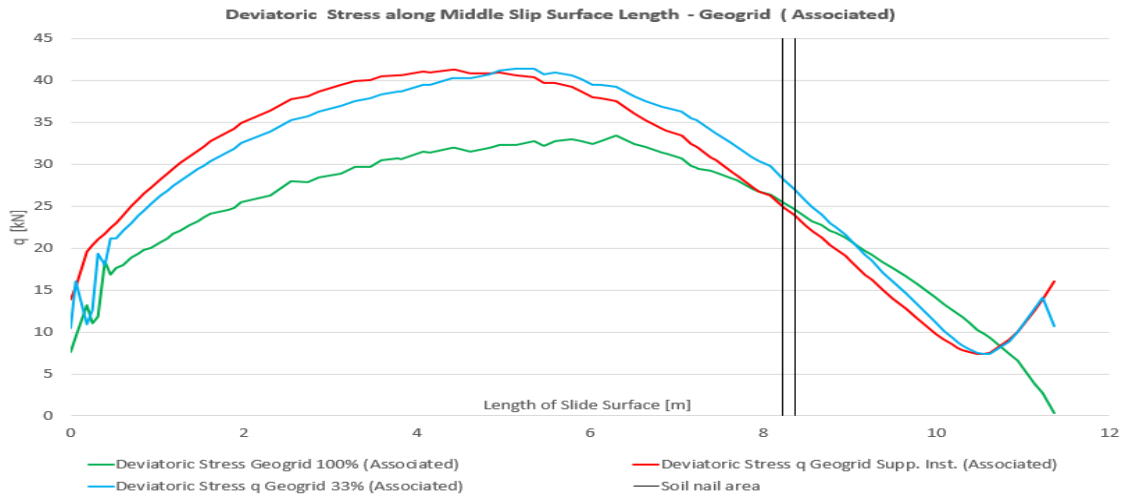

Figure D 3 Deviatoric stress along the slip surface of the 1-nail supported MC model (associated flow rule)

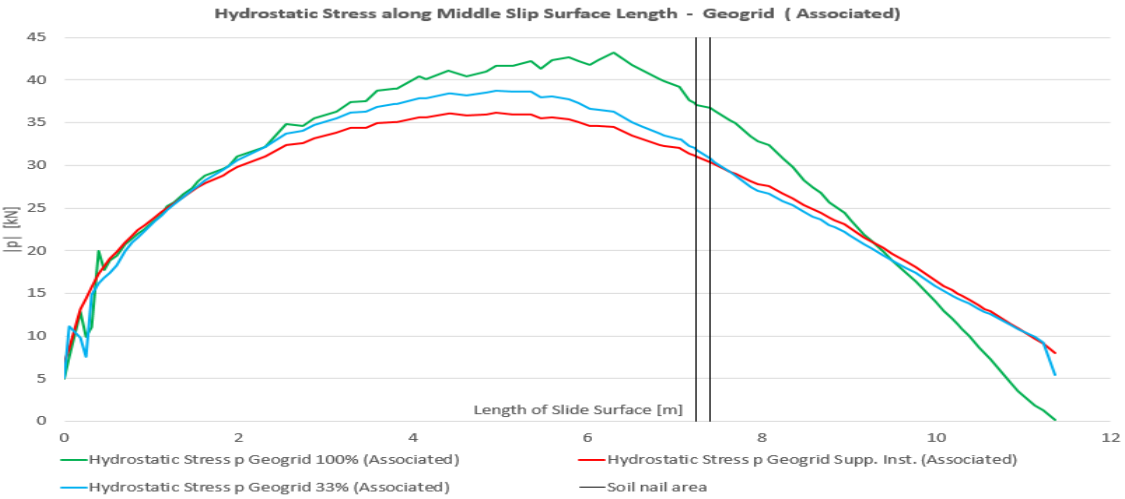

Figure D 4 Effective hydrostatic p' stress along the slip surface of the 1-nail supported MC model (non-associated flow rule)

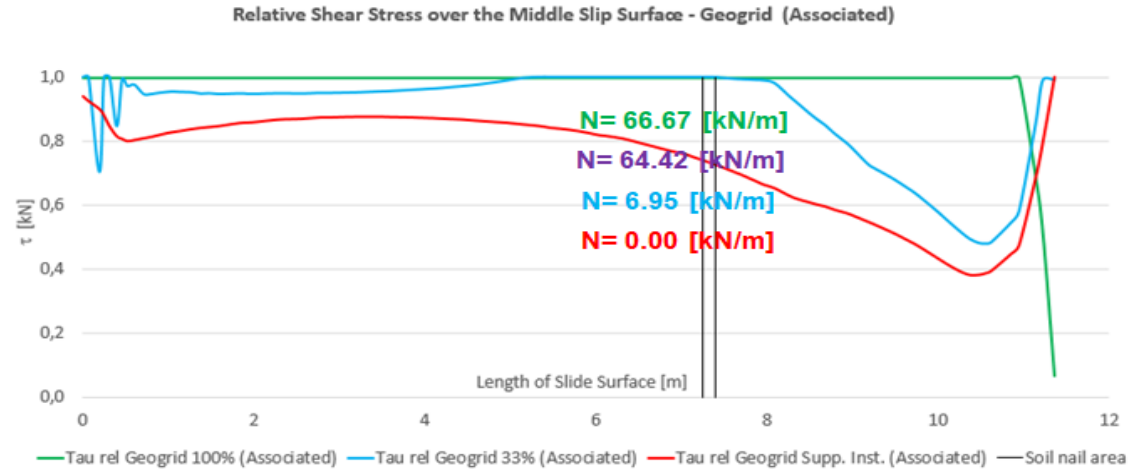

Figure D 5 Relative shear stress with corresponding maximal soil nail normal force over the slip surface length of the 1-nail supported MC slope model (associated flow rule)

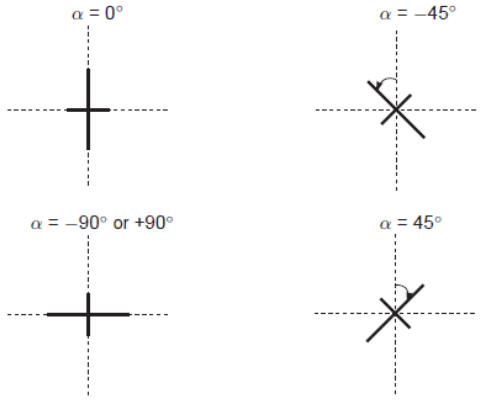

Figure D 6 Illustration of positive and negative angles of the principal effective stress

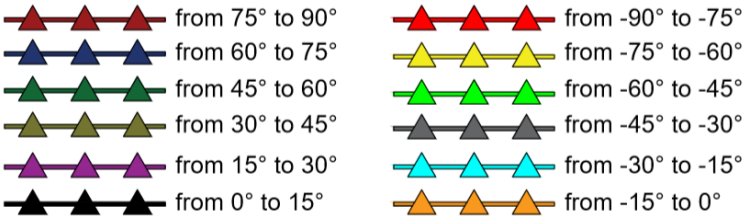

Figure D 7 The colouring of the triangles corresponds to a certain principal stress direction degree interval

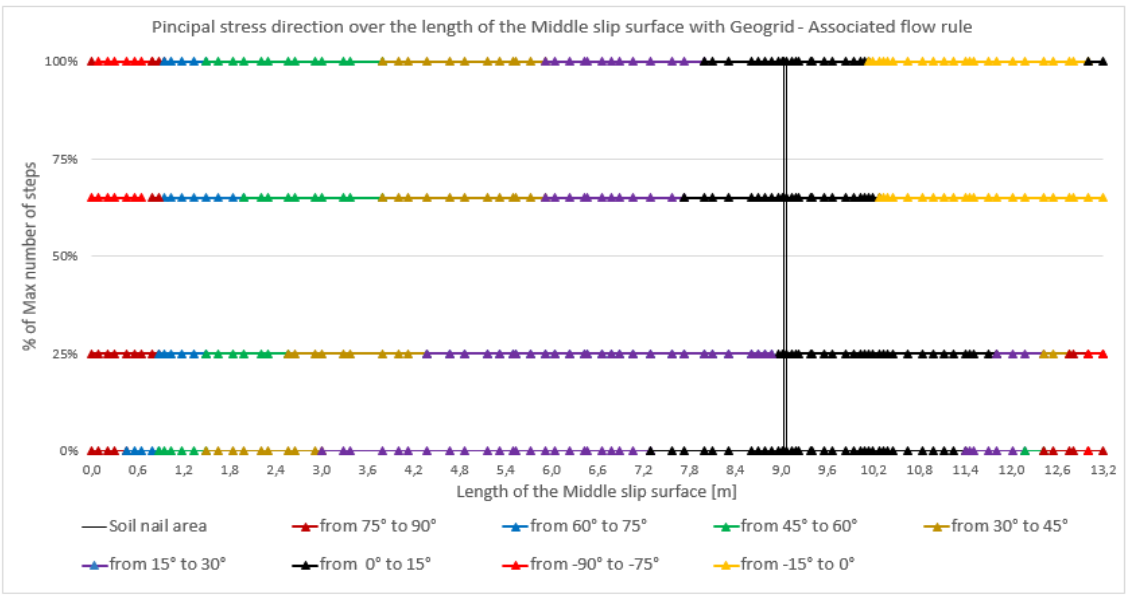

Figure D 8 Evolution of the principal stress directions with the increase of the safety calculation step for the MC model with 1 soil nail (associated flow rule)

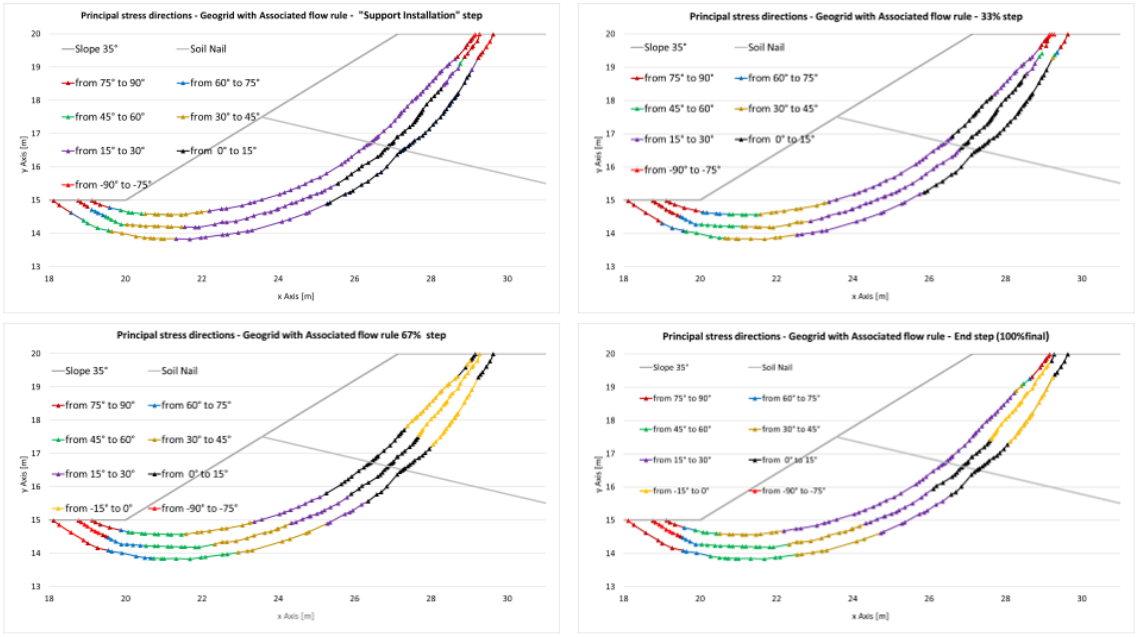

Figure D 9 Principal stress direction evolution between the safety calculation steps, along the slip surface (associated flow rule) for the 1-nail supported MC model

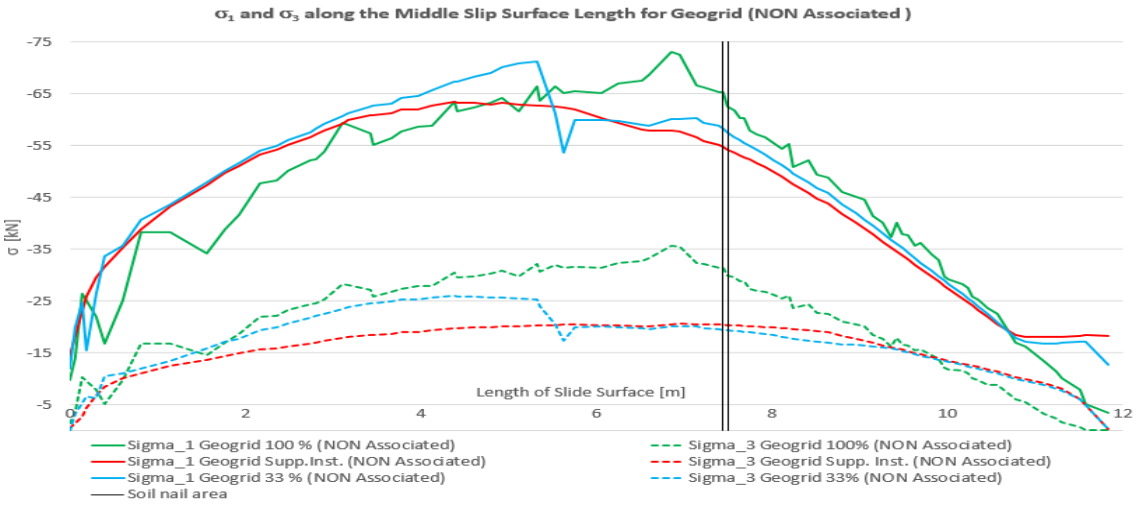

Figure D 10 $\sigma_{1,3}$' over the slip surface length for the non-associated calculation of the 1-nail supported MC model

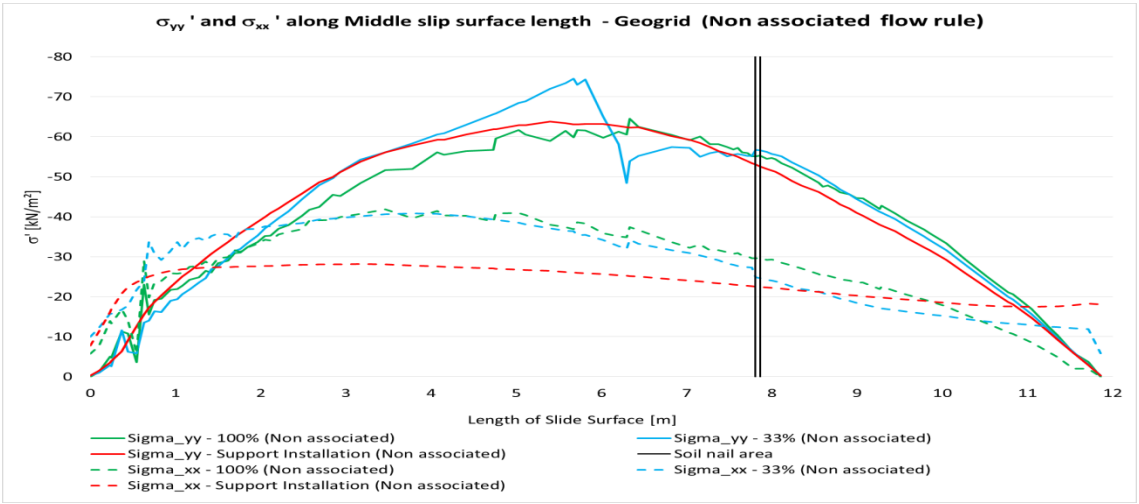

Figure D 11 $\sigma_{xx,yy}$' over the slip surface length for the non-associated calculation of the 1-nail supported MC model

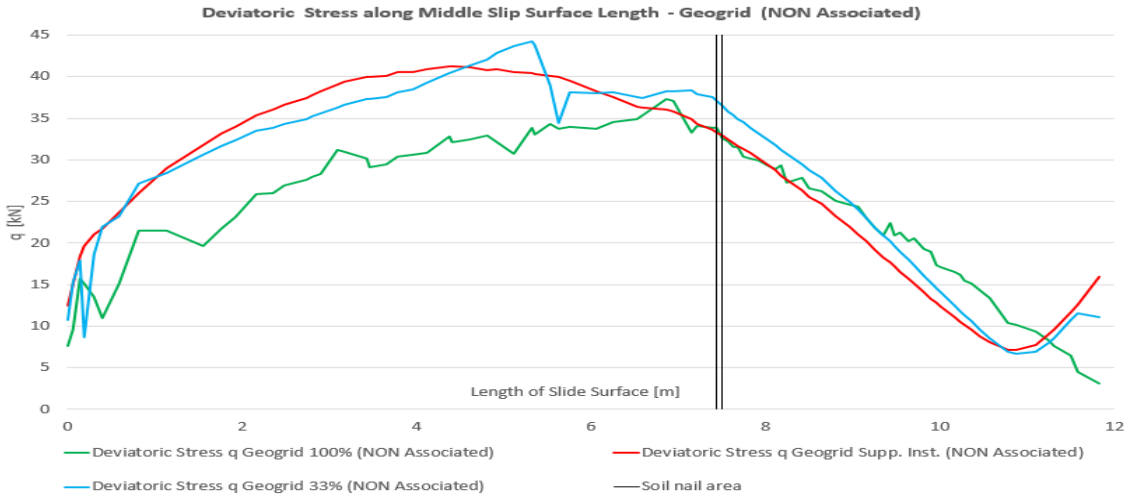

Figure D 12 Deviatoric stress along the slip surface of the 1-nail supported MC model (non-associated flow rule)

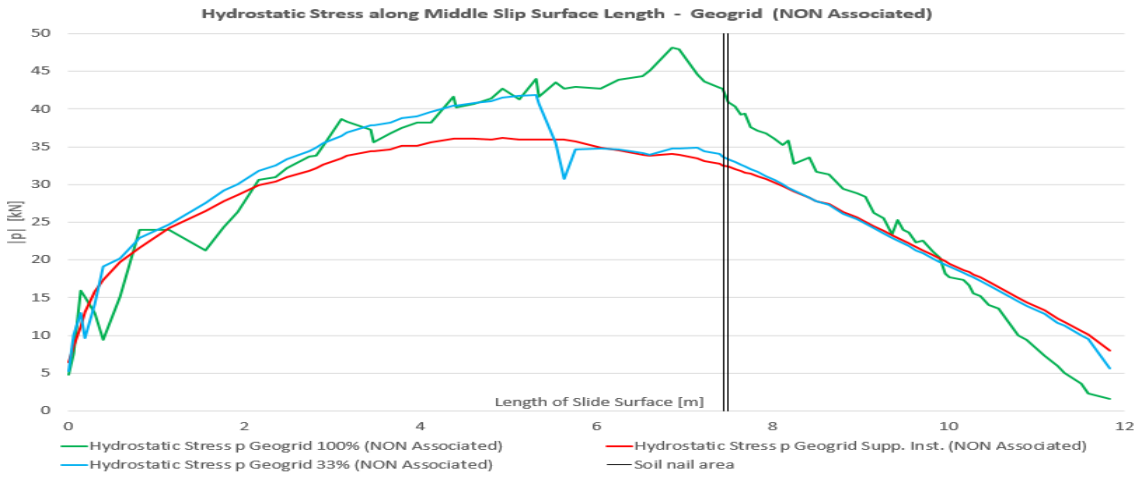

Figure D 13 Effective hydrostatic stress along the slip surface of the 1-nail supported MC model (non-associated flow rule)

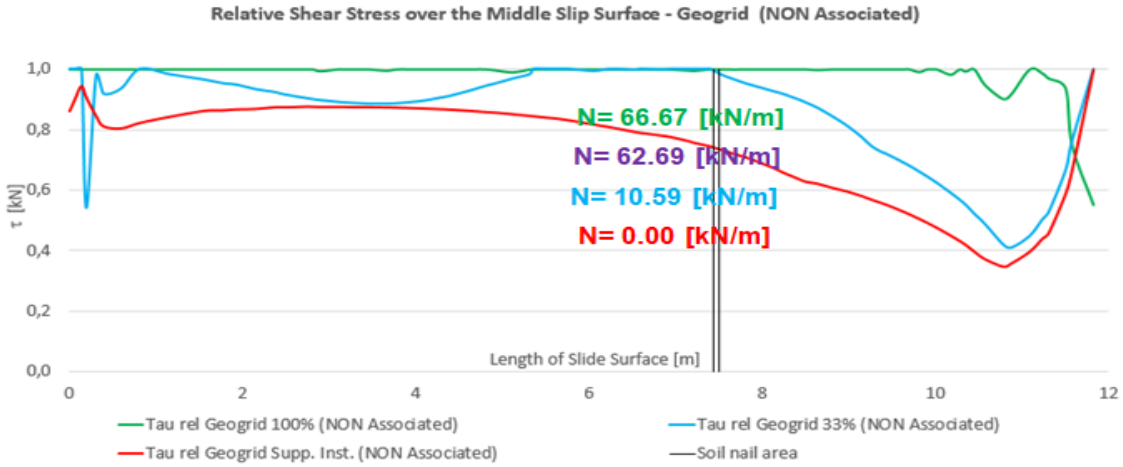

Figure D 14 Relative shear stress with corresponding maximal soil nail normal force over the slip surface length of the 1-nail supported MC slope model (non-associated flow rule)

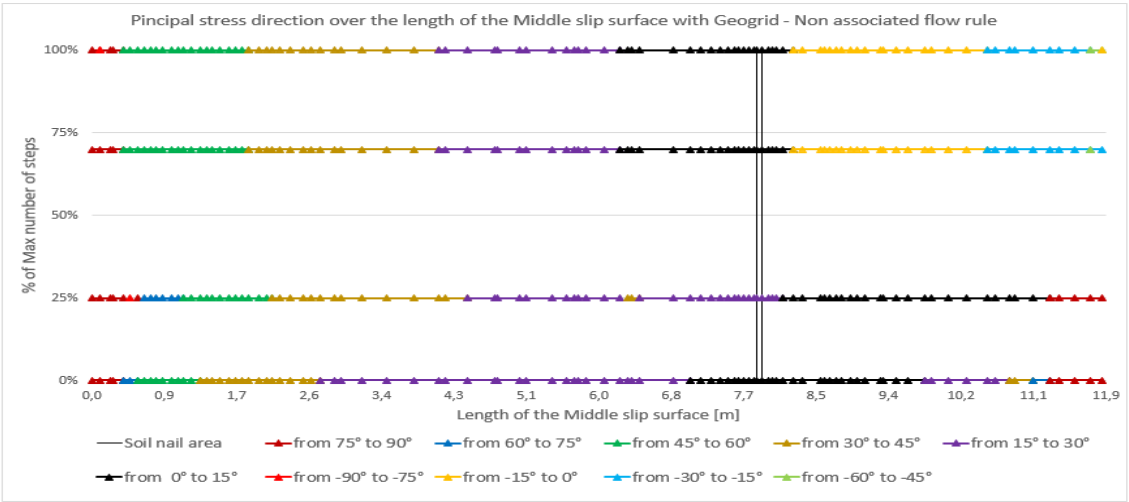

Figure D 15 Evolution of the principal stress directions with the increase of the safety calculation step for the MC model with 1 soil nail (non-associated flow rule)

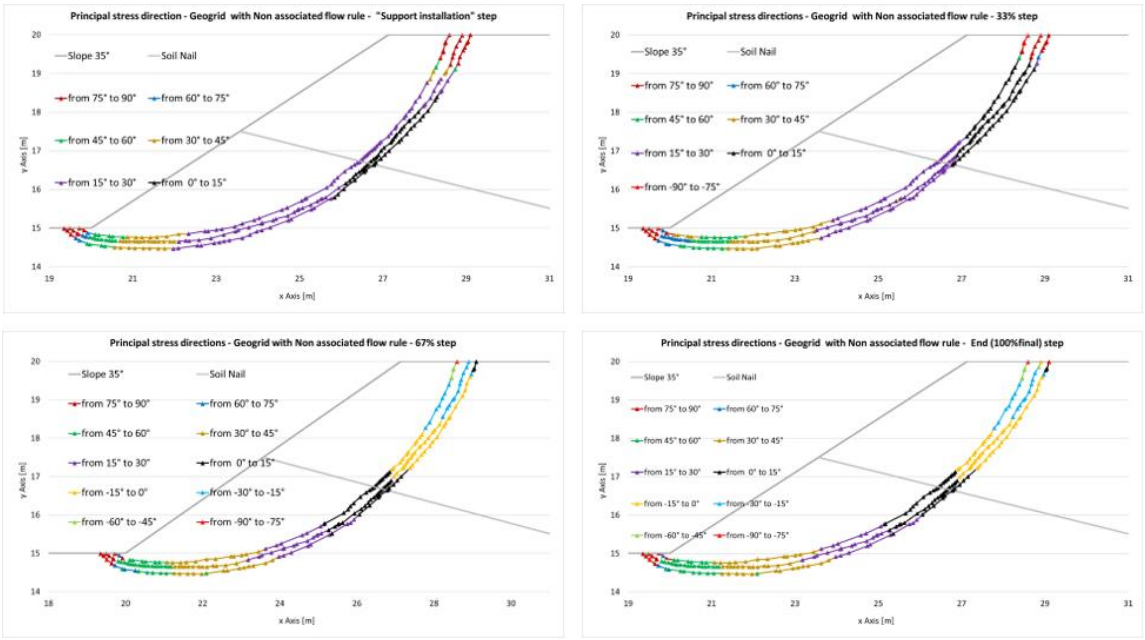

Figure D 16 Principal stress direction evolution between the safety calculation steps, along the slip surface (associated flow rule) for the 1-nail supported MC model

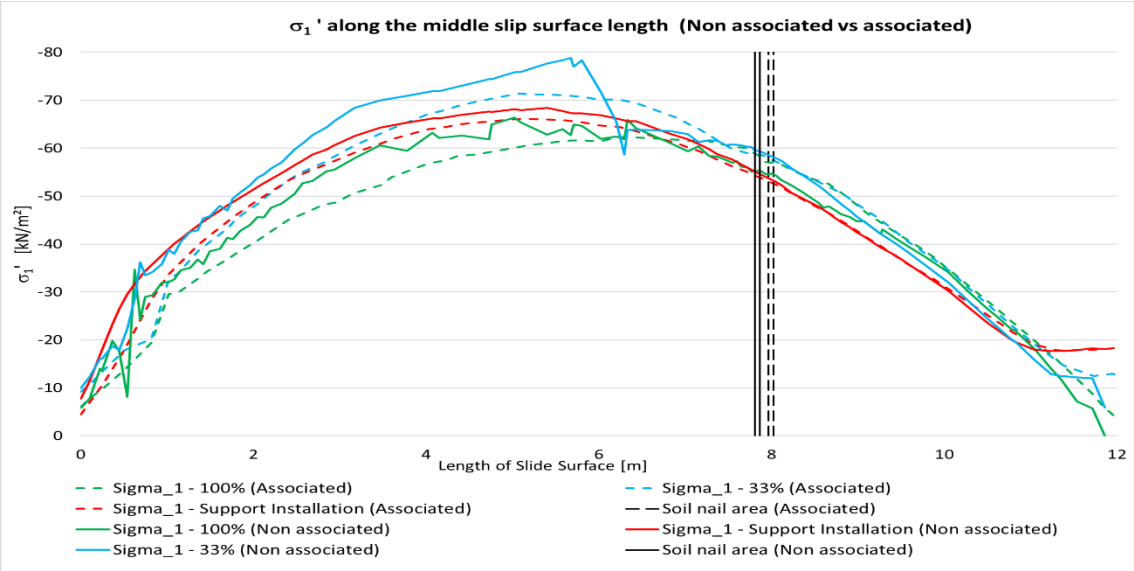

Figure D 17 σ_1' over the slip surface length for the 1-nail supported MC model (associated vs. non-associated flow rule)

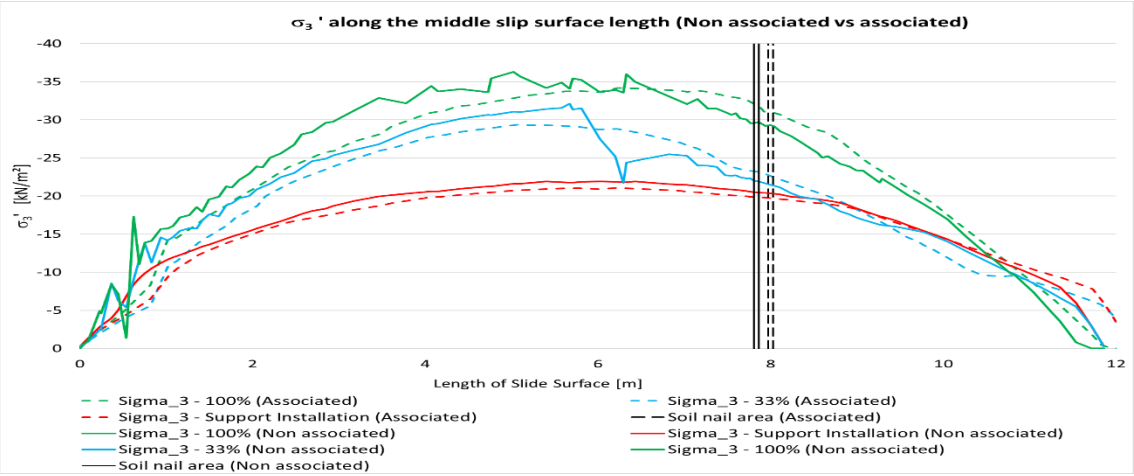

Figure D 18 σ_3' over the slip surface length for the 1-nail supported MC model (associated vs. non-associated flow rule)

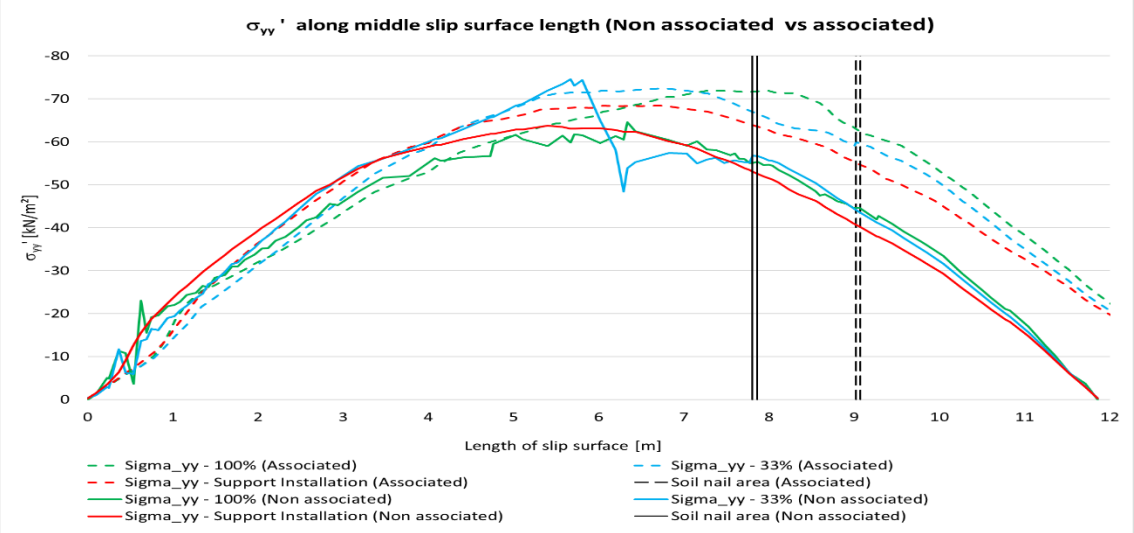

Figure D 19 σ_{yy}' over the slip surface length for the 1-nail supported MC model (associated vs. non-associated flow rule)

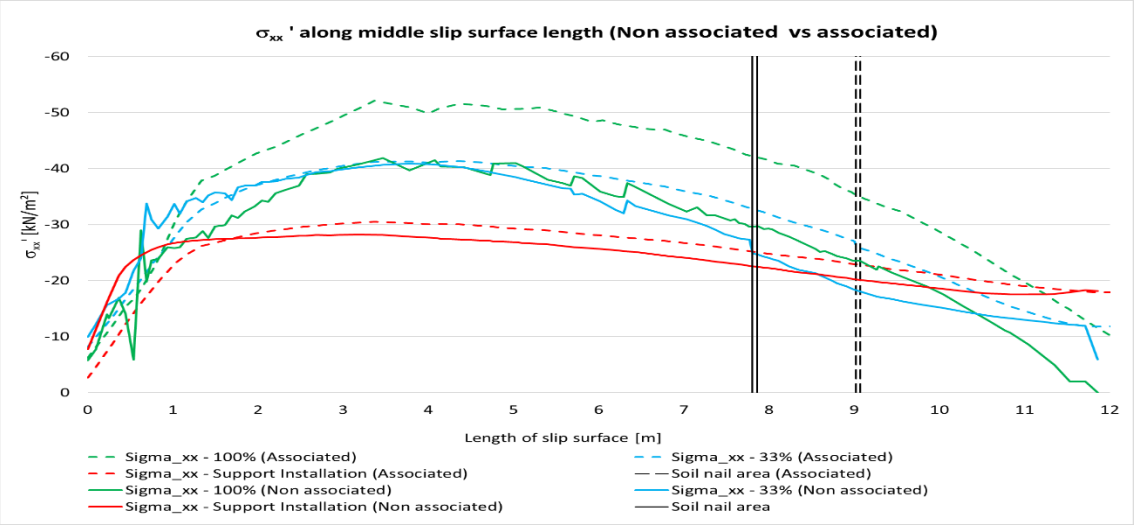

Figure D 20 σ_{xx}' over the slip surface length for the 1-nail supported MC model (associated vs. non-associated flow rule)

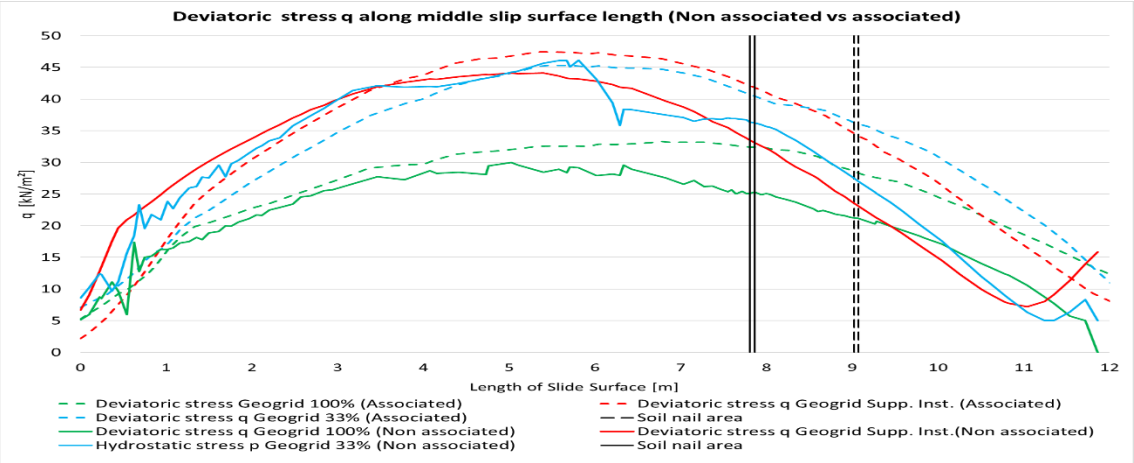

Figure D 21 Deviatoric stress q over the slip surface length for the 1-nail supported MC model (associated vs. non-associated flow rule)

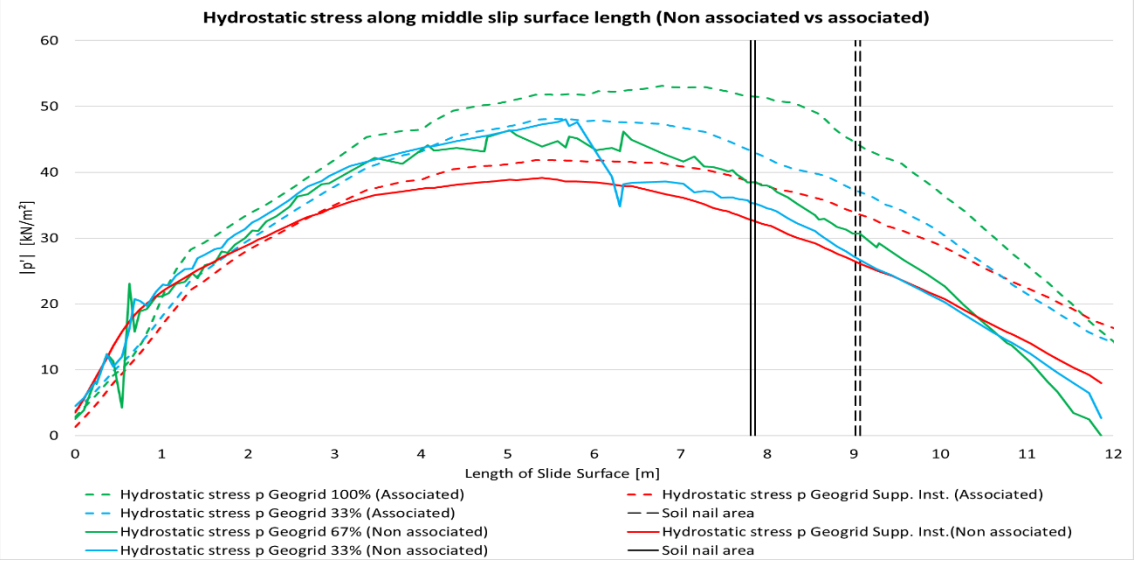

Figure D 22 Hydrostatic effective stress p' over the slip surface length for the 1-nail supported MC model (associated vs. non-associated flow rule)

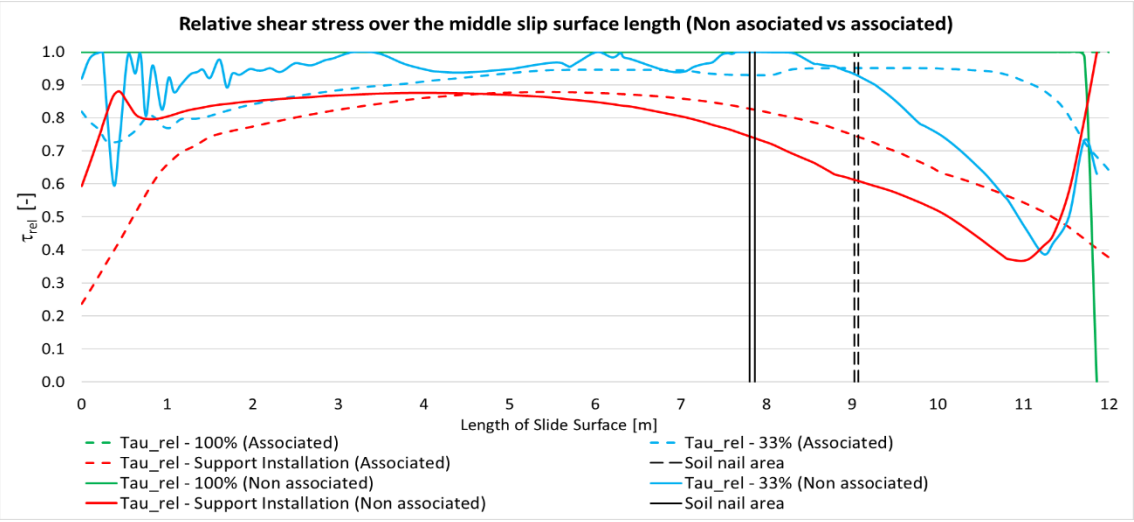

Figure D 23 Relative shear stress over the slip surface length for the 1-nail supported MC model (associated vs. non-associated flow rule)

MC 1-nail slope			
Stress	Associated		Non-associated
σ_n'			
σ_1'	↑	<	↑
σ_3'/σ_2'	↑	=	↑
σ_{yy}'	↑	>	↑
σ_{xx}'	↑	>	↑
p'	↑	>	↑
q	↓	>	↓
τ_{rel}	↑	>	↑

Trend between steps over the slip surface:
↑ increasing trend
↓ decreasing trend
– no bigger change between steps
↕ scattering/no evident trend

> associated shows higher stresses
< non-associated shows higher stresses
= almost equal

Figure D 24 Trend of the stress indicators for the 1-nail supported MC model

Appendix E

The results displayed in this appendix are the stress indicators over the slip surface for the associated and non-associated flow rule of the MC model with a 3-nail reinforced slope.

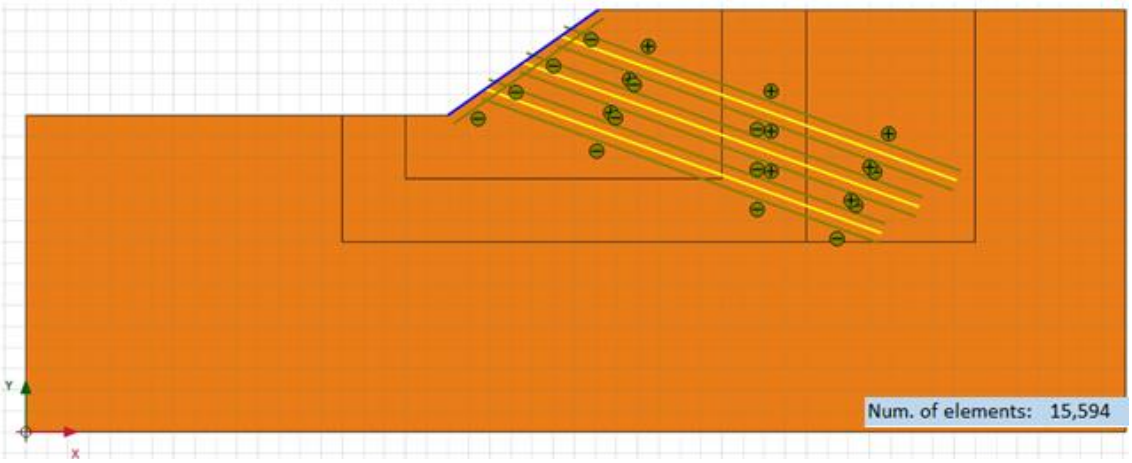

Figure E 1 MC model of the 3-nail reinforced slope

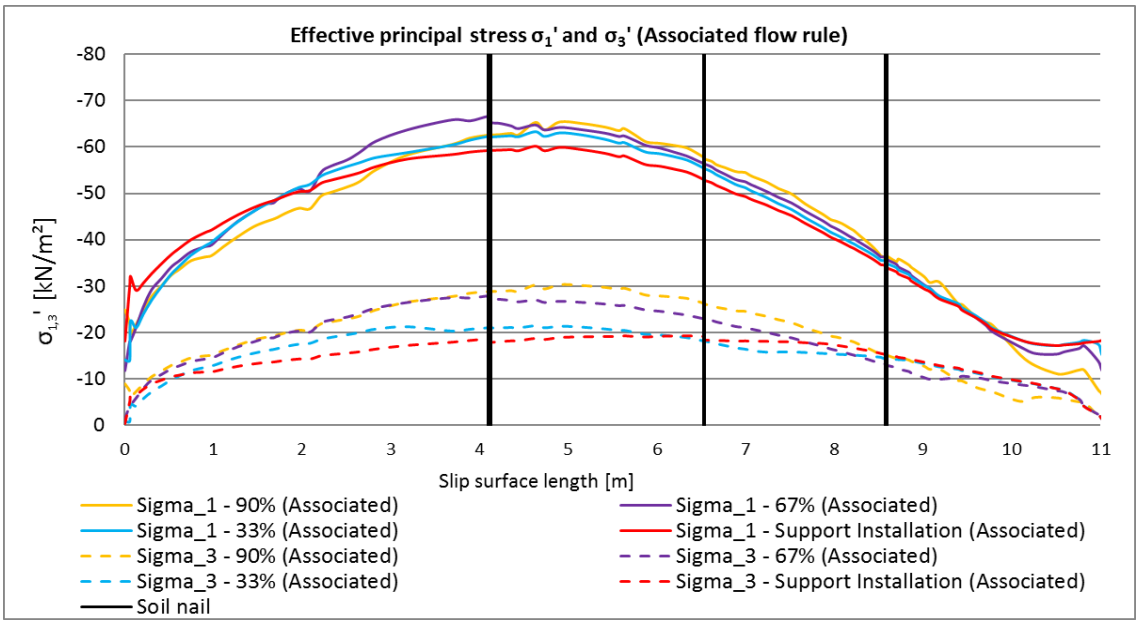

Figure E 2 $\sigma_{1,3}$' over the slip surface length for the associated calculation of the 3-nail supported MC model

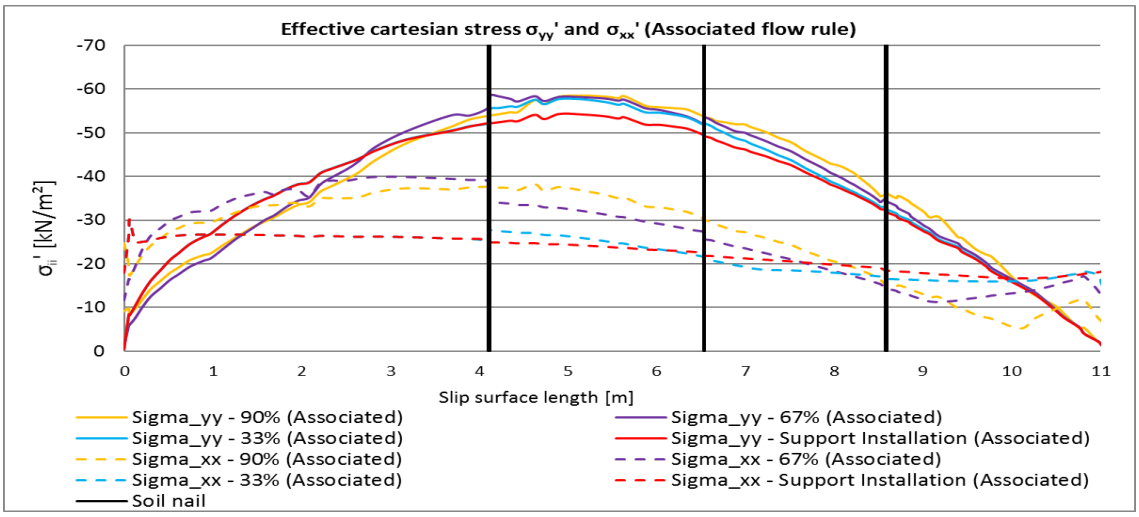

Figure E 3 $\sigma_{xx,yy}'$ over the slip surface length for the associated calculation of the 3-nail supported MC model

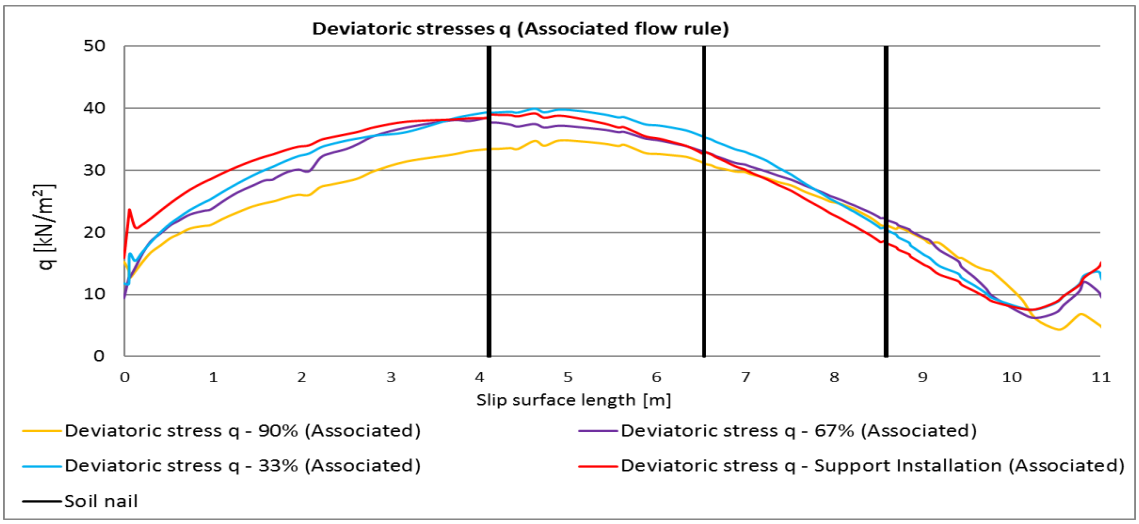

Figure E 4 q over the slip surface length for the associated calculation of the 3-nail supported MC model

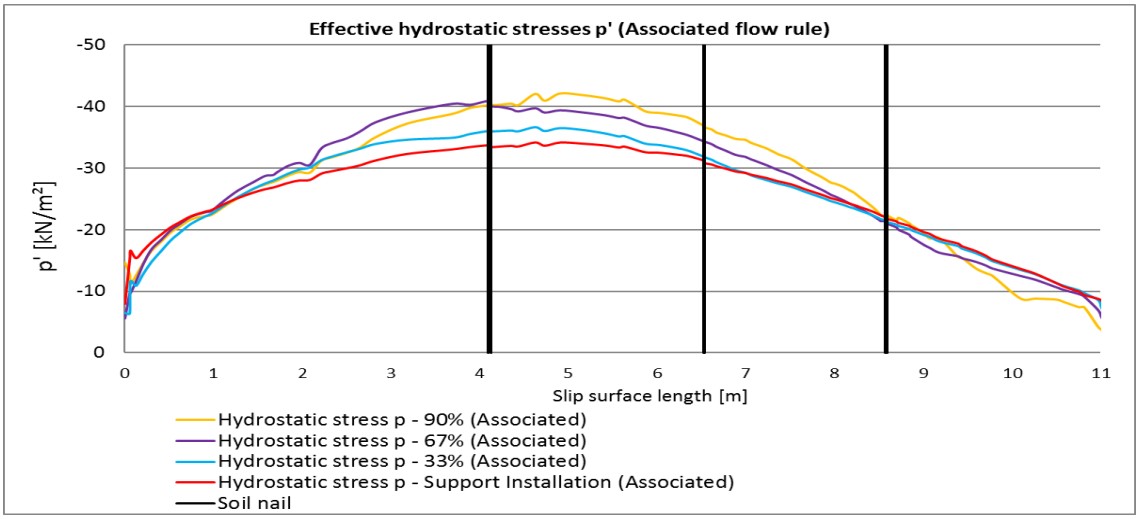

Figure E 5 p' over the slip surface length for the associated calculation of the 3-nail supported MC model

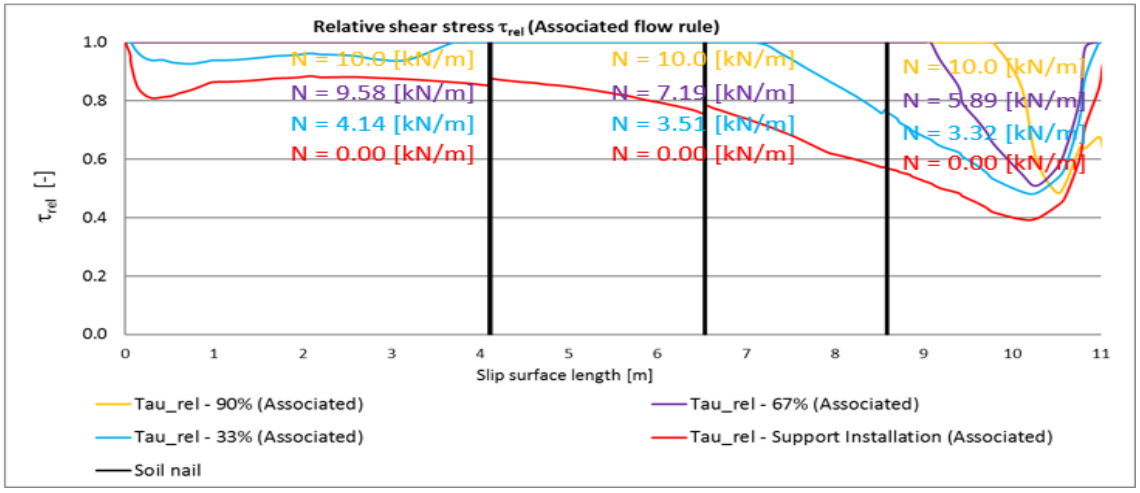

Figure E 6 Relative shear stress over the slip surface length for the non-associated calculation of the 3-nail supported MC model

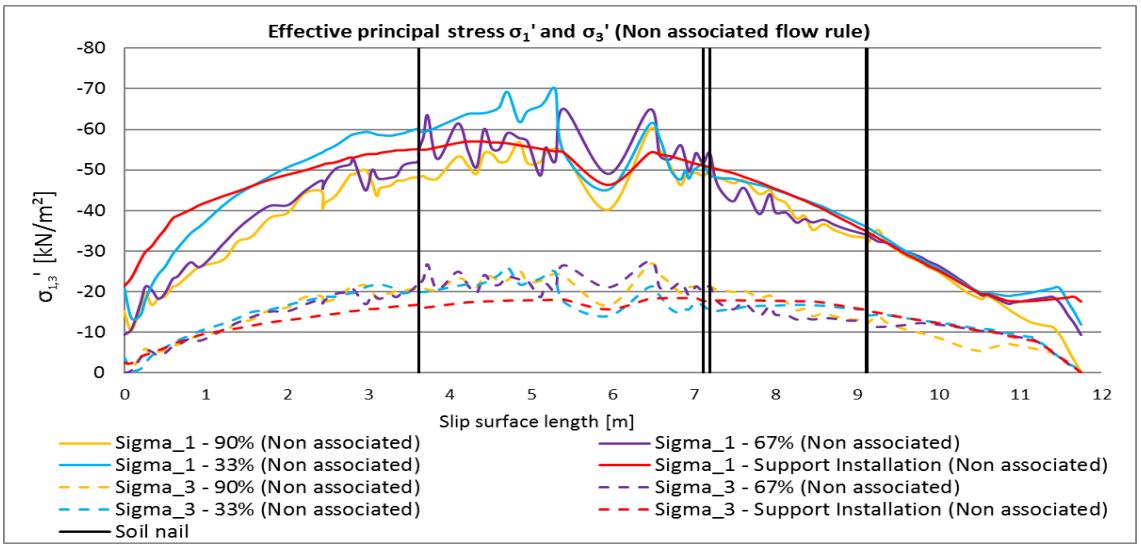

Figure E 7 $\sigma_{1,3}'$ over the slip surface length for the non-associated calculation of the 3-nail supported MC model

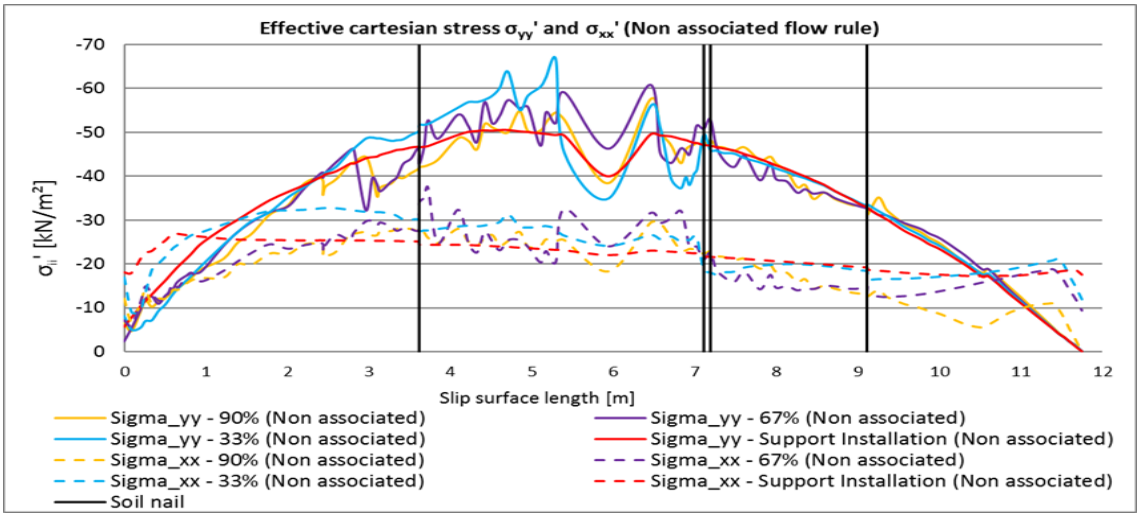

Figure E 8 $\sigma_{xx,yy}'$ over the slip surface length for the non-associated calculation of the 3-nail supported MC model

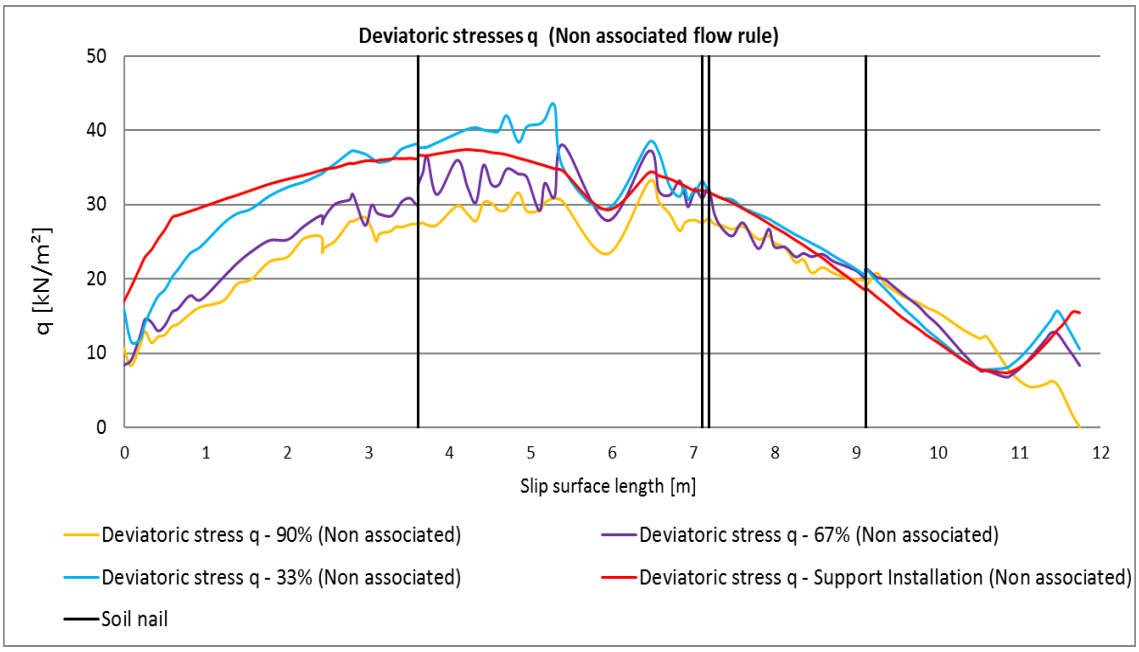

Figure E 9 Deviatoric stresses along the slip surface of the 3-nail supported MC model (non-associated flow rule)

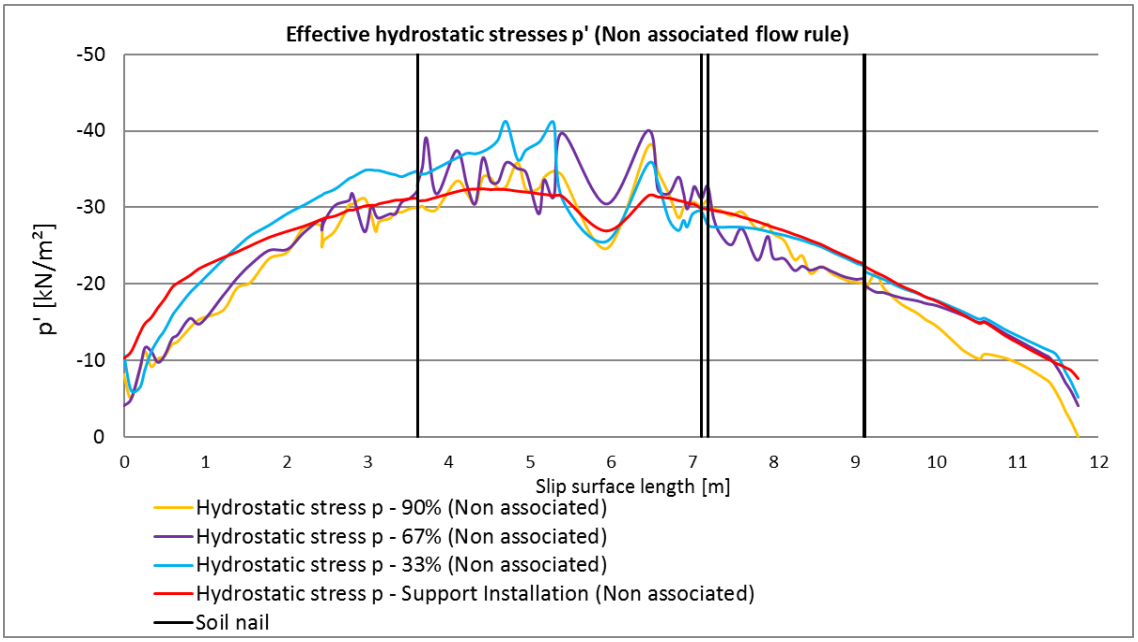

Figure E 10 Effective hydrostatic stresses along the slip surface of the 3-nail supported MC model (non-associated flow rule)

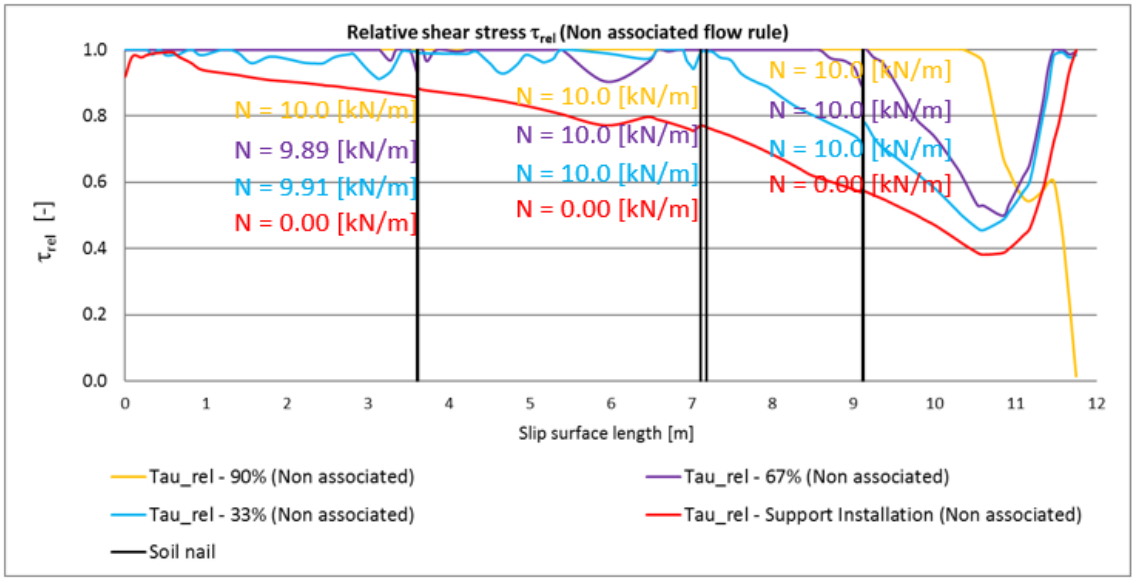

Figure E 11 Relative shear stress along the slip surface of the 3-nail supported MC model (non-associated flow rule)

MC 3-nail slope			
Stress	Associated		Non-associated
σn'			
σ1'	↑	>	↕
σ3'/σ2'	↑	>	↕
σyy'	↑	=	-
σxx'	↑	>	-
p'	↑	>	↕
q	↓	>	↓
τrel	↑	<	↑

Trend between steps over the slip surface:
↑ increasing trend
↓ decreasing trend
- no bigger change between steps
↕ scattering/no one unique trend

> associated shows higher stresses
< non-associated shows higher stresses
= almost equal

Figure E 12Trend of the stress indicators for the 3-nail supported MC model

Appendix F

The results displayed in this appendix are the stress indicators over the slip surface for the associated and non-associated flow rule of the MC-LE model of the unsupported slope.

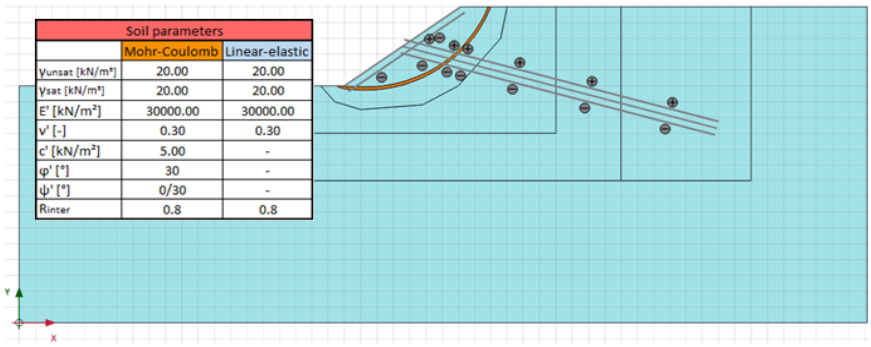

Figure F 1 MC-LE model without reinforcement

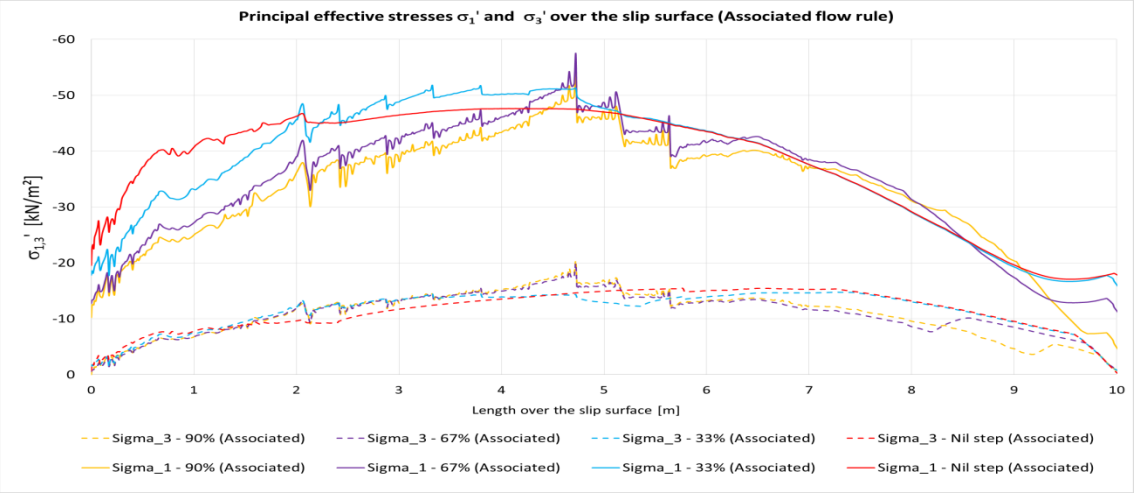

Figure F 2 Principal effective stresses $\sigma_{1,3}$' over the slip surface length for the associated calculation of the unsupported MC-LE model

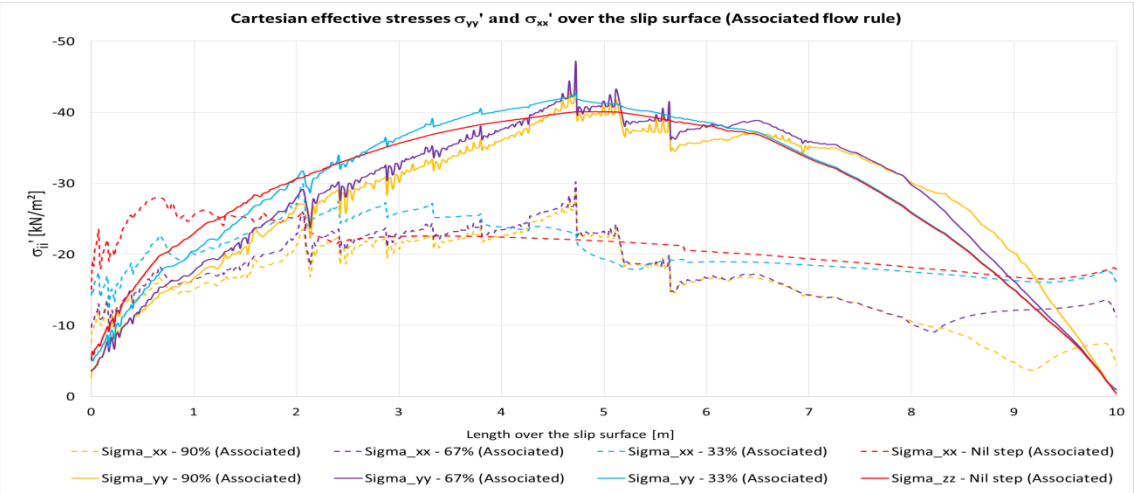

Figure F 3 Cartesian effective stresses $\sigma_{xx,yy}$' over the slip surface length for the associated calculation of the unsupported MC-LE model

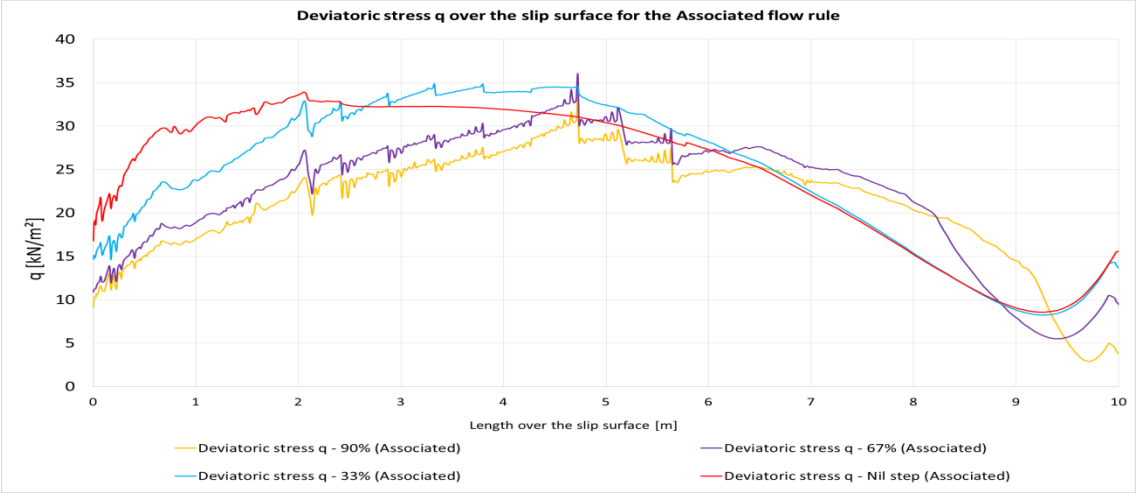

Figure F 4 Deviatoric stress q over the slip surface length for the associated calculation of the unsupported MC-LE model

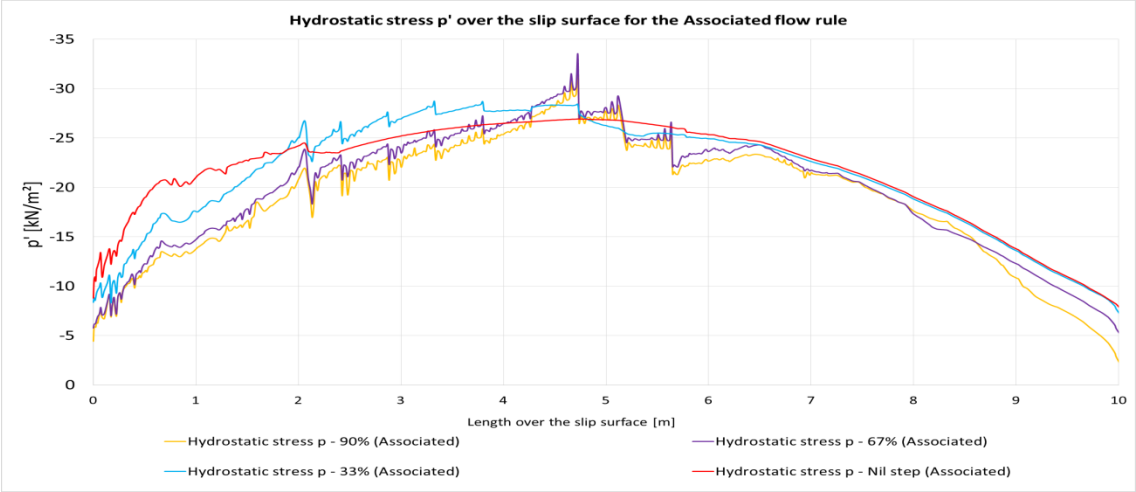

Figure F 5 Hydrostatic effective stress p' over the slip surface length for the associated calculation of the unsupported MC-LE model

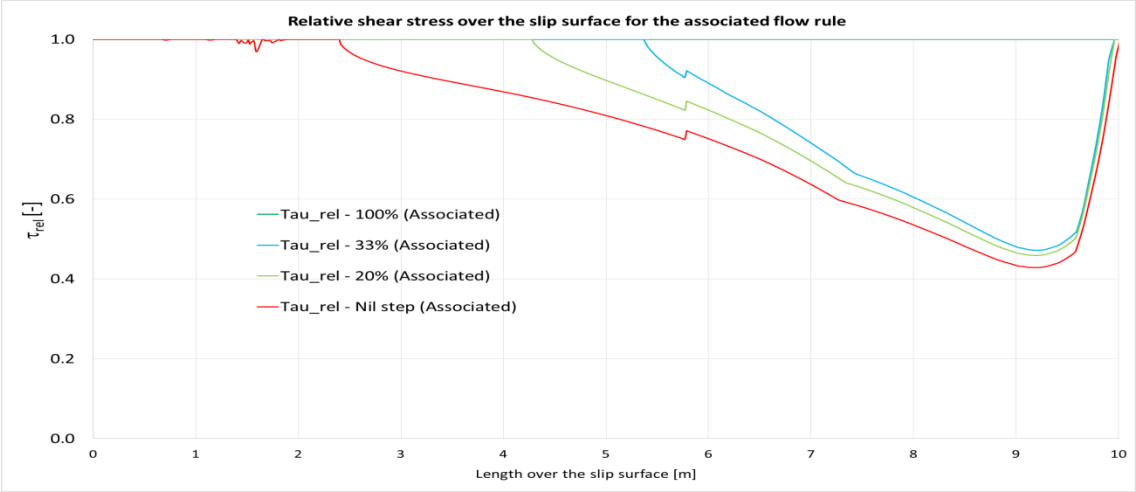

Figure F 6 Relative shear stress over the slip surface length for the associated calculation of the unsupported MC-LE model

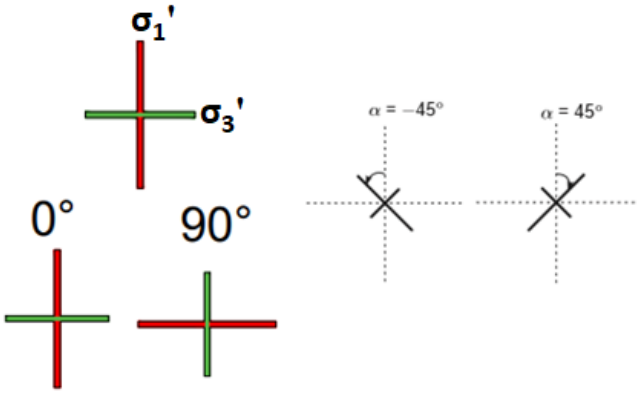

Figure F 7 Principal effective stress cross with the sign convection for the positive and negative inclination [1]

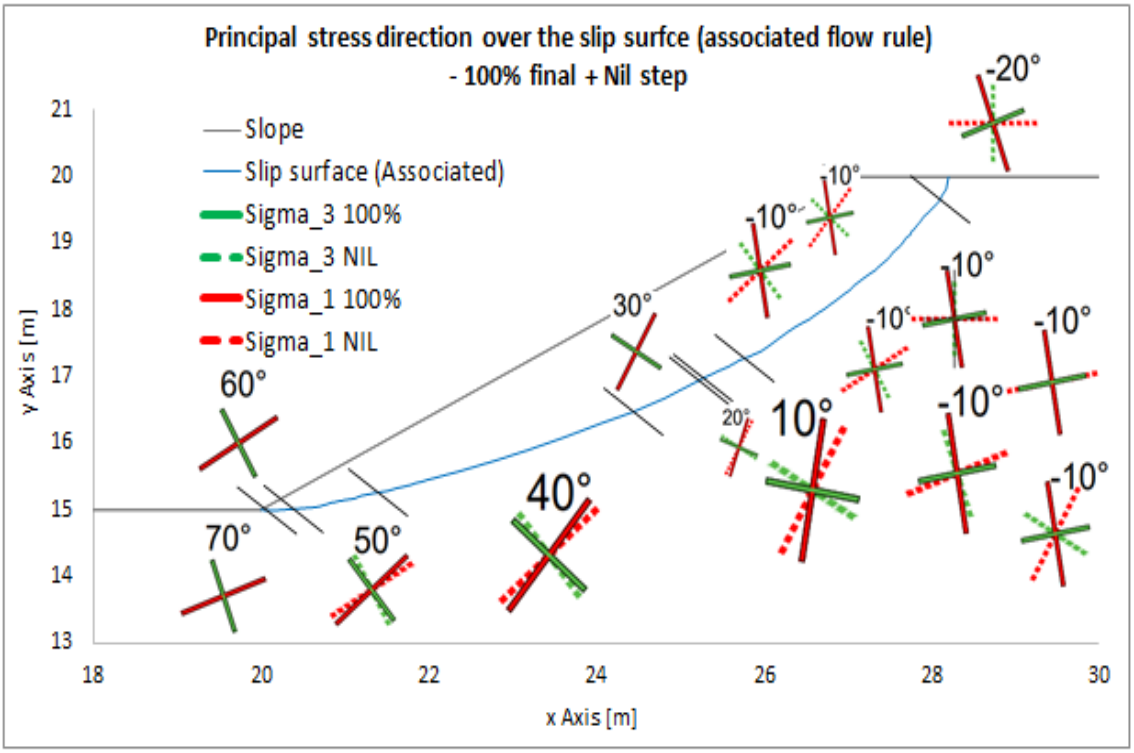

Figure F 8 Principal stress evolution over the slip surface for the associated flow rule (unsupported MC-LE model)

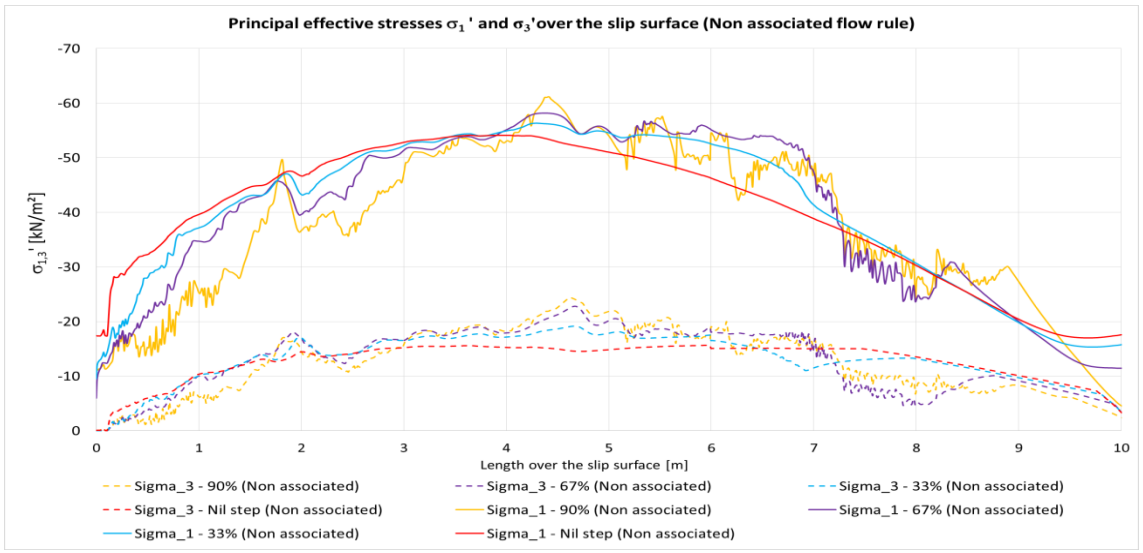

Figure F 9 Principal effective stresses $\sigma_{1,3}$' over the slip surface length for the non-associated calculation of the unsupported MC-LE model

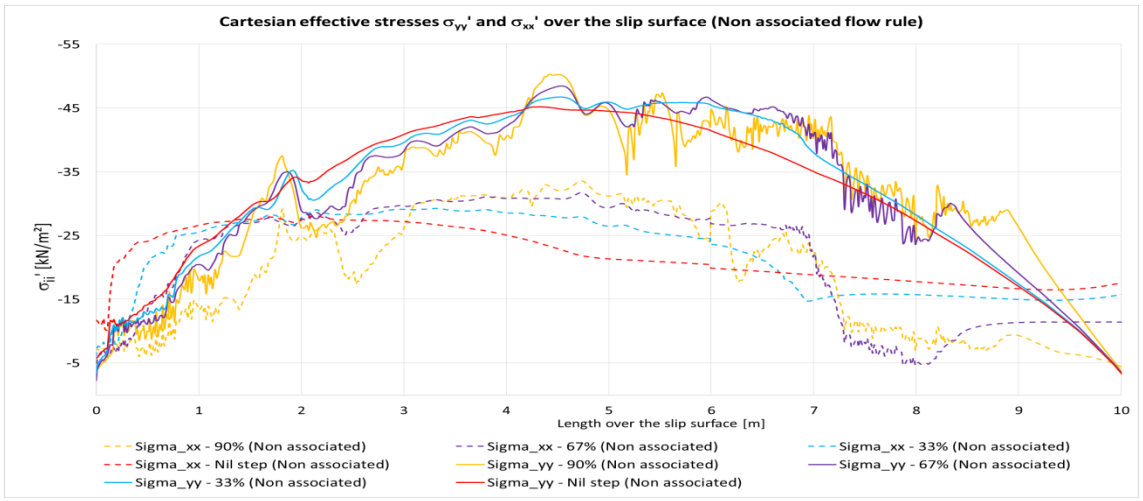

Figure F 1 Cartesian effective stresses σxx,yy' over the slip surface length for the non-associated calculation of the unsupported MC-LE model

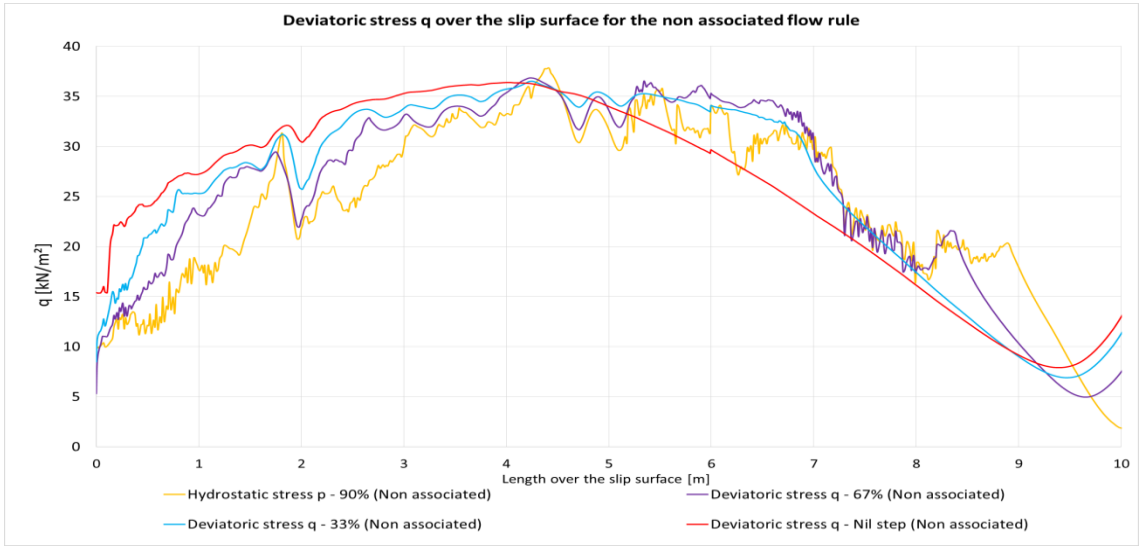

Figure F 11 Deviatoric stress q over the slip surface length for the non-associated calculation of the unsupported MC-LE model

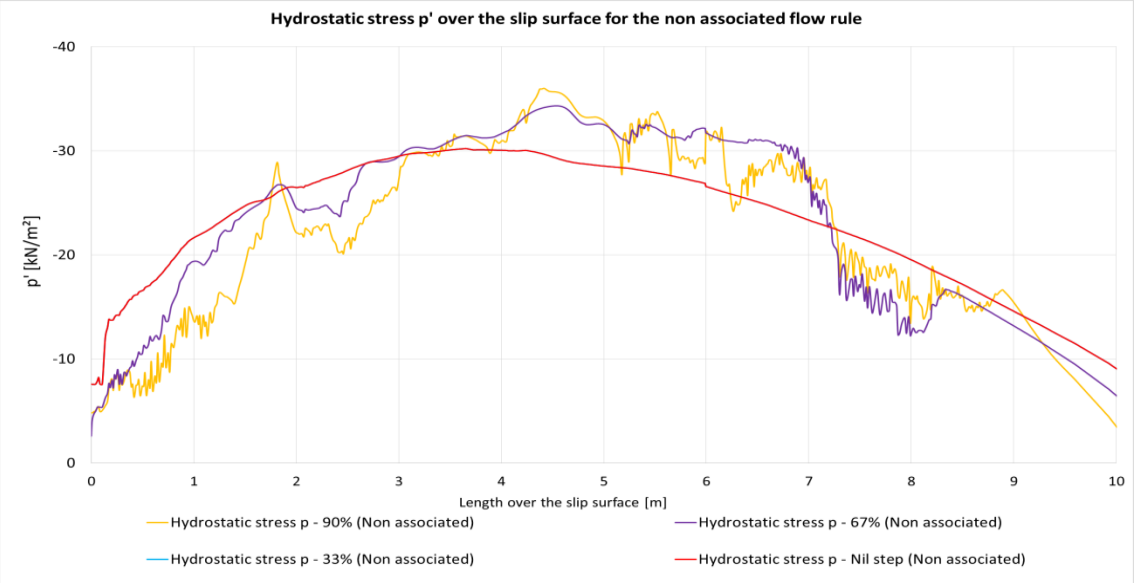

Figure F 12 Hydrostatic effective stress p' over the slip surface length for the non-associated calculation of the unsupported MC-LE model

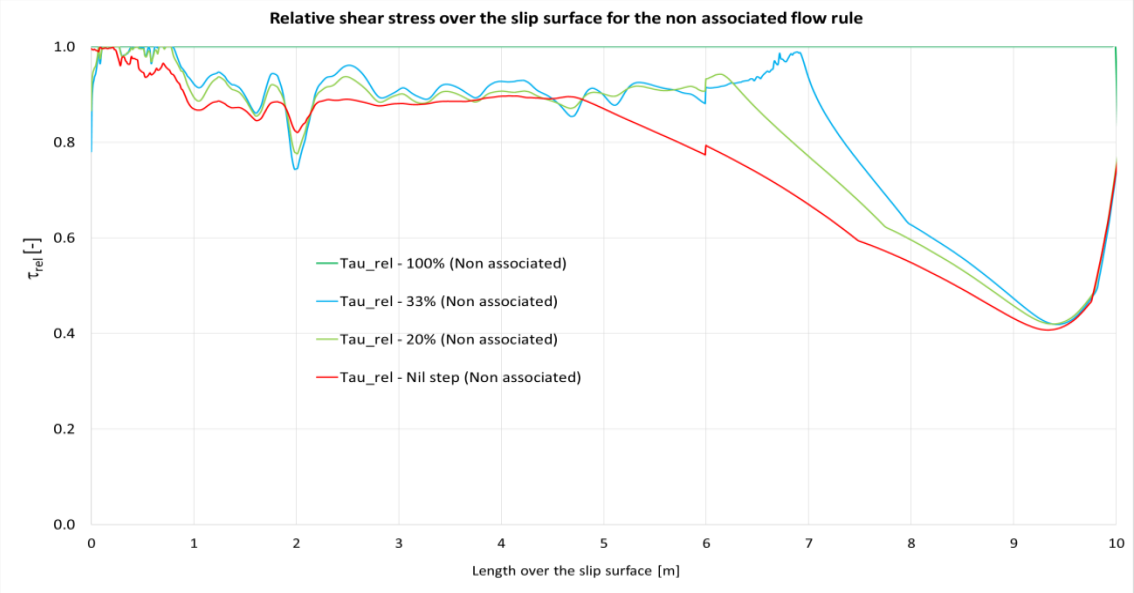

Figure F 13 Relative shear stress over the slip surface length for the non-associated calculation of the unsupported MC-LE model

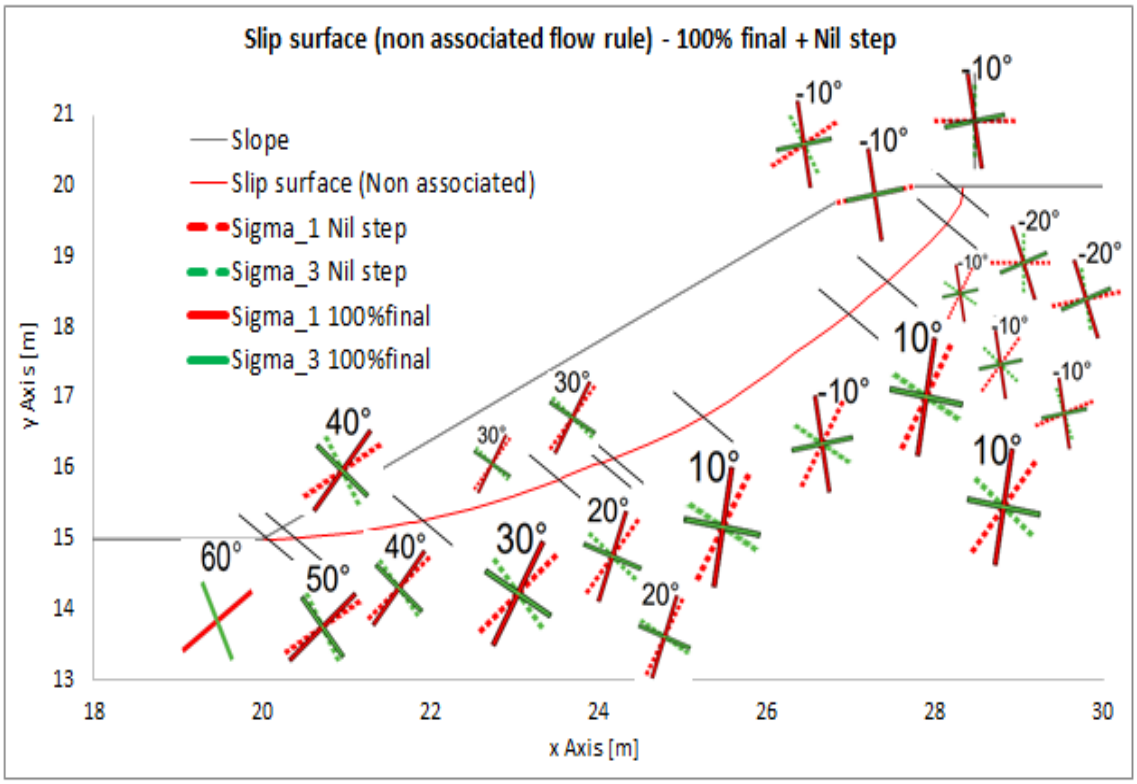

Figure F 14 Principal stress evolution over the slip surface for the non-associated flow rule (unsupported MC-LE model)

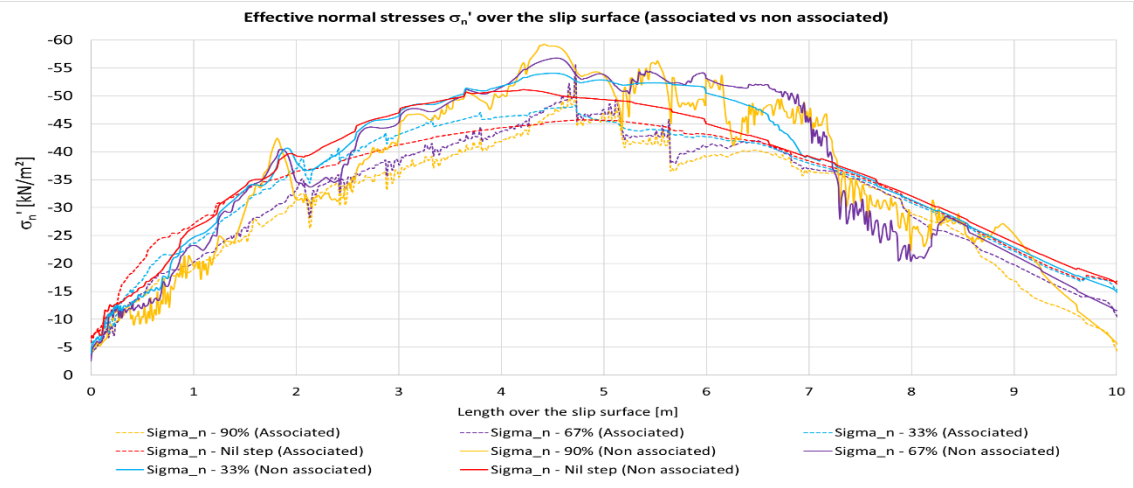

Figure F 15 Normal effective stress σ_n' over the slip surface length for the unsupported MC-LE model (associated vs. non-associated flow rule)

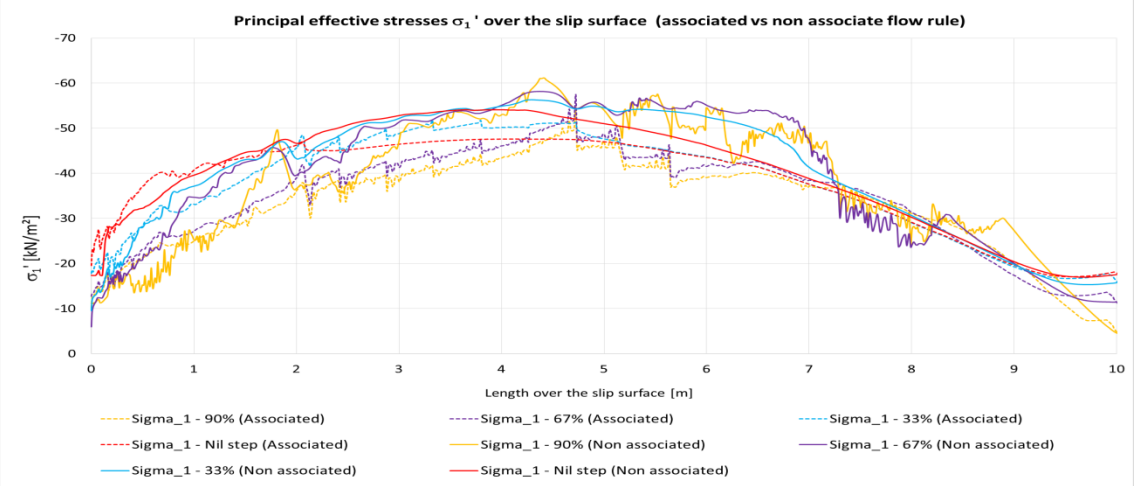

Figure F 16 σ_1' over the slip surface length for the unsupported MC-LE model (associated vs. non-associated flow rule)

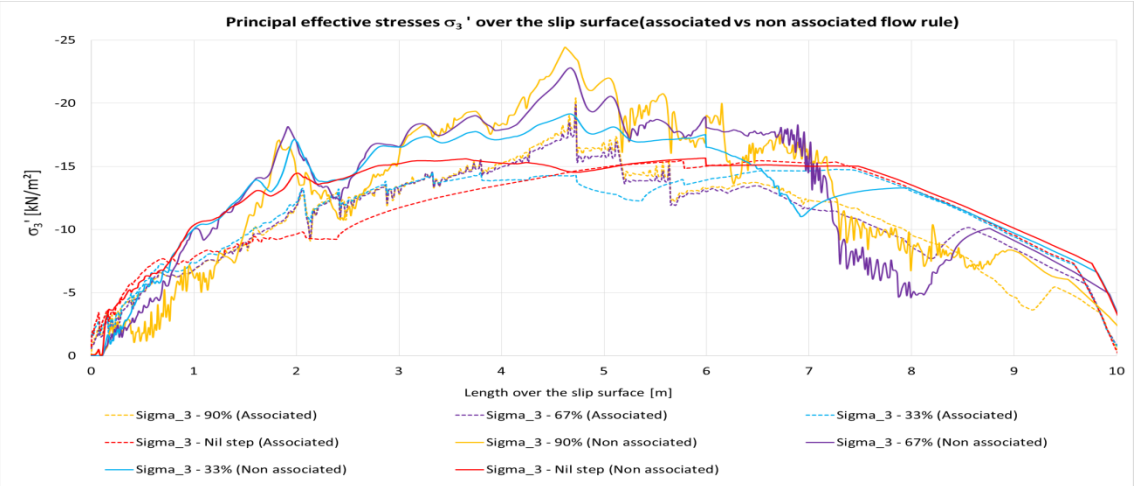

Figure F 17 σ_3' over the slip surface length for the unsupported MC-LE model (associated vs. non-associated flow rule)

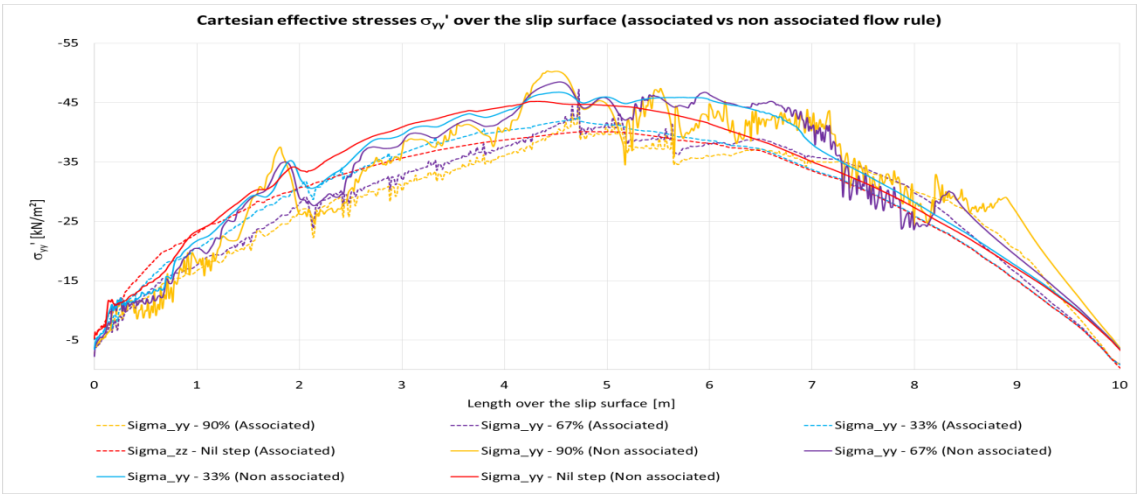

Figure F 18 σ_{yy}' over the slip surface length for the unsupported MC-LE model (associated vs. non-associated flow rule)

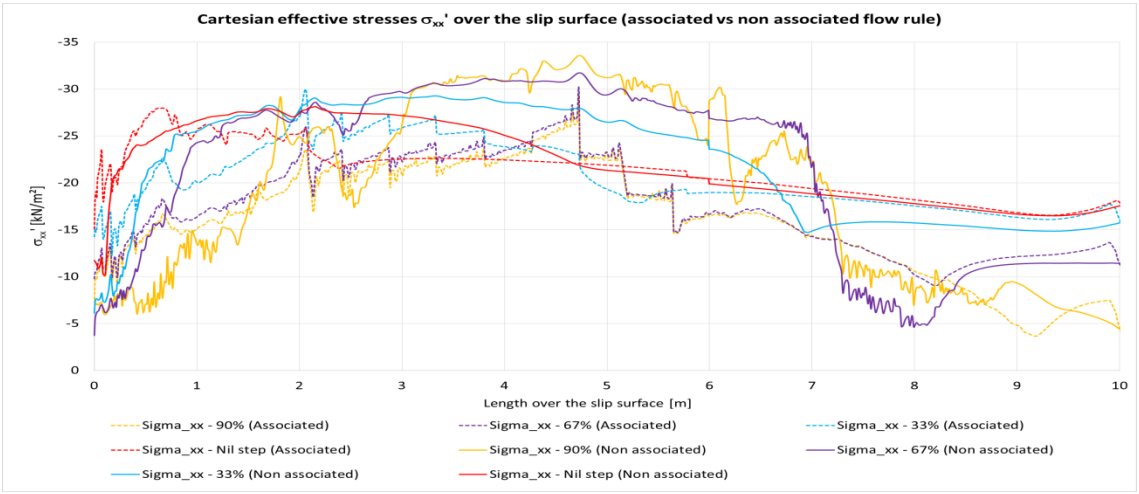

Figure F 19 σ_{xx}' over the slip surface length for the unsupported MC-LE model (associated vs. non-associated flow rule)

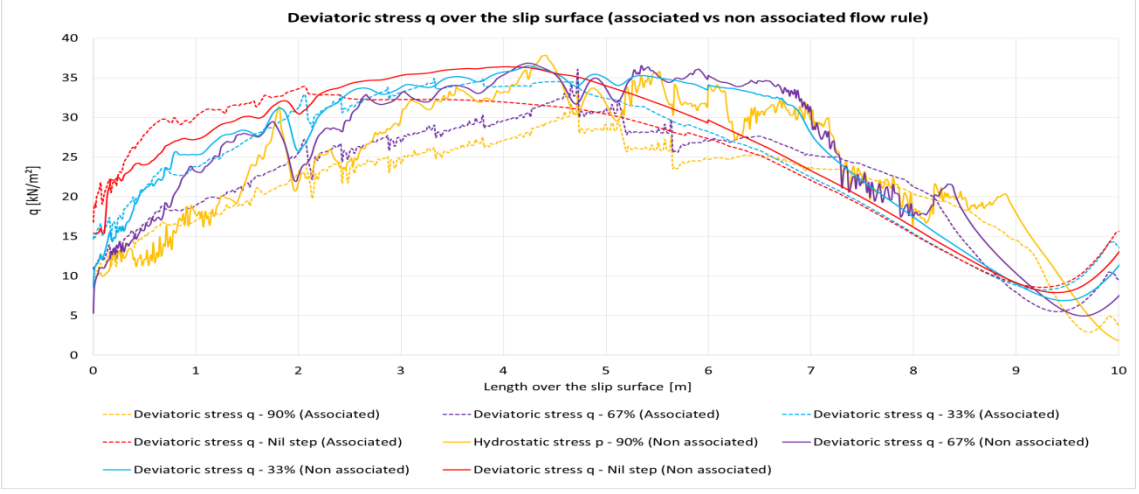

Figure F 20 Deviatoric stress q over the slip surface length for the unsupported MC-LE model (associated vs. non-associated flow rule)

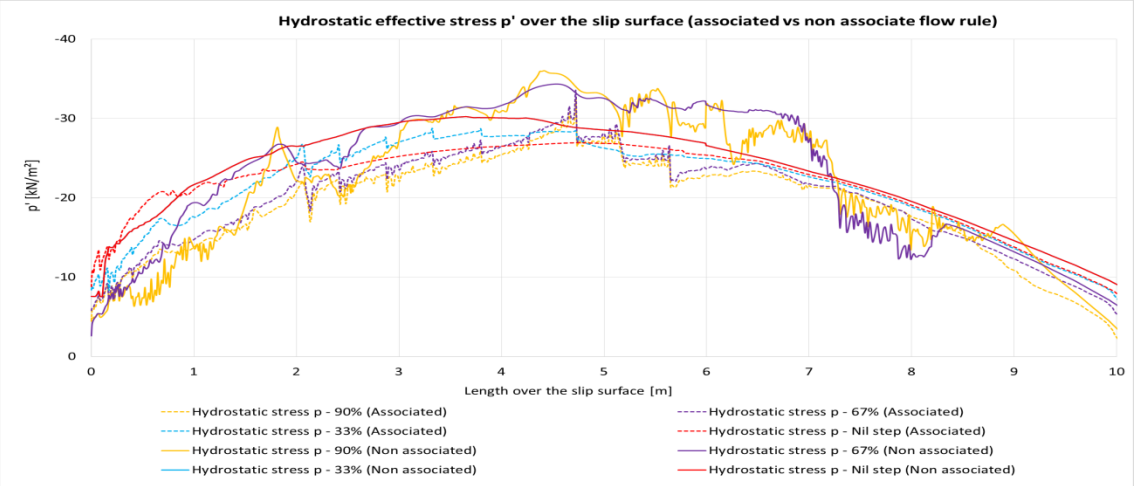

Figure F 21 Effective hydrostatic stress p' over the slip surface length for the unsupported MC-LE model (associated vs. non-associated flow rule)

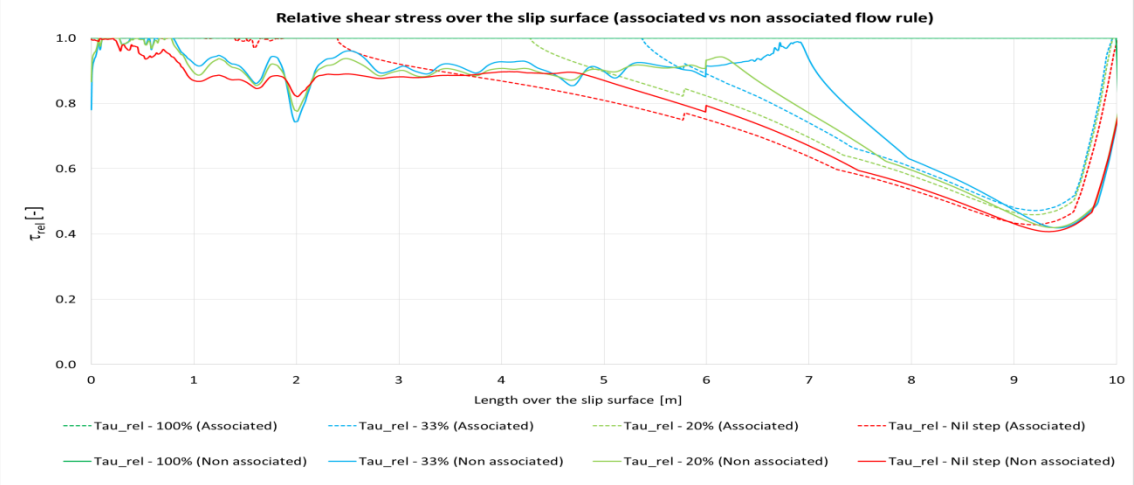

Figure F 22 Relative shear stress over the slip surface length for the unsupported MC-LE model (associated vs. non-associated flow rule)

MC-LE unsupported slope			
Stress	Associated		Non-associated
σn'	↓	<	↕
σ1'	↓	<	↕
σ3'/σ2'	-	<	↕
σyy'	-	<	↕
σxx'	↕	<	↕
p'	↓	<	↕
q	↓	<	↕
τrel	↑	<	↑

Trend between steps over the slip surface:
↑ increasing trend
↓ decreasing trend
- no bigger change between steps
↕ scattering/no evident trend

> associated shows higher stresses
< non-associated shows higher stresses
= almost equal

Figure F 23 Trend of the stress indicators for the unsupported MC-LE model

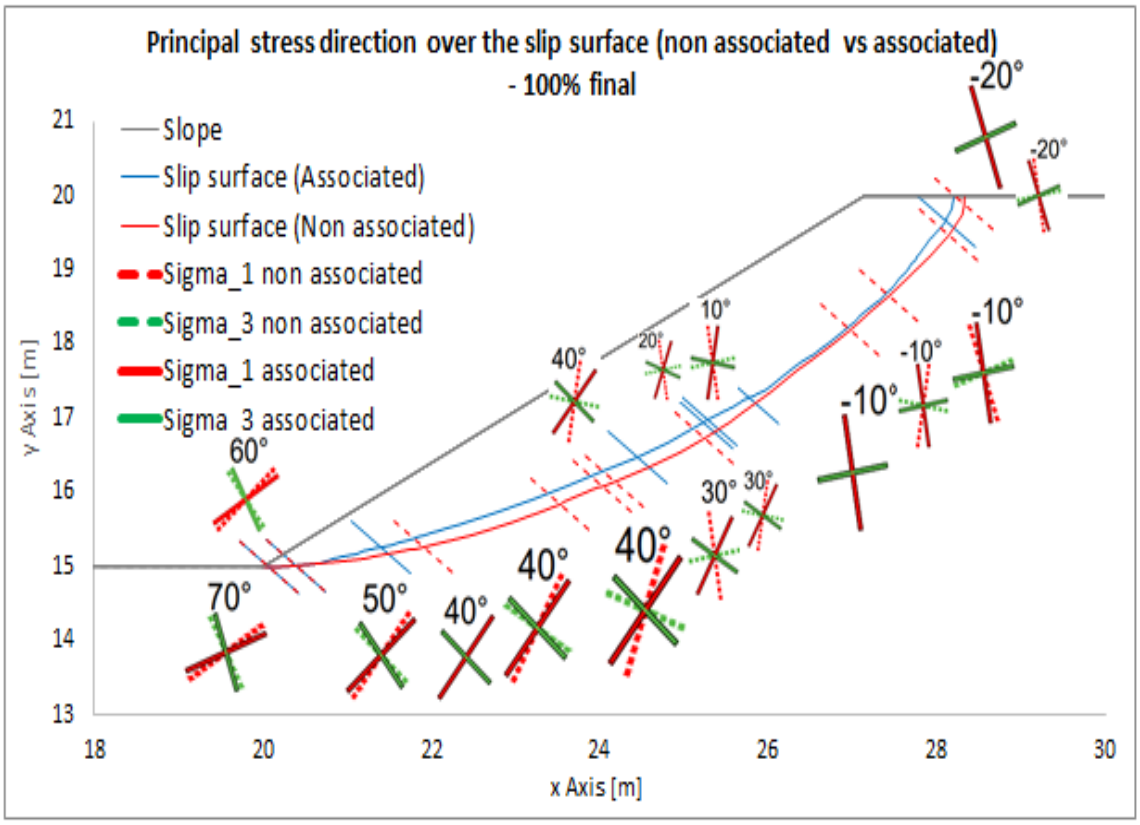

Figure F 24 Principal stress evolution over the slip surface for the unsupported MC-LE model (associated vs. non-associated flow rule)

Appendix G

The results displayed in this appendix are the stress indicators over the slip surface for the associated and non-associated flow rule of the MC-LE model with a 3-nail reinforced slope.

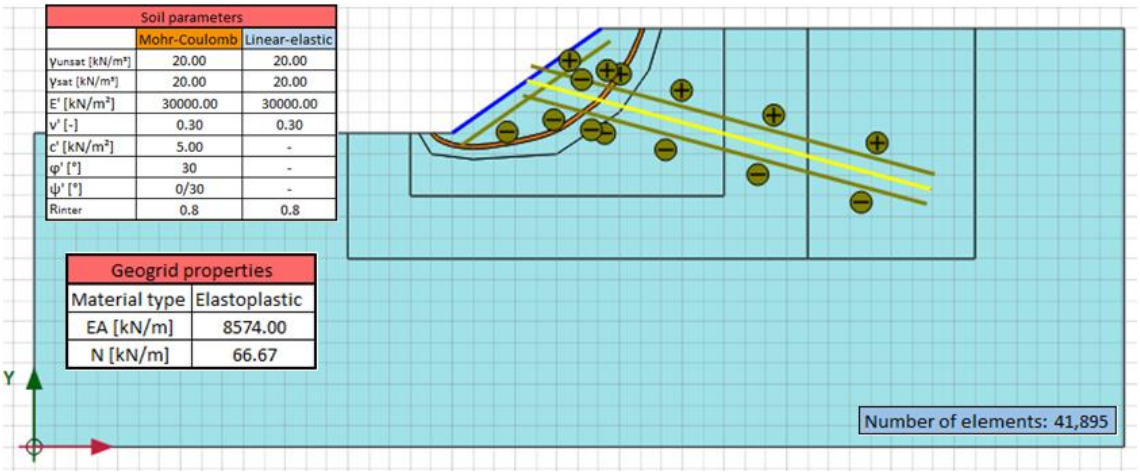

Figure G 1 MC-LE model with a support with one soil nail (geogrid + interface)

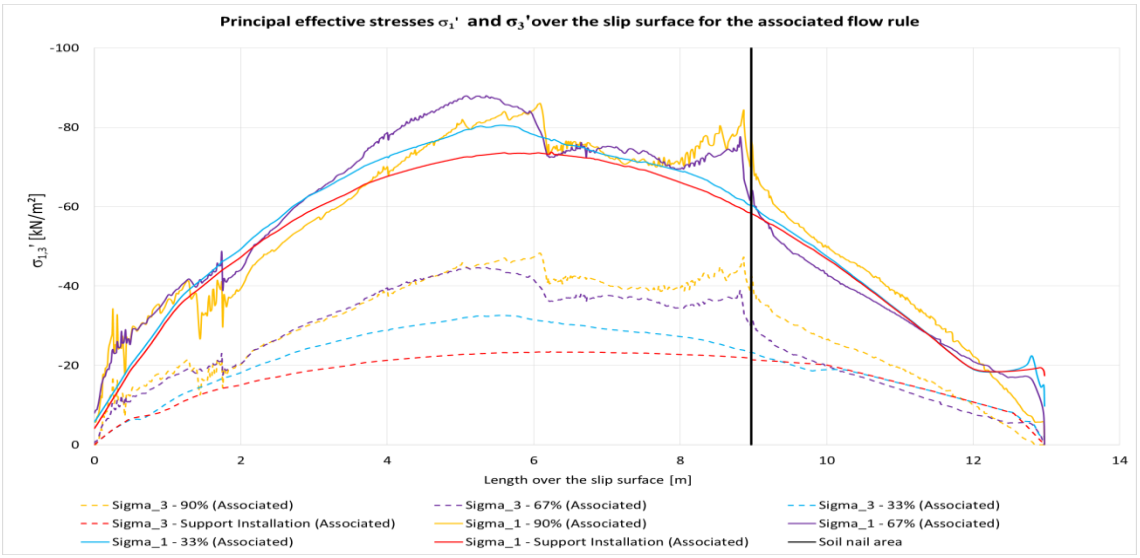

Figure G 2 Principal effective stresses $\sigma_{1,3}'$ over the slip surface length for the associated calculation of the 1-nail supported MC-LE model

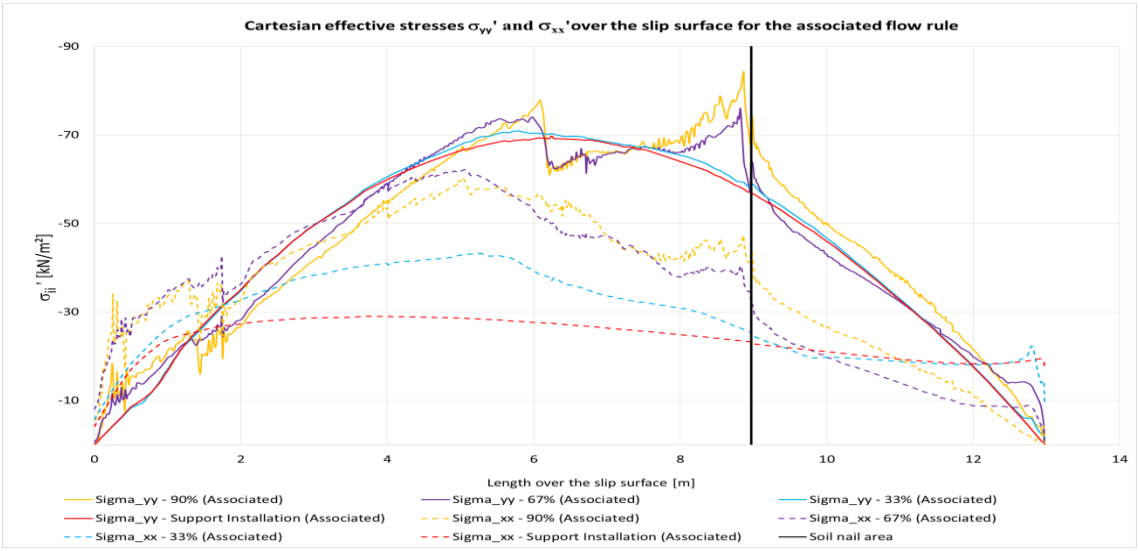

Figure G 3 Cartesian effective stresses $\sigma_{xx,yy}$' over the slip surface length for the associated calculation of the 1-nail supported MC-LE model

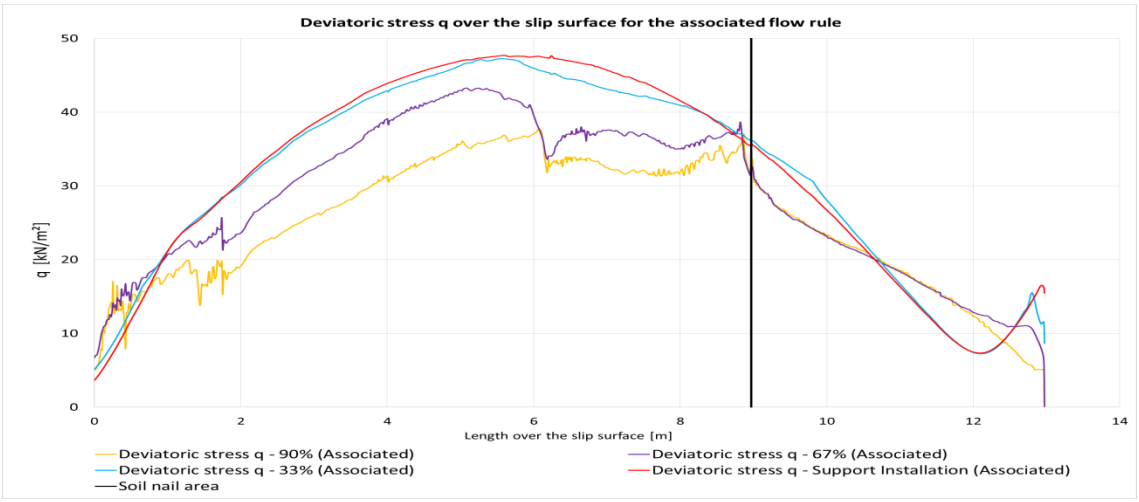

Figure G 4 Deviatoric stress q over the slip surface length for the associated calculation of the 1-nail supported MC-LE model

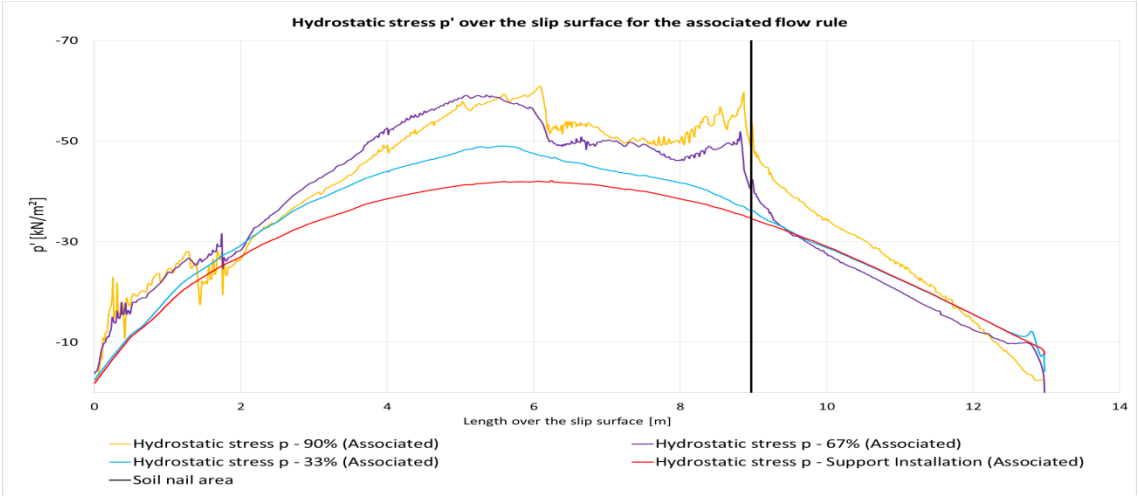

Figure G 5 Effective hydrostatic stress p' over the slip surface length for the associated calculation of the 1-nail supported MC-LE model

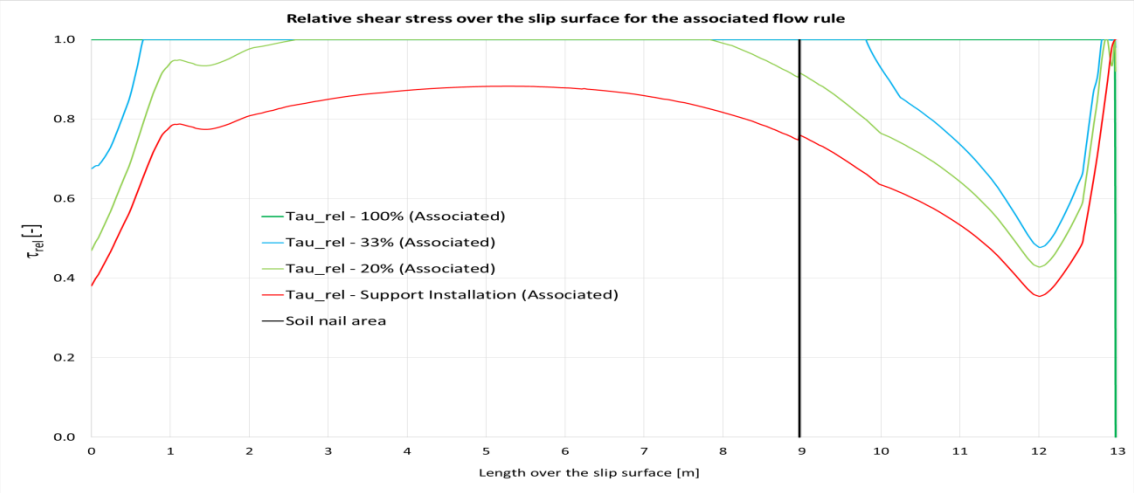

Figure G 3 Relative shear stress over the slip surface length for the associated calculation of the 1-nail supported MC-LE model

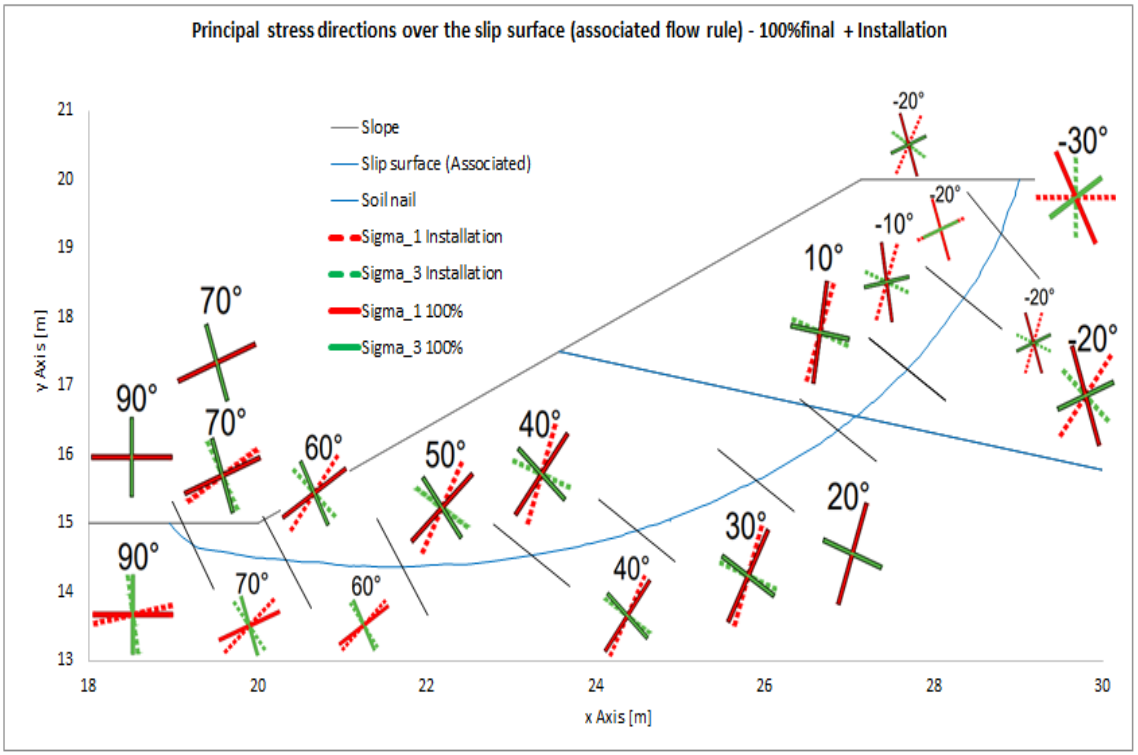

Figure G 4 Principal stress direction evolution over the slip surface for the associated calculation of the 1-nail supported MC-LE model

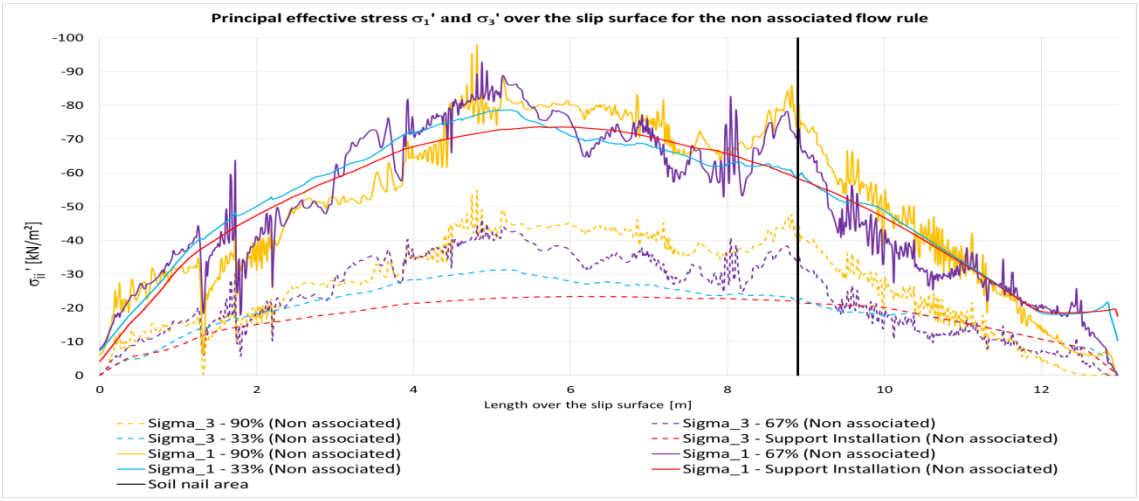

Figure G 8 Principal effective stresses $\sigma_{1,3}$' over the slip surface length for the non-associated calculation of the 1-nail supported MC-LE model

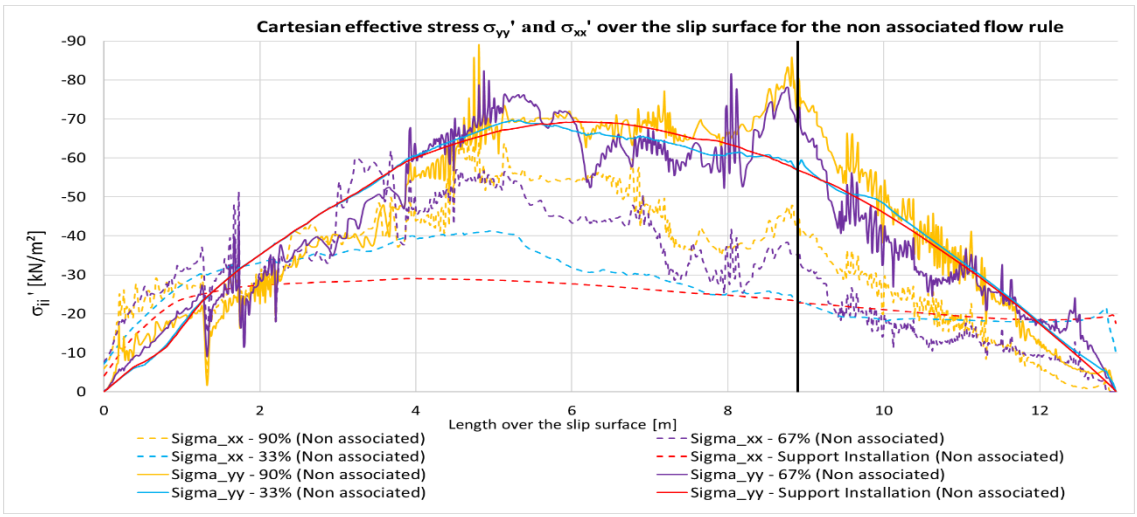

Figure G 9 Cartesian effective stresses $\sigma_{xx,yy}$' over the slip surface length for the non-associated calculation of the 1-nail supported MC-LE model

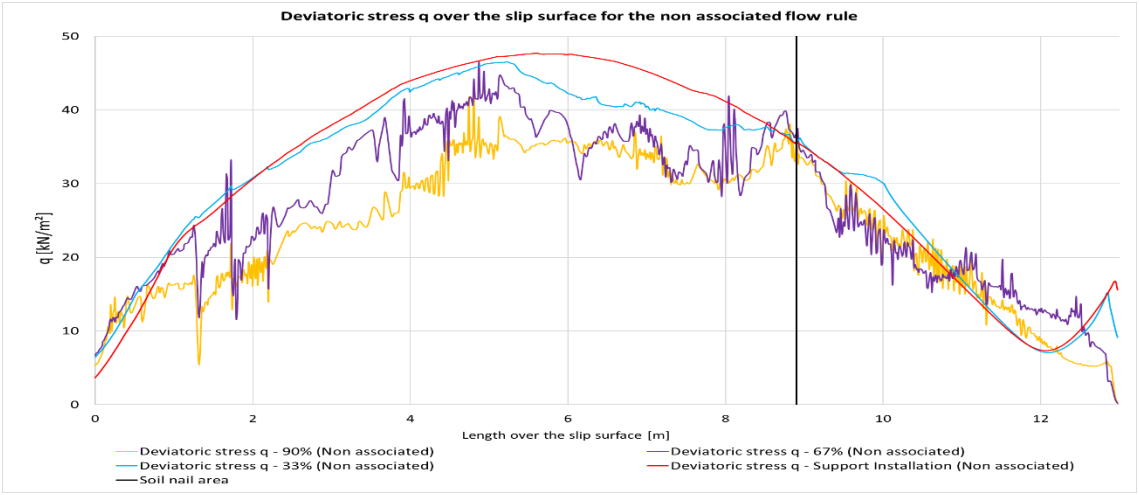

Figure G 10 Deviatoric stress q over the slip surface length for the associated calculation of the 1-nail supported MC-LE model

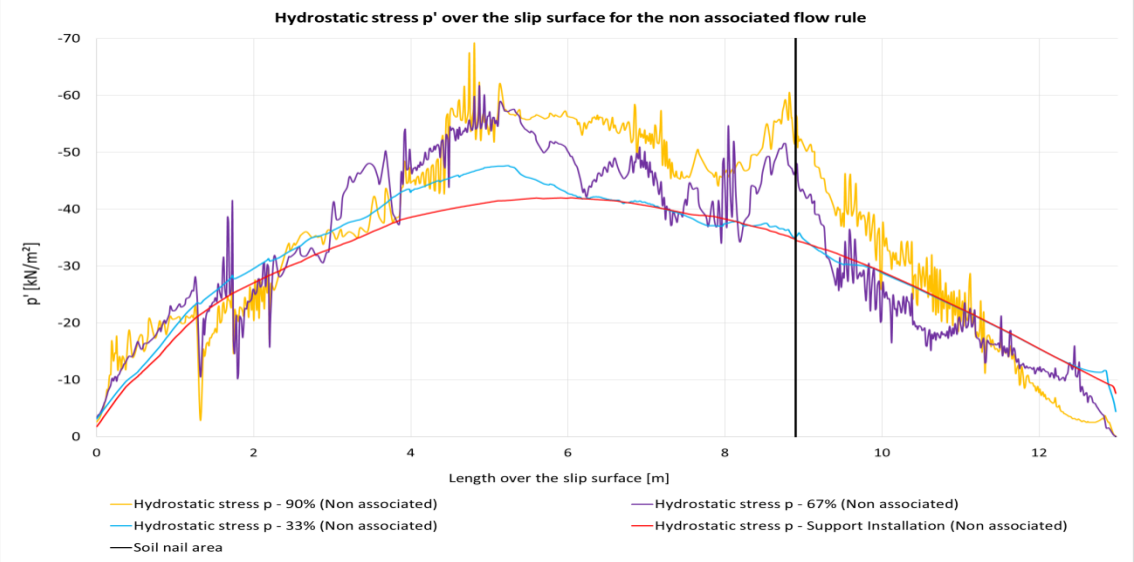

Figure G 5 Effective hydrostatic stress p' over the slip surface length for the non-associated calculation of the 1-nail supported MC-LE model

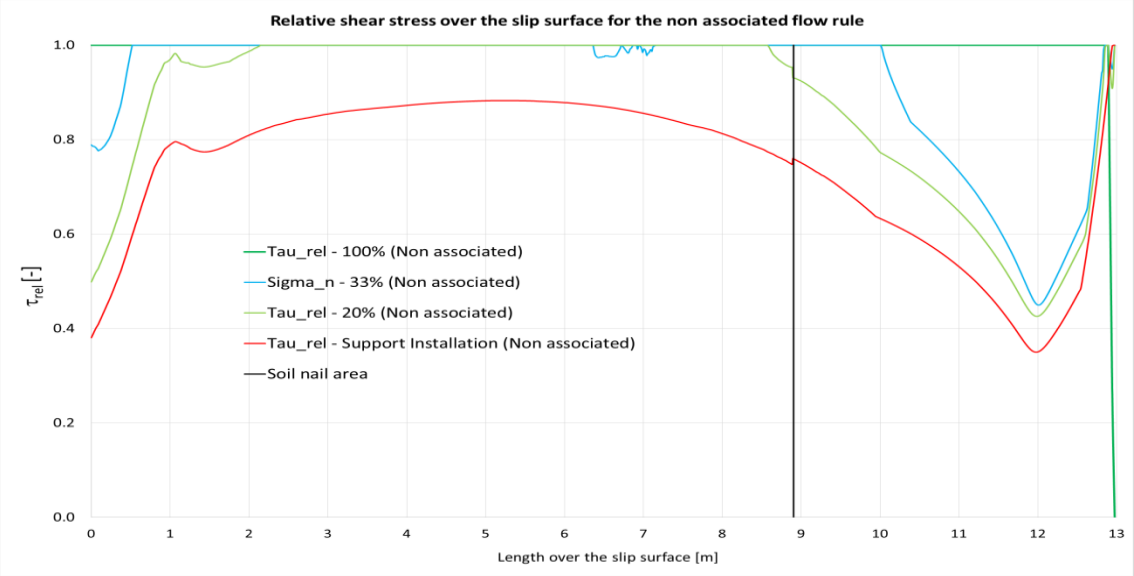

Figure G 6 Relative shear stress over the slip surface length for the non-associated calculation of the 1-nail supported MC-LE model

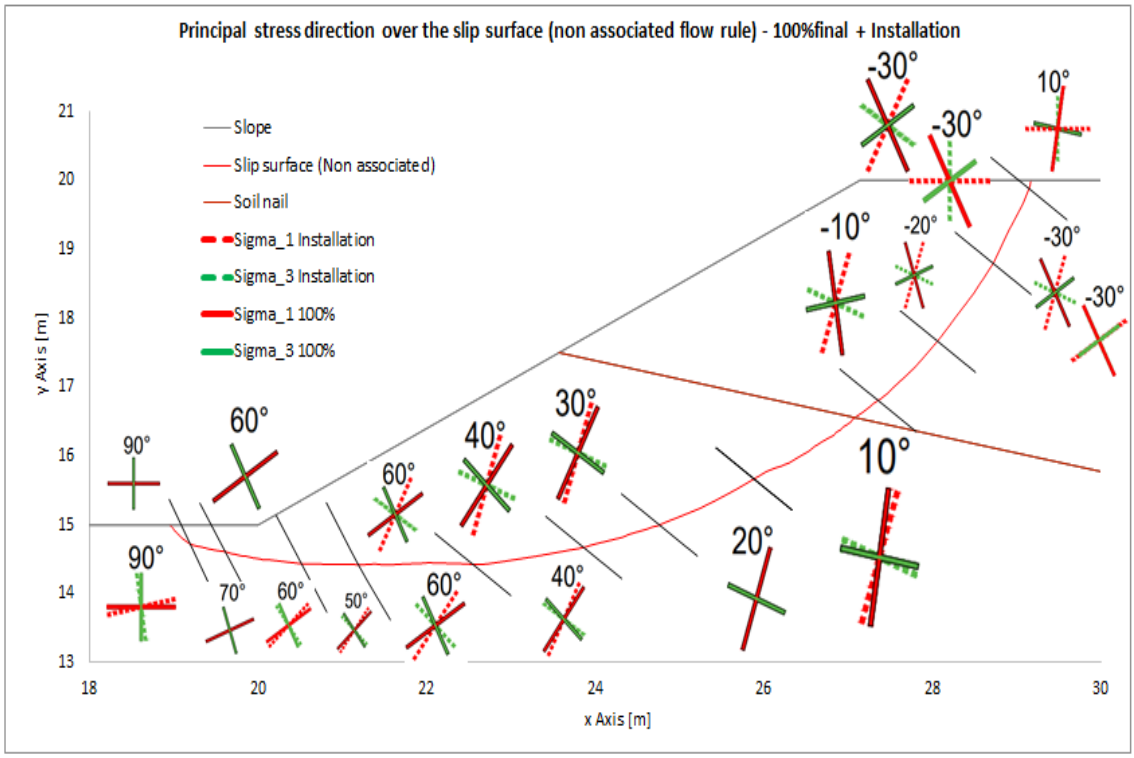

Figure G 7 Principal stress direction evolution over the slip surface for the non-associated calculation of the 1-nail supported MC-LE model

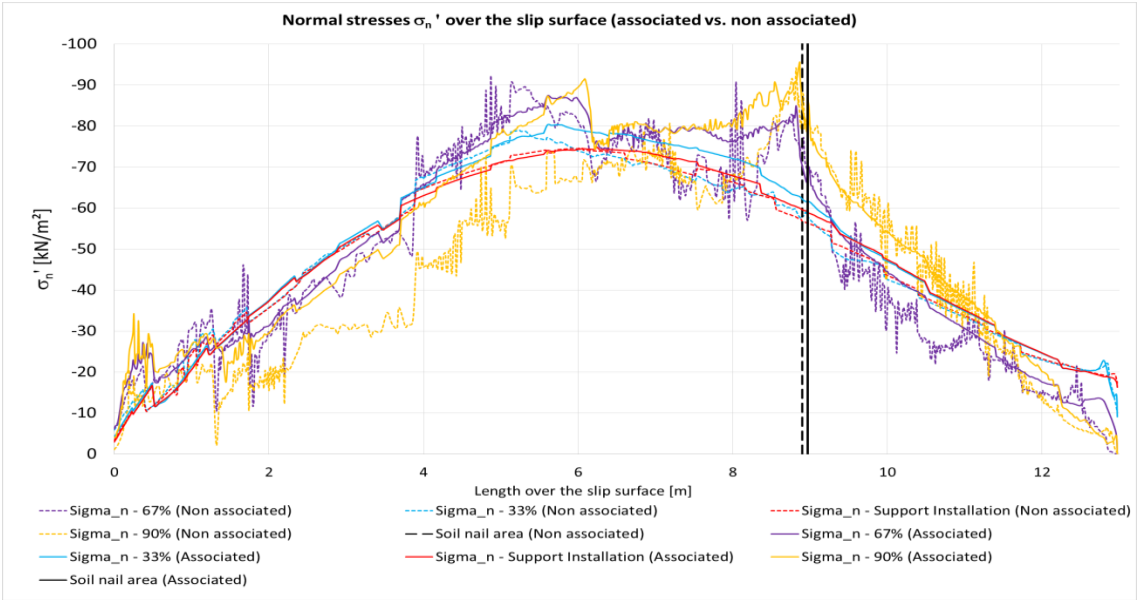

Figure G 8 Normal effective stress σ_n' over the slip surface length for the 1-nail supported MC-LE model (associated vs. non-associated flow rule)

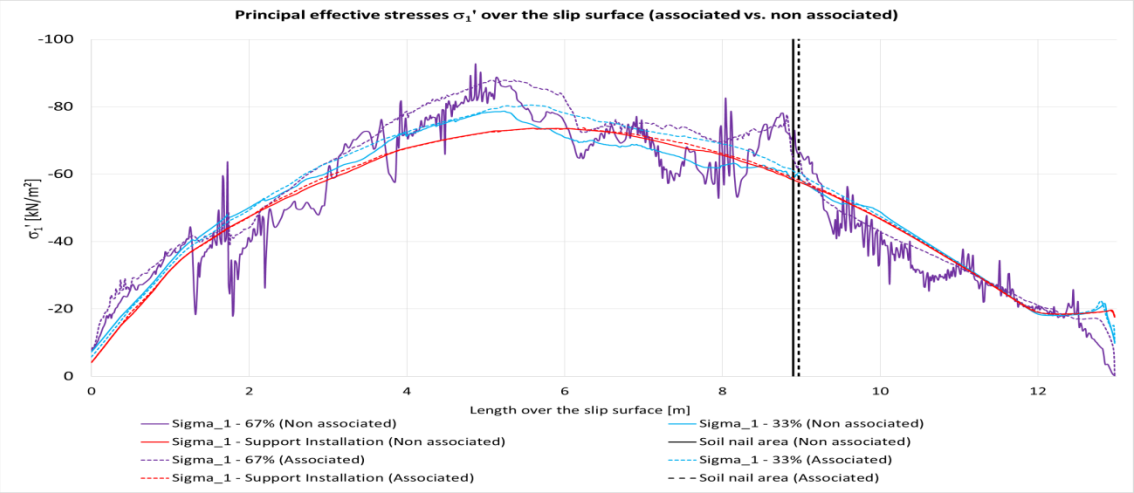

Figure G 15 σ_1' over the slip surface length for the 1-nail supported MC-LE model (associated vs. non-associated flow rule)

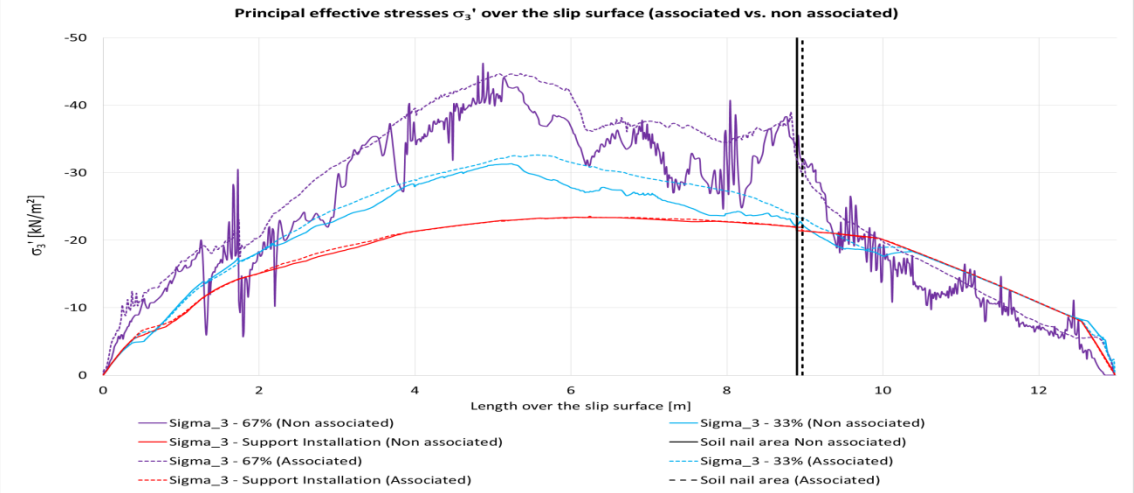

Figure G 16 σ_3' over the slip surface length for the 1-nail supported MC-LE model (associated vs. non-associated flow rule)

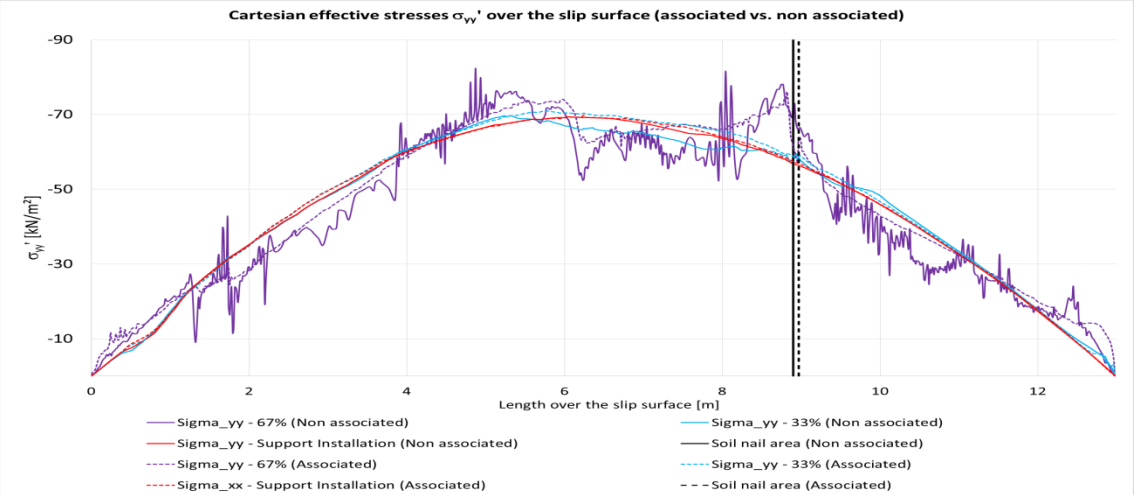

Figure G 17 σ_{yy}' over the slip surface length for the 1-nail supported MC-LE model (associated vs. non-associated flow rule)

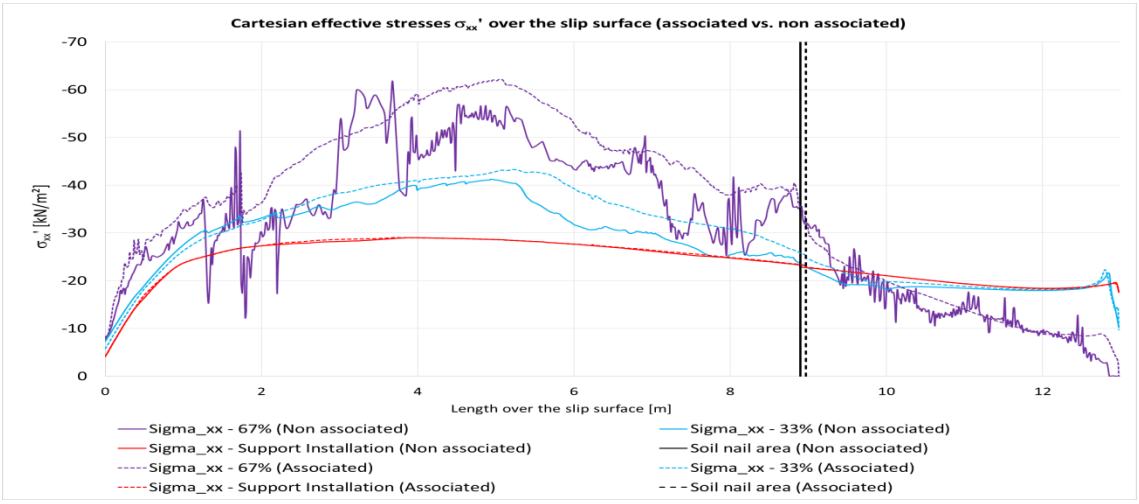

Figure G 18 σ_{xx}' over the slip surface length for the 1-nail supported MC-LE model (associated vs. non-associated flow rule)

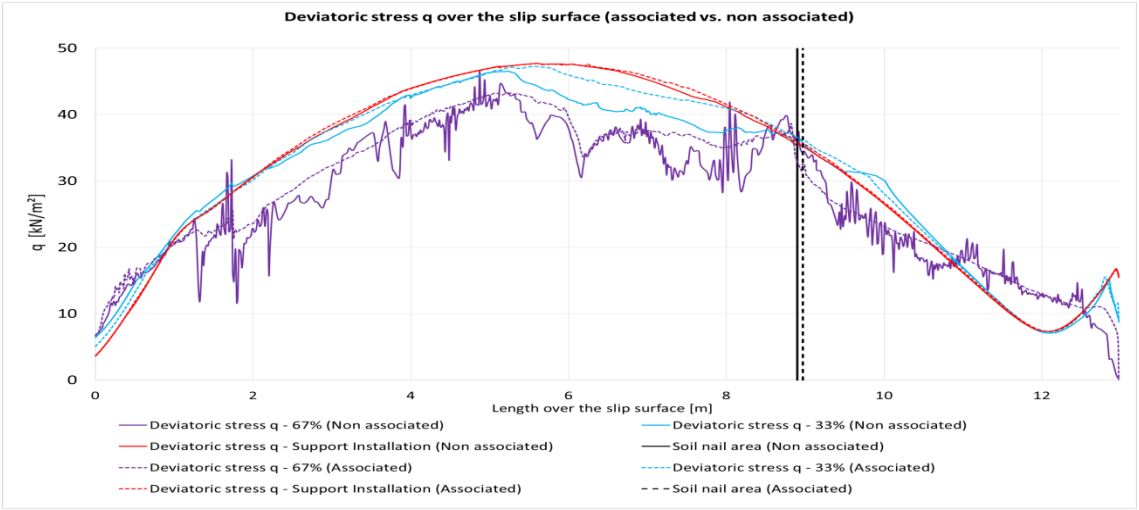

Figure G 9 Deviatoric stress q over the slip surface length for the 1-nail supported MC-LE model (associated vs. non-associated flow rule)

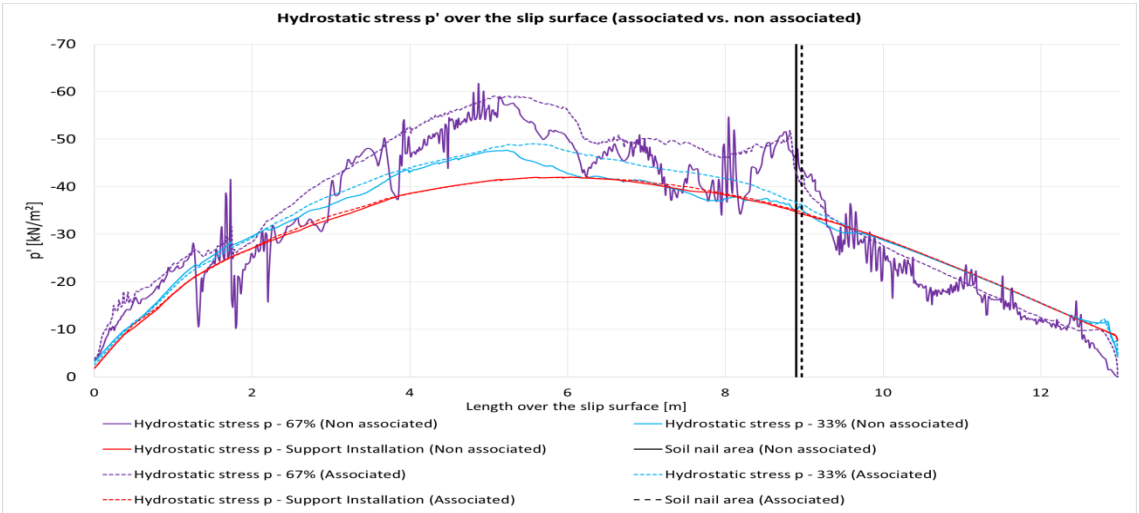

Figure G 20 Effective hydrostatic stress p' over the slip surface length for the 1-nail supported MC-LE model (associated vs. non-associated flow rule)

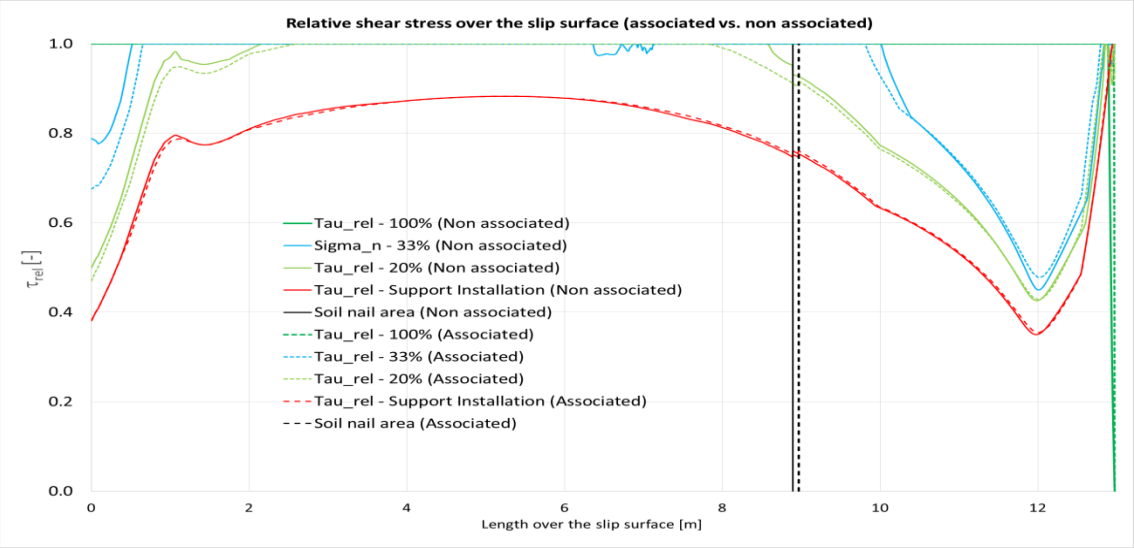

Figure G 21 Relative shear stress over the slip surface length for the 1-nail supported MC-LE model (associated vs. non-associated flow rule)

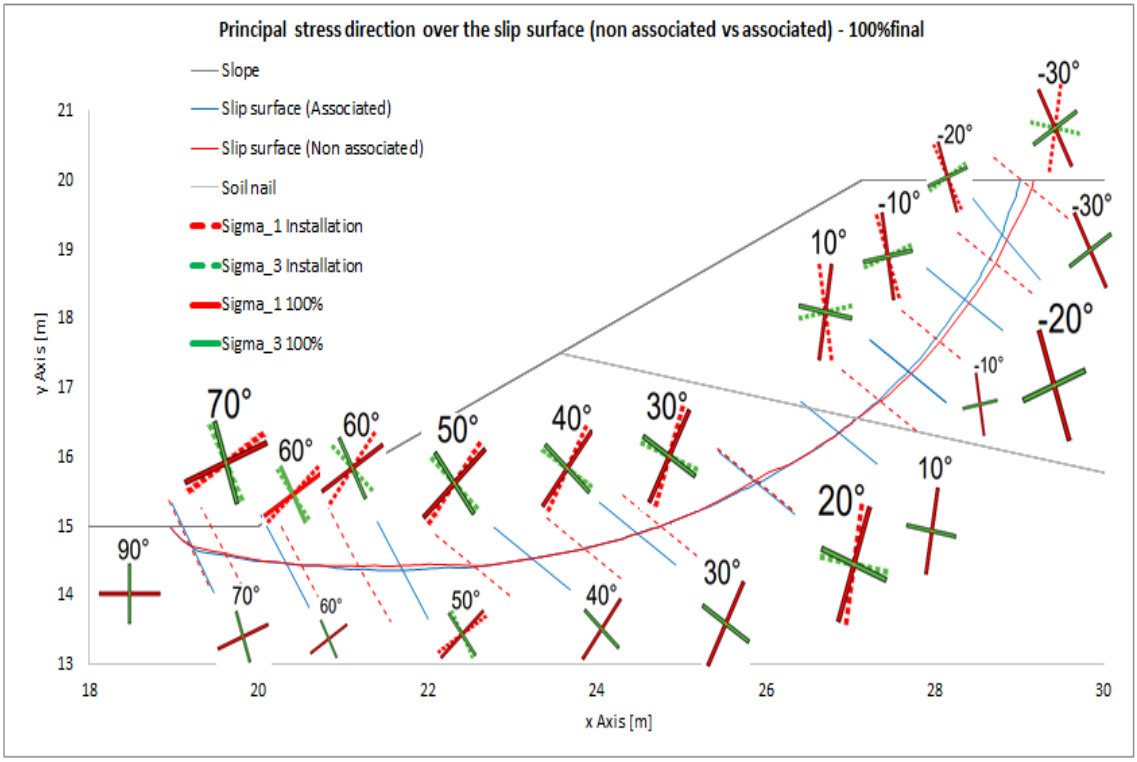

Figure G 22 Evolution of the principal stress direction over the slip surface for the 1-nail supported MC-LE model (associated vs. non-associated flow rule)

MC-LE 1-nail slope			
Stress	Associated		Non-associated
σ_n'	↕	>	↑
σ_1'	↑	>	↑
σ_3'/σ_2'	↑	>	↑
σ_{yy}'	↑	=	↑
σ_{xx}'	↑	>	↑
p'	↑	>	↑
q	↓	=	↓
τ_{rel}	↑	=	↑

Trend between steps over the slip surface:
↑ increasing trend
↓ decreasing trend
– no bigger change between steps
↕ scattering/no evident trend

> associated shows higher stresses
< non-associated shows higher stresses
= almost equal

Figure G 23 Trend of the stress indicators for the 1-nail supported MC-LE model

Appendix H

The results displayed in this appendix are the stress indicators over the slip surface for the associated and non-associated flow rule of the MC-LE model with a 3-nail reinforced slope.

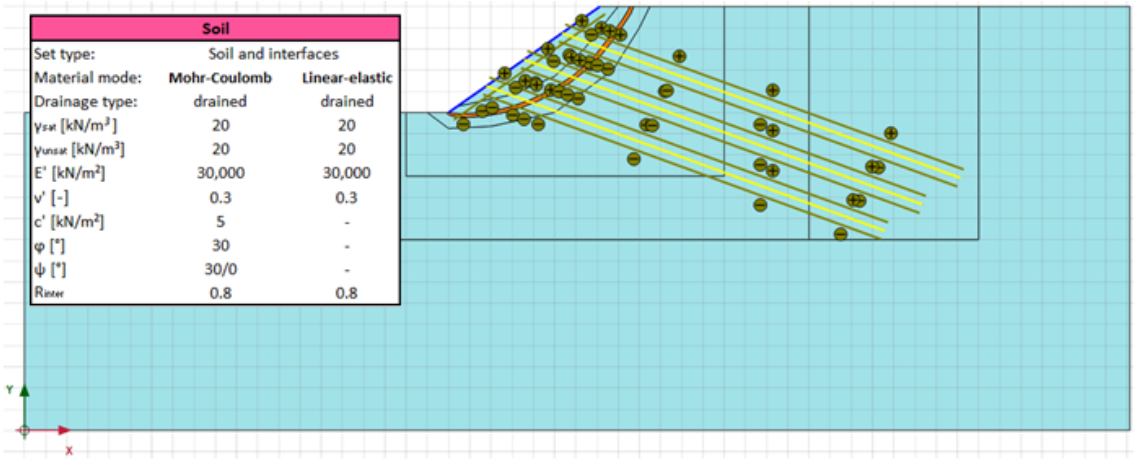

Figure H 1 MC-LE model with three soil nail (geogrid + interface) horizons as support

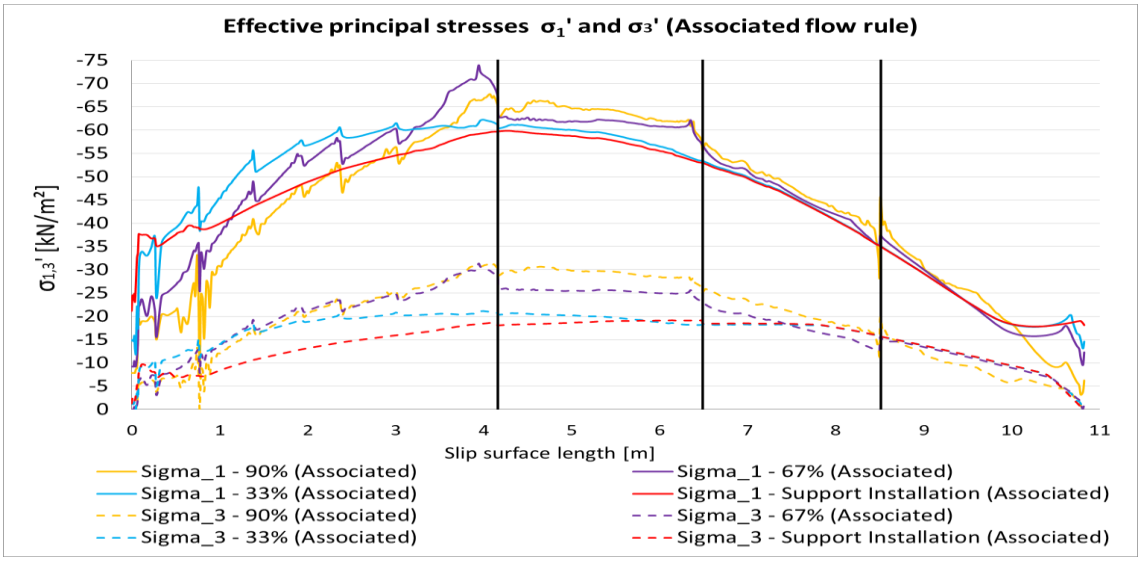

Figure H 2 Principal effective stresses $\sigma_{1,3}'$ over the slip surface length for the associated calculation of the 3-nail supported MC-LE model

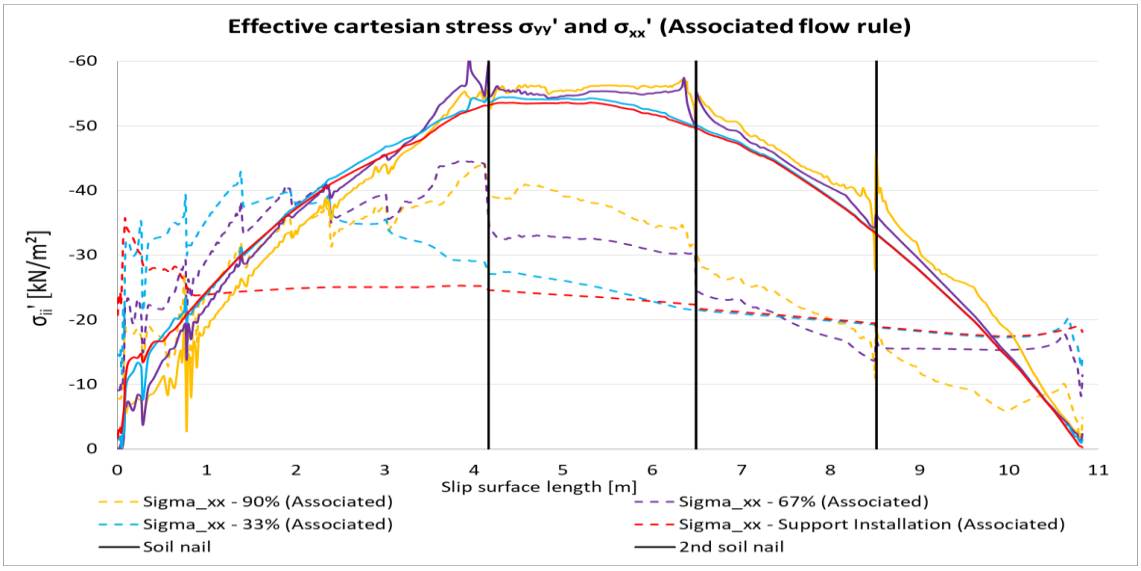

Figure H 3 Cartesian effective stresses $\sigma_{xx,yy}$' over the slip surface length for the associated calculation of the 3-nail supported MC-LE model

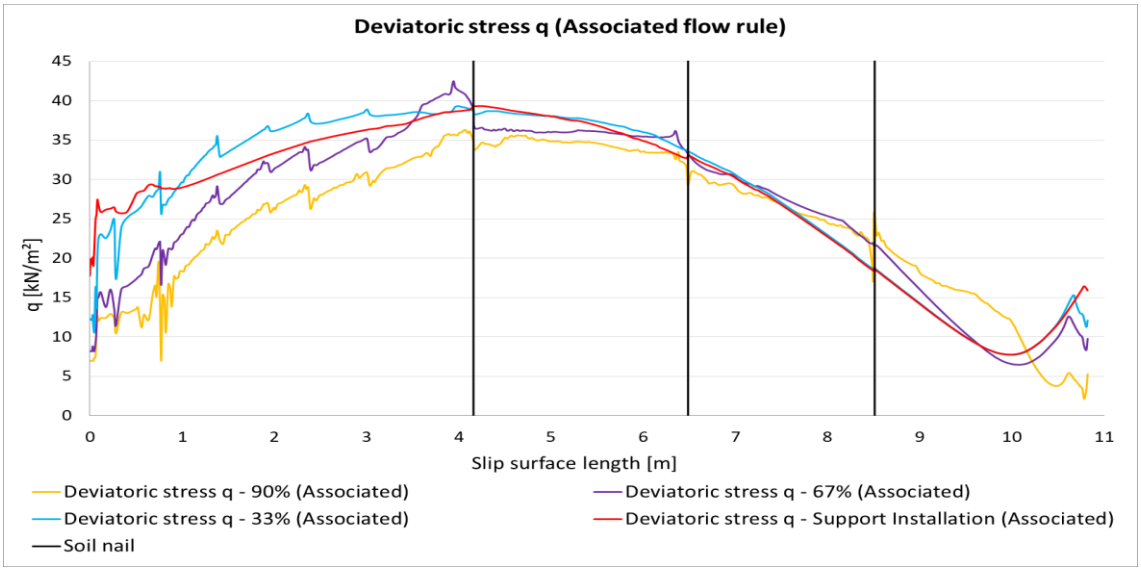

Figure H 4 Deviatoric stress q over the slip surface length for the associated calculation of the 3-nail supported MC-LE model

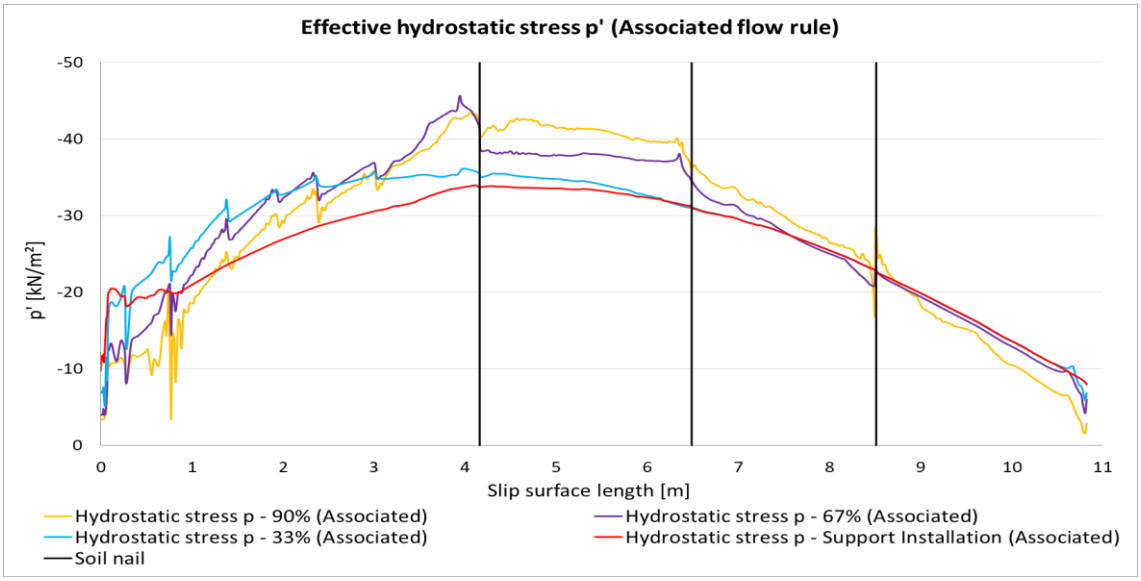

Figure H 5 Effective hydrostatic stress p' over the slip surface length for the associated calculation of the 3-nail supported MC-LE model

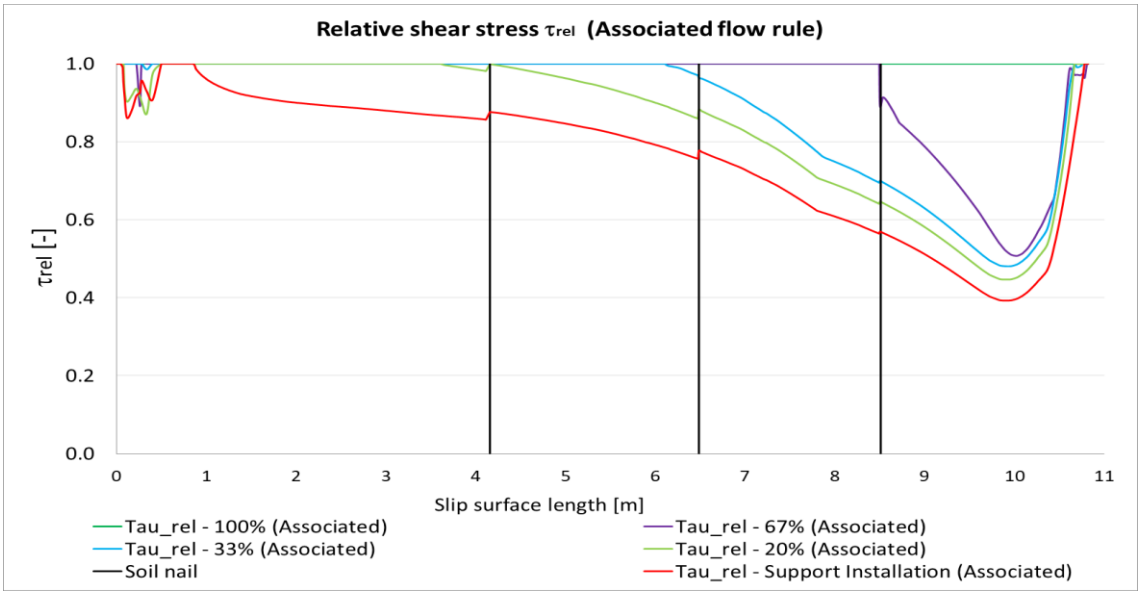

Figure H 6 Relative shear stress over the slip surface length for the associated calculation of the 3-nail supported MC-LE model

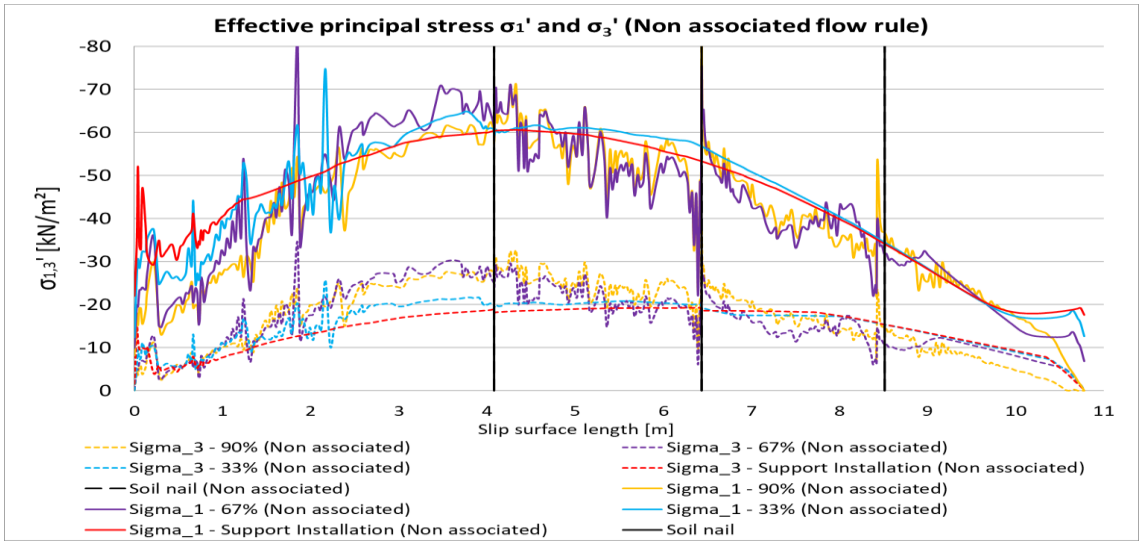

Figure H 7 Principal effective stresses $\sigma_{1,3}'$ over the slip surface length for the non-associated calculation of the 3-nail supported MC-LE model

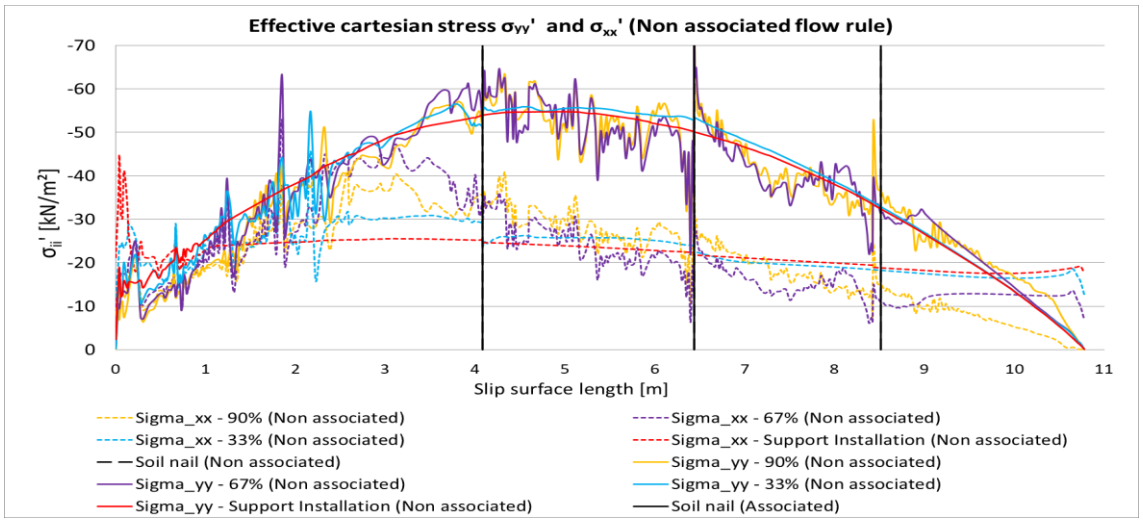

Figure H 8 Cartesian effective stresses $\sigma_{xx,yy}'$ over the slip surface length for the non-associated calculation of the 3-nail supported MC-LE model

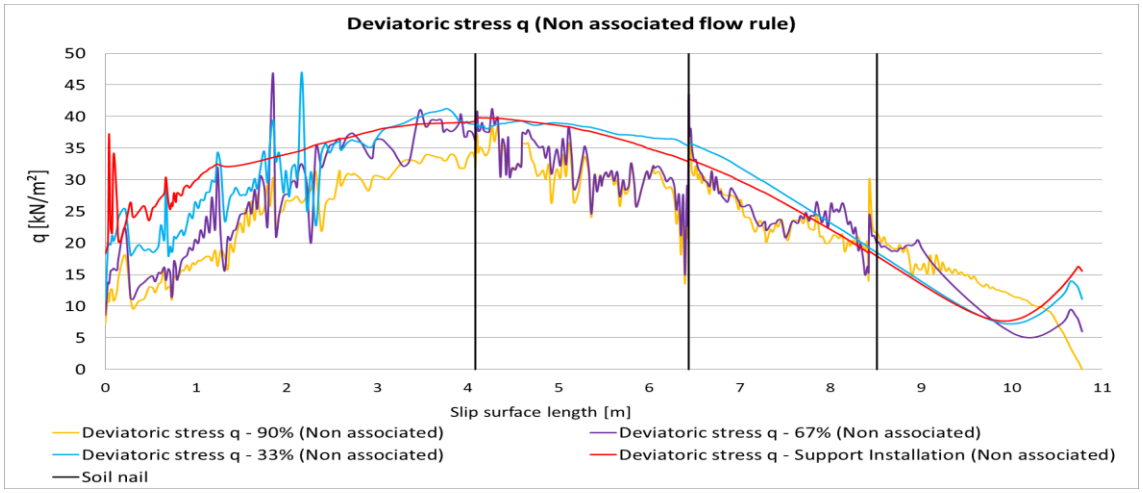

Figure H 9 Deviatoric stress q over the slip surface length for the non-associated calculation of the 3-nail supported MC-LE model

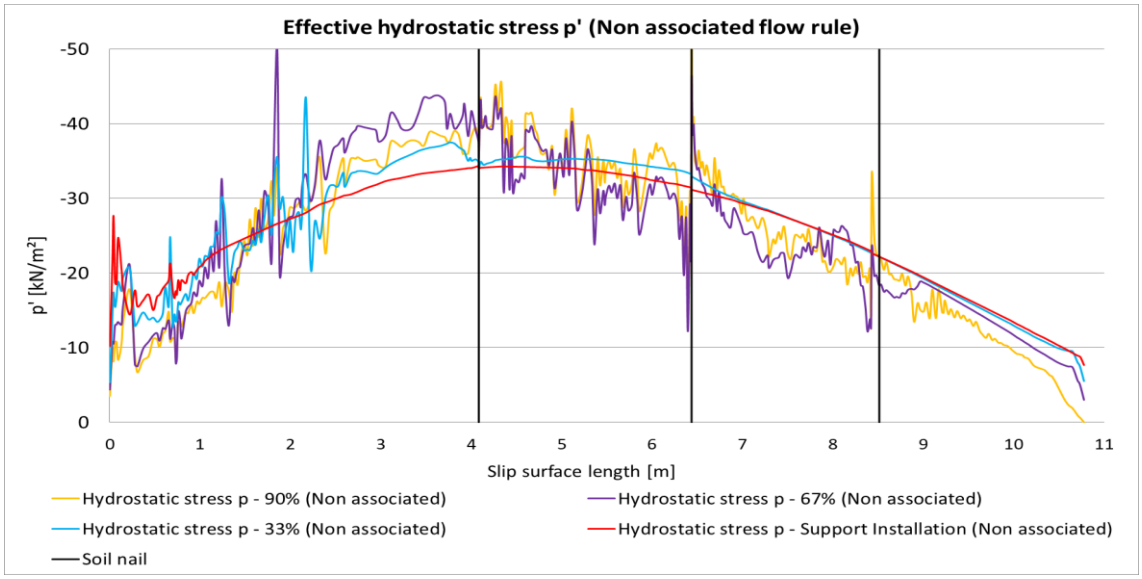

Figure H 10 Effective hydrostatic stress p' over the slip surface length for the non-associated calculation of the 3-nail supported MC-LE model

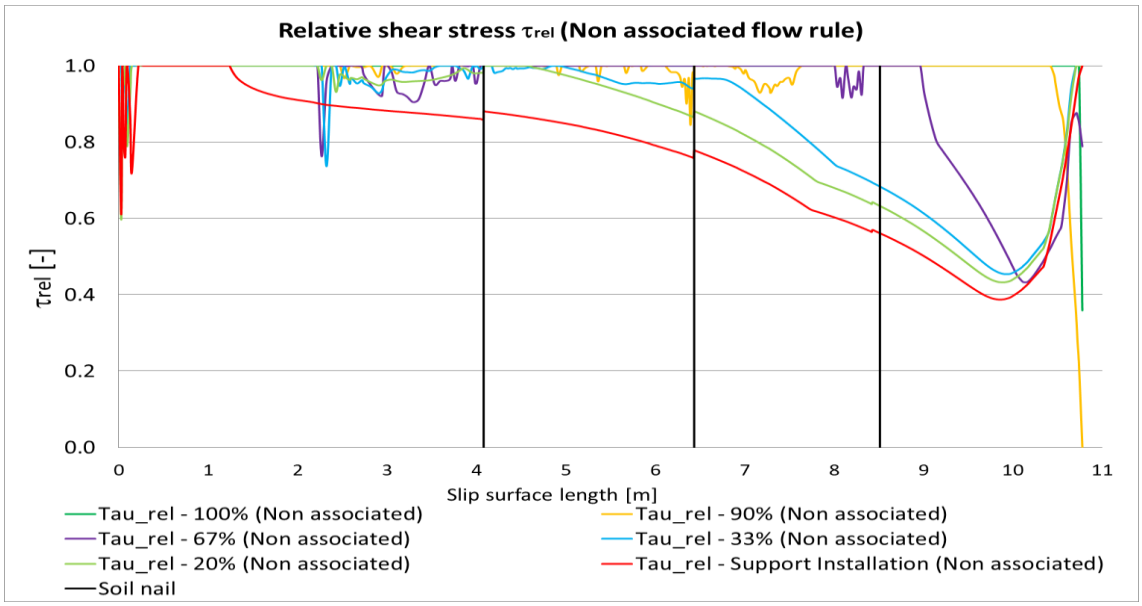

Figure H 11 Relative shear stress over the slip surface length for the non-associated calculation of the 3-nail supported MC-LE model

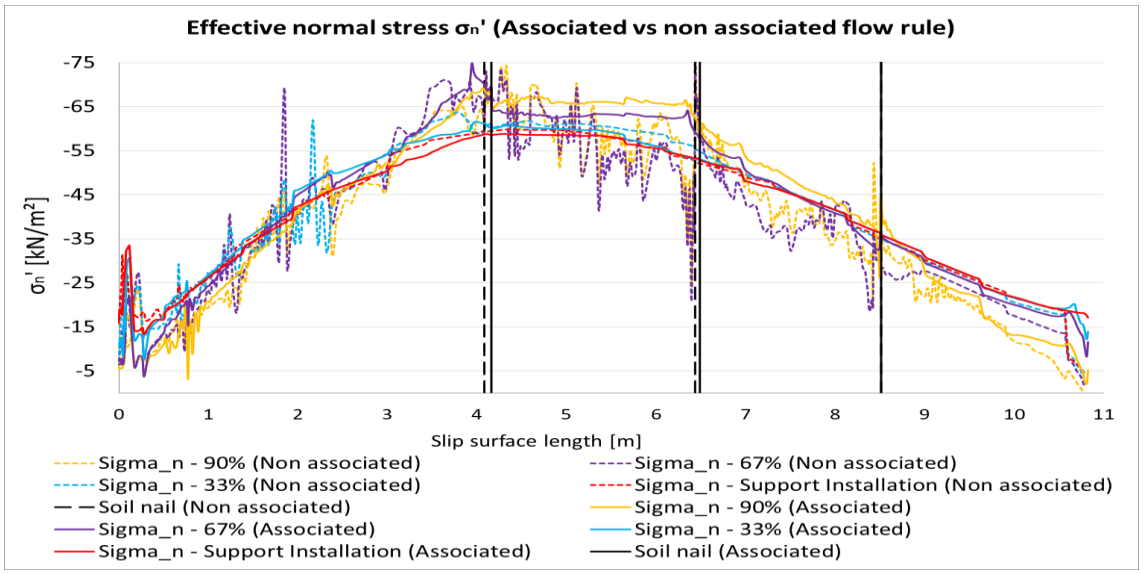

Figure H 12 Effective normal stress σ_n' over the slip surface length for the 3-nail supported MC-LE model (associated vs. non-associated flow rule)

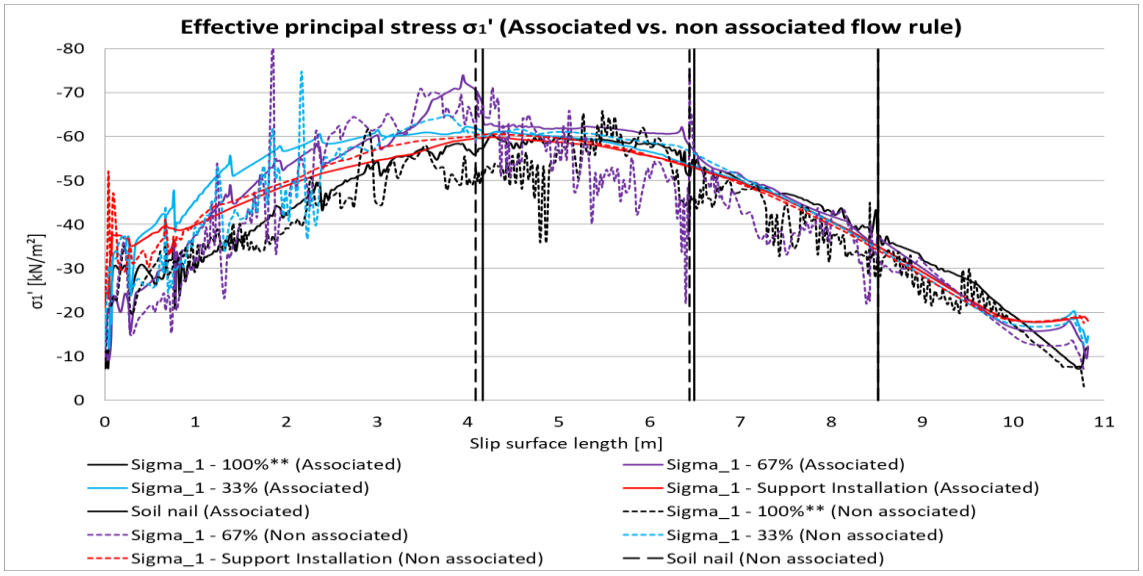

Figure H 73 σ_1' over the slip surface length for the 3-nail supported MC-LE model (associated vs. non-associated flow rule)

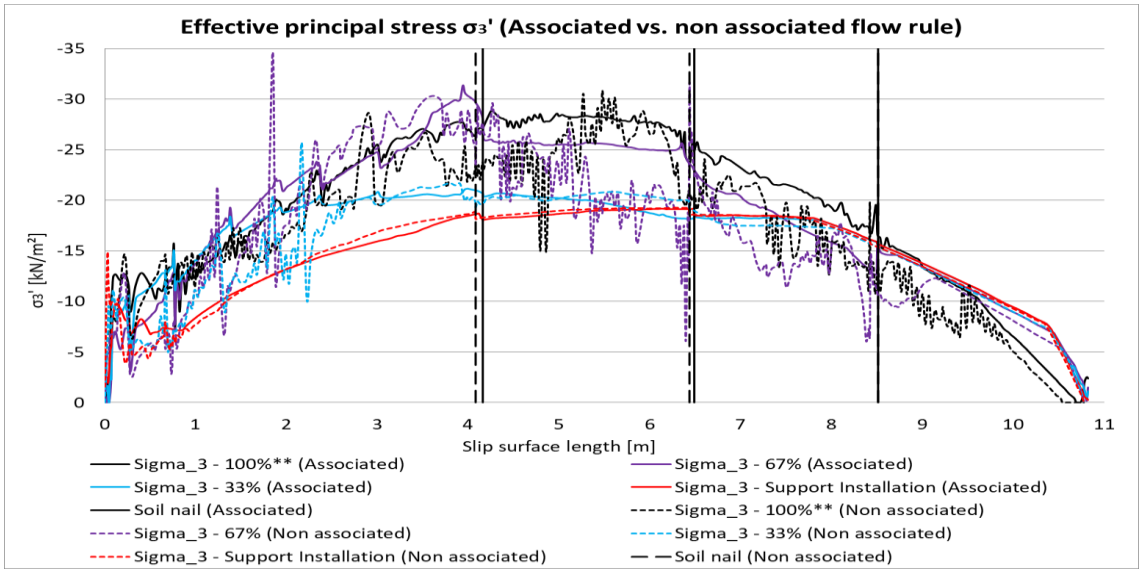

Figure H 84 σ_3' over the slip surface length for the 3-nail supported MC-LE model (associated vs. non-associated flow rule)

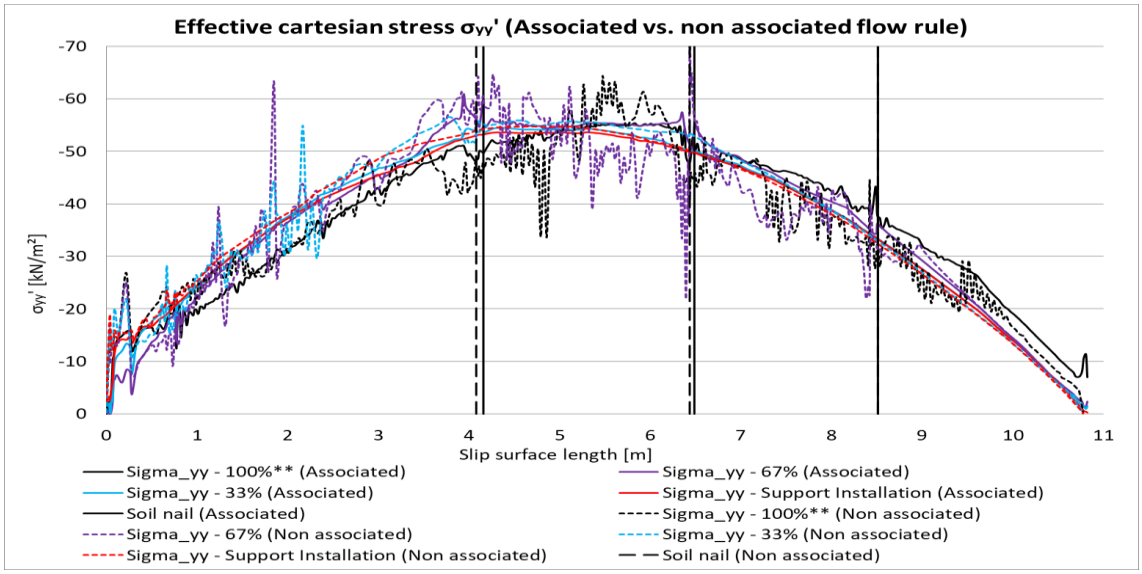

Figure H 15 σ_{yy}' over the slip surface length for the 3-nail supported MC-LE model (associated vs. non-associated flow rule)

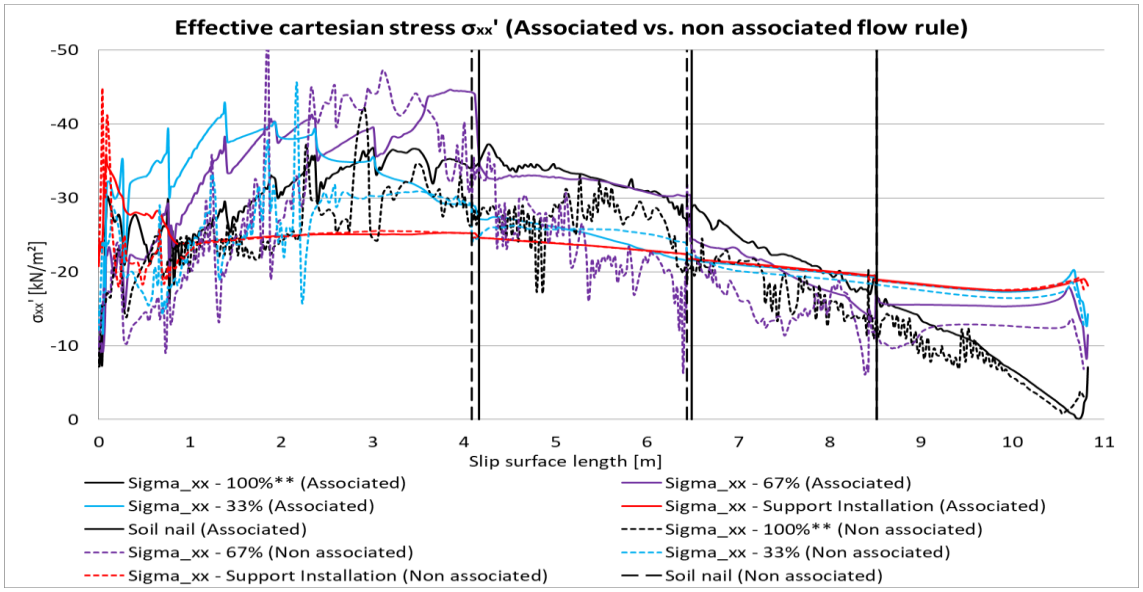

Figure H 16 σ_{xx}' over the slip surface length for the 3-nail supported MC-LE model (associated vs. non-associated flow rule)

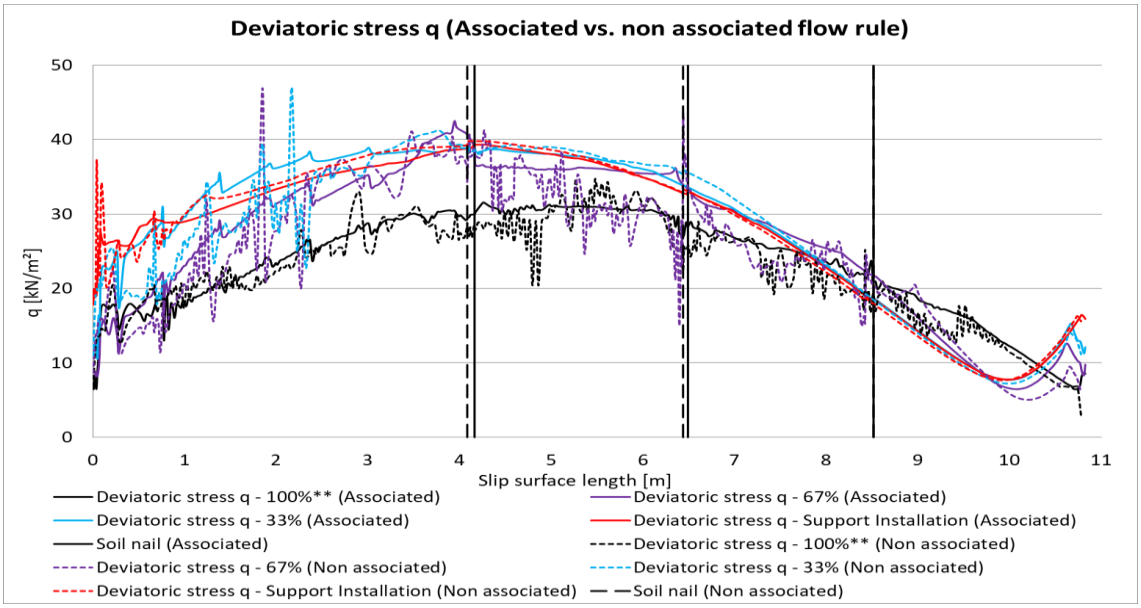

Figure H 17 Deviatoric stress q over the slip surface length for the 3-nail supported MC-LE model (associated vs. non-associated flow rule)

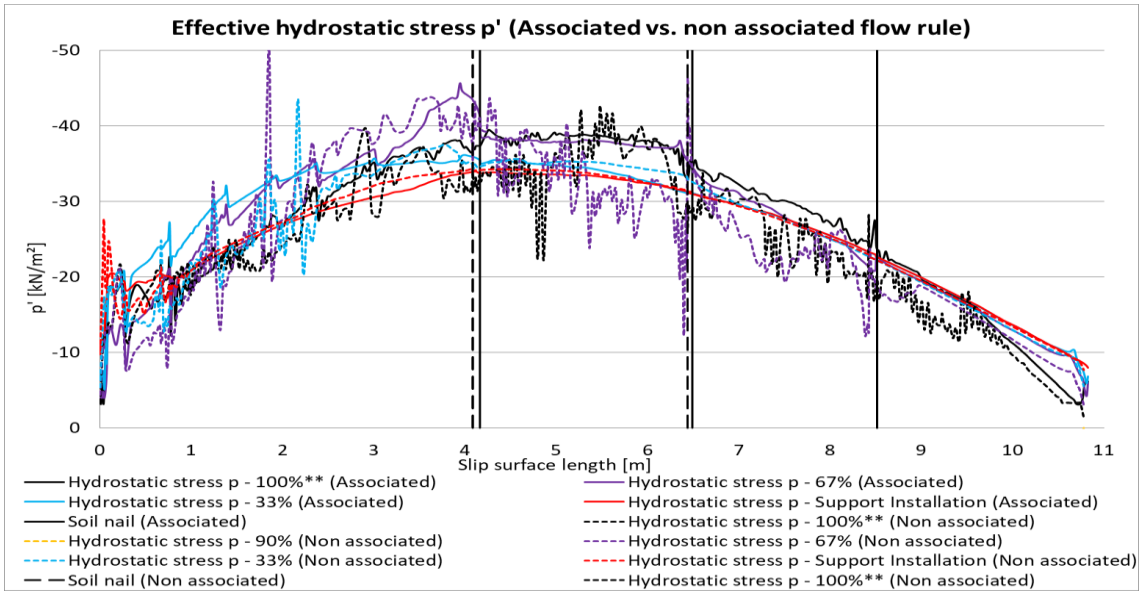

Figure H 18 Effective hydrostatic stress p' over the slip surface length for the 3-nail supported MC-LE model (associated vs. non-associated flow rule)

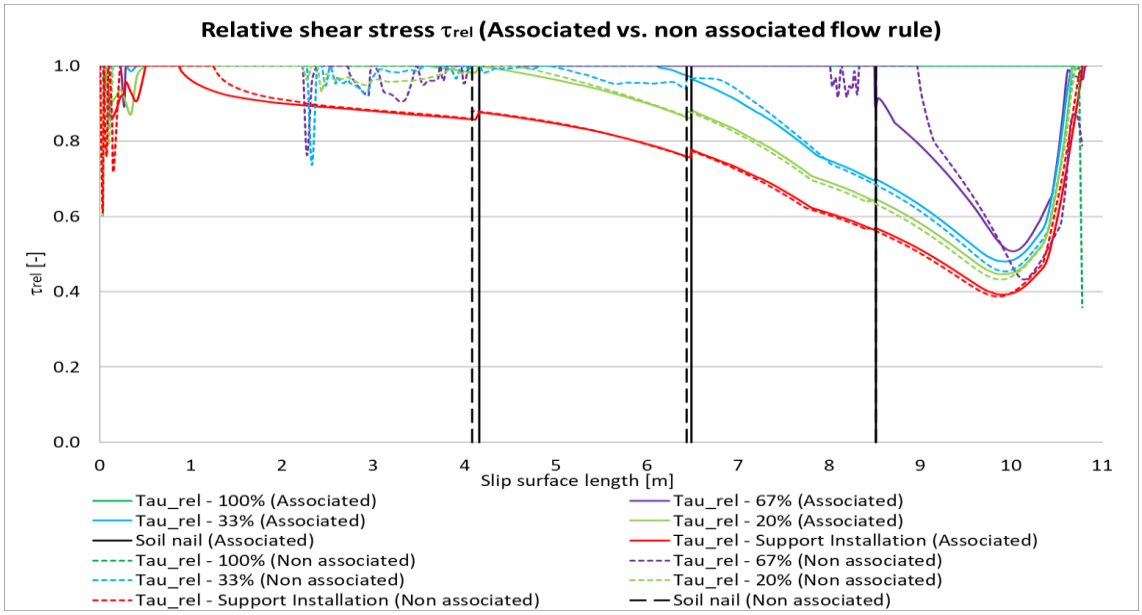

Figure H 19 Relative shear stress over the slip surface length for the 1-nail supported MC-LE model (associated vs. non-associated flow rule)

MC-LE 3-nail slope			
Stress	Associated		Non-associated
σ_n'	↑	>	–
σ_1'	↑	=	↑
σ_3'/σ_2'	↑	>	↑
σ_{yy}'	↑	=	–
σ_{xx}'	↑	>	↕
p'	↑	=	↕
q	↓	=	↓
τ_{rel}	↑	=	↑

Trend between steps over the slip surface:
↑ increasing trend
↓ decreasing trend
– no bigger change between steps
↕ scattering/no evident trend

> associated shows higher stresses
< non-associated shows higher stresses
= almost equal

Figure H 20 Trend of the stress indicators for the 1-nail supported MC-LE model

Appendix I

This appendix containing the parameters and coordinates (of all the used surfaces) used to model the investigated soil body where the Unzmarkt - soil nail wall is located.

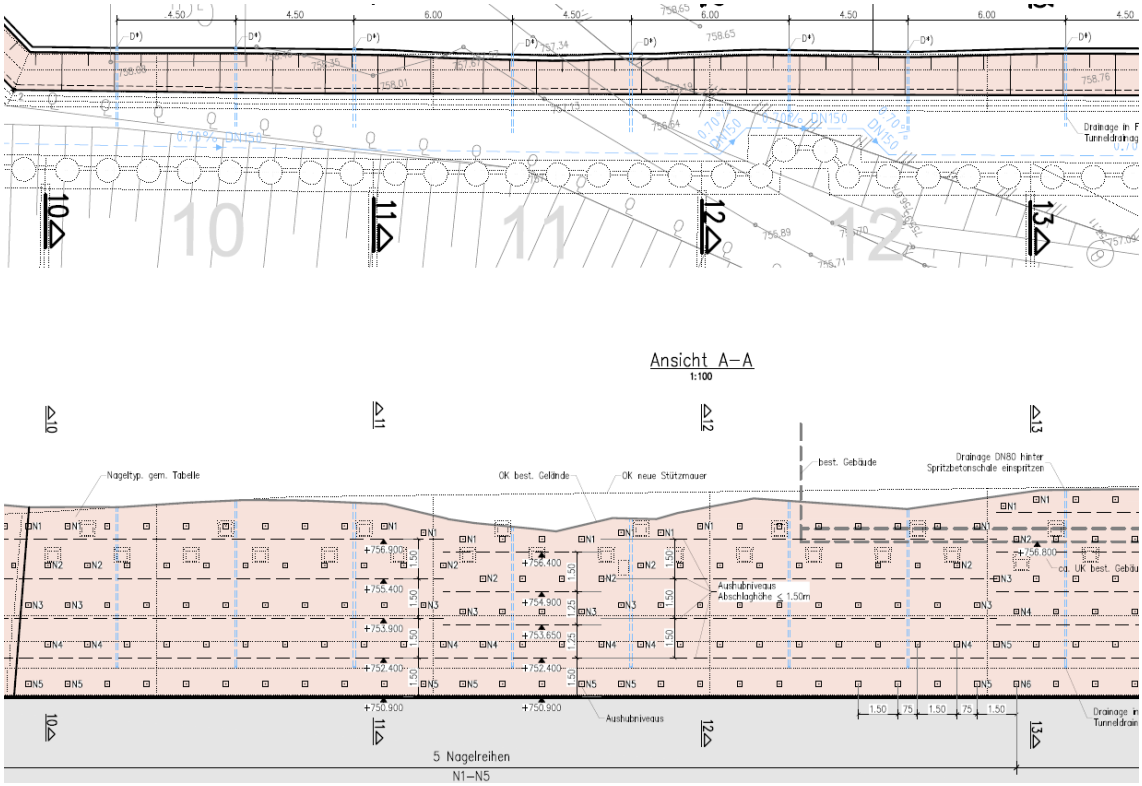

Figure I 1 Plan view and front view of the Unzmarkt soil nail wall

Volumen bottom surface		
x	y	z
0	0	0
38.47	0	0
38.47	41.5	0
0	41.5	0

Figure I 2 Coordinates of the extruded square

Border surface			
Surf. Num.	x	y	z
1	-1	-1	30
	-1	20	30
	40	20	30
	40	-1	30
2	-1	20	30
	40	20	30
	-1	23	45.48
	40	23	45.48

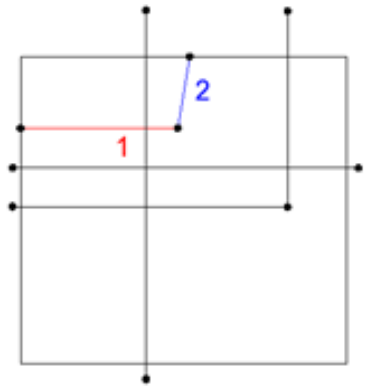

Figure I 3 Border-surfaces of the final (4th) excavation and slope (2)

Ground surface border (soil body "roof")					
x	y	z	x	y	z
-3.39	0	35.95	-3.39	41.5	38.85
0.00	0	35.67	0.00	41.5	38.57
6.70	0	36.02	6.70	41.5	38.92
12.70	0	35.81	12.70	41.5	38.71
15.17	0	35.17	15.17	41.5	38.07
19.34	0	34.75	19.34	41.5	37.65
21.59	0	35.31	21.59	41.5	38.21
23.36	0	35.31	23.36	41.5	38.21
27.10	0	36.16	27.10	41.5	39.06
33.31	0	35.60	33.31	41.5	38.5
38.47	0	36.24	38.47	41.5	39.14
41.49	0	36.24	41.49	41.5	39.14

Figure I 4 Border-surfaces of the final (4th) excavation and slope (2)

Mesh border			
	x	y	z
1 - 9	-1	-1	25
	42	-1	25
	-1	43	25
	42	43	25
2 - 7	-1	-1	20
	42	-1	20
	-1	34	20
	42	34	20
7 - 8	-1	34	20
	42	34	20
	-1	34	45
	42	34	45
5 - 6	-1	29	-2
	42	29	-2
	-1	29	45
	42	29	45
3 - 4	-1	16	-2
	42	16	-2
	-1	16	45
	42	16	45

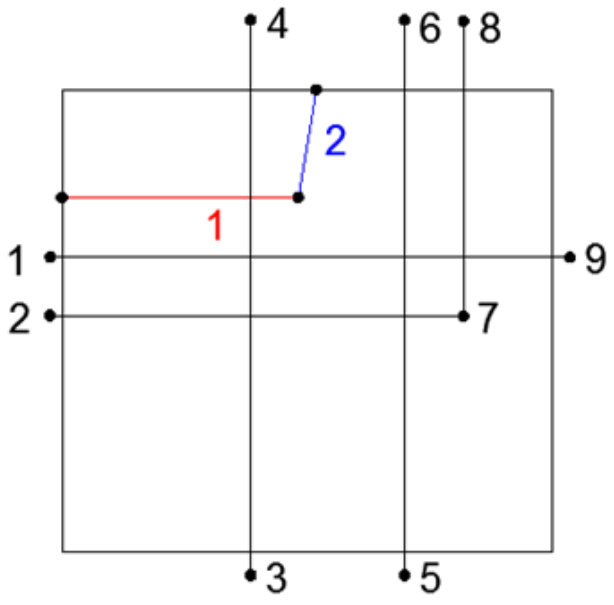

Figure I 5 Mesh borders coordinates

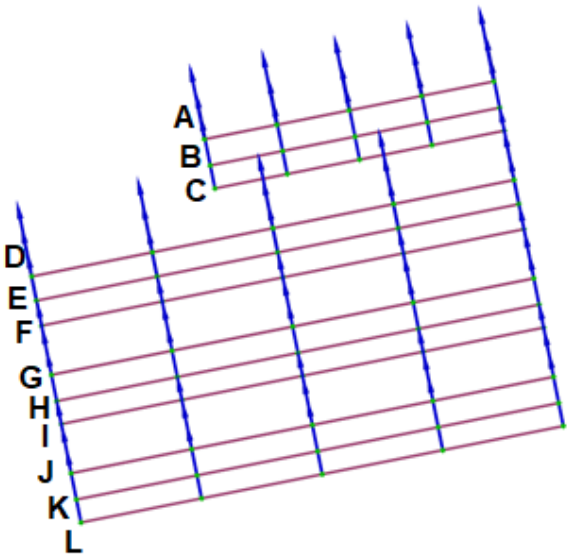

Figure I 6 Side view of the soil nail wall

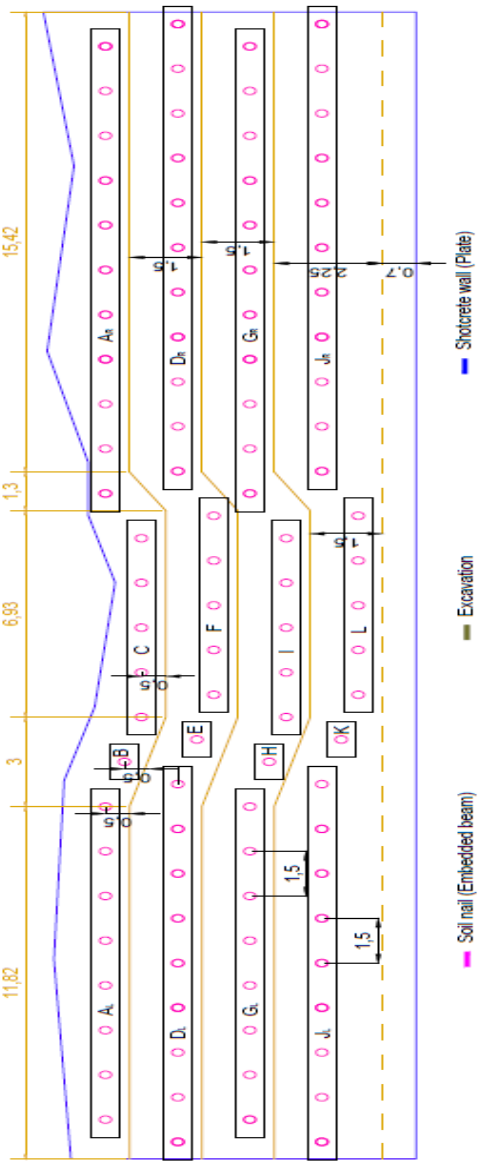

Figure I 7 Front view of the soil nail wall (all four rows and three subrows per row)

Embedded beams coordinates							
Soil nail name	x	y	z	Soil nail name	x	y	z
AR_1	22.32	21.60 / 25.71	36.51 / 35.57	GR_1	22.32	20.99 / 28.04	33.51 / 31.98
AR_2	23.82			GR_2	23.82		
AR_3	25.32			GR_3	25.32		
AR_4	26.82			GR_4	26.82		
AR_5	28.32			GR_5	28.32		
AR_6	29.82			GR_6	29.82		
AR_7	31.32			GR_7	31.32		
AR_8	32.82			GR_8	32.82		
AR_9	34.32			GR_9	34.32		
AR_10	35.82			GR_10	35.82		
AR_11	37.32			GR_11	37.32		
AL_1	1.32	21.60 / 25.71	36.51 / 35.57	GL_1	1.32	20.99 / 28.04	33.51 / 31.98
AL_2	2.82			GL_2	2.82		
AL_3	4.32			GL_3	4.32		
AL_4	5.82			GL_4	5.82		
AL_5	7.32			GL_5	7.32		
AL_6	8.82			GL_6	8.82		
AL_7	10.32			GL_7	10.32		
AL_8	11.82			GL_8	11.82		
B	13.32	21.51 / 25.62	36.11 / 35.17	H	13.32	20.91 / 27.96	33.11 / 31.58
C_1	14.82	21.44 / 25.55	35.76 / 34.82	I _1	14.82	20.84 / 27.89	32.76 / 31.23
C_2	16.32			I _2	16.32		
C_3	17.82			I _3	17.82		
C_4	19.32			I _4	19.32		
C_5	20.82			I _5	20.82		
DR_1	23.07	21.29 / 28.34	35.01 / 33.48	JR_1	23.07	20.69 / 27.74	32.01 / 30.48
DR_2	24.57			JR_2	24.57		
DR_3	26.07			JR_3	26.07		
DR_4	27.57			JR_4	27.57		
DR_5	29.07			JR_5	29.07		
DR_6	30.57			JR_6	30.57		
DR_7	32.07			JR_7	32.07		
DR_8	33.57			JR_8	33.57		
DR_9	35.07			JR_9	35.07		
DR_10	36.57			JR_10	36.57		
DR_11	38.07			JR_11	38.07		
DL_1	0.57	21.29 / 28.34	35.01 / 33.48	JL_1	0.57	20.69 / 27.74	32.01 / 30.48
DL_2	2.07			JL_2	2.07		
DL_3	3.57			JL_3	3.57		
DL_4	5.07			JL_4	5.07		
DL_5	6.57			JL_5	6.57		
DL_6	8.07			JL_6	8.07		
DL_7	9.57			JL_7	9.57		
DL_8	11.07			JL_8	11.07		
DL_9	12.57			JL_9	12.57		
E	14.07	21.22 / 28.27	34.64 / 33.11	K	14.07	20.61 / 27.66	31.61 / 30.08
F_1	15.57	21.44 / 28.19	34.26 / 32.73	L_1	15.57	20.54 / 27.59	31.26 / 29.73
F_2	17.07			L_2	17.07		
F_3	18.57			L_3	18.57		
F_4	20.07			L_4	20.07		
F_5	21.57			L_5	21.57		

Figure I 8 Coordinates of the embedded beams

Black x- and y-coordinates are the x- and y-coordinates are of the soil nail head, and the violet ones are the coordinates of the soil nail tail. With this coordinates the soil nails are slightly longer than the one given in the cross section (4.5 m and 7.5 m). But, by cutting them with the shotcrete plate, their resulting length is equal to the lengths given in the cross section of the soil nail wall.

Excavations									
1	x	y	z	2	x	y	z	3	x	y	z
	-1.00	-1.00	35.95		-1.00	-1.00	34.45		-1.00	-1.00	32.95
	-1.00	45.00	35.95		-1.00	45.00	34.45		-1.00	45.00	32.95
	11.82	-1.00	35.95		11.82	-1.00	34.45		11.82	-1.00	32.95
	11.82	45.00	35.95		11.82	45.00	34.45		11.82	45.00	32.95
	14.82	-1.00	35.20		14.82	-1.00	33.70		14.82	-1.00	32.20
	14.82	45.00	35.20		14.82	45.00	33.70		14.82	45.00	32.20
	21.75	-1.00	35.20		21.75	-1.00	33.70		21.75	-1.00	32.20
	21.75	45.00	35.20		21.75	45.00	33.70		21.75	45.00	32.20
	23.05	-1.00	35.95		23.05	-1.00	34.45		23.05	-1.00	32.95
	23.05	45.00	35.95		23.05	45.00	34.45		23.05	45.00	32.95
	40.00	-1.00	35.95		40.00	-1.00	34.45		40.00	-1.00	32.95
	40.00	45.00	35.95		40.00	45.00	34.45		40.00	45.00	32.95

Figure I 9 Coordinates for the borders of the excavation surfaces

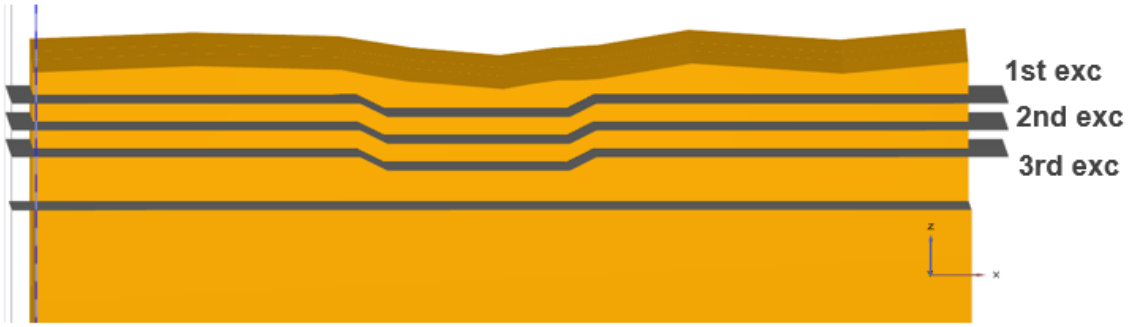

Figure I 10 Borders of the excavation surfaces

Shotcrete	
Set type:	**Plate**
Material type:	Elastic
d [m]	0.2
γ [kN/m³]	30
E_1 [kN/m²]	$26*10^6$
ν_{12} [-]	0.3
G_{12} [kN/m²]	$10*10^6$

Figure I 11 Shotcrete parameters

Appendix J

The generated $M_{sf}/|u|$ diagrams after the safety calculation of the 3D soil nail investigation.

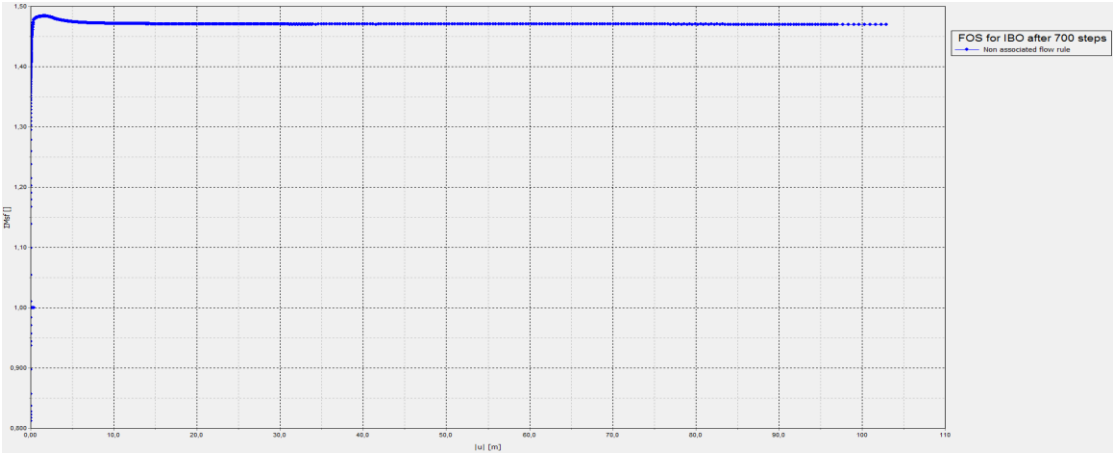

Figure J 1 IBO (φ'=32.5° and ψ'=0°) – FoS = 1.47

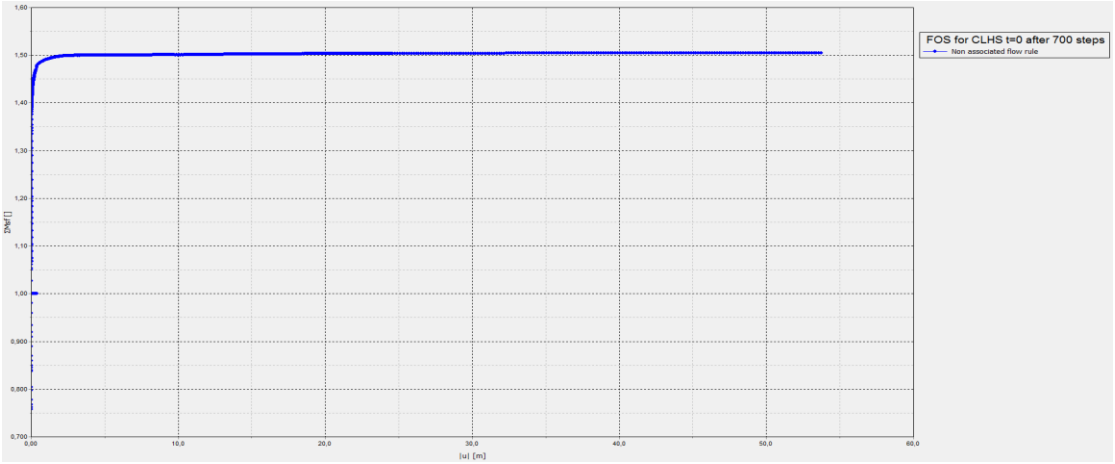

Figure J 2 CLHS (t=0) (φ'=32.5° and ψ'=0°) – FoS = 1.50

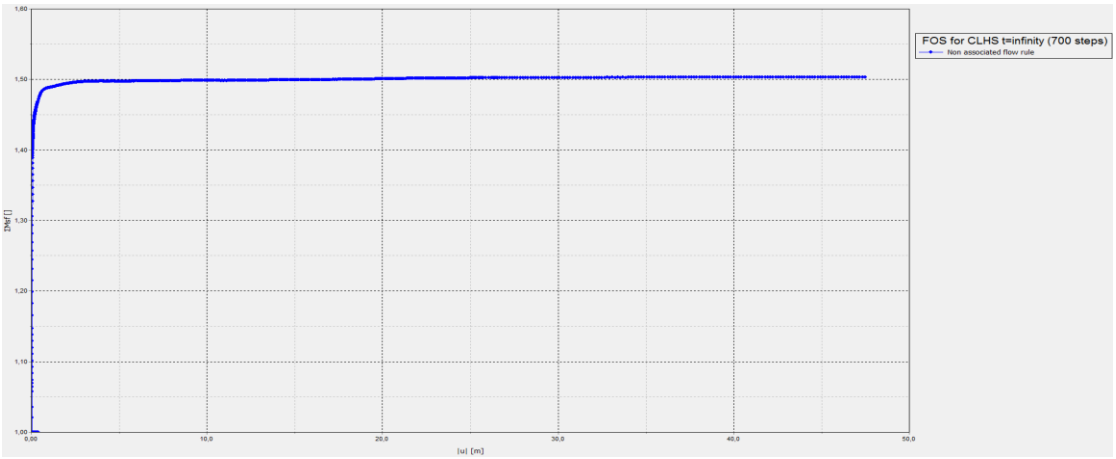

Figure J 3 CLHS (t=∞) (φ'=32.5° and ψ'=0°) – FoS = 1.50

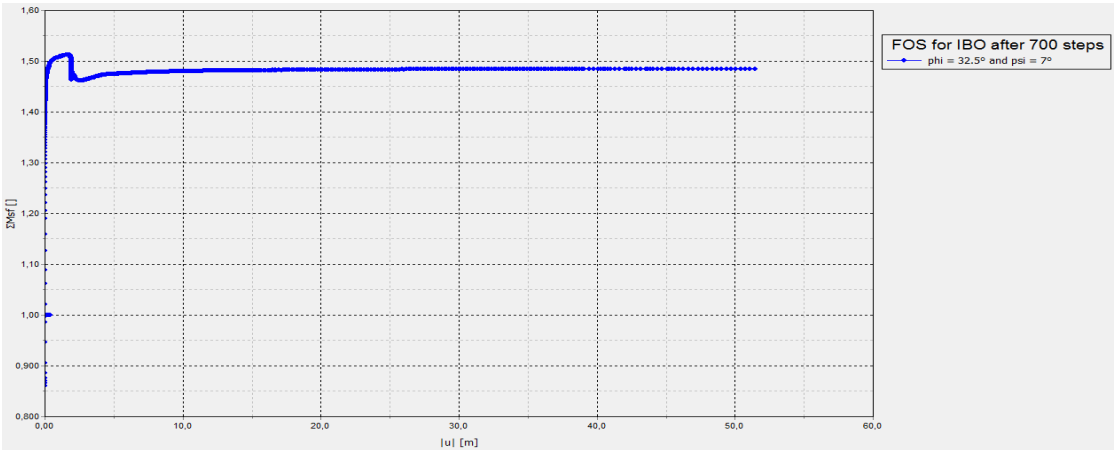

Figure J 4 IBO (φ'=32.5° and ψ'=7°) – FoS = 1.49

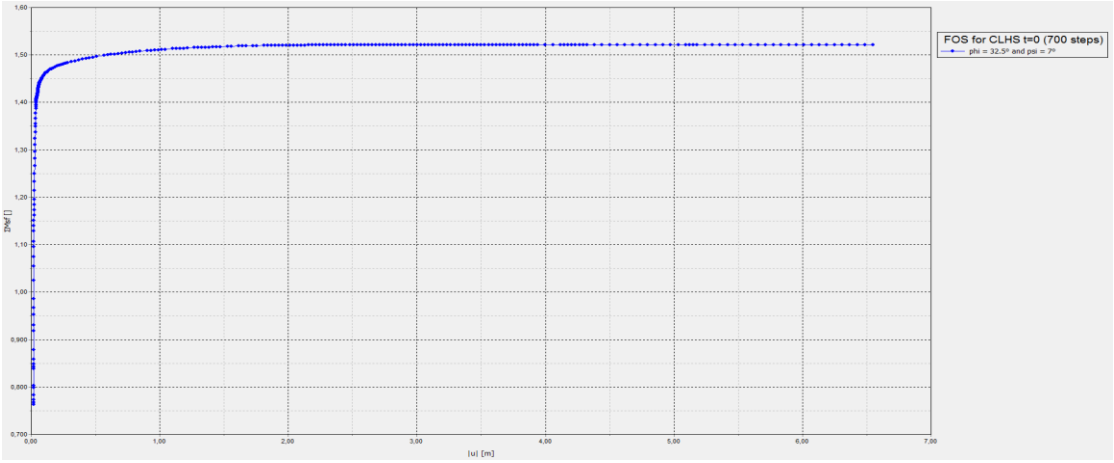

Figure J 5 CLHS (t=0) (φ'=32.5° and ψ'=7°) – FoS = 1.52

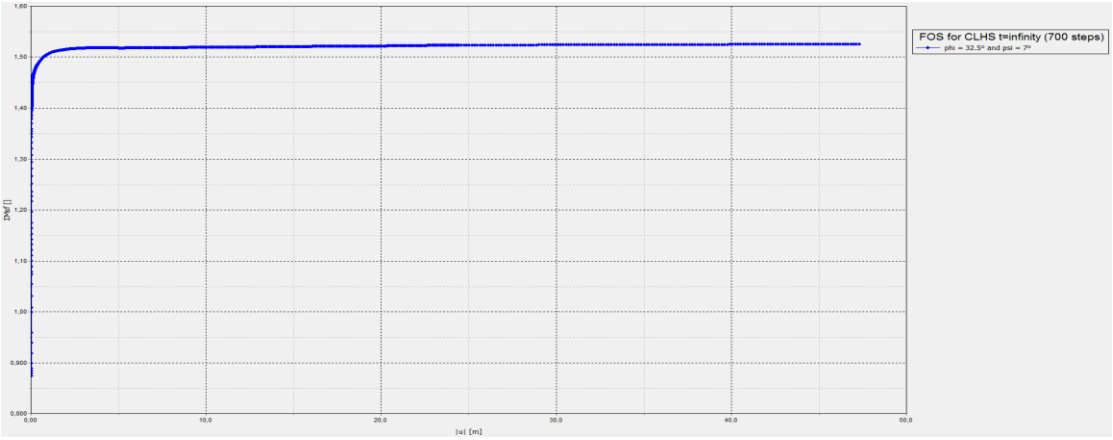

Figure J 6 CLHS (t=∞) (φ'=32.5° and ψ'=7°) – FoS = 1.52

Appendix K

Displacement results of the four investigated soil nails, for all the different soil nail types and soil body parameters are depicted in this Appendix.

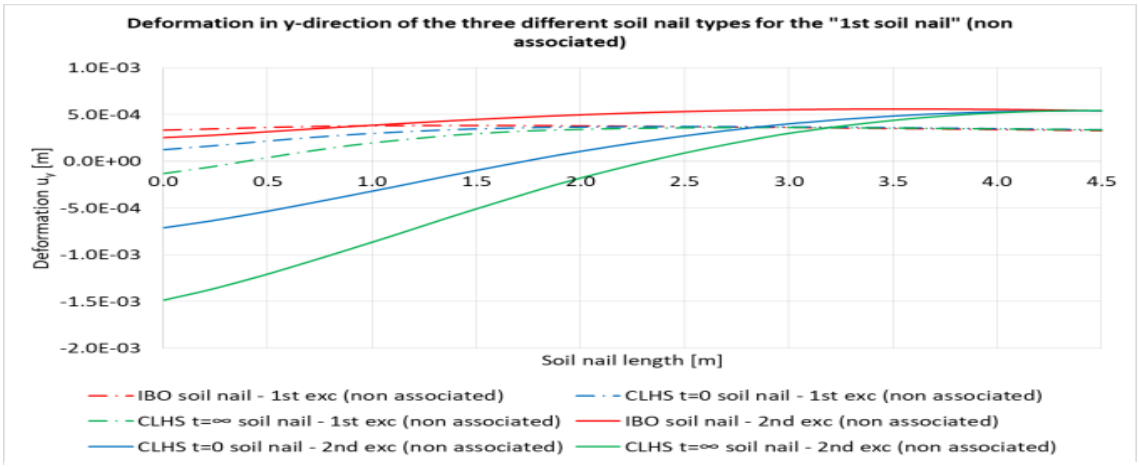

Figure K 1 u_y for the 1st soil nail (excavation steps: 1 and 2) – ψ'=0°

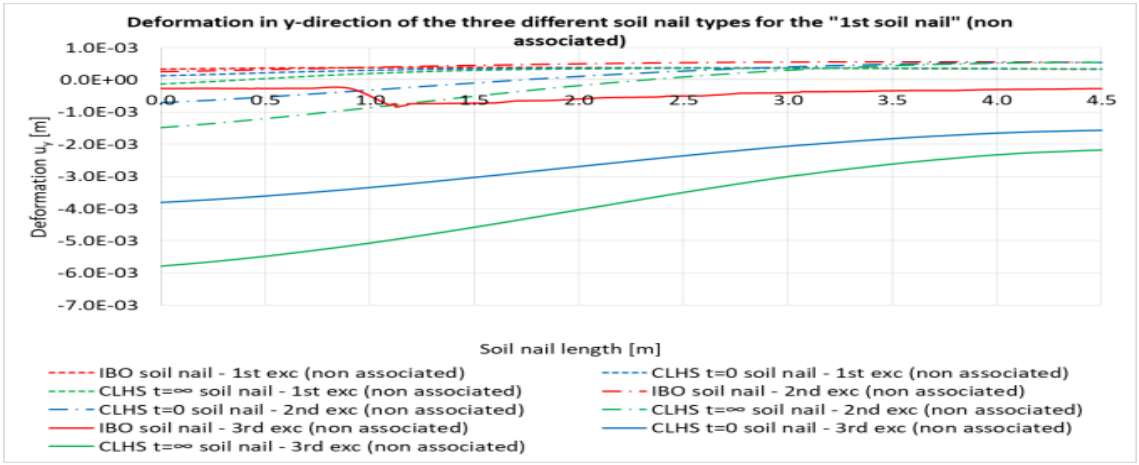

Figure K 2 u_y for the 1st soil nail (excavation steps: 1, 2 and 3) – ψ'=0°

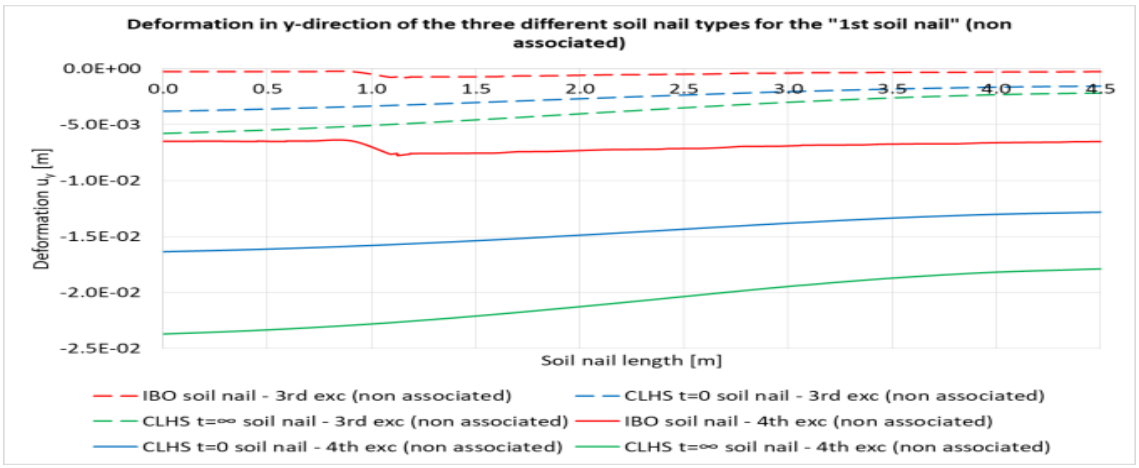

Figure K 3 u_y for the 1st soil nail (excavation steps: 3 and 4) – ψ'=0°

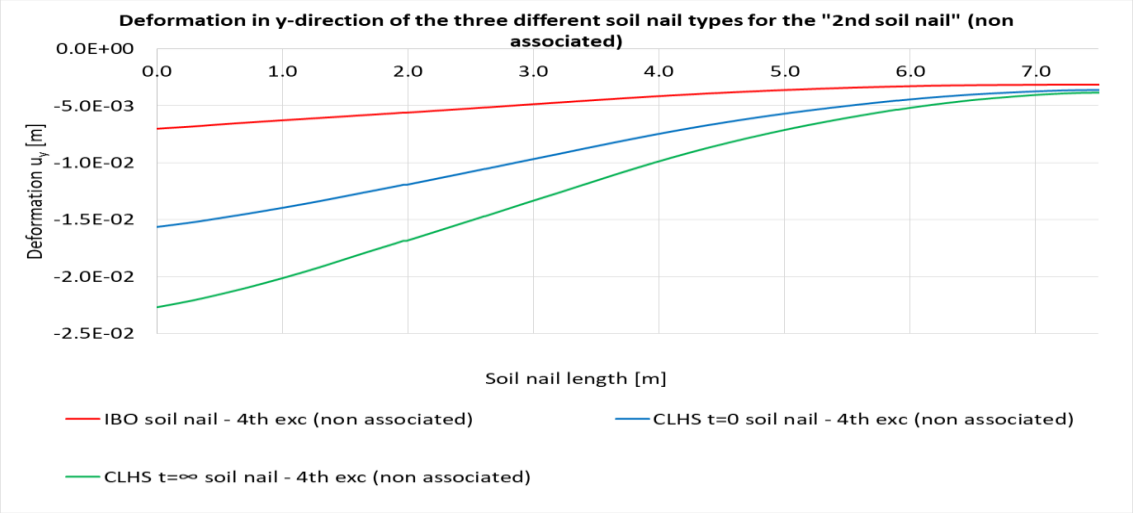

Figure K 4 u_y for the 2nd soil nail (excavation steps: 2 and 3) – ψ'=0°

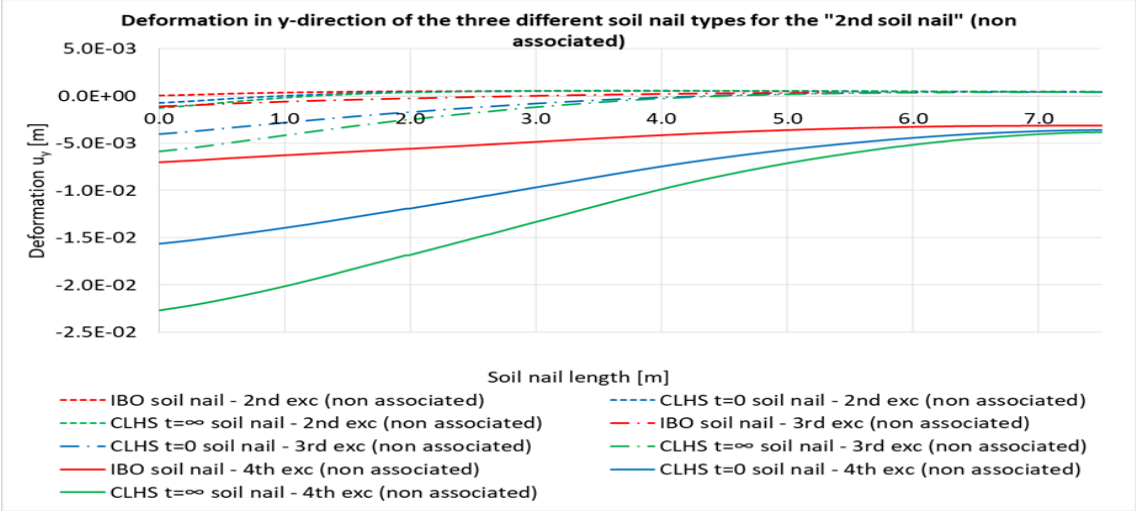

Figure K 5 u_y for the 2nd soil nail (excavation steps: 2, 3 and 4) – ψ'=0°

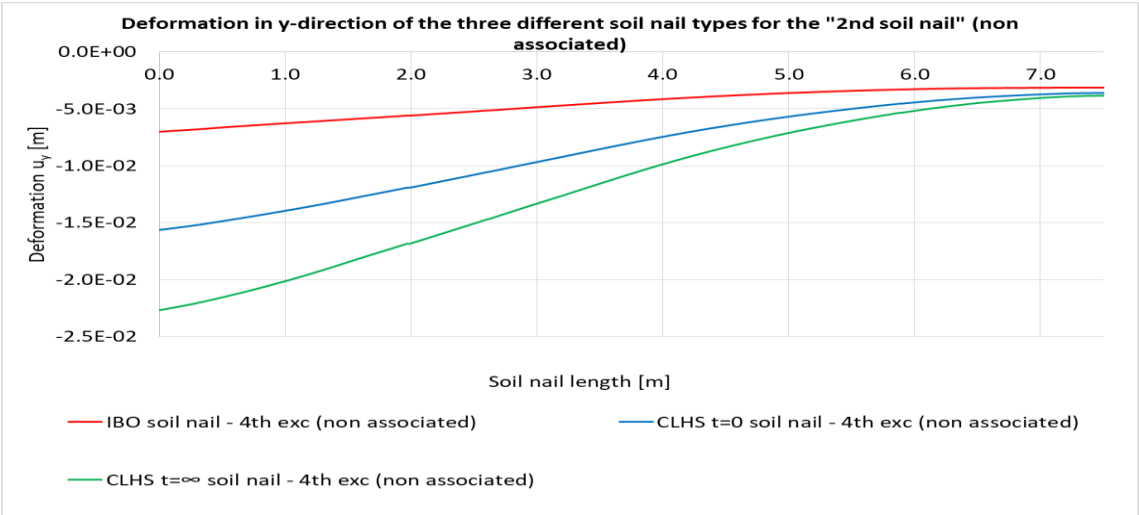

Figure K 6 u_y for the 4th soil nail (excavation steps: 2, 3 and 4) – ψ'=0°

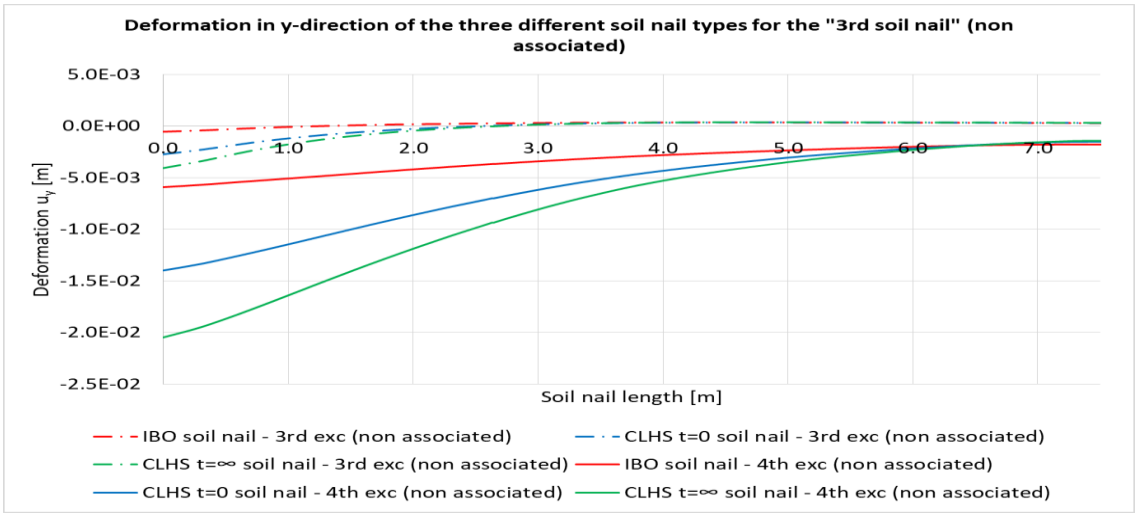

Figure K 7 u_y for the 3rd soil nail (excavation steps: 3 and 4) – $\psi'=0°$

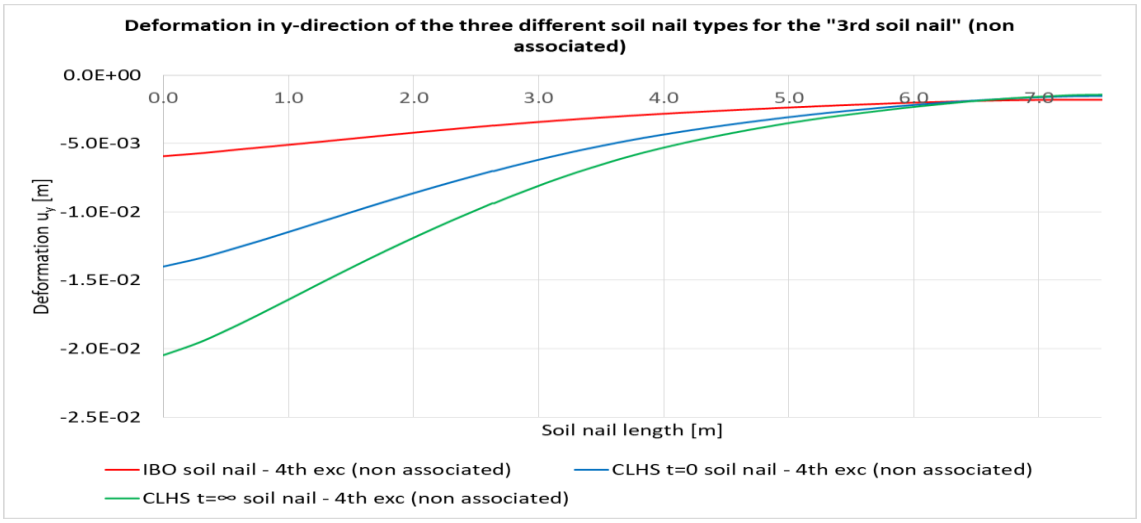

Figure K 8 u_y for the 2nd soil nail (excavation step 4) – $\psi=0°$

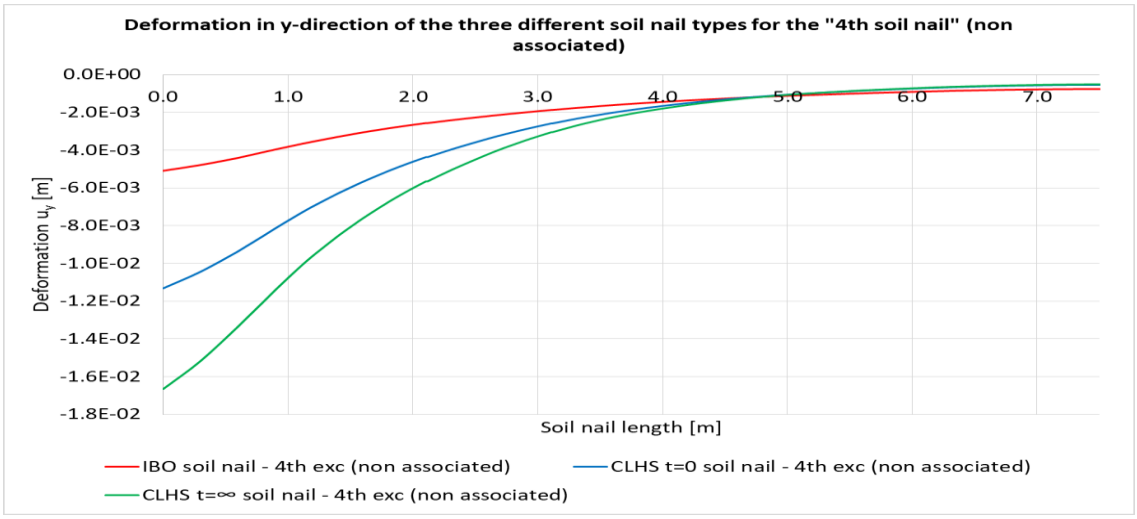

Figure K 9 u_y for the 3rd soil nail (excavation step 4) – $\psi'=0°$

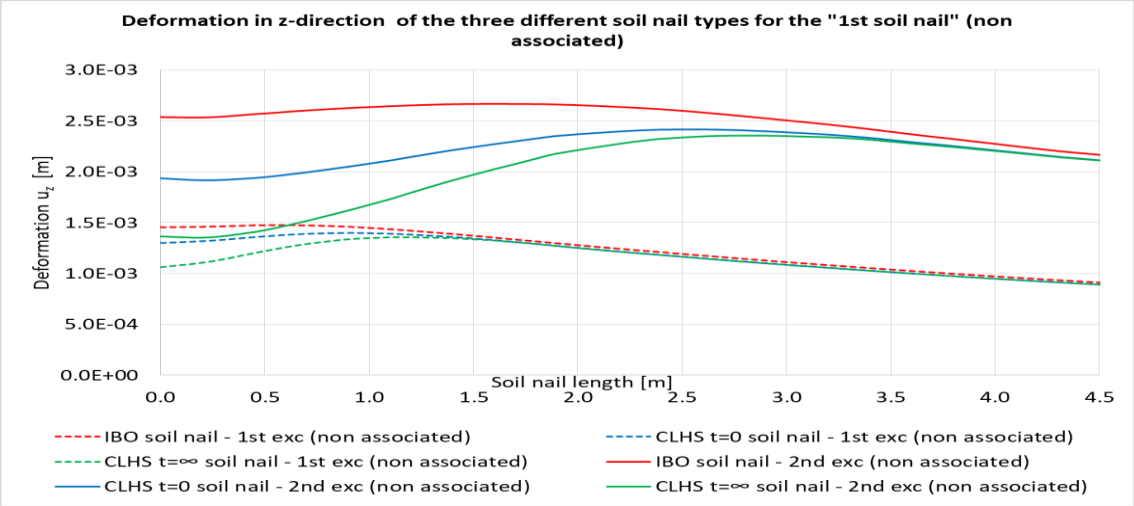

Figure K 1 u_z for the 1st soil nail (excavation steps: 1 and 2) – ψ'=0°

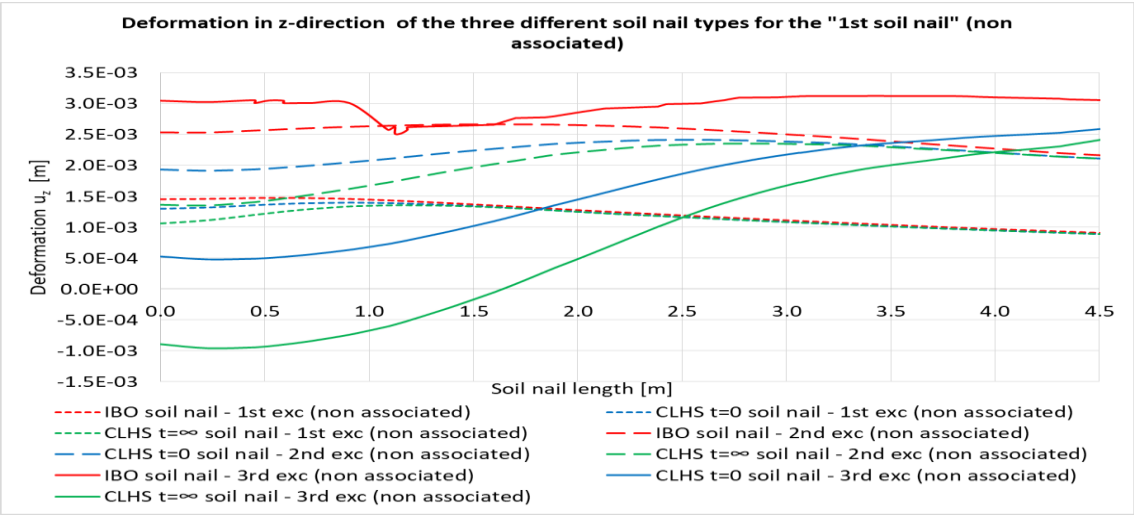

Figure K 11 u_z for the 1st soil nail (excavation steps: 1, 2 and 3) – ψ'=0°

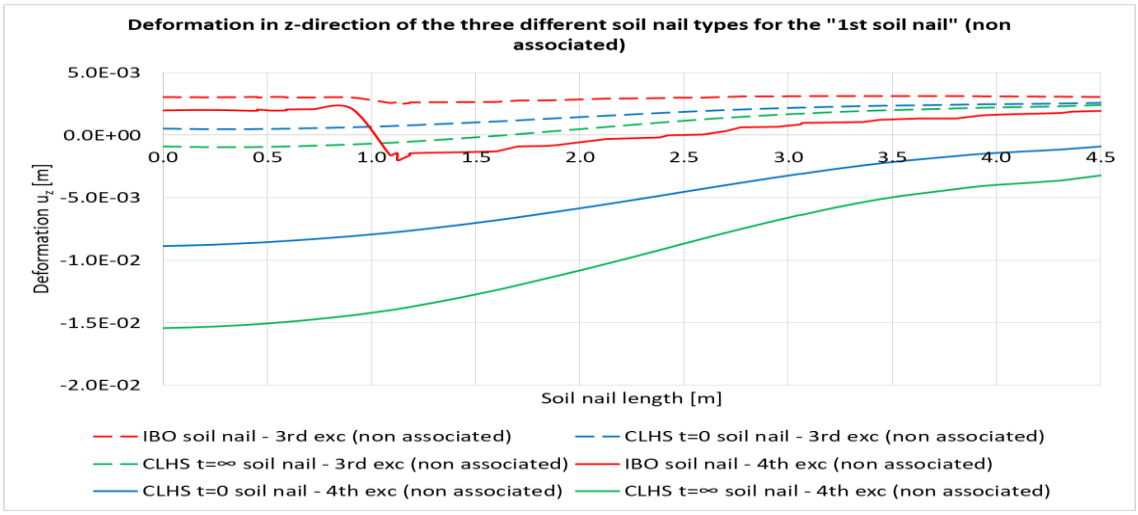

Figure K 12 u_z for the 1st soil nail (excavation steps: 3 and 4) – ψ'=0°

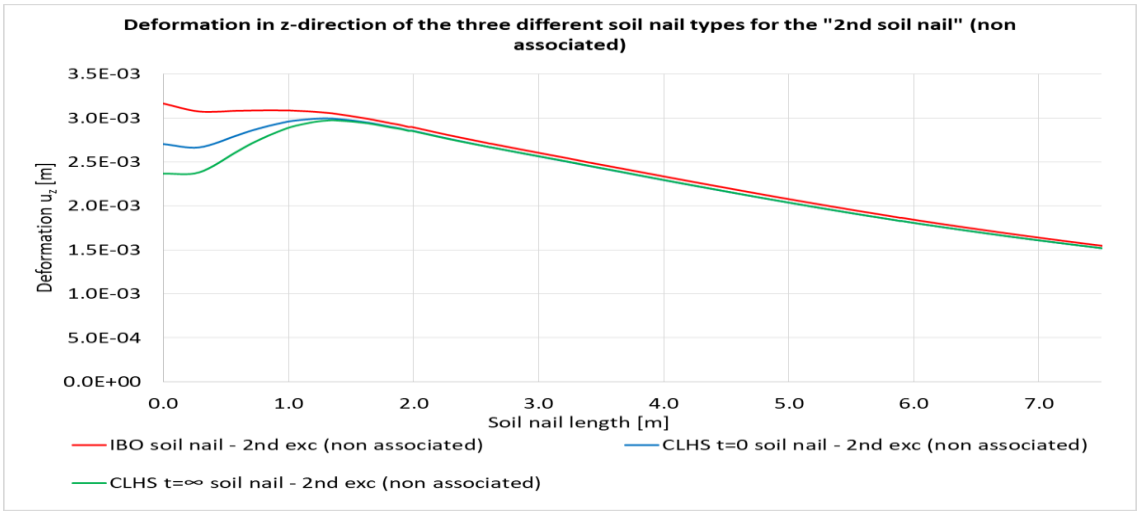

Figure K 13 u_z for the 2nd soil nail (excavation step 2) – ψ'=0°

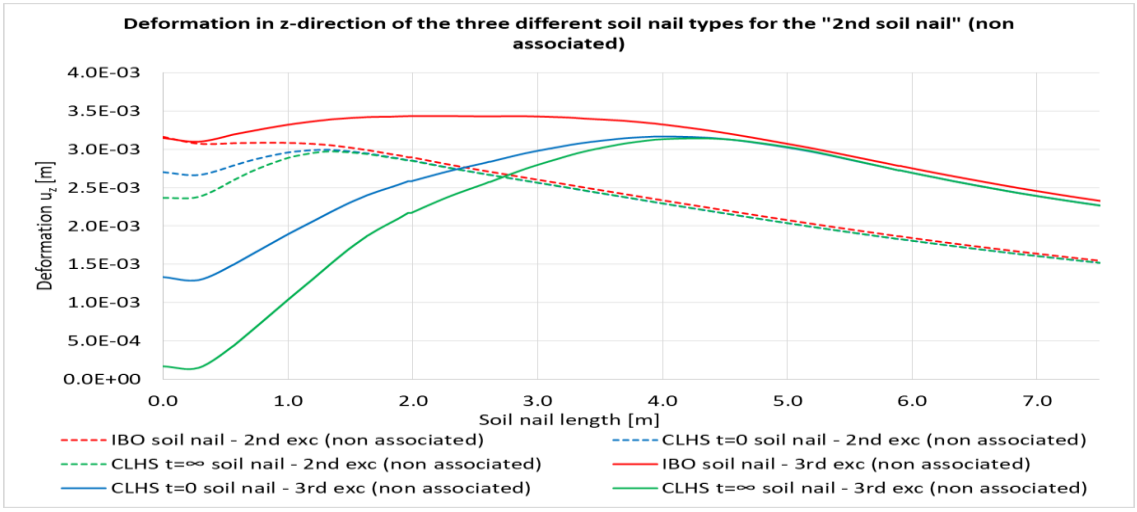

Figure K 14 u_z for the 2nd soil nail (excavation steps: 2 and 3) – ψ'=0°

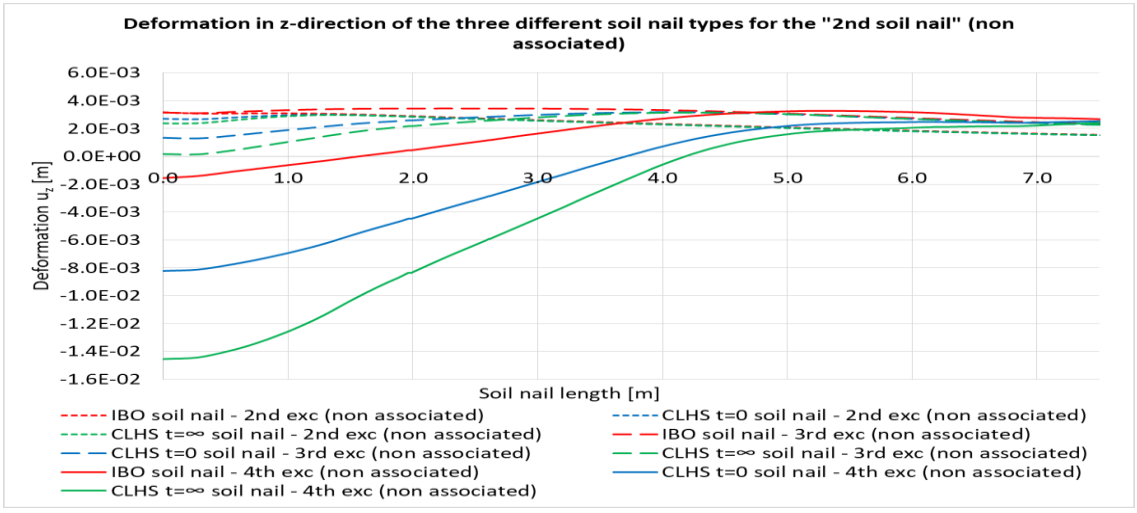

Figure K 15 u_z for the 2nd soil nail (excavation steps: 2, 3 and 4) – ψ'=0°

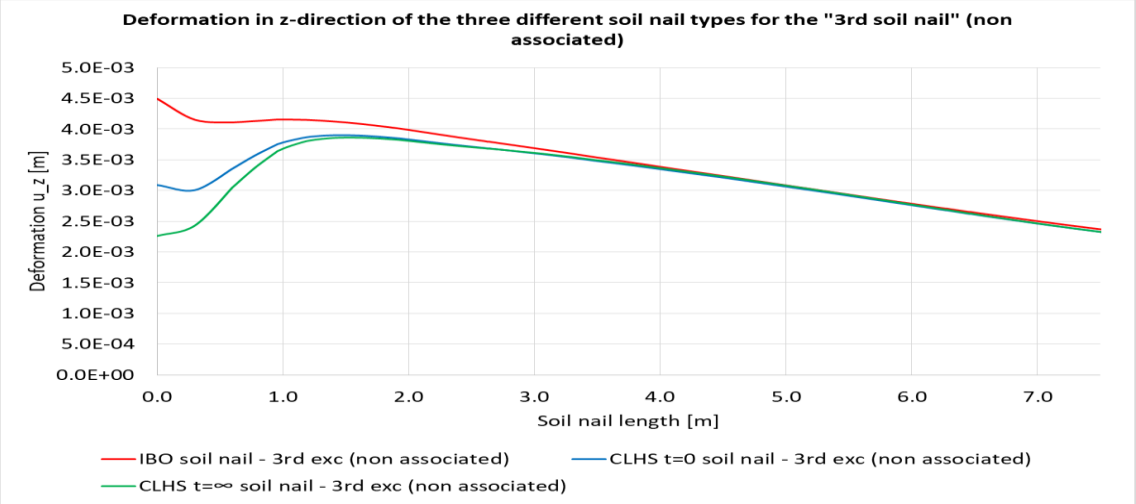

Figure K 16 u_z for the 3rd soil nail (excavation step 3) – $\psi'=0°$

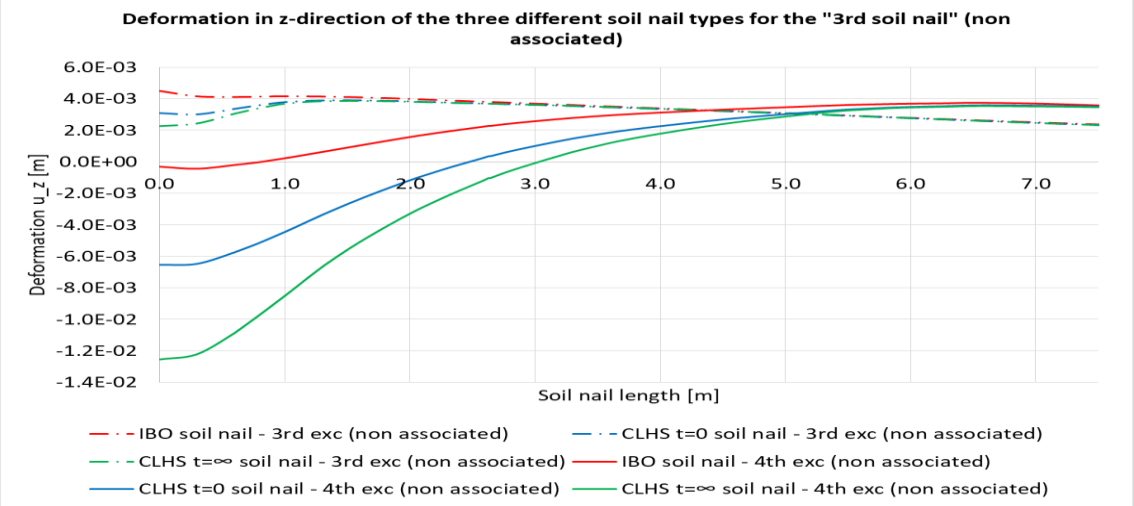

Figure K 17 u_z for the 3rd soil nail (excavation steps: 3 and 4) – $\psi'=0°$

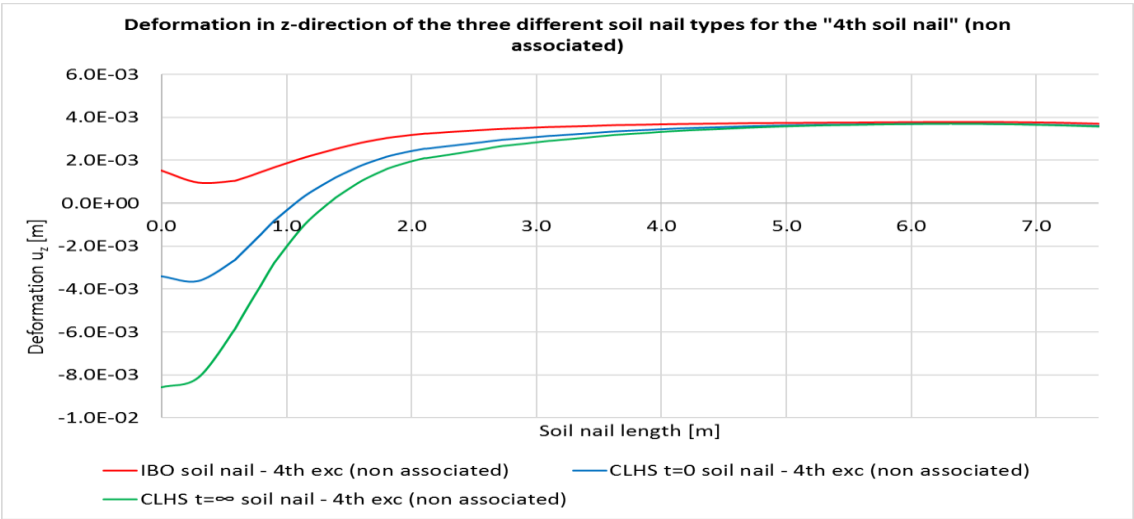

Figure K 18 u_z for the 4th soil nail (excavation step 4) – $\psi'=0°$

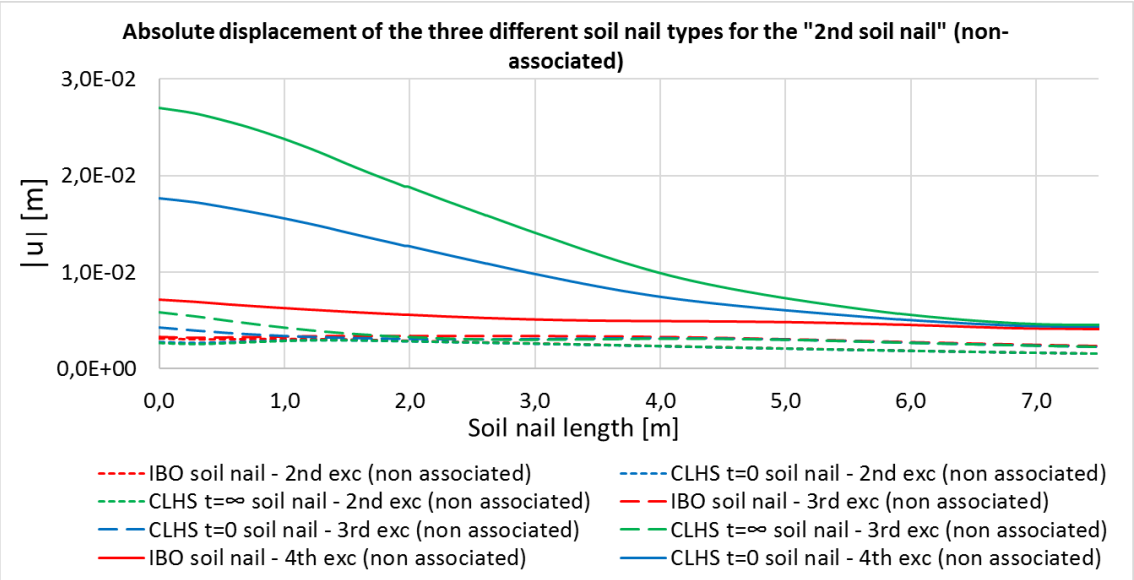

Figure K 19 $|u|$ for the 2nd soil nail (excavation step 2, 3 and 4) – ψ'=0°

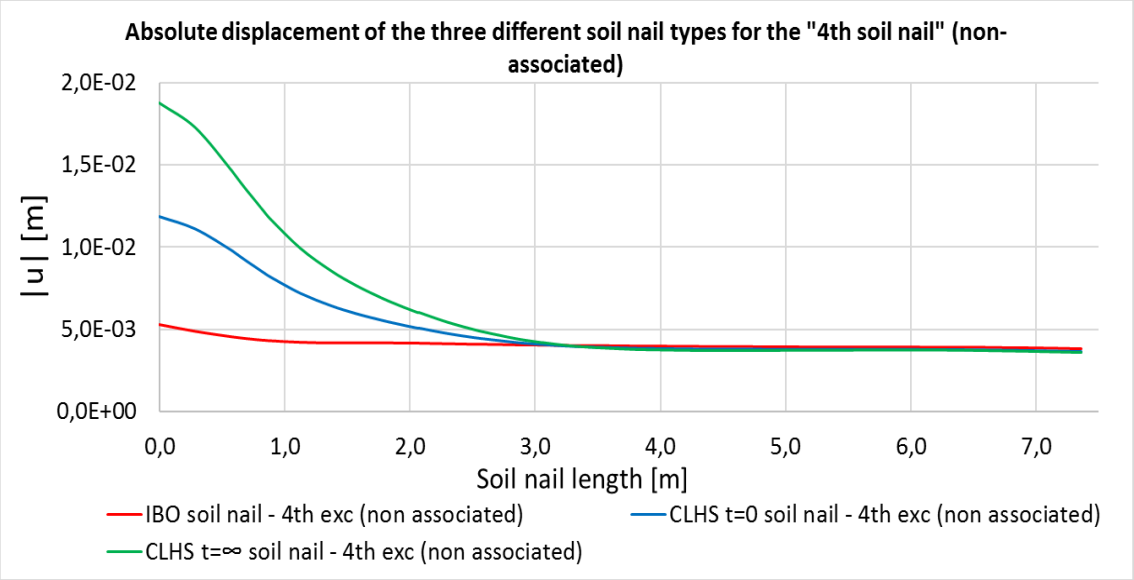

Figure K 20 $|u|$ for the 4th soil nail (excavation 4) – ψ'=0°

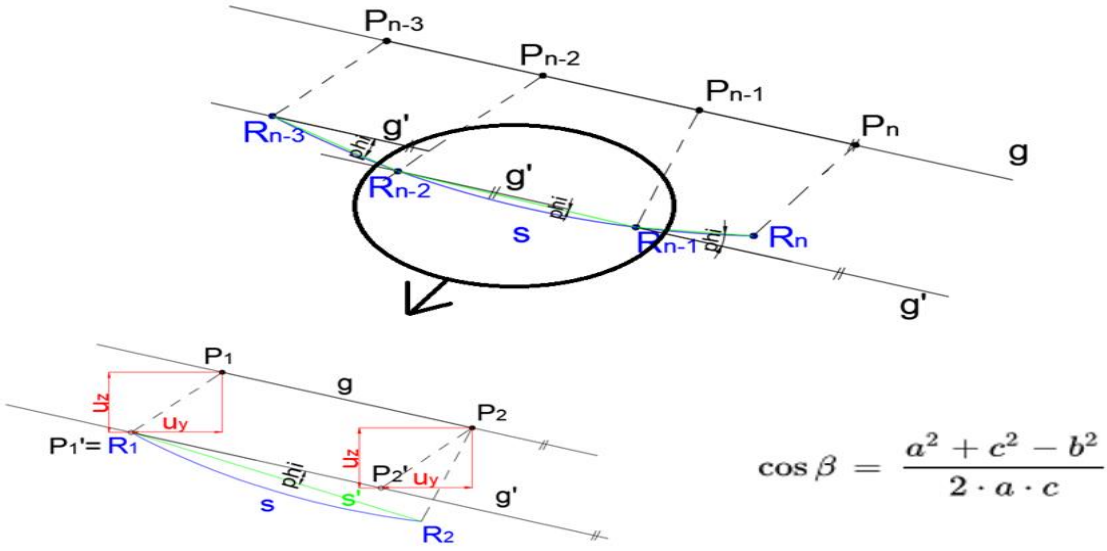

$$\cos\beta = \frac{a^2 + c^2 - b^2}{2 \cdot a \cdot c}$$

Figure K 21 Bending approximation approach

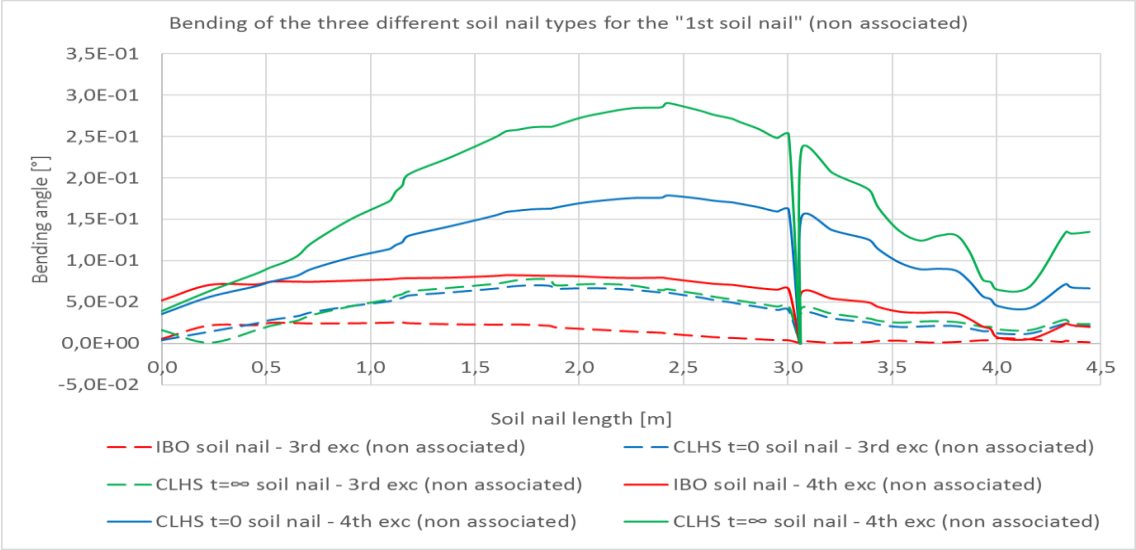

Figure K 22 Bending of the 1st soil nail for all the soil nail types (3rd and 4th excavation) – ψ'=0°

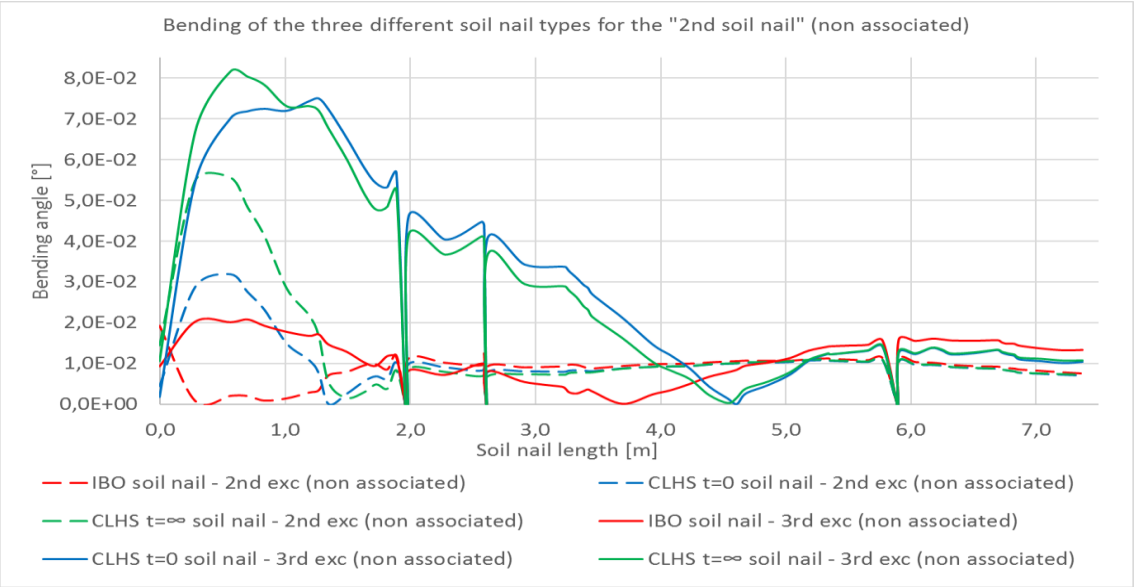

Figure K 23 Bending of the 2nd soil nail for all the soil nail types (2nd and 3rd excavation) – ψ'=0°

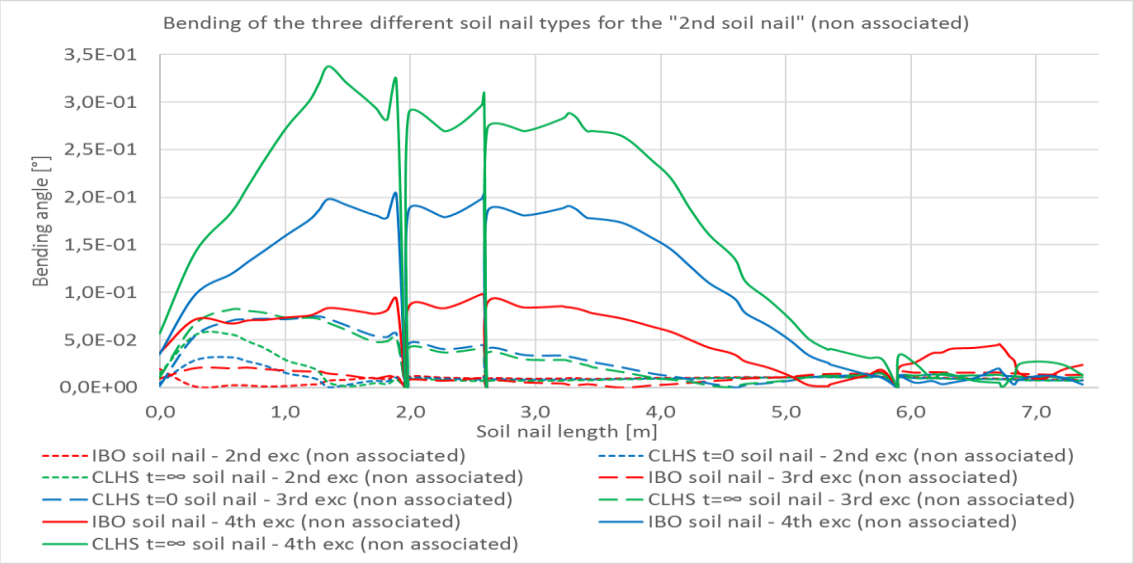

Figure K 24 Bending of the 2nd soil nail for all the soil nail types (2nd, 3rd and 4th excavation) – ψ'=0°

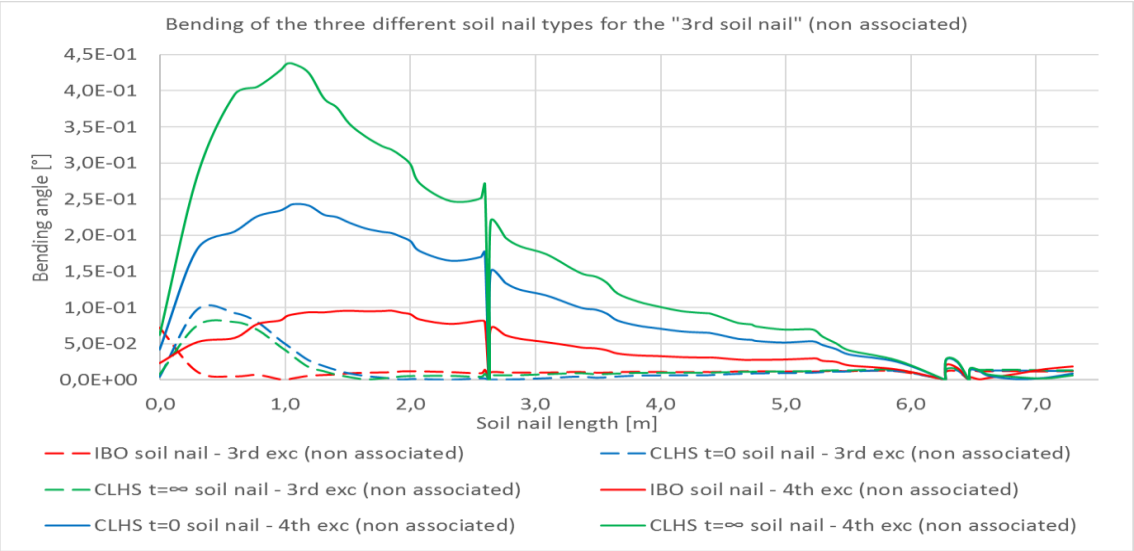

Figure K 25 Bending of the 3rd soil nail for all the soil nail types (3rd and 4th excavation) – ψ'=0°

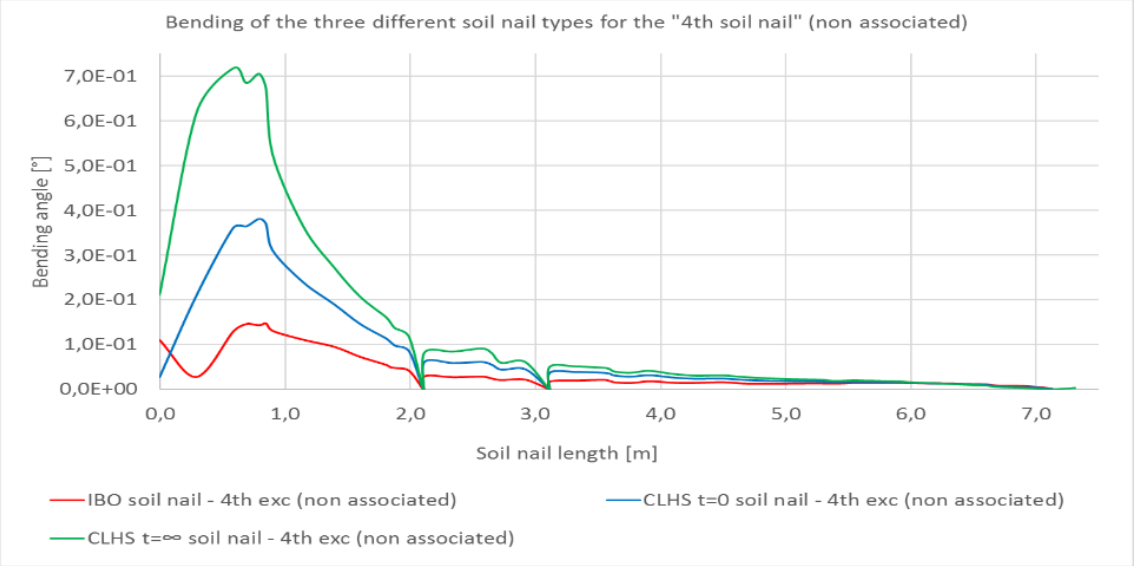

Figure K 26 Bending of the 4th soil nail for all the soil nail types (4th excavation) – ψ'=0°

Appendix L

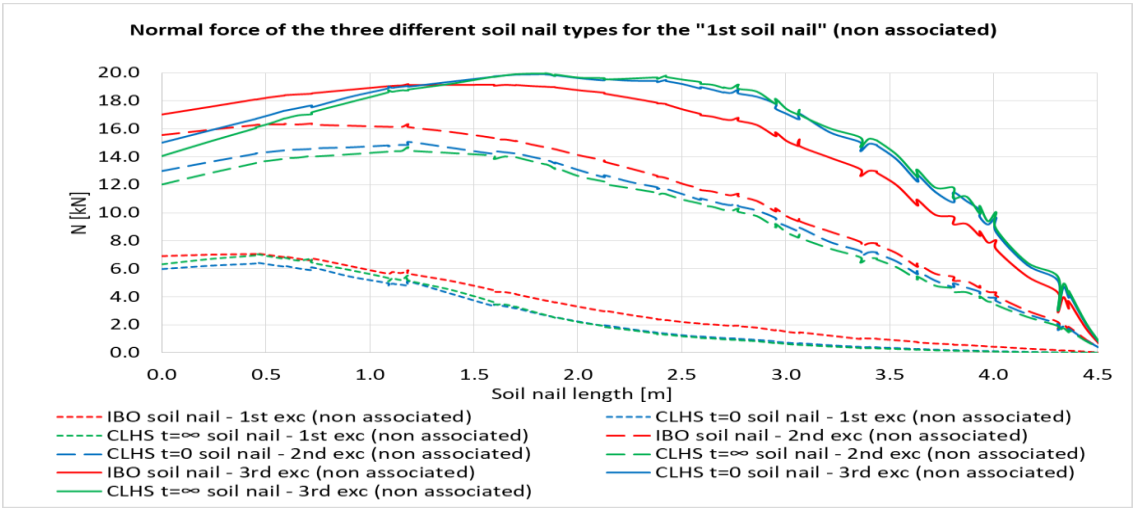

Figure L 1 1st soil nail normal force (excavation steps: 1, 2 and 3) – ψ'=0°

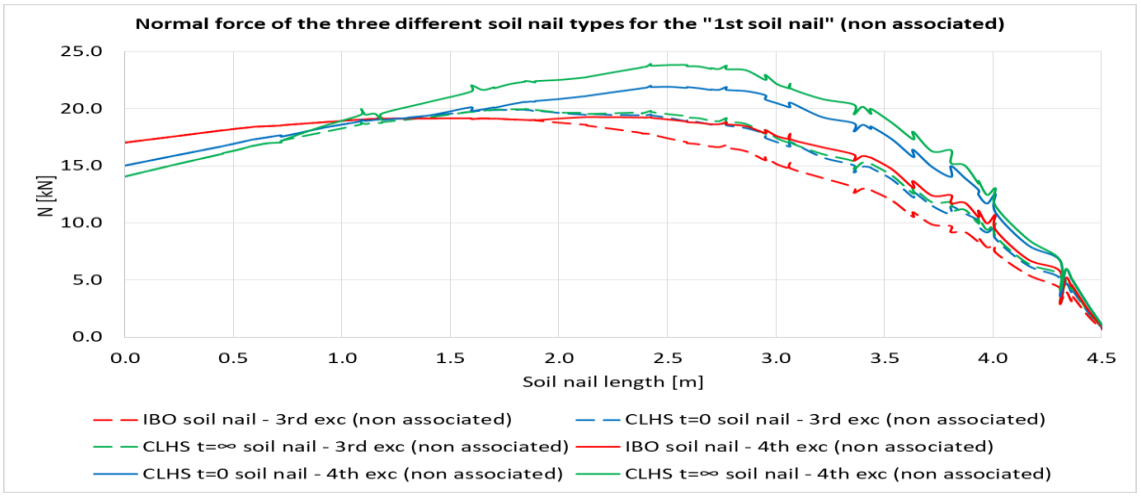

Figure L 2 1st soil nail normal force (excavation steps: 3 and 4) – ψ'=0°

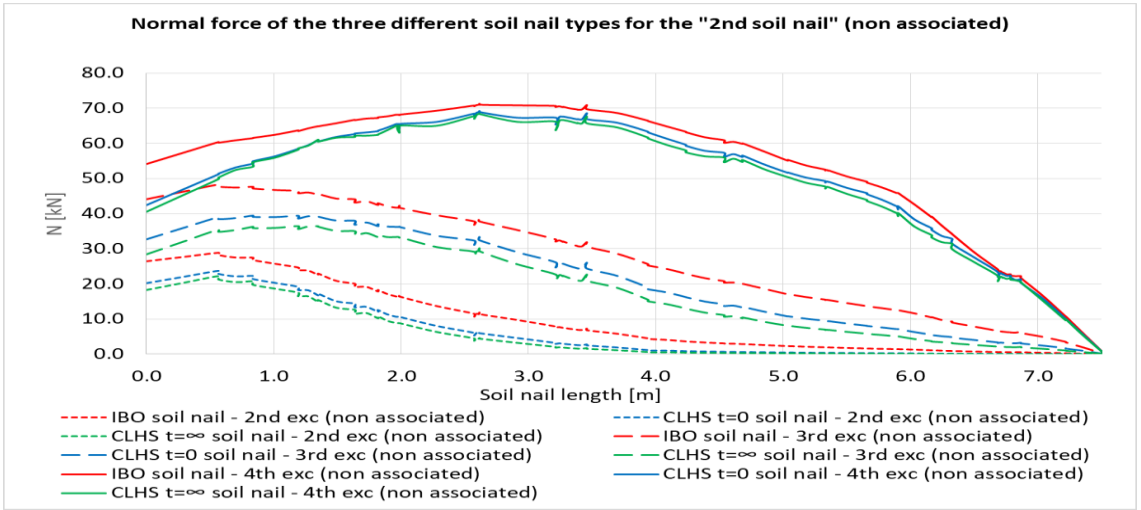

Figure L 3 2nd soil nail normal force (excavation steps: 2, 3 and 4)– ψ'=0°

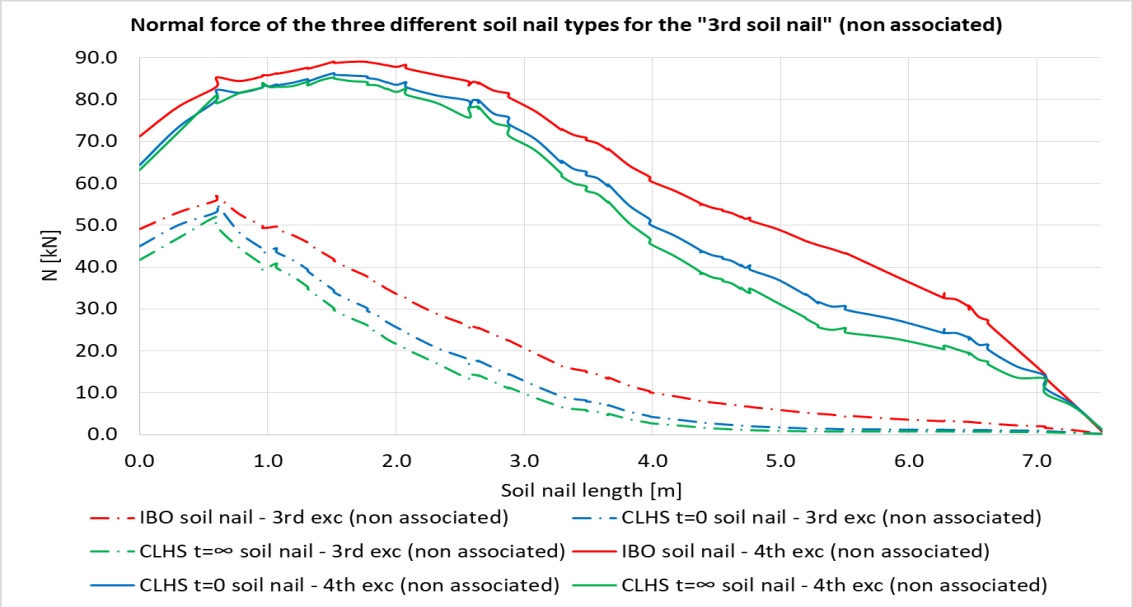

Figure L 2 3rd soil nail normal force (excavation steps: 3 and 4)– ψ'=0°

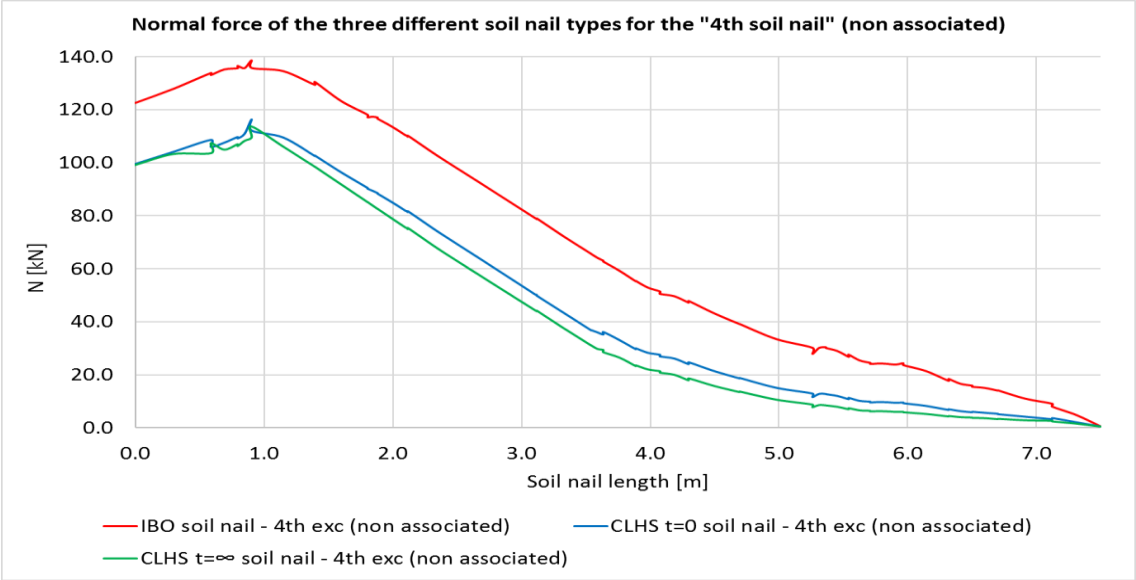

Figure L 3 4th soil nail normal force (excavation step 4)– ψ'=0°

Appendix M

The calculated plastic points, incremental displacements and deviatoric incremental strains of the 3D Unzmarkt soil nail wall model(-s), for the three cross sections (shown in Figure L 1) are depicted in the figures of Appendix L, for the non-associated flow rule calculations only.

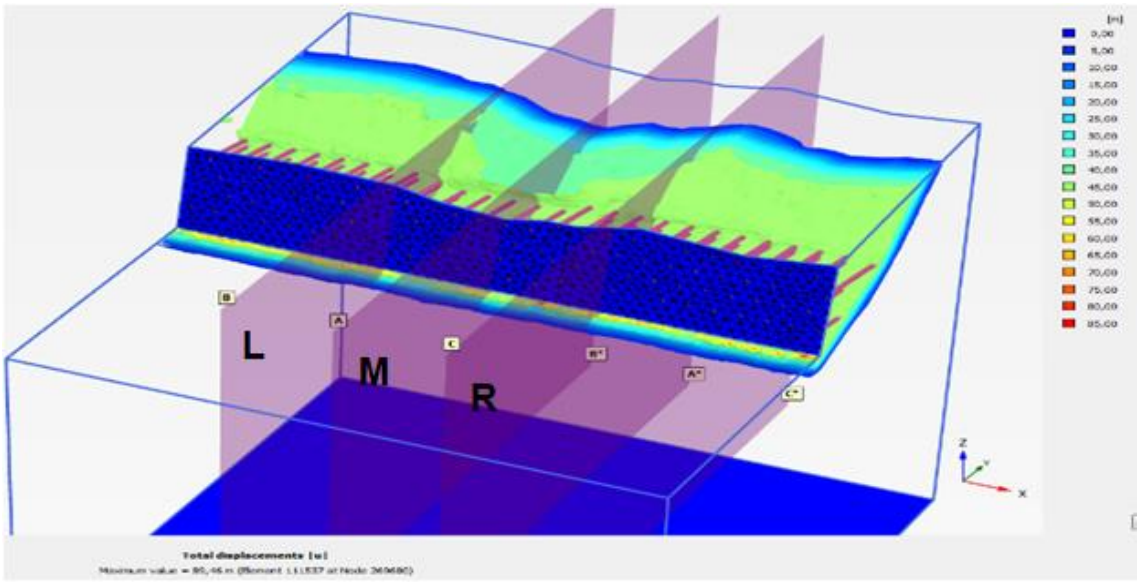

Figure M 1 Three examined cross sections (L-left, M-middle, R-right cross section)

Figure M 3 Plastic points of the three examined cross sections for the IBO soil nail type

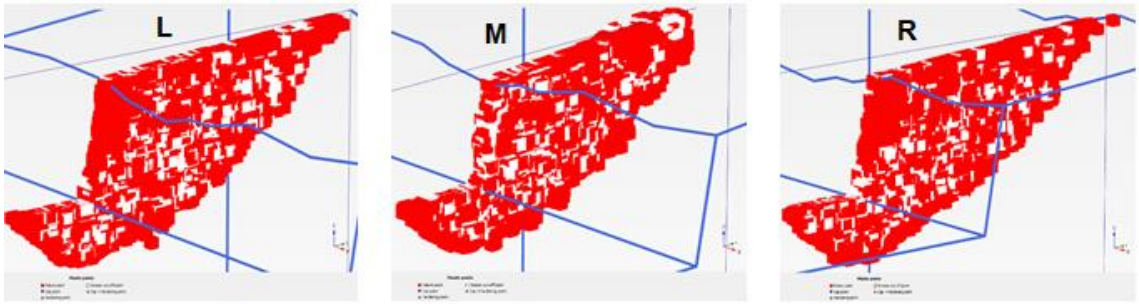

Figure M 2 Plastic points of the three examined cross sections for the CLHS (t=0) soil nail type

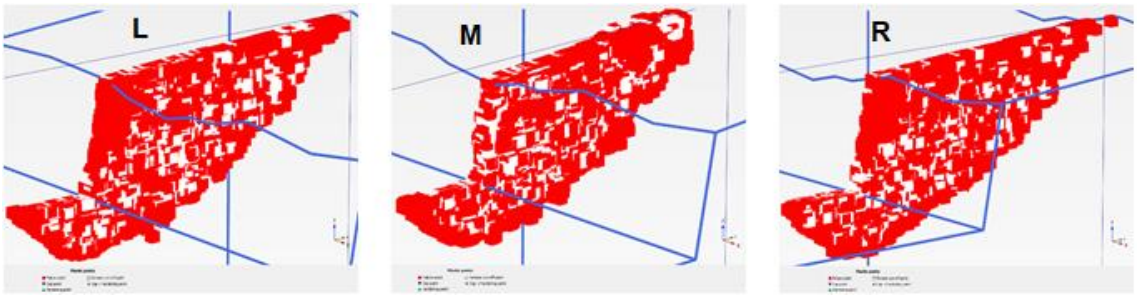

Figure M 5 Plastic points of the three examined cross sections for the CLHS (t=∞) soil nail type

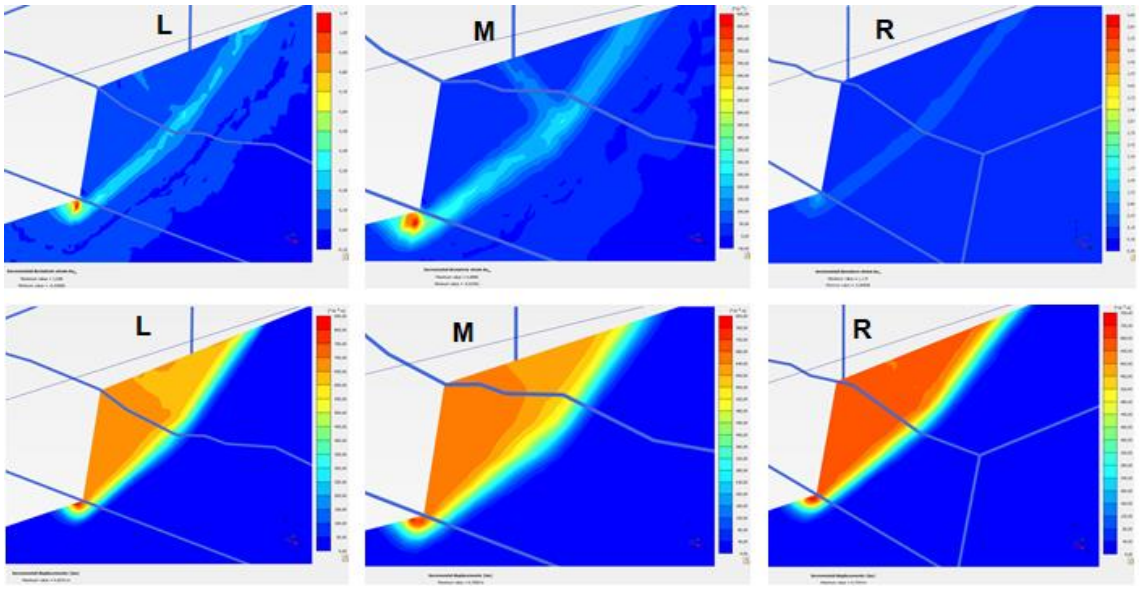

Figure M 4 Illustration of the incremental deviatoric strains (upper row) and incremental displacements (lower row) for the Unzmarkt soil nail wall with the parameters of IBO

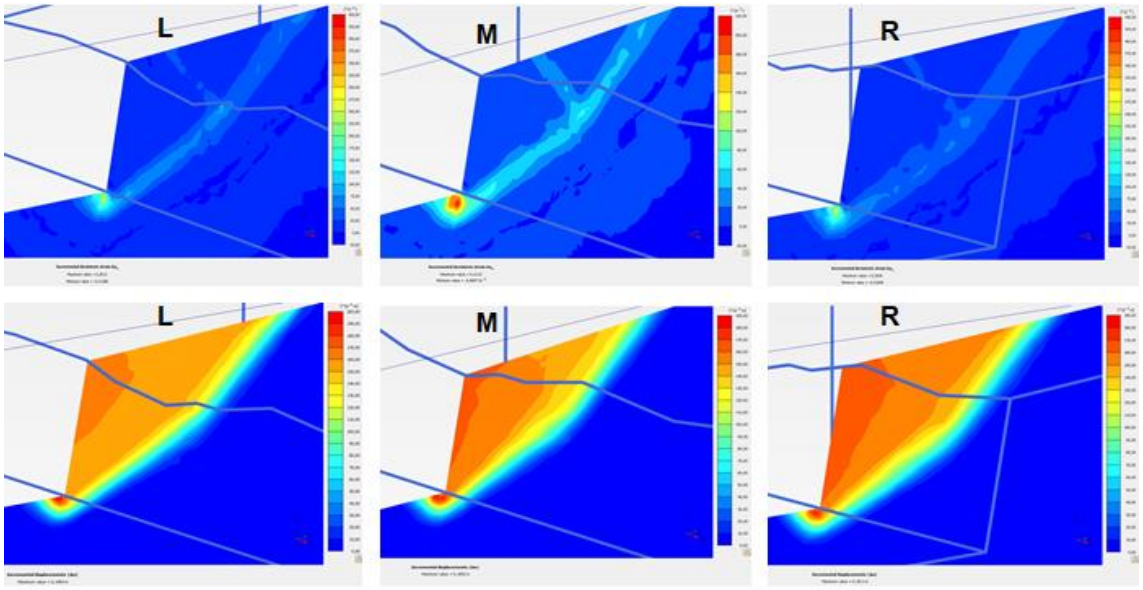

Figure M 6 Illustration of the incremental deviatoric strains (upper row) and incremental displacements (lower row) for the Unzmarkt soil nail wall with the parameters of CLHS (t=0)

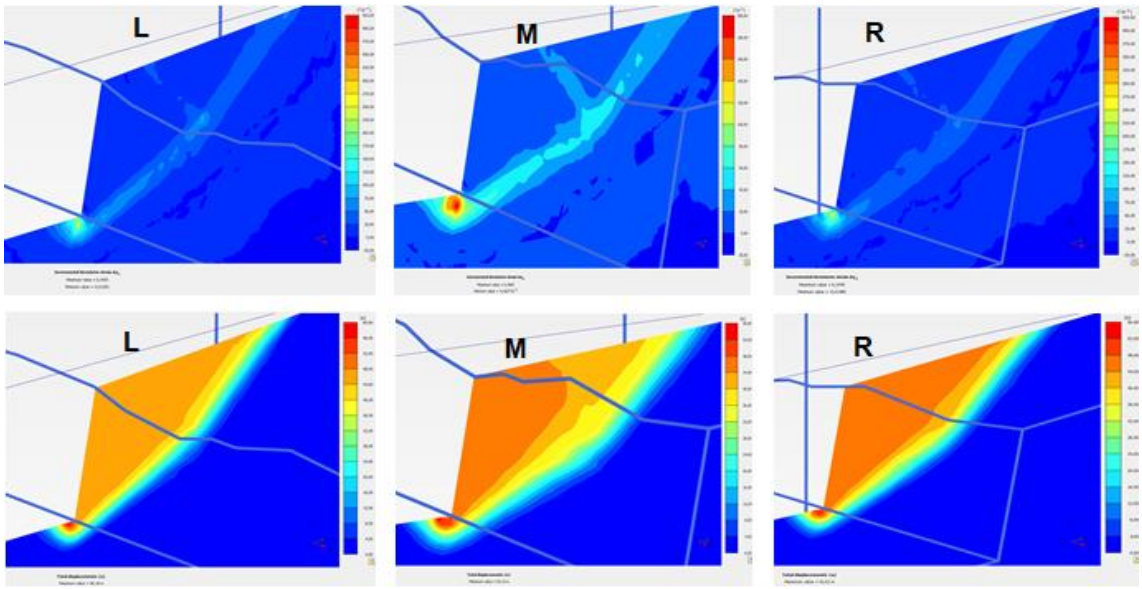

Figure M 7 Illustration of the incremental deviatoric strains (upper row) and incremental displacements (lower row) for the Unzmarkt soil nail wall with the parameters of CLHS (t=∞)